The Complex Narrowband UHF Mobile Radio Channel.

by

Michael Thomas Feeney

Thesis submitted in accordance with the requirements of the University of Liverpool for the degree of Doctor in Philosophy.

August 1989

Department of Electrical Engineering & Electronics.

ABSTRACT

The first part of this thesis is devoted to reviewing the characteristics of the complex signal received in a mobile radio environment. Two models are used, firstly a two-dimensional model in which the incoming multipath waves are constrained to the horizontal plane and secondly a more general three dimensional model in which the incoming vertically polarised waves do not, necessarily, travel horizontally. The second model is more realistic and more relevant to a study of propagation in small cells. Results, in particular those pertaining to correlational properties, are presented which show the different effects of the two models.

A review of predetection diversity strategies, is presented in terms of the cumulative distribution function, level crossing rate and average fade duration of the signal envelope together with a derivation of the cumulative distribution function of random FM for selection diversity. This review collates together, for the first time, first and second order envelope statistics in terms of uncorrelated and correlated diversity branches.

A novel receiver is described which was used to measure the complex correlation between the signals on two spaced antennas. The data gathered, using the receiver, enabled a realistic comparison to be made between several predetection diversity strategies in terms of both envelope and phase-related statistics. Cross-correlation measurements at both the base and mobile stations suggest that antennas vertically separated by 8λ to 13λ (base station) and $< 1\lambda$ (mobile station), can be usefully employed, in a cell of radius 1.3km, in conjunction with various diversity strategies. Measured envelope, phase and correlational statistics show considerable improvement for each of the diversity strategies considered at both stations using vertically separated antennas.

ACKNOWLEDGEMENTS.

In a work of this kind, in which so many people have been involved, it is difficult to acknowledge every individual, and therefore, the author wishes to apologise if any such persons do not see their name mentioned.

I would particularly like to thank my supervisor Professor J.D. Parsons for his unstinting help and guidance throughout this and earlier work. Also, appreciation and thanks go to Dr. F. Adachi for his invaluable contribution to the many papers referred to in this work. A considerable amount of technical support was required for this research, and therefore, I would like to express my gratitude to Mr. D.G. Lewis and Mr. R. Smith and members of the department's Electronic and Mechanical workshops. Colleagues in Professor Parsons' Mobile Radio Group provided many valued discussions during the course of this study, and therefore, my thanks go to them.

Finally, I would like to acknowledge and express my thanks to Catherine E. Pearce for her continued support and help throughout this and earlier work. I am deeply indebted to her, for without her support this thesis would never have been completed.

This thesis is dedicated
to my late parents,
Bernard and Marie Feeney.

LIST OF PRINCIPAL SYMBOLS.

ADC	Analogue to Digital Convertor.
AFD	Average Fade Duration.
AM	Amplitude Modulation.
ASCII	American national Standards institute Code for Information Interchange.
BER	Bit Error Rate.
CDF	Cumulative Distribution Function.
CNR	Carrier to Noise Ratio.
COV	COVariance.
CRO	Cathode Ray Oscilloscope.
CW	Continuous Wave.
DCR	Direct Conversion Receiver.
EBCDIC	Extended Binary Coded Decimal Interchange Code.
EGC	Equal Gain Combiner.
FDMA	Frequency Division Multiple Access.
FFT	Fast Fourier Transform.
FM	Frequency Modulation.
FOCC	FOrward Control Channel.
FSK	Frequency Shift Key.
GMSK	Gaussian Minimum Shift Key.
GSM	Groupe Speciale Mobile.
IF	Intermediate Frequency.
LCR	Level Crossing Rate.
LO	Local Oscillator.
MRC	Maximal Ratio Combiner.
PDF	Probability Density Function.

QPSK	Quaternary Phase Shift Key.
SAE	Switch And Examine.
SAS	Switch And Stay.
SEL	SELection.
SNR	Signal to Noise Ratio.
TACS	Total Access Communications System.
TDMA	Time Division Multiple Access.
$a(.)$	generalised quadrature autocorrelation function.
$\dot{a}$	first derivative, wrt time, of a.
$\ddot{a}$	second derivative, wrt time, of a.
a	10/ln10 = 4.34
C	Euler's constant = 0.5772
d_v	vertical antenna separation.
d	dominant envelope value in Rician PDF/CDF.
E{.}	expectation of {.}.
E_n	amplitude of nth wave.
erf(.)	error function.
erfc(.)	complementary error function.
F{.}	Fourier transform of {.}.
F(.)	Confluent hypergeometric function.
f	frequency.
f_c	carrier frequency.
f_D	maximum Doppler frequency.
f_s	sampling frequency.
$G_n(.)$	directivity of antenna n.
$I_0(.)$	modified Bessel function of first kind zero order.
$I(.)$	in-phase time varying component.
Im{.}	Imaginary part of {.}.

$J_0(.)$	zero order Bessel function.
$J_1(.)$	first order Bessel function.
K[.]	complete elliptic integral of the first kind.
L	distance of test area from base station.
L	sample distance over which local mean is estimated.
l	separation distance between two sample points.
m^2	local mean power.
$\hat{m}^2$	estimate of local mean power.
med	median.
m	mean of a random variable.
N	number of samples.
N_R	level crossing rate at envelope value R.
$P(.)$	CDF of (.).
$p(.)$	PDF of (.).
$p(a,b)$	joint PDF of a and b.
$p(a\|b)$	conditional PDF of a given b.
$Q(.)$	quadrature time varying component.
$Q(a,b)$	Marcum's Q-function.
R	envelope value.
$R(.)$	received signal envelope.
R_t	envelope switching threshold level.
Re{.}	Real part of {.}.
$r(.)$	normalised received signal envelope.
$r_{dB}(.)$	dB expressed envelope sequence.
$\hat{r}(.)$	estimate of fast fading component.
r_{mean}	mean of the linear expressed envelope.
r_{med}	median of the linear expressed envelope.
$r_{med}(dB)$	median of the dB expressed envelope.

r_v	distance of scatterers from mobile.
$S_{carr}(f)$	RF input or Doppler spectrum.
$S_{env}(f)$	envelope spectrum.
$S_{FM}(f)$	random FM spectrum.
$s(t)$	received signal.
T	sampling interval.
V	vehicle speed.
$z(.)$	complex sequence.
$< z(.) >$	ensemble average of complex sequence.
$z^*(.)$	complex conjugate of $z(.)$.
$\|z(.)\|$	modulus of complex value.
α_n	azimuth angle of arrival of nth multipath wave.
β	$2\pi/\lambda$
γ	direction of vehicle motion relative to base station.
γ	instantaneous carrier to noise ratio.
γ_0	average CNR.
ε_n	elevation angle of arrival of nth multipath wave.
ε_v	elevation angle at which multipath waves are centred.
$\zeta(.)$	normalised autocorrelation function i.e. $a(\tau)/a(0)$.
θ_n	phase angle of nth multipath wave.
λ	wavelength.
$\xi(.)$	autocorrelation function of the dB expressed envelope.
ρ_{12}	complex cross-correlation between antennas 1 and 2.
ρ_{env}	envelope cross-correlation between antennas 1 and 2.
$\rho_{11}(\tau)$	autocorrelation function at delay τ.
σ^2	average signal power.
σ_n^2	noise power.
σ_r^2	variance of linear expressed envelope.

$\sigma_r^2(dB)$	variance of dB expressed envelope.
τ	time delay.
τ_R	AFD at envelope value R.
$\phi(.)$	received signal phase.
$\dot{\phi}(.)$	first derivative of ϕ wrt to time.
ϕ_n	phase angle of nth multipath wave.
$\psi(.)$	autocovariance of the dB expressed envelope.
$\psi_{nR}(.)$	phase noise of receiver.
$\psi_{nT}(.)$	phase noise of transmitter.
$\psi_n(.)$	combined phase noise of transmitter and receiver.
Ω	$\omega_D/\sqrt{2}$
ω_c	carrier angular frequency.
ω_D	maximum angular Doppler frequency.
ω_n	angular frequency of nth multipath wave.
ω_o	local oscillator angular frequency.

TABLE OF CONTENTS

CHAPTER 1. INTRODUCTION.

Man has always had the need to communicate quickly and faultlessly with his fellow man, such communication being required for social, business, political or emergency reasons. Ideally, the means by which the information is conveyed should be simple, inexpensive and be able to operate from any location and without excessive delay. Radio communications provides an attractive solution, but the RF spectrum over which the information is carried is a natural resource that requires both efficient and effective management if the information transmitted is to reach its destination intact. Mobile radio, i.e. when one of the parties is not fixed to a specific location, attempts to meet each of the above criteria; however, it is not a universal panacea. Mobile radio systems have to operate under the adverse effects of severe and rapid fading (especially whilst one or both of the terminals is in motion) which arises from the destructive interference of multipath waves.

Notwithstanding these problems, mobile radio has seen a steady growth from the 1950s, when the invention of the transistor facilitated the design of reliable and lightweight communication systems. Since the beginning of 1985 commercial cellular radio (which is just one aspect of mobile radio) has seen a spectacular growth in the number of subscribers. The current UK cellular radio system, TACS (Total Access Communications System), employs analogue techniques. Second generation systems will employ digital techniques[1] that will provide an improved and greater choice of services to the user because of the greater flexibility provided by digital modulation, compared with analogue techniques. The Pan-European Digital Cellular Mobile Radio Network (i.e. Groupe Speciale Mobile-GSM) that will be introduced in 1991 is a wideband scheme with 270kb/s GMSK[2] modulation in a Time Division Multiple Access (TDMA) mode. The GSM systems contrasts markedly with the current narrowband scheme employed in the FDMA (Frequency Division Multiple Access) TACS system (FM modulation with 25kHz channel spacing). It is not known, at this stage, what schemes will be employed in future generation systems beyond GSM. The consensus in

Japan[3], and to a certain extent in the USA, is towards narrowband schemes employing narrow channel spacings (e.g. 12.5 Hz) with spectrally efficient digital modulation techniques such as GMSK together with diversity to combat the adverse effects of multipath. There is no reason to suggest that future generation systems in Europe might not follow similar trends. It is therefore vitally important for the success of these future generation systems that the narrowband channel is fully quantified in terms of both the envelope and phase characteristics in order that both diversity strategies and spectrally efficient high order modulation schemes can be evaluated.

To the author's knowledge the envelope and phase characteristics of the narrowband channel have never been investigated with the specific purpose of implementing diversity strategies employing spatial antenna separation. The author has previously investigated several diversity strategies for vertically separated antennas at the base station, only in terms of the envelope[4-10]. Appendix A of this thesis contains several publications reporting this work. The extent of the improvement provided by spaced antenna diversity is dependent upon the degree of correlation between the signals received on the two antennas. In this work therefore, the cross-correlation is examined for complex signals received on vertically separated antennas at both base and mobile stations. The effects of cross-correlation on the performance of several diversity strategies is then examined in terms of statistics associated with the envelope and phase. The thesis can be summarised as follows;

Chapter 2 contains a review of the received signal statistics for two propagation models. The well-known, two-dimensional model in which the incoming multipath waves are constrained to propagate in a horizontal direction is considered and this leads to statistical results principally based on classical Rayleigh fading. A three-dimensional model is also considered in which the constraint of horizontal propagation is removed. In this later model the statistics show a departure from those of the two dimensional model for the correlational properties (i.e. spectra etc.). but not for the envelope and phase. The three dimensional model, it is considered, probably becomes more important for small cells where the effects of height are more apparent.

In the third chapter a variety of diversity schemes are reviewed with predetection diversity combining using spaced antennas, being considered in detail. The statistics of several diversity combiners are discussed in terms of an equivalent envelope and phase which results from the action of the diversity system on two correlated signals which exhibit Rayleigh statistics. The statistical parameters of the envelope considered are the Cumulative Distribution Function (CDF), the Level Crossing Rate (LCR) and Average Fade Duration (AFD). In addition, selection diversity is considered in terms of the instantaneous frequency (i.e. random FM) of the complex signal received on the individual branches and that of the equivalent output of a selection diversity receiver. The CDF of the random FM for selection diversity is derived and compared with that for a single branch.

Chapter 4 outlines the basic concept of a direct conversion, vector demodulator receiver, in which the carrier envelope and phase are determined at baseband frequencies using the quadrature outputs of the receiver. Several sources of error associated with such a receiver are discussed in terms of their effect on the envelope and phase measured at the output of the receiver. The sources of error considered are; quadrature channel mismatch, quadrature dc offset and quadrature error. Several methods are described by which these sources of error can be quantified and reduced. The concept of the vector demodulator receiver is then advanced to the development of a dual-branch amplitude and phase measuring receiver. This receiver has been used in conjunction with two vertically spaced antennas, for a direct study of the effects of complex cross-correlation between the signals received on two spaced antennas (at base and mobile stations). It is believed that this is the first time such a study has been undertaken. In addition, it is the first time that a realistic evaluation of several diversity combiners has been carried out in terms of statistics associated with both the envelope and phase. This novel receiver is discussed in terms of its phase noise performance with respect to a transmitter/receiver arrangement which was used to measure the complex signals on two vertically spaced antennas at base and mobile stations.

Chapter 5 discusses the experimental arrangements in which the receiver was operated. Firstly, the receiver was used in conjunction with two vertically separated antennas at the base station. The transmitter, located at the mobile, was driven around a preplanned route. Antenna displacements of 2λ to 20λ were used, in steps of 1λ. Secondly, the transmitter and receiver locations were reversed and antenna separations from 0.5λ to 4.0λ in steps of 0.5λ were used at the mobile. The data digitisation is discussed together with initial data reduction. The data reduction includes normalisation of the data to remove the slow fading component, which is caused by variations in the gross terrain features along the propagation path. This procedure also allows the subsequent comparison of simulated diversity schemes with results predicted by theory for a pure fast fading (i.e. Rayleigh) environment. The slow fading component is estimated by a moving average technique.

The results of the various field trials are presented in Chapter 6 in three distinct sections. Firstly, results are presented in terms of a single branch for the envelope, phase and various spectra (e.g. Doppler, envelope and random FM) for signals received in both Rayleigh and non-Rayleigh fading conditions. The results for non-Rayleigh fading conditions are considered in terms of a two-ray propagation model where there exists direct and indirect paths which combine to form a standing wave pattern which produces a CDF with a considerably higher probability of deep fades than that experienced under pure Rayleigh fading conditions. In addition, the results, particularly those pertaining to correlational properties (i.e. spectra), are considered for a three dimensional propagation model in which the multipath waves arriving in elevation can significantly modify the Doppler and envelope spectra. These phenomena are probably of considerable importance for propagation in small cells. Secondly, the cross-correlation between the signals received on two vertically separated antennas, at various values of displacement, are presented for the cases when the receiver is located at the base and mobile stations. A scattering model is then developed which describes the degree of cross-correlation between the two antennas, in terms of how the spaced antennas view the scatterers surrounding the mobile. Finally, several predetection diversity strategies are simulated and their

performance evaluated using the data recorded by the dual branch vector demodulator receiver. The diversity simulation, which enables a realistic comparison between the various schemes, is considered in terms of the quadrature signals, which allows the various strategies to be assessed in terms of the statistics related to the envelope and various spectra (e.g. Doppler, envelope and random FM).

The final chapter summarises the results of the work and discusses several proposals for future work which have arisen out of this research.

1.1 REFERENCES.

[1] Balston, D.M., "Pan-European Cellular Radio: or 1991 and all that", Electronics and Communication Engineering J. Jan/Feb., 1989.

[2] Murota, K. and Hirade, K., "GMSK Modulation for Digital Mobile Radio", IEEE Trans., COM-29, No.7, pp.1044-1050, 1981.

[3] Kuramoto, M. and Shinji, M., "Second Generation Mobile Radio System in Japan", IEEE Magazine, Vol.24, No.2, pp.17-21, 1986.

[4] Williamson, A.G., Adachi, F., Feeney, M.T. and Parsons, J.D., "Base Station Space Diversity for Mobile Radio Systems", Presented at the IREECON (Melbourne Australia) Oct. 1985, pp.228-231.

[5] Adachi, F., Feeney, M.T., Williamson, A.G. and Parsons, J.D., "Cross-correlation Between the Envelopes of 900MHz Signals Received at a Radio Base Station Site", IEE Proc. Pt.F., Vol.133, No.6, 1986, pp.506-512.

[6] Feeney, M.T., and Adachi, F., "The Performance of Various Diversity Combiners on Signals Received at a Base Station Site", Presented at the IERE Third International Conference on 'Land Mobile Radio', Publication No.65, pp.55-62, 1985.

[7] Adachi, F., Feeney, M.T. and Parsons, J.D., "An Evaluation of Specific Diversity Combiners Using Signals Received by Vertically Spaced Base Station Antennas", J. of IERE Vol. 57, No.6 (Supl.) pp.S218-S224 1987.

[8] Adachi, F., Feeney, M.T. and Parsons, J.D., "Effects of Correlated Fading on Level Crossing Rates and Average Fade Duration with Predetection Diversity Reception", IEE Proc. Pt.F, Vol.135, No.1, pp.11-17, 1988.

[9] Parsons, J.D. and Feeney, M.T., "Comparison of Selection and Switched Diversity Systems for Error-Rate Reduction at Base-Station Sites in Digital Radio Systems", 37th IEEE Vehicular Technology Conference, 1-3rd June 1987, Tampa Florida, pp.393-398.

[10] Adachi, F., Feeney, M.T. and Parsons, J.D., "Level Crossing Rate and Average Fade Duration for Time Diversity in

Rayleigh Fading Conditions", IEE Proc. Pt.F, Vol.135, No.6, pp.501-506, 1988.

CHAPTER 2. THE COMPLEX SIGNAL FOR A NARROWBAND MOBILE RADIO CHANNEL.

2.1 INTRODUCTION.

In this and the following chapter no attempt is made at a complete derivation of statistical formulae which can, in any case, be found elsewhere. The purpose of Chapters 2 and 3 is to bring together pertinent information from various texts[1,2,3] and recent papers regarding the nature of the complex narrowband mobile radio channel and the improvements afforded by various predetection diversity schemes.

The signal received, both at the mobile and base stations, is subject to rapid fluctuations in field intensity, as the vehicle progresses along a route. These rapid variations in signal strength occur due to the superposition of multipath waves, at the receiving antenna, which have undergone propagation by various modes e.g. reflection and diffraction. Naturally, such phenomena would have a deleterious effect on information transmitted over the mobile radio channel, especially when digital techniques are employed. To quantify the phenomena exhibited by such a channel the statistics associated with a mathematical channel model will be reviewed in this chapter.

In the ensuing discussion only those statistics pertaining to the fast fading component in a narrowband channel will be described. By fast fading we mean that the slow fading associated with the local mean, which is due to variations in the gross terrain features, will not be considered. By narrowband we mean that frequency-selective fading does not occur across the band. In addition, we shall assume the statistics to be stationary over a distance of the order of tens of wavelengths.

The model used to describe the channel is that of Aulin[4]. This model is an extension of the more commonly used Clarke model[5], which is confined to the superposition of waves travelling in a horizontal plane only. Aulin's model includes those vertically polarised waves which are not travelling horizontally. This later aspect is of particular importance to this work, where the use of small cells in urban areas is considered. The statistics presented will be related only to the electric field component i.e. the signal as sensed by a vertical monopole or dipole antenna. In addition, the results will be elucidated to give the more familiar results associated with waves only travelling horizontally. Aulin's results only show departure from those of Clarke because of the non-zero distribution of waves out of the horizontal plane. This distribution of waves in elevation is generally unspecified. In general Aulin's model shows a departure from that of Clarke's for correlational properties (e.g. spectra) but not for the envelope and phase statistics.

2.2 THE MATHEMATICAL MODEL.

Aulin[4] considered several component plane waves combining together in three dimensional space (see Fig.2.1). A single component has an amplitude c_n, an angle of arrival, relative to the x-z plane, α_n, and ε_n relative to the x-y plane and a phase angle ϕ_n. The parameters c_n, α_n, ε_n and ϕ_n are random and statistically independent. The resultant wave at a point (x_0,y_0,z_0) is given by

$$E(t) = \sum_{n=1}^{N} E_n(t) \tag{2.1}$$

where

$$E_n(t) = c_n \cos[\omega_c t - \frac{2\pi}{\lambda}(x_0 \cos\alpha_n \cos\varepsilon_n + y_0 \sin\alpha_n \cos\varepsilon_n + z_0 \sin\varepsilon_n) + \phi_n] \tag{2.2}$$

In the above ω_c and λ are the carrier angular frequency and wavelength respectively. This reduces to Clarke's model[5] if all the plane waves

are confined to the x-y plane (i.e. $\cos \varepsilon_n = 1$). If the point (x_0,y_0,z_0) is now displaced with a velocity V in the direction γ, relative to the x-z plane (i.e.$(x_0,y_0,z_0) \rightarrow (V \cos \gamma, V \sin \gamma, z_0)$) then the resultant field is

$$E(t) = I(t) \cos \omega_c t - Q(t) \sin \omega_c t \tag{2.3}$$

where I(t) and Q(t) are the in-phase and quadrature components seen by a quadrature detector receiver[6] *viz*,

$$\begin{aligned} I(t) &= \sum_{n=1}^{N} c_n \cos[\omega_n t + \theta_n] \\ Q(t) &= \sum_{n=1}^{N} c_n \sin[\omega_n t + \theta_n] \end{aligned} \tag{2.4}$$

and

$$\begin{aligned} \omega_n &= \omega_D \cos(\gamma - \alpha_n) \cos \varepsilon_n \\ \theta_n &= 2\pi \frac{z_0}{\lambda} \sin \varepsilon_n + \phi_n \end{aligned} \tag{2.5}$$

ω_n is the Doppler angular frequency component of the nth wave and ω_D is the maximum Doppler angular frequency ($= 2\pi f_D$, f_D is the maximum Doppler frequency). Waves arriving from ahead of the vehicle have a positive Doppler shift, those arriving from behind have a negative shift. Again the above simplify to Clarke's model[5] when confined to the horizontal plane, i.e. $p(\varepsilon = 0) = 1$.

2.2.1 The Quadrature Components I(t) and Q(t).

When N becomes sufficiently large (typically $N \geq 6$) I(t) and Q(t), by the central limit theorem, become zero mean Gaussian processes with equal variance (σ^2). Thus I(t) and Q(t) have a Probability Density Function (PDF) of the form

$$p(x) = \frac{1}{\sigma\sqrt{2\pi}} \exp\left\{ -\frac{x^2}{2\sigma^2} \right\} \quad x = I(t) \text{ or } Q(t) \tag{2.6}$$

The Cumulative Distribution Function (CDF) of the quadrature components is given by

$$P(x \leq X) = \int_{-\infty}^{X} p(x)\,dx = \frac{1}{2}\left[1 + \text{erf}\left(\frac{X}{\sigma\sqrt{2}}\right)\right] \tag{2.7}$$

where erf if the error function defined as

$$\text{erf}\,(y) = \frac{2}{\sqrt{\pi}}\int_{0}^{y} e^{-t^2}dt \tag{2.8}$$

The PDF and CDF of a zero mean Gaussian distribution, which could have either I(t) or Q(t) as the variate, is shown in Figure 2.2. Note that for a zero mean Gaussian distribution the median and the mean are identical.

2.2.2 The Received Signal Envelope r(t).

The envelope of the received signal is defined in terms of the quadrature components as,

$$r(t) = \sqrt{I^2(t) + Q^2(t)} \tag{2.9}$$

The envelope has been shown by Rice[7] to be Rayleigh distributed with a PDF given by

$$p(r) = \frac{r}{\sigma^2}\exp\left\{\frac{-r^2}{2\sigma^2}\right\} \tag{2.10}$$

where σ^2 is the local mean power and $r^2/2$ is the short-term signal power. The CDF is then given by

$$P(R) = \int_{0}^{R} p(r)\,dr = 1 - \exp\left\{-\frac{R^2}{2\sigma^2}\right\} \tag{2.11}$$

Appendix B shows how the Rayleigh PDF can be expressed in dB terms. Figures 2.3 and 2.4 show the PDF and CDF, expressed in dB terms, of a normalised signal envelope respectively. Notice that the PDF is

asymmetric such that a fade of 10dB below the local mean (0dB) is more likely to occur than a 10dB enhanced signal above the local mean.

2.2.3 Statistical Parameters of the Envelope.

The envelope is the most commonly recorded parameter of the received signal. If the envelope conforms to a Rayleigh distribution then the following parameters apply.

2.2.3.1 Mean strength of the envelope.

The mean value of the envelope r_{mean} is given by the expectation of r(i.e. $E\{r\}$) which, since we are dealing with ergodic processes[3], is given by the ensemble average of r[1] (i.e. $< r >$). The expectation of a variate is then given by the integration of that variate with its PDF over all possible values of the variate i.e.

$$r_{mean} = E\{r\} = < r > = \int_0^\infty r\,p(r)\,dr = \sigma\sqrt{\frac{\pi}{2}} \tag{2.12}$$

The variance of the envelope σ_r^2 is given by

$$\sigma_r^2 = E\{r^2\} - E\{r\}^2 = 2\sigma^2 - \frac{\sigma^2\pi}{2} = \sigma^2\left(\frac{4-\pi}{2}\right) \tag{2.13}$$

---

[1] $\bar{r}$ is not used here since this representation is used for the arithmetic sample average and not ensemble average and in addition, is confusing in complicated expressions.

2.2.3.2 Median signal strength.

The median of the envelope, r_{med}, which represents the envelope value at which 50% of the distribution lie below and 50% lie above this value is found from

$$\int_0^{r_{med}} p(r)\,dr = 0.5 \tag{2.14}$$

$$r_{med} = \sigma\sqrt{2\ \ln 2}$$

Hence the median of the envelope is $0.94 r_{mean}$ i.e. expressed in dB terms the median is 0.54dB below the mean value of the envelope.

2.2.3.3 Mean signal strength in dB units.

Commercial signal strength measuring receivers usually have a logarithmic IF(Intermediate Frequency) detector whose output voltage is linearly proportional to the input power expressed in dB units. In this situation the envelope, expressed in dB units, can be written as

$$r_{dB}(t) = 20 \log r(t) = a\ \ln r^2(t) \tag{2.15}$$

where

$$a = 10/\ln 10 = 4.34$$

Again the mean of the dB-expressed envelope values i.e. $< r_{dB} >$ is given by

$$< r_{dB} > = \int_0^{\infty} r_{dB}\, p(r_{dB})\, dr_{dB} \tag{2.16}$$

However $< r_{dB} >$ can be expressed in linear envelope terms with the appropriate conservation of probability space (i.e. $p(r)dr = p(r_{dB})dr_{dB}$), hence

$$< r_{dB} > = \int_0^\infty a \ln r^2 p(r)\, dr \tag{2.17}$$

$$= a\{ \ln(2\sigma^2) - C\} \tag{2.18}$$

where C = Euler's constant = 0.5772.

$$< r_{dB} > = 10 \log(2\sigma^2) - 2.51 \tag{2.19}$$

Hence the average of the dB expressed envelope values is 2.51dB below the mean envelope power ($2\sigma^2$).

The standard deviation of the dB expressed envelope values, $\sigma_r(dB)$, can be determined in the manner of equation (2.13). This form of derivation is shown in appendix C. Another derivation of $\sigma_r(dB)$ can be determined by considering the autocorrelation, $\xi(\tau)$, of the dB expressed envelope values i.e.

$$\xi(\tau) = < r_{dB}(t).r_{dB}(t+\tau) > \tag{2.20}$$

The autocovariance of a random variable is related to the autocorrelation, $\xi(\tau)$, and mean, m, of the random variable by[8]

$$\psi(\tau) = \xi(\tau) - < m >^2 \tag{2.21}$$

The autocorrelation of the dB expressed envelope values has been found[9] such that

$$\xi(\tau) = a^2 \sum_{n=1}^{\infty} \frac{|\rho|^{2n}}{n^2} + a^2(\ln(2\sigma^2) - C)^2 \tag{2.22}$$

Now the second term in $\xi(\tau)$ is simply $< r_{dB} >^2$ (see equation (2.18)) i.e. m^2, hence the autocovariance is simply

$$\psi(\tau) = a^2 \sum_{n=1}^{\infty} \frac{|\rho|^{2n}}{n^2} \tag{2.23}$$

The variance of the dB expressed envelope values, $\sigma_r^2(dB)$, is given by $\psi(\tau)$ at $\tau = 0$ i.e.

$$\sigma_r^2(dB) = \psi(0) = a^2 \sum_{n=1}^{\infty} \frac{1}{n^2} \tag{2.24}$$

since $|\rho| = |\rho(\tau)| = |\rho(0)| = 1$. The summation term can be further simplified[10]

$$\sum_{n=1}^{\infty} \frac{1}{n^2} = \frac{\pi^2}{6} \tag{2.25}$$

hence

$$\sigma_r^2(dB) = \frac{a^2\pi^2}{6} \tag{2.26}$$

$$\sigma_r(dB) = \frac{a\pi}{\sqrt{6}} = 5.57dB \tag{2.27}$$

Regardless of whether the envelope values are expressed in linear or dB terms the median occurs at the same point in the distribution. In other words for a given set of envelope values the number of values that lie above and below the median is the same for both cases. The dB median value is then simply the linear median value expressed in dB terms, i.e.

$$r_{med}(dB) = 20 \log r_{med} = 10 \log(2\sigma^2) - 1.59 \text{ dB} \tag{2.28}$$

Hence the median of the dB expressed envelope values is 1.59dB below the mean envelope power (i.e. $E\{r^2\}$).

2.2.4 The Received Signal Phase.

The received signal phase $\phi(t)$ is given in terms of the quadrature components by

$$\phi(t) = \tan^{-1}\left\{ \frac{Q(t)}{I(t)} \right\} \tag{2.29}$$

If viewed in the complex plane, where I(t) and Q(t) are the real and imaginary parts respectively, the point $z(t)(z(t) = I(t) + jQ(t))$, moves in a random manner. The PDF of the received phase is rectangularly distributed[2] between 0 and 2π such that

$$p(\phi) = \frac{1}{2\pi} \qquad 0 \le \phi < 2\pi \tag{2.30}$$

The mean phase value, $< \phi >$, is given by

$$< \phi > = \int_0^{2\pi} \phi \, p(\phi) \, d\phi = \pi \tag{2.31}$$

The mean square value of the phase is therefore

$$< \phi^2 > = \int_0^{2\pi} \phi^2 p(\phi) \, d\phi = \frac{4\pi^2}{3} \tag{2.32}$$

hence the variance of the phase, σ_ϕ^2 is given by

$$\sigma_\phi^2 = < \phi^2 > - < \phi >^2 = \frac{\pi^2}{3} \tag{2.33}$$

---

[2] The term rectangularly distributed is also referred to as uniformly distributed.

Figure 2.5 shows the random motion of the phase and the absolute signal strength of the received signal envelope corresponding to the phase shown. The in-phase and quadrature signals, used to determine the signal envelope and phase, shown in Figure 2.5 were obtained using the dual branch vector demodulator receiver (see Chapter 4). The motion of the vector can be related in phase from one position to another. If we consider a vector having an envelope and phase of r_1 and ϕ_1, and at another point r_2 and ϕ_2 then there exists a four-fold joint PDF, between the envelopes and phases, given by[1]

$$p(r_1, r_2, \phi_1, \phi_2) = \frac{r_1 r_2}{(2\pi\mu)^2(1-\lambda^2)} \times \exp\left\{ -\frac{r_1^2 + r_2^2 - 2r_1 r_2 \lambda \cos(\phi_2 - \phi_1 - \theta)}{2\mu(1-\lambda^2)} \right\} \tag{2.34}$$

$$\text{where} \qquad \tan\theta = \frac{\mu_2}{\mu_1}, \qquad \lambda^2 = \frac{\mu_1^2 + \mu_2^2}{\mu^2}$$

$$\begin{aligned} \mu &= <(r_1 \cos\phi_1)^2> \\ \mu_1 &= <(r_1 \cos\phi_1)(r_2 \cos\phi_2)> \\ \mu_2 &= <(r_1 \cos\phi_1)(r_2 \sin\phi_2)> \end{aligned} \tag{2.35}$$

now r_1 and r_2 are such that $0 \le r_1, r_2, < \infty$, therefore the joint PDF between ϕ_1 and ϕ_2 can be found from[1,4]

$$p(\phi_1, \phi_2) = \int_0^\infty \int_0^\infty p(r_1, r_2, \phi_1, \phi_2)\, dr_1\, dr_2 \qquad 0 \le \phi_1, \phi_2 < 2\pi \tag{2.36}$$

$$p(\phi_1, \phi_2) = \frac{1-\zeta^2}{4\pi^2} \times \frac{\sqrt{1-\zeta^2\cos^2(\phi_1-\phi_2)} + \zeta\cos(\phi_1-\phi_2)\cos^{-1}[-\zeta\cos(\phi_1-\phi_2)]}{(1-\zeta^2\cos^2(\phi_1-\phi_2))^{3/2}} \tag{2.37}$$

where $\zeta = \zeta(\tau) = a(\tau)/a(0)$, is the normalised autocorrelation function (see section on spectra for $a(\tau)$). If we now consider the phase difference between the phase at two separated points in space (i.e. $\Delta\phi = \phi_2 - \phi_1$) then the PDF for $\Delta\phi$ is given by

$$p(\Delta\phi) = \frac{1-\zeta^2}{4\pi^2} \times \frac{\sqrt{1-\zeta^2\cos^2(\Delta\phi)} + \zeta\cos(\Delta\phi)[\pi - \cos^{-1}(\zeta\cos(\Delta\phi))]}{(1-\zeta^2\cos^2(\Delta\phi))^{3/2}} (2\pi - |\Delta\phi|) \tag{2.38}$$

which reduces to the simpler model[5] when $p(\varepsilon = 0) = 1$, i.e. $\zeta(\tau)$ is the normalised autocovariance function given by $J_0(\beta V\tau)$ ($\beta = 2\pi/\lambda$, J_0 is the zero-order Bessel function of the first kind).

The PDF of the phase difference is shown in Figure 2.6 for various separation distances (l/λ) between two points, using the autocorrelation function of the Clarke two dimensional model. Naturally, the smallest separations are associated with the highest probability and a π phase change occurs at separations of $\lambda/2$. When the two points are separated by a distance of 0.38λ they are uncorrelated and hence the joint PDF becomes that of two uniform distributions i.e. $p(\phi_1, \phi_2) = p(\phi_1).p(\phi_2) = 1/4\pi^2$.

The statistics associated with the phase gradient, $\dot{\phi}$, are considered separately in the section titled 'Random FM'.

2.3 SECOND ORDER STATISTICS.

In this section we consider the higher order statistics associated with the envelope i.e. those which are dependent upon time. Since the distribution of the multipath waves in elevation has little effect on these statistics[4] the simpler two dimensional model[5] will be considered here. The Level Crossing Rate (LCR) and Average Fade Duration (AFD) are important statistical parameters which must be considered when digital transmission systems are employed. The AFD is particularly important when choosing transmission bit rates, word lengths and coding schemes in relation to vehicle speed and carrier frequency.

2.3.1 The Level Crossing Rate (LCR).

As a vehicle proceeds along a route the fading rate and hence the rate of change of the envelope varies with vehicle speed. This can be quantitatively expressed in terms of the LCR, N_R, defined as the rate a particular signal level R, is crossed in either a positive or negative sense (but not both). The LCR is shown schematically in Figure 2.7 for a threshold level of -10dB. The LCR is given by the number of times that a particular threshold level is crossed in a one second period. This is expressed by[1]

$$N_R = \int_0^\infty \dot{r}\, p(r, \dot{r})\, d\dot{r} \tag{2.39}$$

where $p(r, \dot{r})$ is the joint PDF of r and $\dot{r}$, which is given by

$$p(r, \dot{r}) = \int_{-\infty}^{\infty} \int_0^{2\pi} p(r, \dot{r}, \phi, \dot{\phi})\, d\phi\, d\dot{\phi} \tag{2.40}$$

now $p(r, \dot{r}, \phi, \dot{\phi})$ is given by[1] as

$$p(r, \dot{r}, \phi, \dot{\phi}) = \frac{r^2}{4\pi^2 b_0 b_2} \exp\left\{ -\frac{1}{2}\left(\frac{r^2}{b_0} + \frac{\dot{r}^2}{b_2} + \frac{R^2\dot{\phi}^2}{b_2} \right) \right\} \tag{2.41}$$

where b_0 and b_2 are the spectral moments given by [1,8]

$$\begin{aligned} b_0 &= < I^2(t) > = < Q^2(t) > = \sigma^2 \\ b_2 &= < (\dot{I}(t))^2 > = < (\dot{Q}(t))^2 > = \frac{\sigma^2 \omega_D^2}{2} \end{aligned} \tag{2.42}$$

$$p(r, \dot{r}) = \frac{r}{\sigma^2} \exp\left\{ -\frac{r^2}{2\sigma^2} \right\} \cdot \frac{1}{\sigma\omega_D\sqrt{\pi}} \exp\left\{ -\frac{\dot{r}^2}{\sigma^2\omega_D^2} \right\} \tag{2.43}$$

$$= p(r) \cdot p(\dot{r}) \tag{2.44}$$

where $p(r, \dot{r}) = p(r).p(\dot{r})$ because r and $\dot{r}$ are independent and uncorrelated. Then N_R is simply

$$N_R = \sqrt{\pi} f_D \frac{R}{\sigma} e^{-R^2/2\sigma^2} \tag{2.45}$$

2.3.2 The Average Fade Duration (AFD).

The AFD is the average duration of a fade below a particular threshold level and is shown schematically in Figure 2.7 for a -10dB threshold. For a particular threshold level, the AFD is given by the total amount of time that the envelope is below that level, divided by the number of times that the envelope faded below that level. Mathematically the AFD is given by[1]

$$\tau_R = \frac{P(R)}{N_R} \tag{2.46}$$

$$\tau_R = \frac{\sigma(e^{R^2/2\sigma^2} - 1)}{\sqrt{\pi} f_D R} \tag{2.47}$$

Figure 2.8 shows N_R and τ_R for a Rayleigh distributed envelope using normalised axes. The normalised LCR and AFD are given by N_R/f_D and $\tau_R f_D$ respectively. Notice that the maximum LCR occurs at -3dB and that N_R and τ_R are linearly dependent upon the normalised signal strength, expressed in dBs, for signal levels less than -10dB.

2.4 THE RECEIVED SIGNAL SPECTRA.

Having dealt with the statistical properties of the envelope we can now turn to a consideration of the received signal spectra. In this section we shall be concerned with two particular spectra associated with the received signal;

(i) The RF input spectrum.
(ii) The spectrum of the envelope.

The spectrum of the differential phase, random FM, will be discussed separately in a later section. The results will be considered for both the three[4] and two[5] dimensional models.

2.4.1 The RF Input (Doppler) Spectrum.

The RF input spectrum, sometimes called the Doppler spectrum, shows how the transmitted carrier frequency is displaced as a result of the vehicle travelling through the scattered field. The shape of the spectrum can be evaluated from a knowledge of the quadrature autocorrelation function, $a(\tau)$[4] which is given by

$$a(\tau) = E\{\cos \omega_n \tau\} \tag{2.48}$$

Now $a(\tau)$ is affected by the PDF of the arrival angles in azimuth, $p(\alpha)$ and elevation $p(\varepsilon)$. A reasonable assumption for $p(\alpha)$ is that it is rectangularly distributed between 0 and 2π. The PDF in the vertical plane, $p(\varepsilon)$, is more difficult to specify. Aulin[4] does not give any general expression although $p(\varepsilon)$ must be known in order to evaluate $a(\tau)$. In the two-dimensional model[5] the autocorrelation function is given by[3]

$$a_0(\tau) = E\{\beta V \tau \cos(\gamma - \alpha)\} = J_0(\beta V \tau) \tag{2.49}$$

The RF input spectrum $S_{RF}(f)$ is simply the Fourier Transform of $a(\tau)$

$$S_{RF}(f) = F\{a(\tau)\} \tag{2.50}$$

where $F\{.\}$ is the Fourier Transform given by

$$F\{a(\tau)\} = \int_{-\infty}^{\infty} a(\tau) e^{-j\omega\tau} d\tau \tag{2.51}$$

Equation (2.50) can be integrated numerically to give the RF input spectrum. A closed form solution, for the two dimensional model, can be obtained by considering the angular contribution of multipath waves received by a vertical monopole antenna[1,11]

---

[3] a_0 is used to represent the two dimensional model autocorrelation function compared with that for the three dimensional model $a(\tau)$.

$$S_{RF}(f) = \frac{\sigma^2}{\omega_D} \frac{3}{\sqrt{\left[1 - \left(\frac{f - f_c}{f_D}\right)^2\right]}} \tag{2.52}$$

The factor of 3 arises from the directivity of a vertical whip antenna (G = 1.5) and the fact that $p(\alpha)$ is an even function[1]. This spectrum together with its autocorrelation (i.e. $a_0(\tau) = J_0(\beta V \tau)$) function is shown in Figure 2.9 where the spectrum is centred on the carrier frequency and the frequency deviation is normalised by the maximum Doppler frequency f_D . This spectrum is 'U' shaped with frequency cutoffs occurring at $\pm f_D$. The observed power spectral density at low frequencies is greater than that predicted by equation (2.52). Aulin[4] therefore, considered $p(\varepsilon)$ in an attempt to predict higher values for this region of the spectrum. No experimental studies have been published which give values for $p(\varepsilon)$. In this work the results will be discussed only qualitatively in terms of $p(\varepsilon)$.

2.4.2 The Spectrum of the Received Envelope.

Earlier we saw that the received signal, when viewed by a quadrature detector receiver, could be represented as a vector moving around the complex plane in a random manner. The magnitude of the vector, i.e. the envelope, clearly has a time varying nature, which is described as fast fading, and conforms to a Rayleigh distribution.[4] The fading spectrum of the envelope can be found from the envelope autocorrelation function. The envelope autocorrelation function, for a Rayleigh fading signal, is given by[1,4]

$$E\{r(t).r(t+\tau)\} = \frac{\pi}{2}\sigma^2 F\left(-\frac{1}{2}, -\frac{1}{2}; 1; \left(\frac{a(\tau)}{a(0)}\right)^2\right) \tag{2.53}$$

---

[4] For this part of the discussion we assume that there is no local mean variation and that there does not exist a dominant specular component.

where F(.) is the hypergeometric function. The Fourier Transform of the above cannot be carried out exactly. The hypergeometric function can, however, be expanded in polynomial form, and approximated by neglecting terms beyond the second degree[7]. In this case the envelope spectrum is given by[1] as

$$S_{env}(f) \simeq \frac{\sigma^2}{8\pi f_D} \mathrm{K}\left[\sqrt{\left(1-\left(\frac{f}{2f_D}\right)^2\right)}\right] \tag{2.54}$$

where K[.] is the complete elliptic integral of the first kind. In this case the frequency cutoff occurs at $2f_D$. Figure 2.10 shows the spectrum of the envelope, given by equation (2.54), with the abscissa normalised by the maximum Doppler frequency together with the envelope autocorrelation function ($a_0^2(\tau) = J_0^2(\beta V \tau)$). The spectrum of the envelope can be determined numerically by noting that

$$S_{env}(f) = F\{ < r(t).r(t+\tau) > \} = F\{a^2(\tau)\} \tag{2.55}$$

In the case of the two dimensional propagation model[5] this is given by

$$S_{env}(f) \simeq F\{J_0^2(\beta V \tau)\} \tag{2.56}$$

Again Aulin[4] considered propagation of multipath waves, out of the horizontal plane, to explain the differences between observed spectra and that derived for the simpler two-dimensional model[5]. The differences most notably occur in the lower frequency region of the spectrum and at the cutoff frequency ($2f_D$). The modified spectra, like the Doppler spectrum, depends upon the expression assumed for the PDF, $p(\varepsilon)$.

In both spectra mentioned so far it was assumed that the PDF of the azimuthal angle of arrival, of the multipath waves, was rectangularly distributed between 0 and 2π. Although this assumption might be reasonable for most cases, situations can arise when it is no longer true. Naturally both forms of spectra, the Doppler and envelope, might be altered if such a situation occurred. The problem then arises of distinguishing between the effects $p(\alpha)$ and $p(\varepsilon)$ on the spectra. The uncertainty involved in distinguishing between the effects of

$p(\alpha)$ and $p(\varepsilon)$ could be resolved by means of a sectored antenna arrangement in both azimuth and elevation.

2.5 RANDOM FM.

If we represent the received signal, $s(t)$, as

$$\begin{aligned} s(t) &= Re\{z(t)e^{-j\omega_c t}\} \\ &= r(t)\cos(\omega_c t) \end{aligned} \tag{2.57}$$

where $z(t)$ is a complex Gaussian process, then the received vector moves in a random manner in the complex plane. This motion introduces a differential phase, $\dot{\phi}$, which appears to the receiver as noise i.e.

$$\dot{\phi} = -Im\left\{ \frac{z(t)\dot{z}(t)^*}{|z(t)|^2} \right\} = \frac{d}{dt}\left\{ \tan^{-1}\left(\frac{Q(t)}{I(t)} \right) \right\} \tag{2.58}$$

which will be superimposed on any desired modulation[9]. This random FM noise can best be described in terms of its PDF and power spectrum.

2.5.1 The PDF and CDF of the Random FM.

The motion of the received vector gives rise to a phase that changes with time. This differential phase manifests itself as noise to the detector of an FM receiver and other receivers that use phase-sensitive demodulators. This noise is often referred to as random FM. The PDF of the random FM, $p(\dot{\phi})$, is obtained by appropriate integration of the joint PDF of the envelope and phase and their differential counterparts. This can be achieved by rearranging the integration of the four-fold joint PDF, $p(r, \dot{r}, \phi, \dot{\phi})$, and leads to

$$p(\dot{\phi}) = \int_0^{2\pi}\int_{-\infty}^{\infty}\int_0^{\infty} p(r, \dot{r}, \phi, \dot{\phi})\, dr\, d\dot{r}\, d\phi \tag{2.59}$$

$$p(\dot{\phi}) = \frac{1}{\omega_D}\sqrt{\frac{1}{2}}\left(1+\frac{2}{\omega_D^2}\dot{\phi}^2\right)^{-3/2} \tag{2.60}$$

The CDF of $\dot{\phi}$ is given by

$$P(\dot{\phi}) = \int_{-\infty}^{\dot{\phi}} p(\dot{\phi})\, d\dot{\phi} \tag{2.61}$$

$$P(\dot{\phi}) = \frac{1}{2}\left[1+\sqrt{2}\,\frac{\dot{\phi}}{\omega_D}\left(1+\frac{2\dot{\phi}^2}{\omega_D^2}\right)^{-1/2}\right] \tag{2.62}$$

Figure 2.11 shows the PDF and CDF of $\dot{\phi}$. Although the differential phase is concentrated at small deviations, there is an appreciable probability of large phase excursions occurring. To see how the phase changes with fade depth we need to consider the conditional PDF $p(\dot{\phi}\,|\,R)$[7]

$$p(\dot{\phi}\,|\,R) = \frac{p(\dot{\phi},R)}{p(R)} = \frac{R}{\sigma\omega_D\sqrt{\pi}}\exp\left\{-\frac{R^2\dot{\phi}^2}{\omega_D^2\sigma^2}\right\} \tag{2.63}$$

The conditional PDF has a Gaussian shape with zero mean. Figure 2.12 shows the conditional PDF for various dB-expressed envelope values. Notice that the probability of large phase excursions occurring increases with the fade depth.

2.5.2 The Random FM Spectrum.

The random FM spectrum can be found from the Fourier Transform of the autocorrelation of $\dot{\phi}$(*i.e.* $<\dot{\phi}(t).\dot{\phi}(t+\tau)>$). The autocorrelation of $\dot{\phi}$ is given by[1,4,12][5]

$$<\dot{\phi}(t).\dot{\phi}(t+\tau)> = \frac{1}{2}\left[\left(\frac{\dot{a}(\tau)}{a(\tau)}\right)^2 - \frac{\ddot{a}(\tau)}{a(\tau)}\right]\ln\left[1-\left(\frac{a(\tau)}{a(0)}\right)^2\right] \tag{2.64}$$

---

[5] The derivative here is with respect to τ

for the two dimensional model[5]

$$< \dot{\phi}(t).\dot{\phi}(t+\tau) > = \frac{\omega_D^2}{2J_0^2(u)} \left[\frac{J_0(u)J_1(u)}{u} - J_0^2(u) - J_1^2(u) \right] \times \ln[1 - J_0^2(u)] \qquad (2.65)$$

$$\text{where u } = \omega_D \tau$$

The random FM spectrum is then given by the Fourier Transform of the autocorrelation function

$$S_{FM}(f) = F\{ < \dot{\phi}(t).\dot{\phi}(t+\tau) > \} \qquad (2.66)$$

Figure 2.13 shows the one-sided power spectrum of the random FM. This was derived directly by Fourier transforming the autocorrelation of the random FM. This spectrum is largely confined to $2f_D$[12], from where the spectrum falls off as $1/f$. Hence, the principal random FM noise is concentrated in the audio band. The asymptotic spectrum beyond $2f_D$ is given by[12]

$$S_{FM}(f) \simeq \frac{\omega_D^2}{4f} \qquad (2.67)$$

2.6 RICIAN FADING.

The discussion so far has been centred around how the various spectra might change with respect to the type of model considered. In small cells another situation might easily arise, namely where the fading contains a dominant specular component. In this situation the statistics are known to differ[7] from those discussed so far. In such a case we might expect less predominance of deep fades and for the specular component to become a dominant feature of the spectra[1,4,7]. Some of the statistics associated with this so called Rician fading will be presented here for completeness.

The joint PDF of envelope and phase, $p(r, \phi)$, with a dominant envelope component d i.e. Rician fading is given by[4][6]

$$p(r, \phi)_{Ric} = \frac{r}{2\pi\sigma^2} \exp\left\{ -\frac{d^2 + r^2 - 2rd\cos(\eta)}{2\sigma^2} \right\} \tag{2.68}$$

$$\text{where } \eta = \phi - \omega_0 t - \theta_0$$

Integrating the joint PDF with respect to ϕ, gives the PDF of r as

$$p(r)_{Ric} = \frac{r}{\sigma^2} \exp\left\{ -\frac{r^2 + d^2}{2\sigma^2} \right\} I_0\left(\frac{rd}{\sigma^2} \right) \tag{2.69}$$

where I_0 is the modified Bessel function of the first kind and zero order. Integrating the joint PDF with respect to r gives the PDF of the phase

$$\begin{aligned} p(\phi)_{Ric} = & \sqrt{\frac{d}{2\pi\sigma^2}} \cos(\eta) \exp\left\{ -\frac{d}{2\sigma^2} \sin^2(\eta) \right\} \\ & \operatorname{erf}\left(-\sqrt{\frac{d}{\sigma^2}} \cos(\eta) \right) + \frac{1}{2\pi} \exp\left\{ -\frac{d}{2\sigma^2} \right\} \end{aligned} \tag{2.70}$$

Appendix D shows how the PDF for dB-expressed envelope values can be derived. Figures 2.14 and 2.15 respectively show the PDF and CDF (with Rayleigh axes)[7] for a Rician distribution, expressed in dB terms, for various values of normalised dominant component d/σ. Notice that when there is no dominant component (i.e. $d/\sigma = 0$) the PDF and CDF become Rayleigh distributed. As the dominant component increases the likelihood of deep fades diminishes and the PDF becomes Gaussian in form.

---

[6] The subscript '0' here refers to the specific parameter associated with the specular component.

[7] By Rayleigh axes we mean that the ordinate is scaled such that a Rayleigh distribution appears as a straight line.

2.7 CONCLUSION.

The basic statistics associated with the complex fast fading signal of a narrowband mobile radio channel have been presented for the case of both two and three dimensional multipath models. Although the three dimensional model is probably a better representation of propagation in urban areas, using small cells, the problem of specifying the PDF of the vertical spatial angle ε remains unresolved. Both models make a reasonable assumption that the PDF of the arrival angles in azimuth is rectangularly distributed. However, in both models the correlational properties (e.g. spectra) are affected if this assumption is not valid. In the following chapter the two dimensional model is assumed. The three dimensional model will be referred to in the Results Chapter.

To overcome the problems associated with fading, various diversity techniques may be employed. The following chapter discusses several methods of diversity together with strategies for combining decorrelated signals from a number of antennas. Quantitative expressions, along the lines of this chapter, are presented assuming Rayleigh fading conditions.

2.8 REFERENCES.

[1] Jakes, W.C.(Ed), "Microwave Mobile Communications", John Wiley and Sons, New York, 1974.

[2] Schwartz, M., Bennett, W.R. and Stein, S., "Communications Systems and Techniques", McGraw-Hill, New York, 1966.

[3] Lee, W.C.Y., "Mobile Communications Engineering", McGraw-Hill, New York, 1982.

[4] Aulin, T. "A Modified Model for the Fading Signal at a Mobile Radio Channel", IEEE Trans. on Veh. Technol., Vol. VT-28, No.3, pp.182-203, 1979.

[5] Clarke, R.H., "A Statistical Theory of Mobile Radio Reception", Bell Sys. Tech. J., Vol.47, pp.957-1000, 1968.

[6] Stremler, F.G., "Introduction to Communication Systems", Addison-Wesley, Reading Massachusetts, 1982 (2nd edn.).

[7] Rice, S.O., "Mathematical Analysis of Random Noise", Bell Sys. Tech. J., Vol.23, pp.292-332, 1944.
---,"Statistical Properties of a Sine Wave Plus Noise", Bell Sys. Tech. J., Vol.27, pp.109-157, 1948.

[8] Papoulis, A., "Probability Random Variables and Stochastic Processes", McGraw-Hill, 11th print, 1981.

[9] Davis, B.R. and Bognor, R.E., "Propagation at 500MHz for Mobile Radio", IEE Proc. Vol.132, Pt-F, No.5, pp.307-320, 1985.

[10] Dwight, H.B., "Tables of Integrals and other Mathematical Data", MacMillan, New York, 1961.

[11] Gans, M.J., "A Power Spectral Theory of Propagation in the Mobile Radio Environment", IEEE Trans. on Veh. Technol., Vol.23, No.1, pp.27-38, 1972.

[12] Davis, B.R., "FM Noise with Fading Channels and Diversity", IEEE Trans. on Commun. Technol., Vol.COM-19, No.6, pp.1189-1200, 1971.
---,"Random FM in Mobile Radio With Diversity", IEEE Trans. on Commun. Technol., Vol.COM-19, No.6, pp.1259-1267, 1971.

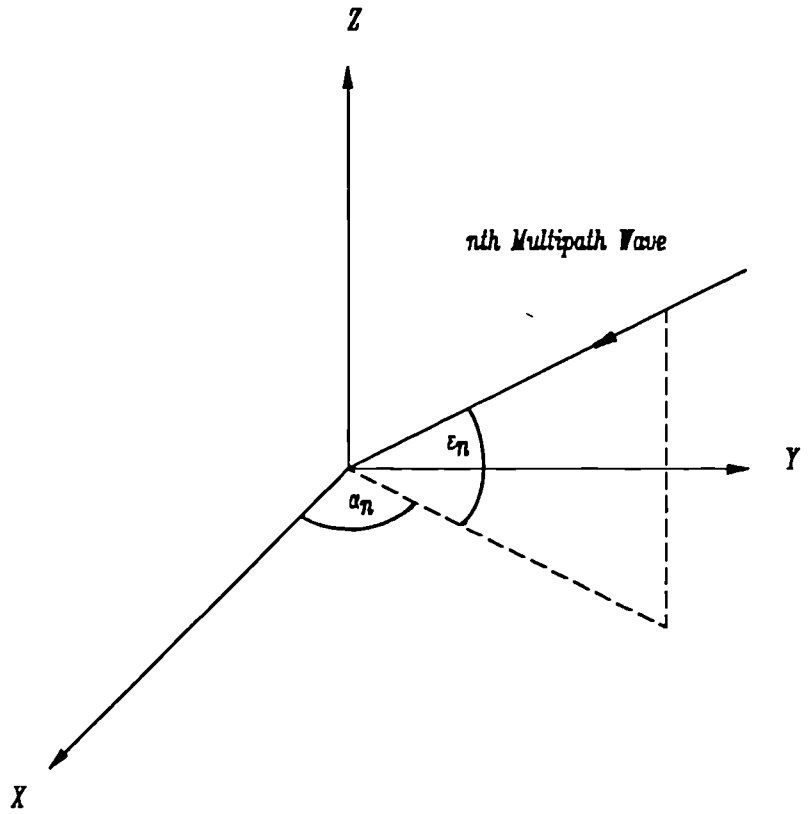

Figure 2.1 The three dimensional propagation model (after Aulin[4]) for a single multipath wave in terms of azimuth, α_n, and elevation, ε_n.

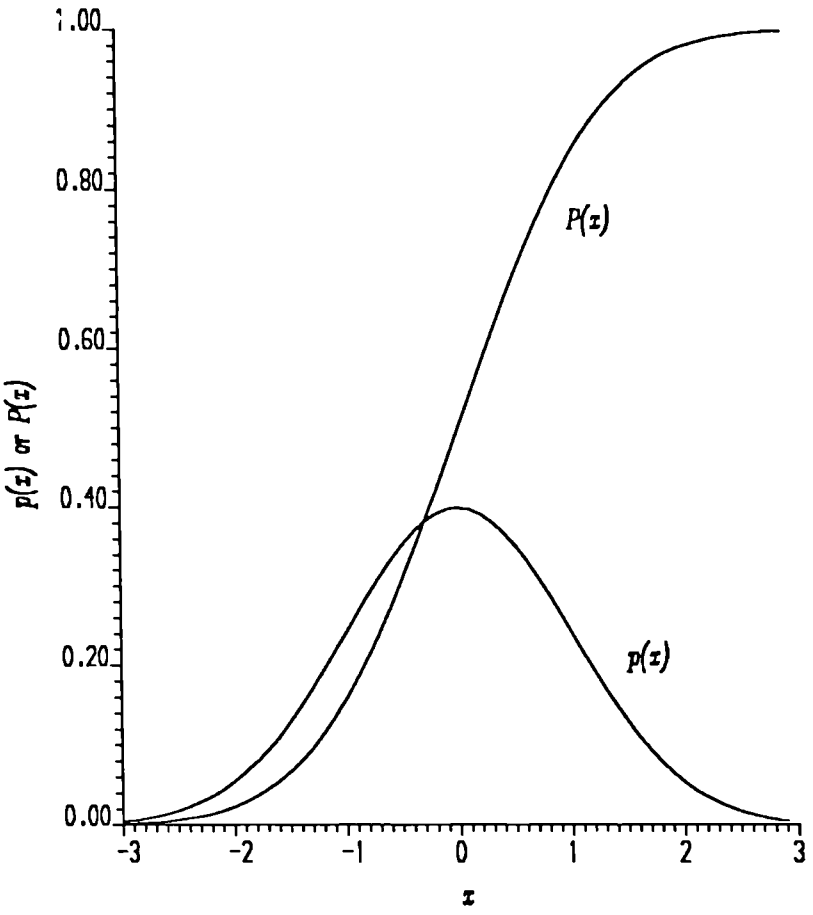

Figure 2.2 Gaussian PDF, $p(x)$, and CDF, $P(x)$, for normally distributed in-phase, I, and quadrature, Q, components.

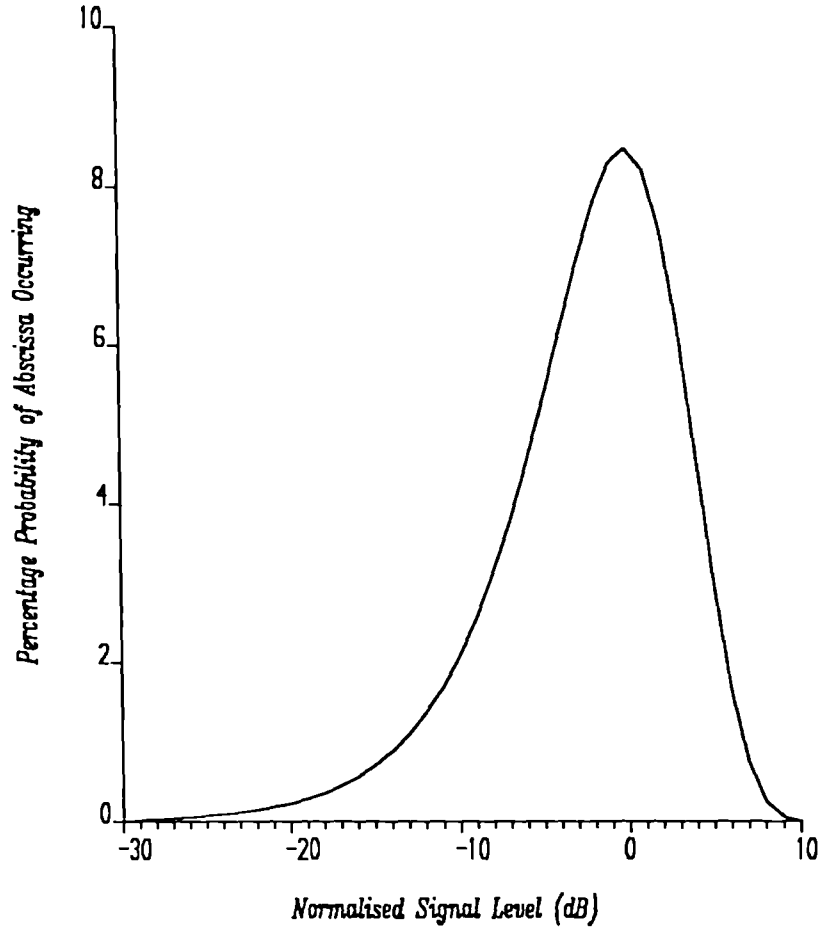

Figure 2.3 PDF of a Rayleigh fading envelope normalised by the average signal power (σ^2) i.e. $p(r/\sqrt{2}\,\sigma)$.

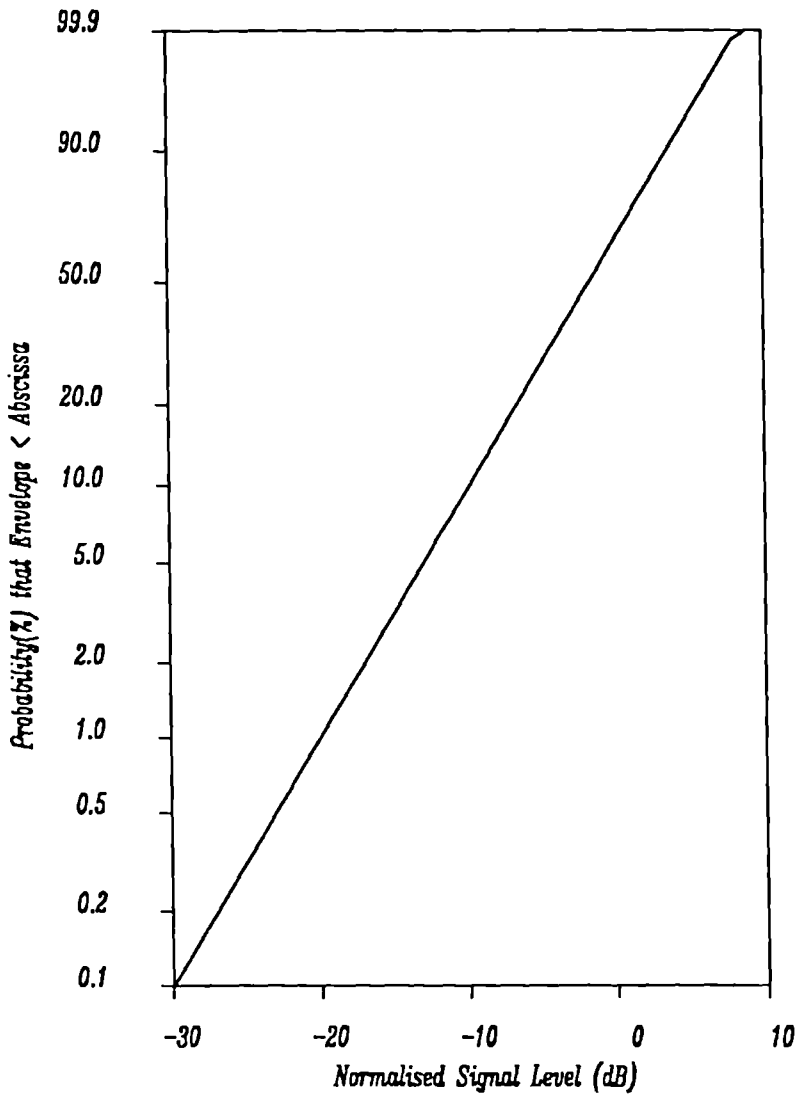

Figure 2.4 CDF of a Rayleigh fading envelope normalised by the average signal power (σ^2) i.e. $p(r/\sqrt{2}\,\sigma)$.

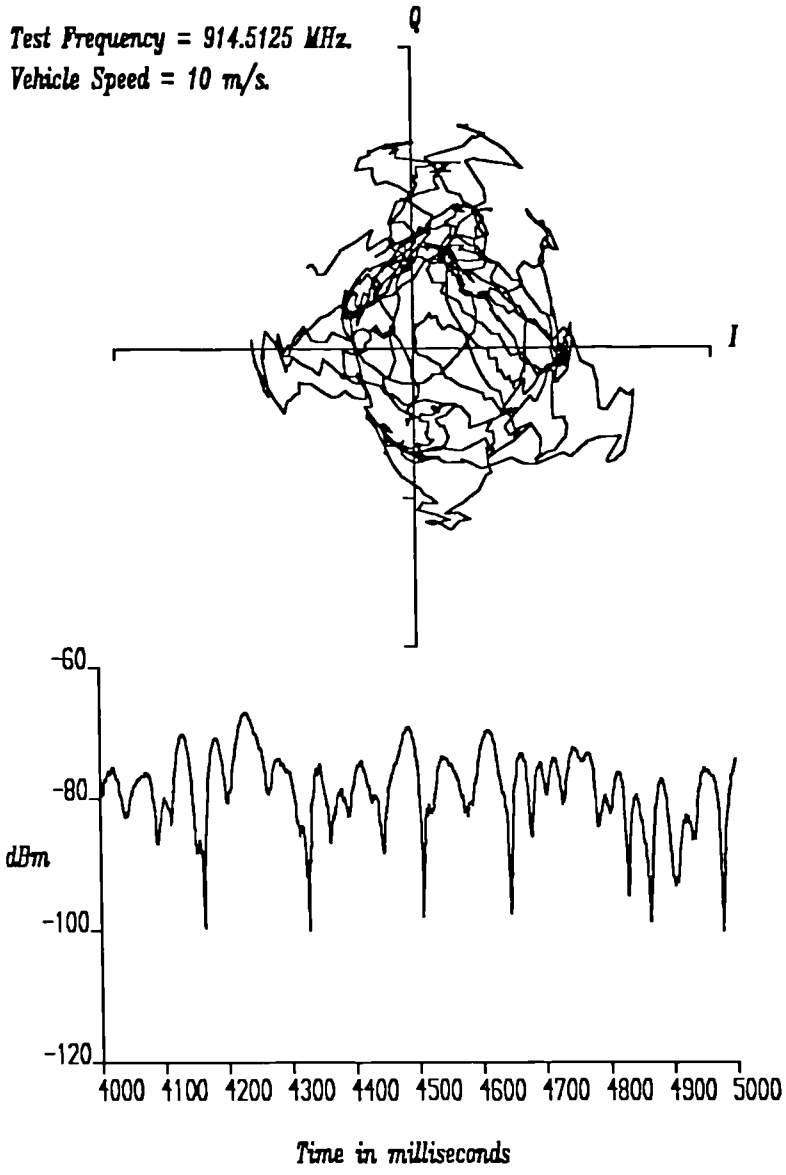

Figure 2.5 Example of quadrature signal and envelope varying with time. The upper plot shows the variation of the quadrature components (I and Q) over a one second period. The lower plot shows the time varying envelope ($\sqrt{I^2 + Q^2}$), for the same period of time as that as the upper diagram.

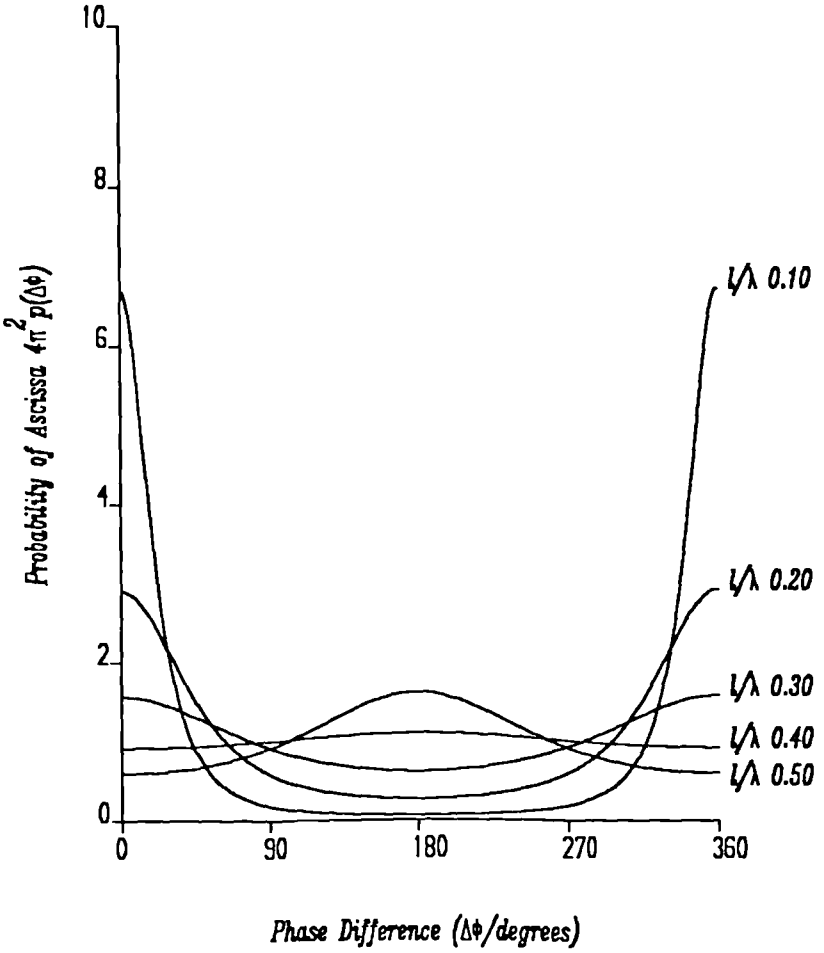

Figure 2.6 The PDF of the phase gradient, $p(\Delta\phi)$, between points separated by l/λ. Note that when $l/\lambda \rightarrow 0.38$ then $p(\Delta\phi)$ becomes that of two independent phases i.e. $p(\Delta\phi) \rightarrow p(\phi_1) \bullet p(\phi_2) = 1/4\pi^2$.

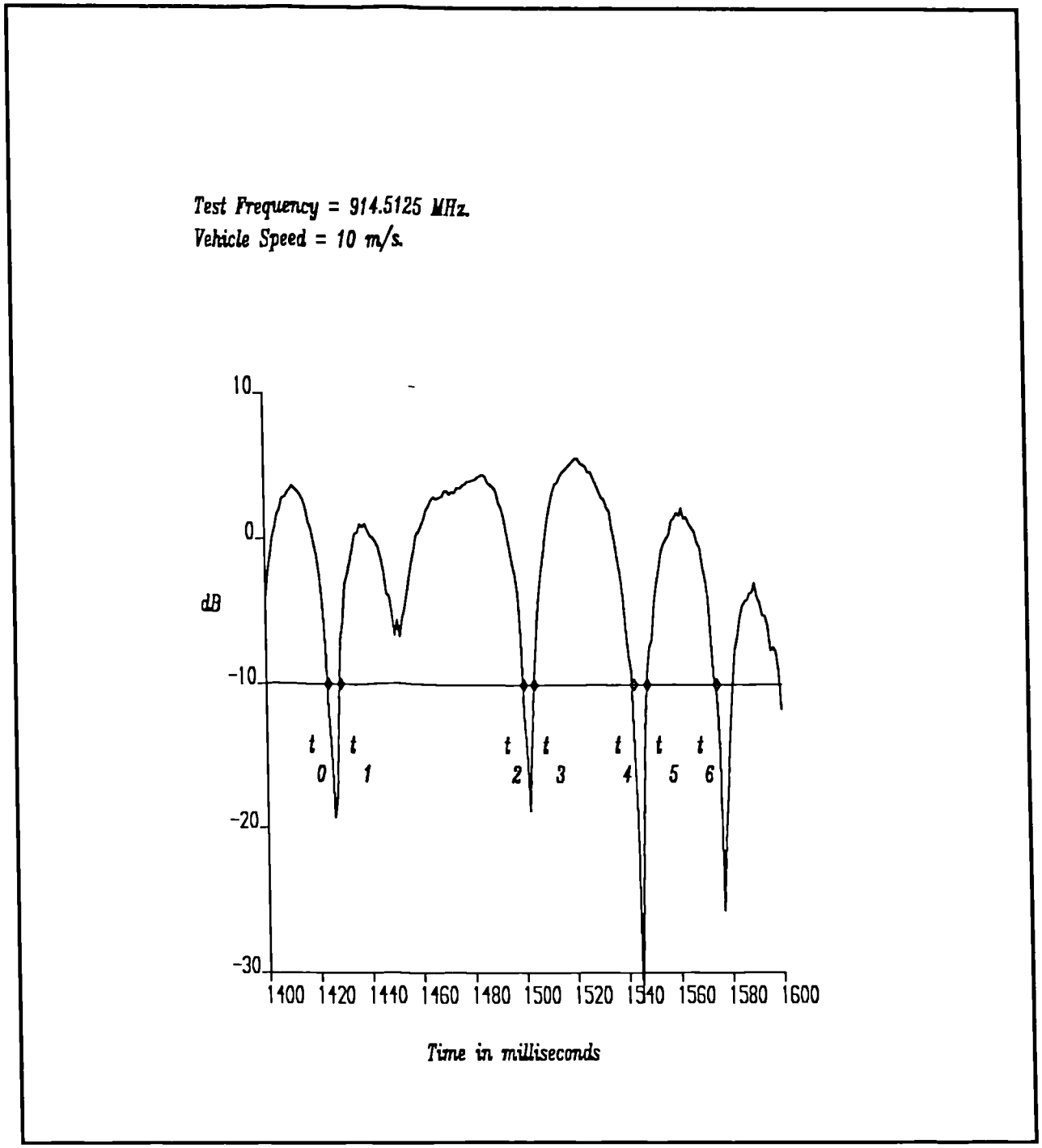

Figure 2.7 Illustrating the definition of LCR and AFD for a normalised Rayleigh fading envelope. The LCR is the average number of crossings per second of a particular threshold. In this example the -10dB threshold is crossed approximately 25 times per second. The AFD here is approximately 8 milliseconds.

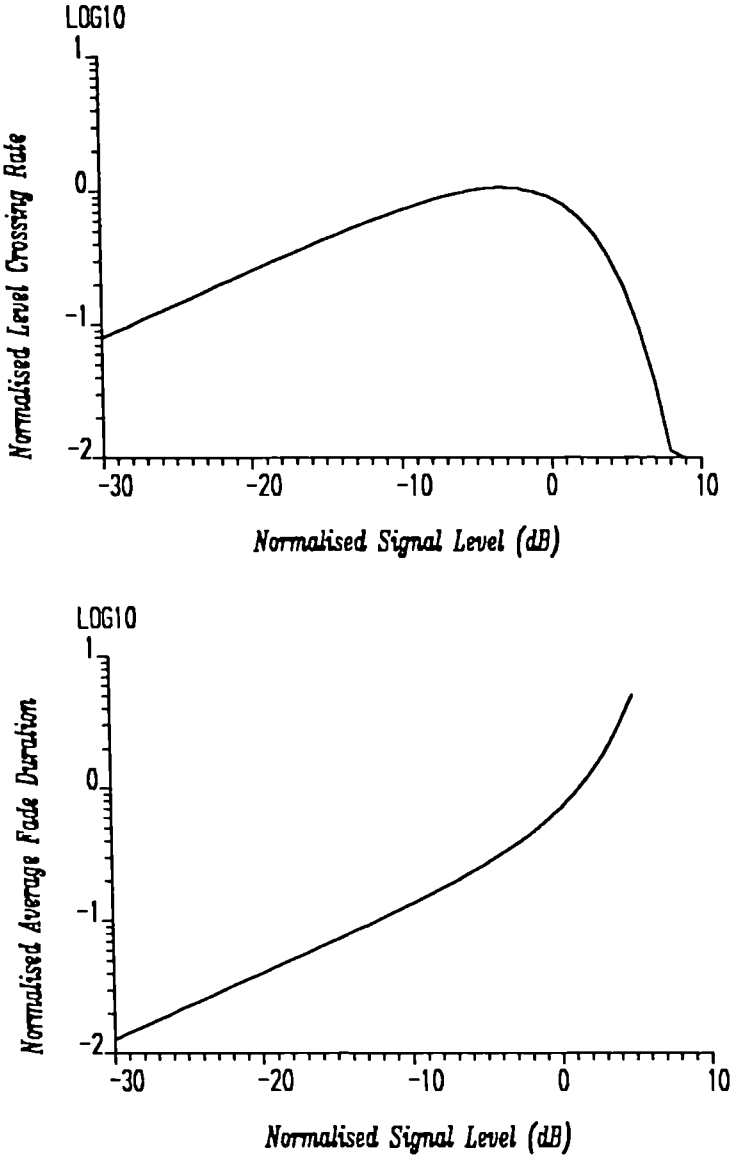

Figure 2.8 Normalised LCR (N_R/f_D) and $AFD(\tau_R f_D)$ for a Rayleigh fading envelope with respect to the average signal power (σ^2).

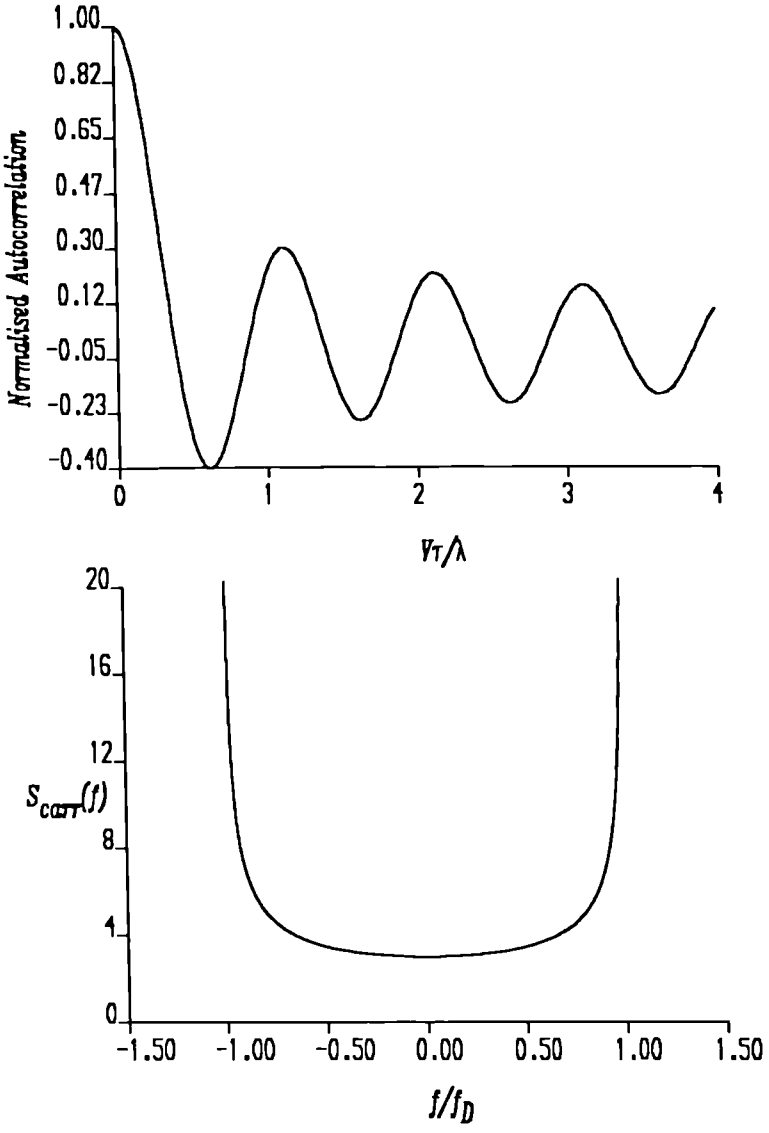

Figure 2.9 Autocorrelation function ($J_0(\beta V\tau)$) of the in-phase or quadrature component and RF input spectrum (Doppler) for a Rayleigh fading signal. Note the small amplitude of the low frequency components and the strict bandlimiting to $\pm f_D$.

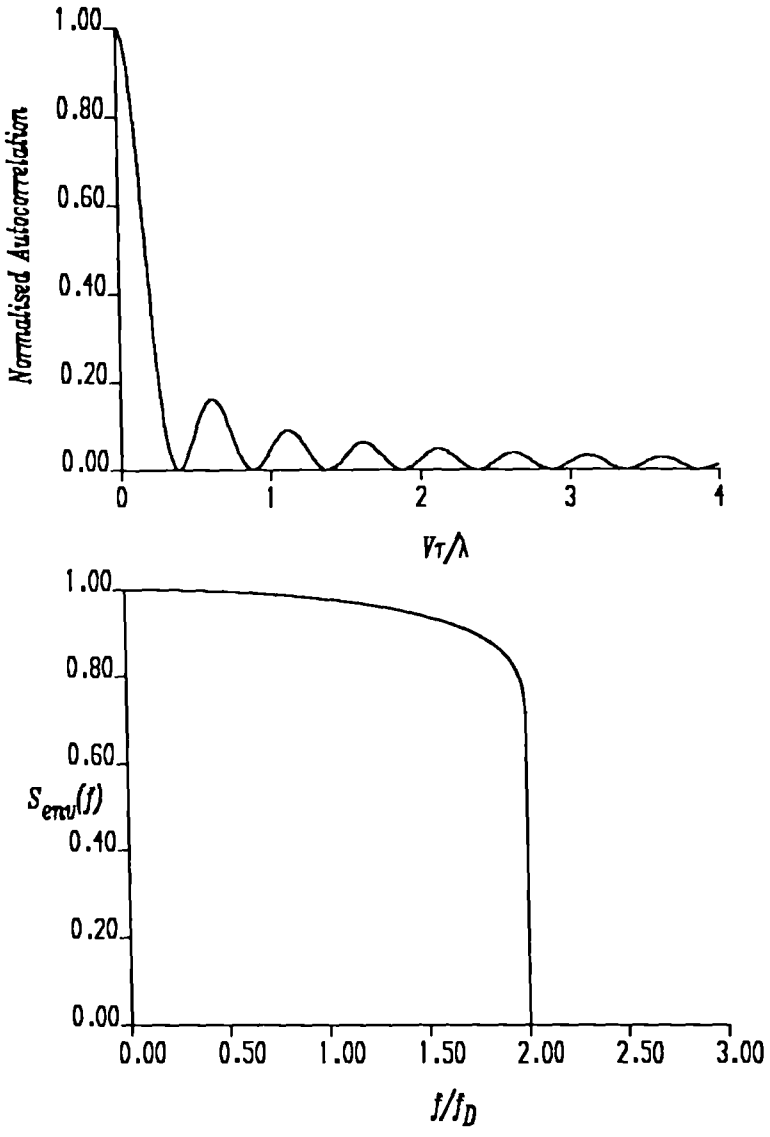

Figure 2.10 Envelope autocorrelation function ($J_0^2(\beta V\tau)$) and spectrum for a Rayleigh fading envelope. Note the flat response up to the sharp frequency cut-off at $2f_D$.

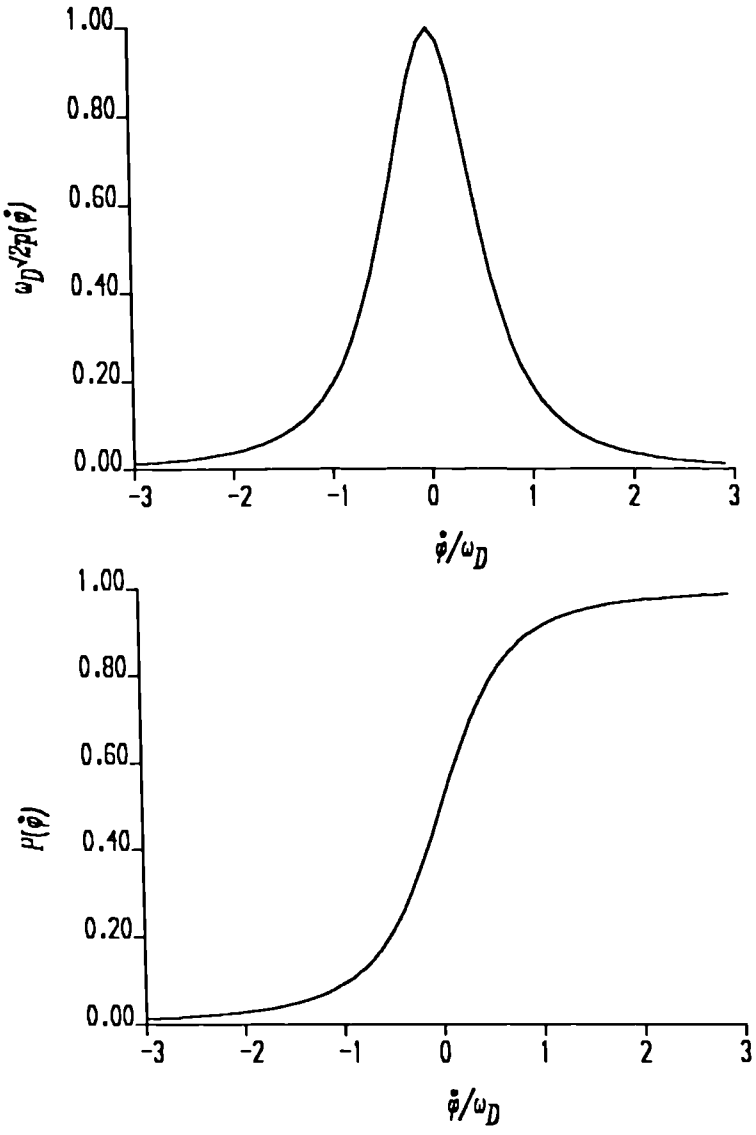

Figure 2.11 PDF and CDF of the instantaneous frequency (i.e. random FM) normalised by the maximum angular Doppler frequency.

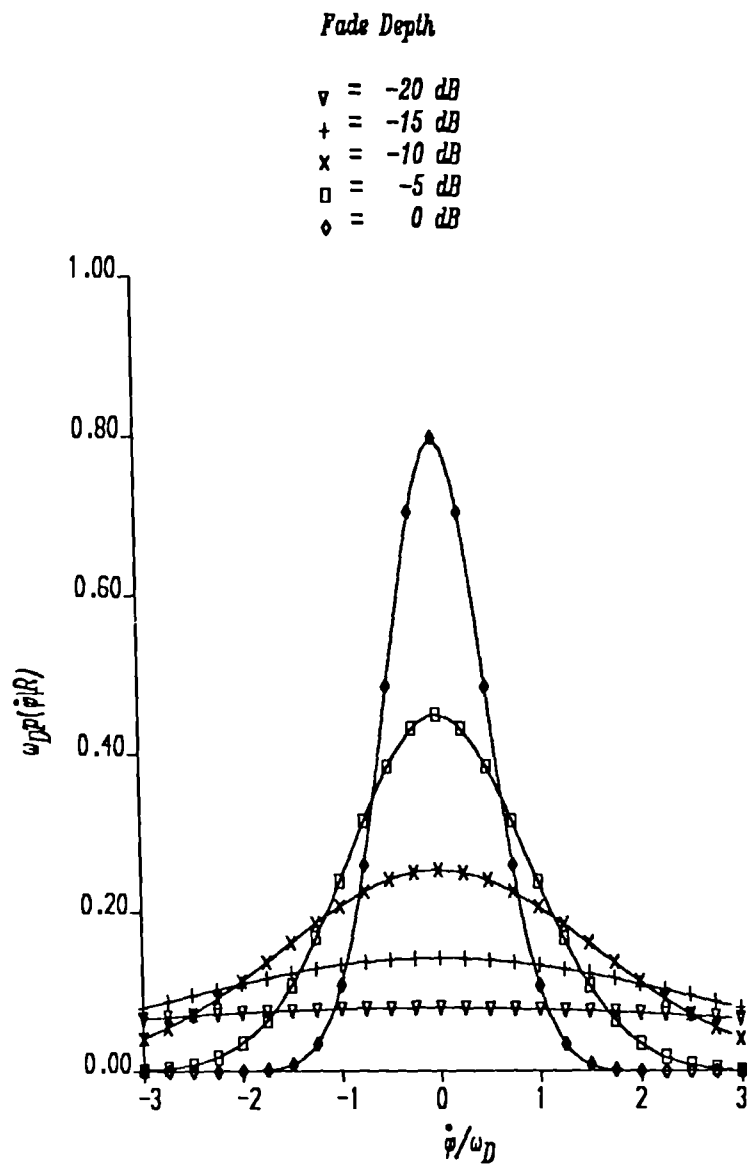

Figure 2.12 Conditional PDF of random FM as a function of fade depth, $p(\dot{\phi}\,|\,R)$ normalised by the maximum angular Doppler frequency.

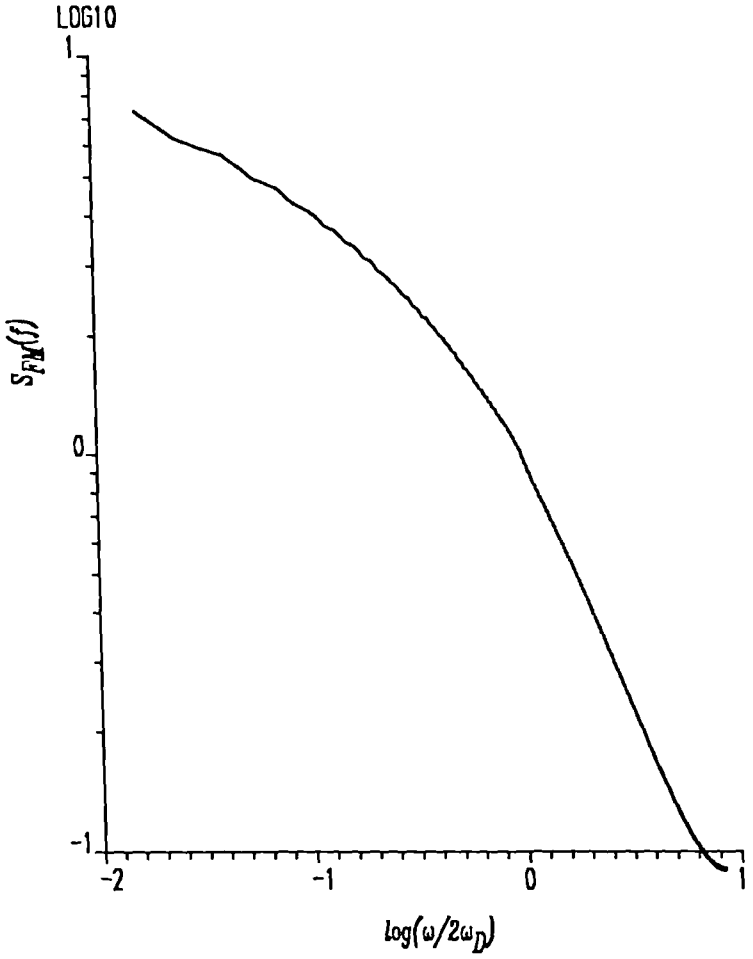

Figure 2.13 One sided spectrum of the instantaneous frequency (random FM).

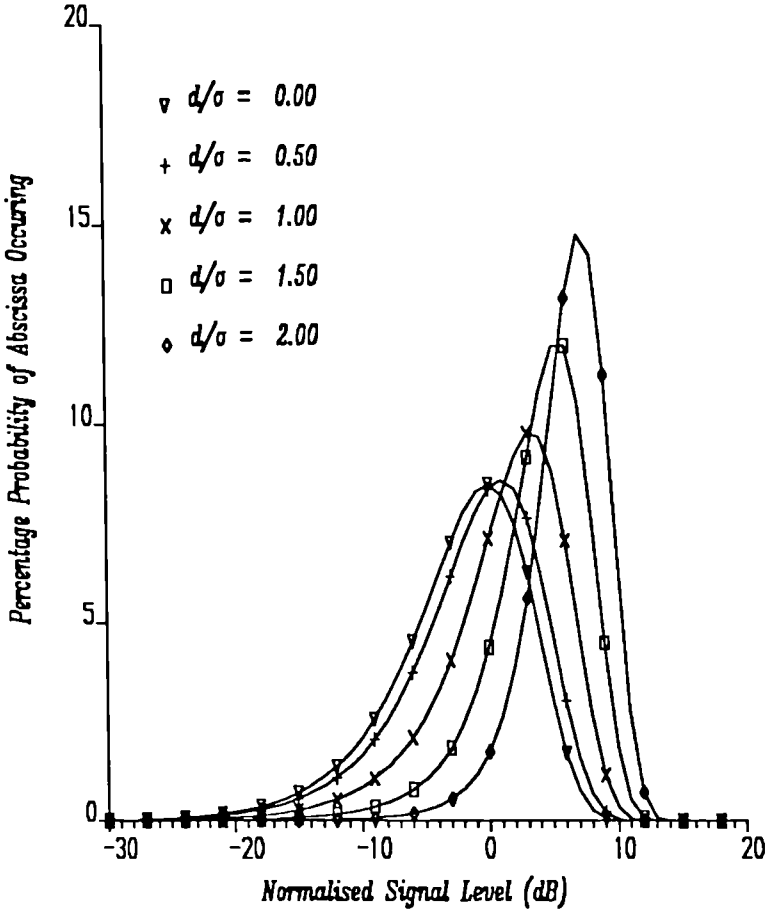

Figure 2.14 PDF of a normalised Rician distributed envelope for various values of dominant component d. The term 'normalised signal level' means that the resultant envelope (i.e. instantaneous plus dominant component) has been normalised by the average signal power (σ^2). The dominant component d has also been normalised by the average signal (σ^2) power (see Appendix D).

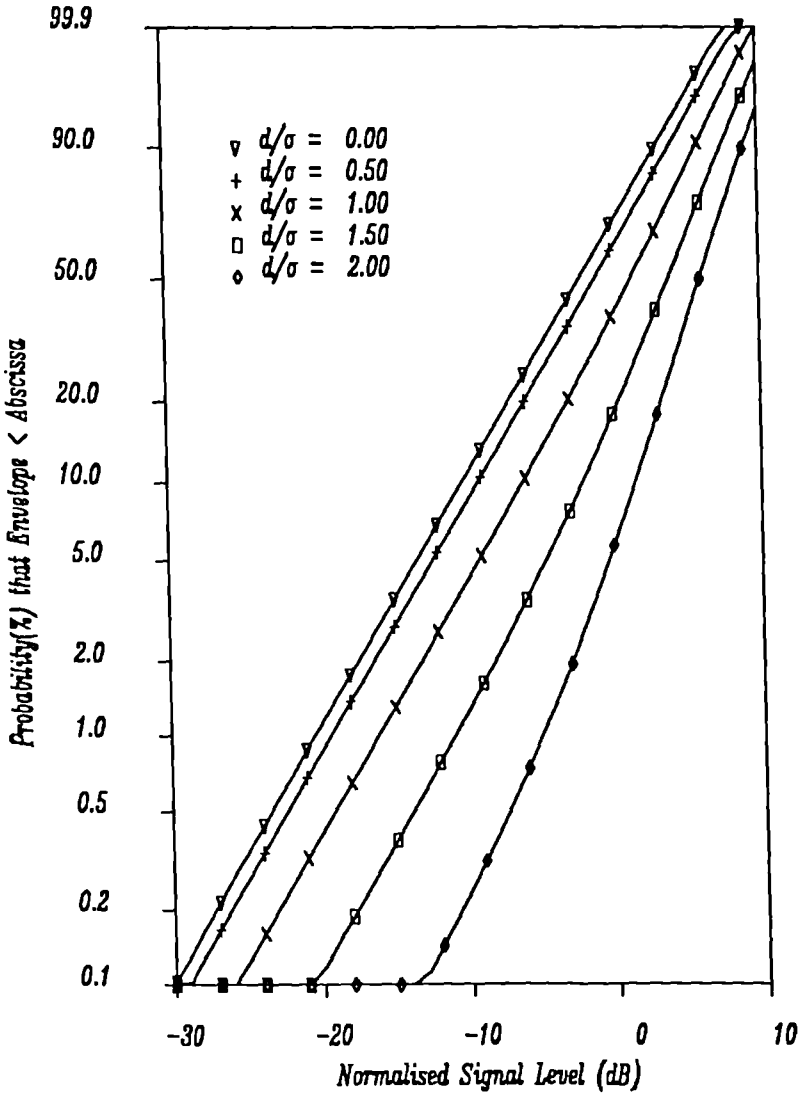

Figure 2.15 CDF of a normalised Rician distributed envelope for various values of dominant component d. The term 'normalised signal level' means that the resultant envelope (i.e. instantaneous plus dominant component) has been normalised by the average signal power (σ^2). The dominant component d has also been normalised by the average signal power (σ^2).

CHAPTER 3. THE NARROWBAND MOBILE RADIO CHANNEL WITH DIVERSITY.

3.1 INTRODUCTION.

In the previous chapter we discussed the statistics associated with the signal received in a mobile radio environment. The deep and rapid fading envelope, caused by relative motion of the transmitter/receiver can be a serious impairment to the system performance, especially when digital transmissions systems are used. During a deep fade, bit errors occur due to the signal falling below the detector threshold, the level becoming indistinguishable from the noise, or, as in the case of phase modulation schemes, undergoing an unexpected phase transition which results from a deep fade. An examination of the Cumulative Distribution Function (CDF) of the fading envelope reveals that the deep fades occur frequently, especially when the scattered field is seriously perturbed e.g. by a high vehicle speed. It is highly desirable therefore, to find some method whereby the occurrence and depth of these fades can be sufficiently reduced to permit an acceptable level of performance.

3.2 DIVERSITY.

Diversity is one means by which the degree of fading can be reduced such that an acceptable level of performance can be achieved. Diversity relies on the combination of two or more signals, containing the same information, which are, to some extent, decorrelated. If two signals are uncorrelated then the probability that both experience the same depth of fade at the same time is the square of the probability that one of them experiences that depth of fade. Various techniques exist[1] which can be used to obtain signals with a sufficient degree of decorrelation. They can be summarised as follows;

1) Polarisation.
2) Frequency.
3) Time.
4) Spaced Antenna.

The first three of these methods will be discussed briefly, followed by a detailed investigation of the fourth, which is used in this work.

3.2.1 Polarisation Diversity.

This scheme utilises the fact that the resultant field, after scattering, is sufficiently depolarised for two orthogonal antennas to be used to receive decorrelated signals. The methods of combining the signals are the same as those to be discussed later. Results from computer simulation[2] and experimental results[3] from field trials, have been obtained for hand-held portable telephones which utilise polarisation diversity. The results show that the use of polarisation diversity is particularly well suited to hand-held phones, which are held in a variety of orientations.

Although not quite the same as polarisation diversity, field component diversity has many similarities. This method uses the magnetic and electric field components of the signal to provide uncorrelated signals for combining. In this situation the signals from co-located antennas are always completely decorrelated. The use of two magnetic loops (orthogonal to each other) in conjunction with a co-located electric whip antenna, ensures that, regardless of the horizontal orientation, there always exists a magnetic component to be combined with the ever present electric component (the whip antenna has omnidirectional coverage in azimuth).

3.2.2 Frequency Diversity.

For frequency diversity the information is transmitted on two or more sufficiently separated carrier frequencies. The amount of frequency separation required, depends upon the time-dispersive nature of the channel. This form of diversity scheme has the disadvantage that different transmitters are required for each frequency and the use of different carrier frequencies, for the same information, entails an inefficient use of the radio spectrum.

3.2.3 Time Diversity.

This is the oldest form of diversity whereby the message is repeated several times to ensure error free interpretation. The time varying nature of the received envelope can be used to advantage in a time diversity scheme which utilises digital transmission techniques. Use is made of the decorrelation between envelope samples as a function of time separation. It has been found[4] that sufficient decorrelation can be achieved for a repetition rate in the order of $0.2f_D$. Indeed, time diversity is employed in the FOrward Control Channel (FOCC) of the UK TACS cellular radio system. This provides a particularly robust protection against bit errors by retransmitting words five times every 10ms. The receiver, which has stored the repeated words, carries out a simple majority vote decision on a bit-by-bit basis. Although this scheme has an inefficient throughput rate, especially when no errors occur, it is simple, easy to implement and does not require sophisticated antenna systems nor does it make additional demands on the RF spectrum.

3.2.4 Spaced Antenna Diversity.

This diversity scheme is possibly the most commonly used in radio communications. Two or more antennas are physically separated in

space to provide decorrelated signals. Naturally, the amount of separation changes the degree of decorrelation, and is different at the mobile than at the base station case. This is due to the angle subtended by the scatterers relative to the mobile antennas being larger than that experienced by the base station antennas (see Results Chapter for further discussion). The amount of separation required for horizontally spaced antennas at the mobile is determined from the autocorrelation function of the envelope. As shown by equation (2.56) this is given by $J_0^2(\beta l)$ (where $\beta = 2\pi/\lambda$ and l is the separation between the antennas). Uncorrelated samples occur for $J_0^2(\beta l) = 0$ i.e. $l = 0.38\lambda$, which at 900MHz is physically small ($\simeq 13cm$). The amount of separation required at both the mobile and base station antennas, for vertically separated antennas, is discussed in the Results Chapter.

The antenna separation discussed above only provides an improvement in the statistics of the fast fading component of the signal. To eliminate the slow fading component would require antenna separations of considerably greater dimensions than those discussed above. The remainder of this work is only applicable to the fast fading component.

Once the decorrelated signals have been obtained they then require combining, in some manner, to provide an improved resultant signal. The combining can be performed prior to or after detection (pre or post detection). In what follows we consider various predetection combining schemes for which we assume the mean noise power to be the same in all branches. Feedforward and feedback combining schemes[5] are not considered here.

3.3 PREDETECTION COMBINING SCHEMES.

There are various methods of combining the signals from the different diversity branches. We shall consider four types in detail and refer to a fifth which is considered elsewhere[6]. The five types are

1) Maximal Ratio.
2) Equal Gain.
3) Selection.
4) Switch and Stay.
5) Switch and Examine.

In the following sections no attempt is made to derive, from first principles, the first and second order envelope statistics for each of the above methods. Instead, the relevant results are quoted from source in order that all pertinent statistical equations are, for the first time, collated in one piece of work.

3.3.1 The Maximal Ratio Combiner.

The predetection Maximal Ratio Combiner (MRC) co-phases the signals from the different branches and sums them together, each branch being weighted in proportion to its own signal voltage to noise power ratio[7]. Provided that the noise in each branch is uncorrelated then the output carrier to noise ratio (CNR) is given by

$$\gamma_{mrc} = \sum_{i=1}^{M} \gamma_i \tag{3.1}$$

where M = No. of branches.
If we consider that the short-term signal power on the i^{th} branch (i.e. the power averaged over one RF cycle) is $R_i^2/2$ (R_i is the envelope received on the i^{th} branch) in the presence of Gaussian noise, of mean power N, then the 'instantaneous' CNR, γ_i, is given by

$$\gamma_i = \frac{R_i^2}{2N} \tag{3.2}$$

thus

$$\gamma_{mrc} = \sum_{i=1}^{M} \gamma_i = \frac{1}{2N} \sum_{i=1}^{M} R_i^2 \tag{3.3}$$

If we now consider the output CNR, γ_{mrc}, to have an associated equivalent envelope R_{mrc} then

$$\gamma_{mrc} = \frac{R_{mrc}^2}{2N} = \sum_{i=1}^{M} \gamma_i = \frac{1}{2N} \sum_{i=1}^{M} R_i^2 \tag{3.4}$$

This gives a resultant envelope $R_{mrc}(t)$

$$R_{mrc}(t) = \sqrt{\sum_{i=1}^{M} R_i^2(t)} \tag{3.5}$$

3.3.2 The Equal Gain Combiner.

The Equal Gain Combiner (EGC) is a simplified version of the MRC in which the weighting factors are all set to unity. The output CNR is then given by

$$\gamma_{egc} = \frac{1}{M} \left(\sum_{i=1}^{M} \sqrt{\gamma_i} \right)^2 \tag{3.6}$$

Again if we consider the instantaneous CNR on each branch is given by (3.2) then the output CNR for an EGC, γ_{egc}, is given by

$$\gamma_{egc} = \frac{1}{M} \left(\sum_{i=1}^{M} \sqrt{\frac{R_i^2}{2N}} \right)^2 = \frac{1}{2MN} \left(\sum_{i=1}^{M} R_i \right)^2 \tag{3.7}$$

Thus the equivalent output envelope of an EGC is such that

$$\gamma_{egc} = \frac{R_{egc}^2}{2N} = \frac{1}{2MN}\left(\sum_{i=1}^{M} R_i\right)^2 \tag{3.8}$$

which gives a resultant envelope $R_{egc}(t)$

$$R_{egc}(t) = \frac{1}{\sqrt{M}}\left(\sum_{i=1}^{M} R_i(t)\right) \tag{3.9}$$

3.3.3 Selection Diversity.

In the SELection (SEL) diversity combiner the branch selected is that with the largest instantaneous CNR i.e.

$$\gamma_{sel} = \max\{\gamma_1, \gamma_2, \ldots \gamma_M\} \tag{3.10}$$

which gives a resultant envelope $R_{sel}(t)$

$$R_{sel}(t) = \max\{R_1, R_2, \ldots R_M\} \tag{3.11}$$

The predetection SEL combiner requires that all the branches are simultaneously monitored, all of the time, in order that the decision to switch to the branch with the highest CNR can be made. Naturally, such an arrangement is impractical for mobile radio use on account of the expense of continually monitoring all of the branches.

3.3.4 Scanning Diversity.

It is sometimes useful to employ a derivative system known as scanning diversity in which there is no attempt to find the best input, just one which is acceptable. In principle, the inputs on the various branches are scanned until an acceptable one i.e. an input above a predetermined threshold, is found. This input is then used until it falls below the

threshold, at which time the scanning process continues until another acceptable input is found. In its simplest form, only two branches are used and a changeover from one to the other occurs whenever the signal on the branch in use falls below the threshold. In this form it is known as switched diversity.

There are two switching strategies that can be used and these cause different behaviour when the signals on both branches fade simultaneously. Firstly there is the Switch And Stay (SAS) strategy in which the receiver is switched to the alternative branch as soon as the input on the branch in use falls below the threshold. The receiver then stays on the new branch irrespective of whether, at that time, the new input is acceptable or not. Secondly there is the Switch And Examine (SAE) strategy in which, if both inputs are unacceptable, the system switches rapidly between the two branches until the signal on one of them rises above the threshold. It is worth mentioning that the occurrence of simultaneous deep fades is a rare event and that in the vast majority of cases a switch to the other branch will result in an acceptable input.

In both the SAS and SAE cases considered above a fixed threshold level was assumed. In practice the threshold could be set to vary according to the average Signal to Noise Ratio (SNR). In this manner both strategies could be set to operate optimally. Although the SAE strategy allows for a marginally quicker return to an acceptable input, when the signals on both branches fade simultaneously, the rapid switching that occurs can cause a noise burst. In most cases the SAS strategy is therefore preferred. In the remainder of this work we shall consider all the above strategies, except SAE.

3.4 EQUIVALENT ENVELOPE AND PHASE FOR TWO BRANCH DIVERSITY.

As the number of diversity branches increases, the additional improvement afforded by each of the diversity schemes becomes less[5] and the receiver structure becomes more complex. Two branch diversity (M = 2), which is probably the most practical, is therefore considered here.

To compare the various diversity combiners we shall consider the concept of an equivalent envelope $R(t)$, mentioned earlier, together with an equivalent phase $\phi(t)$, determined from the output CNR. Using the equivalent envelope formula given earlier the envelopes, for the various diversity strategies are given by

$$\begin{aligned} R_{mrc} &= \sqrt{R_1^2 + R_2^2} \\ R_{egc} &= \frac{R_1 + R_2}{\sqrt{2}} \\ R_{sel} &= \begin{cases} R_1 & R_1 \geq R_2 \\ R_2 & R_1 < R_2 \end{cases} \end{aligned} \tag{3.12}$$

The equivalent phase for the MRC and EGC cases depends upon whether; one branch is co-phased to the other, both branches are co-phased relative to a reference or both branches are co-phased relative to some other function of ϕ_1 and ϕ_2. In the first case the phase statistics are identical with that of a single branch. In the second and third cases the phase perturbations can sometimes be completely removed. In the scanning strategies the phase of the output is simply that of the branch selected. In summary therefore

$$\begin{aligned} \phi_{mrc} &= \phi_1, \phi_2, 0 \text{ or some function of } \phi_2 \text{ and } \phi_2 \\ \phi_{egc} &= \phi_1, \phi_2, 0 \text{ or some function of } \phi_2 \text{ and } \phi_2 \\ \phi_{sel} &= \begin{cases} \phi_1 & R_1 \geq R_2 \\ \phi_2 & R_1 < R_2 \end{cases} \end{aligned} \tag{3.13}$$

we have assumed perfect co-phasing for the MRC and EGC cases and $R = R(t), R_1 = R_1(t), \phi = \phi(t), \phi_1 = \phi_1(t)$ etc.. The derivative of the envelope and phase, which are used to determine the second order statistics and the random FM, are given by

$$\dot{R}_{mrc} = \frac{R_1\dot{R}_1 + R_2\dot{R}_2}{\sqrt{R_1^2 + R_2^2}}$$

$$\dot{R}_{egc} = \frac{\dot{R}_1 + \dot{R}_2}{\sqrt{2}} \qquad (3.14)$$

$$\dot{R}_{sel} = \begin{matrix} \dot{R}_1 & R_1 \geq R_2 \\ \dot{R}_2 & R_1 < R_2 \end{matrix}$$

$\dot{\phi}_{mrc} = \dot{\phi}_1, \dot{\phi}_2, 0$ or some derivative of ϕ_1 and ϕ_2

$\dot{\phi}_{egc} = \dot{\phi}_1, \dot{\phi}_2, 0$ or some derivative of ϕ_1 and ϕ_2

$$\dot{\phi}_{sel} = \begin{matrix} \dot{\phi}_1 & R_1 \geq R_2 \\ \dot{\phi}_2 & R_1 < R_2 \end{matrix}$$

The equivalent envelope, for the various diversity strategies, is shown in Figure 3.1 using data gathered using the two branch amplitude and phase measuring receiver that will be described in Chapter 4. Notice that the MRC strategy is more resilient to the deep fades than EGC, and that the MRC envelope is always greater than, or at least equal to, the higher of the branch envelopes. In contrast, the EGC envelope can sometimes fall below the higher branch envelope value, particularly when the other branch is in a deep fade (see 1580ms). Selection diversity always follows the higher of the two branch envelopes. In the case of SEL the resultant envelope is noticeably more variable than those of the MRC and EGC strategies. The SAS strategy can be seen in the lower diagram. Notice that a switch between branches occurs (e.g. 1480 and 1570ms) when one of the branches falls below the threshold (-10dB). However, when both branches are below the threshold a disadvantageous switch occurs (see 1545ms).

In the following section some theoretical results for the various diversity schemes, in correlated fading, will be presented along the lines used in Chapter 2. The degree of correlation between the two branches will be given by the complex correlation ρ_{12}.[8]

---

[8] The complex correlation ρ_{12}, between the two branches, will be discussed in detail in the Results Chapter.

3.5 THE CDF OF THE EQUIVALENT ENVELOPE.

A measure of the improvement afforded by diversity is provided by the envelope statistics, in particular the PDF, and hence CDF, of the equivalent envelope. Earlier, the equivalent envelope was discussed in terms of the output CNR. If we return to this notation for a moment then the PDF for a Rayleigh distributed signal is given by

$$p(\gamma) = \frac{1}{\gamma_0} e^{-\gamma/\gamma_0} \tag{3.15}$$

γ is the 'instantaneous' CNR (i.e. $r^2/2\sigma_n^2$), σ_n^2 is the noise power, and γ_0 is the average CNR. The CDF is therefore given by

$$P(\gamma) = 1 - e^{-\gamma/\gamma_0} \tag{3.16}$$

The relationship between the average CNR and envelope is given by

$$\gamma_0 = <\gamma> = \frac{<r^2>}{2\sigma_n^2} = \frac{\sigma^2}{\sigma_n^2} \tag{3.17}$$

The relationship between $p(r)$ and $p(\gamma)$ can readily be seen if it is remembered that $p(\gamma)d\gamma = p(r)dr$.

3.5.1 Uncorrelated Fading.

3.5.1.1 Selection Diversity.

If we consider SEL with uncorrelated branches then the probability that the output CNR is below a particular level is simply the product of the probability that each of the branches are also below that level. In other words the output CDF is simply the product of the individual branch CDFs. Hence, for M branches with the same γ_0 on each of the branches

$$P_{sel}(\gamma) = (1 - e^{-\gamma/\gamma_0})^M \tag{3.18}$$

In terms of the envelope

$$P_{sel}(R) = (1 - e^{-R^2/2\sigma^2})^M \tag{3.19}$$

In the case of two branch selection diversity the CDF of the output CNR is given by

$$P_{sel}(\gamma) = (1 - e^{-\gamma/\gamma_0})^2 \tag{3.20}$$

$$P_{sel}(R) = (1 - e^{-R^2/2\sigma^2})^2 \tag{3.21}$$

The PDF is given by the differential of the CDF with respect to γ or R which for an M branch system is

$$p_{sel}(\gamma) = \frac{d}{d\gamma} P(\gamma) = \frac{M}{\gamma_0} \left[1 - e^{-\gamma/\gamma_0}\right]^{M-1} \exp\left\{ - \frac{\gamma}{\gamma_0} \right\} \tag{3.22}$$

$$p_{sel}(r) = \frac{d}{dr} P(r) = M \frac{r}{\sigma^2} \left[1 - e^{-r^2/2\sigma^2}\right]^{M-1} \exp\left\{ - \frac{r^2}{2\sigma^2} \right\} \tag{3.23}$$

3.5.1.2 Maximal Ratio Combining.

Earlier we saw that when each branch was co-phased and suitably weighted, then the output CNR was provided by the sum of the individual branch CNRs. Now the signal on each branch is composed of in-phase and quadrature components (I and Q respectively). These components are independent of one another and can be described in terms of zero-mean Gaussian random variables with a variance of σ^2 (see Chapter 2). The output CNR therefore consists of 2M Gaussian random variables in a joint distribution of I and Q, which is a χ^2 distribution [9]. In this situation the PDF of the output CNR for M branches is given by [5]

$$p_{mrc}(\gamma) = \frac{\gamma^{M-1} e^{-\gamma/\gamma_0}}{\gamma_0^M (M-1)!} \tag{3.24}$$

In terms of the envelope the PDF is given by

$$p_{mrc}(r) = r\left(\frac{r^2}{2\sigma^2}\right)^{M-1} \frac{e^{-r^2/2\sigma^2}}{(M-1)!} \tag{2.25}$$

The CDF is determined by integrating the PDF over the range of the variable

$$P_{mrc}(\gamma) = \int_0^{\gamma} p_{mrc}(\gamma)\, d\gamma = 1 - e^{-\gamma/\gamma_0} \sum_{n=1}^{M} \frac{(\gamma/\gamma_0)^{n-1}}{(n-1)!} \tag{3.26}$$

For the envelope

$$P_{mrc}(R) = \int_0^{R} p_{mrc}(r)\, dr = 1 - e^{-R^2/2\sigma^2} \sum_{n=1}^{M} \frac{(R^2/2\sigma^2)^{n-1}}{(n-1)!} \tag{3.27}$$

3.5.1.3 Equal Gain Combining.

A good approximation for the CDF of EGC can be obtained by multiplying the average signal power in the expression for the CDF of MRC by $\sqrt{3/2}$ [5]. Thus

$$P_{egc}(R) = 1 - e^{-R^2/2\sigma_1^2} \sum_{n=1}^{M} \frac{(R^2/2\sigma_1^2)^{n-1}}{(n-1)!} \tag{3.28}$$

$$\sigma_1^2 = \sigma^2 \sqrt{3/2} \tag{3.29}$$

3.5.1.4 Switch and Stay.

In the case of SAS diversity the PDF over the whole range of envelope values consists of two regions, with a discontinuity occurring at the switching threshold level. The PDF above and below the threshold have been found to be such that [8]

$$\begin{aligned} p_{sas}(r) &= (1+q)\,p(r) && r > R_t \\ &= q\,p(r) && r \le R_t \end{aligned} \tag{3.30}$$

where

$$\begin{aligned} q &= 1 - \mathrm{e}^{-R_t^2/2\sigma^2} \\ R_t &= \text{switching threshold} \end{aligned} \tag{3.31}$$

The CDF is found by integrating the appropriate expression for the two regions. Thus

$$\begin{aligned} P_{sas}(R) &= (1+q)(1-\mathrm{e}^{-R^2/2\sigma^2}) - q && R > R_t \\ &= q\,P(R) && R \le R_t \end{aligned} \tag{3.32}$$

Figure 3.2 shows the CDF of SAS for switching thresholds of -5 and -10dB with zero correlated branches. Clearly the improvement in the CDF afforded by SAS is dependent upon the choice of threshold level. Too high a threshold provides limited improvement for the deep fades, whilst, too low a threshold only reduces the occurrence of the more rare deepest fades. Figure 3.3 shows the CDF of MRC, EGC, SEL and SAS (at a -10dB switching threshold) for uncorrelated branches. MRC exhibits the biggest improvement followed by EGC, SEL and SAS. It has been shown that[10] MRC gives the best improvement with EGC and SEL showing reduced improvements, relative to MRC, of -0.88dB (*i.e.* $10\log\sqrt{3/2}$) and -1.5dB respectively.

3.5.2 Correlated Fading.

When the two branches become correlated, e.g. if the antennas are not sufficiently separated, the CDF for the various diversity strategies is given by[5,11]

$$P(R)_{mrc} = 1 - \frac{(1+|\rho_{12}|)}{2|\rho_{12}|}\exp\left(-\frac{R^2}{2\sigma^2(1+|\rho_{12}|)}\right) - \frac{(1-|\rho_{12}|)}{2|\rho_{12}|}\exp\left(-\frac{R^2}{2\sigma^2(1-|\rho_{12}|)}\right)$$

$$P(R)_{sae} \simeq 1 - e^{(-R_t^2/2\sigma^2)}Q\left(\frac{R}{\kappa}, \frac{|\rho_{12}|R_t}{\kappa}\right) - e^{(-R^2/2\sigma^2)}\left\{1 - Q\left(\frac{|\rho_{12}|R}{\kappa}, \frac{R_t}{\kappa}\right)\right\} \quad (3.33)$$

$$P(R)_{sel} = 1 - e^{(-R^2/2\sigma^2)}\left\{1 - Q\left(\frac{|\rho_{12}|R}{\kappa}, \frac{R}{\kappa}\right) + Q\left(\frac{R}{\kappa}, \frac{|\rho_{12}|R}{\kappa}\right)\right\}$$

$$\kappa = \sigma\sqrt{(1-|\rho_{12}|^2)}$$

$Q(a,b)$ is Marcum's Q-function defined as

$$\begin{aligned} Q(a,b) &= \int_b^\infty x\exp\left(-\frac{a^2+x^2}{2}\right)I_0(ax)\,dx \\ &= 1 - \int_0^b x\exp\left(-\frac{a^2+x^2}{2}\right)I_0(ax)\,dx \end{aligned} \quad (3.34)$$

$I_0(.)$ is the modified zero-order Bessel function. Again a good approximation for EGC can be obtained by multiplying the average signal power in the expression for the CDF of MRC by $\sqrt{3/2}$ [5]. An expression for the CDF of SAS has not yet been found for correlated fading, but it is identical with that of SAE for independent fading[8]. Note that the CDFs given above reduce to the no-diversity case for perfectly correlated branches (i.e. $|\rho_{12}| = 1$).

Figures 3.4, 3.5 and 3.6 show the improvement in the CDF for MRC, SEL and SAS (-10dB threshold), for $|\rho_{12}|^2$ ($\simeq\rho_{env}$), in steps of 0.25 from 0 to

1, respectively. Both MRC and SEL are particularly tolerant to high values of correlation, whereas, the SAS strategy shows considerably reduced improvement, relative to MRC and SEL, for high values of branch correlation. The CDF for correlated fading can be approximated for small signal envelopes, which is when errors are most likely to occur, to

$$P(R)_{sas} = \left[\frac{RR_t}{2\sigma^2\sqrt{1-|\rho_{12}|^2}} \right]^2 \qquad R \ll R_t$$

$$P(R) = A\left[\frac{R^2}{2\sigma^2\sqrt{1-|\rho_{12}|^2}} \right]^2 \qquad \text{for MRC, EGC and SEL.} \tag{3.35}$$

$$A = \begin{cases} 1 & SEL \\ 2/3 & EGC \\ 1/2 & MRC \end{cases} \tag{3.36}$$

Since $\rho_{env} \simeq |\rho_{12}|^2$ in Rayleigh fading[5], equation 3.35 shows that the envelope cross-correlation reduces the effective average power by a factor of $\sqrt{1-\rho_{env}}$ for all of the diversity combiners. When ρ_{env} = 0.25, 0.5, 0.75 and 0.9 the diversity gain reduces by 0.6, 1.5, 3.0 and 5dB respectively.

3.6 THE LCR AND AFD FOR THE EQUIVALENT ENVELOPE.

The degree to which the envelope fluctuations are smoothed out by the various diversity strategies, and therefore their effectiveness in reducing the rate and length of fades, is apparent from the LCR and AFD. The LCR for diversity can be found in the same manner as that used in Chapter 2. The derivative of the equivalent envelope, which was derived earlier, is used to determine N_R for each of the strategies. Closed form solutions for the LCR and AFD, for uncorrelated fading, are given by[12]

$$N_{\substack{R\\mrc}} = \sqrt{\left(-\frac{\ddot{\rho}_{11}}{\pi}\right)}\left(\frac{R}{\sigma\sqrt{2}}\right)^3 \exp\left(-\frac{R^2}{2\sigma^2}\right)$$

$$N_{\substack{R\\egc}} = \sqrt{\left(-\frac{\ddot{\rho}_{11}}{\pi}\right)}\exp\left(-\frac{R^2}{2\sigma^2}\right) \left[\frac{R}{\sigma\sqrt{2}}\exp\left(-\frac{R^2}{2\sigma^2}\right)+\left\{\frac{R^2}{\sigma^2}-1\right\}\frac{\sqrt{\pi}}{2}\operatorname{erf}\left(\frac{R}{\sigma\sqrt{2}}\right)\right] \tag{3.37}$$

$$N_{\substack{R\\sel}} = 2\sqrt{\left(-\frac{\ddot{\rho}_{11}}{\pi}\right)}\frac{R}{\sigma\sqrt{2}}\exp\left(-\frac{R^2}{2\sigma^2}\right)\left\{1-\exp\left(-\frac{R^2}{2\sigma^2}\right)\right\}$$

$$\tau_{\substack{R\\mrc}} = \sqrt{\left(\frac{\pi}{-\ddot{\rho}_{11}}\right)}\frac{\exp\left(\frac{R^2}{2\sigma^2}\right)-\left(1+\frac{R^2}{2\sigma^2}\right)}{\left(\frac{R}{\sigma\sqrt{2}}\right)^3}$$

$$\tau_{\substack{R\\egc}} = \sqrt{\left(\frac{\pi}{-\ddot{\rho}_{11}}\right)}\times \frac{1-\exp\left(-\frac{R^2}{\sigma^2}\right)-\frac{R}{\sigma\sqrt{2}}\exp\left(-\frac{R^2}{2\sigma^2}\right)\sqrt{\pi}\operatorname{erf}\left(\frac{R}{\sigma\sqrt{2}}\right)}{\exp\left(-\frac{R^2}{2\sigma^2}\right)\left[\frac{R}{\sigma\sqrt{2}}\exp\left(-\frac{R^2}{2\sigma^2}\right)+\left\{\frac{R^2}{\sigma^2}-1\right\}\frac{\sqrt{\pi}}{2}\operatorname{erf}\left(\frac{R}{\sigma\sqrt{2}}\right)\right]} \tag{3.38}$$

$$\tau_{\substack{R\\sel}} = \frac{1}{2}\sqrt{\left(\frac{\pi}{-\ddot{\rho}_{11}}\right)}\frac{\exp\left(\frac{R^2}{2\sigma^2}\right)-1}{\left(\frac{R}{\sigma\sqrt{2}}\right)}$$

Assuming that all the multipath waves received either at the mobile or base stations result from scatterers surrounding the mobile

uniformly[5] (we assume no scatterers at the base station) then $\ddot{\rho}_{11}$, the second derivative of the autocorrelation $\rho(\tau)$[9] is given by

$$\ddot{\rho}_{11} = \frac{d^2\rho}{d\tau^2} = \frac{d^2 J_0(BV\tau)}{d\tau^2} = -2(f_D)^2 \tag{3.39}$$

Figure 3.7 shows N_R and τ_R for MRC, EGC, SEL and SAS(-10 dB) strategies for zero correlated branches. Notice that each of the strategies results in a considerable reduction in the level crossing rate at low signal levels. In the case of τ_R all the strategies show the same improvement below -10dB (except SAS), namely that τ_R is approximately halved.

When the two branches become correlated, for example when the antenna spacing becomes small, the LCR and AFD can be approximated by [6,12]

$$N_R \simeq \nu \left(-\frac{\ddot{\rho}_{11} + \left(\frac{|\dot{\rho}_{12}|^2}{1-|\rho_{12}|^2} \right)}{\pi} \right) \frac{\left(\frac{R}{\sigma\sqrt{2}} \right)^3}{1-|\rho_{12}|^2} \qquad \text{for } \frac{R}{\sigma\sqrt{2}} \ll 1 \tag{3.40}$$

$$\frac{N_R}{sas} = \frac{\sqrt{2\pi} f_D \left(\frac{R}{\sigma\sqrt{2}} \right) \left(\frac{R_t}{\sigma\sqrt{2}} \right)^2}{\left(1-|\rho_{12}|^2 \right)}$$

$$\nu = \begin{cases} 1 & MRC \\ 4/3 & EGC \\ 2 & SEL \end{cases}$$

---

[9] ρ_{11} is used here for the autocorrelation function to distinguish it from $a(\tau)$ in Chapter 2, which is a general term for both the two and three dimensional models. Here we consider only the two dimensional model.

$$\tau_R \simeq \frac{1}{2}\sqrt{\left(-\frac{\pi}{\ddot{\rho}_{11}+\left(\frac{|\dot{\rho}_{12}|^2}{1-|\rho_{12}|^2}\right)}\right)}\frac{R}{\sigma\sqrt{2}} \qquad \text{for } \frac{R}{\sigma\sqrt{2}} \ll 1 \quad (3.41)$$

$$\tau_{sas R} = \frac{1}{\sqrt{2\pi} f_D}\left(\frac{R}{\sigma\sqrt{2}}\right) \quad R \ll R_t$$

In the above cases $|\rho_{12}|$ and hence $\dot{\rho}_{12}$ are dependent upon the antenna geometry in relation to the direction of vehicle motion[12]. No analytical expression is available for $\dot{\rho}_{12}$ with vertically separated antennas. However for horizontally spaced antennas the effect of $\dot{\rho}_{12}$ can be assumed to be small, provided that the antenna separation is not too small[12], hence $\dot{\rho}_{12} \sim 0$. The above equations show that N_R increases as the correlation between the branches increases and becomes 1.3 times, twice, 4 times and ten times as large as that for the independent fading case for $|\rho_{12}|^2$ = 0.25, 0.5, 0.75 and 0.9 respectively. The AFD for SAS is unaffected whilst again τ_R for MRC, EGC and SEL is approximately halved.

Figure 3.8 shows N_R for MRC and SAS (-10dB threshold) for correlations (i.e. $|\rho_{12}|^2$) in steps of 0.25 from 0 to 1 for small envelope values. Of these two diversity schemes MRC shows the best tolerance to high values of correlation.

3.7 THE RF INPUT AND ENVELOPE SPECTRA.

No closed form expressions exist for the autocorrelation function of either the in-phase or quadrature components or of the envelope for the equivalent output signal of the various diversity strategies. Hence, no closed form expressions can be derived for the Doppler and envelope spectra. The effects of the various diversity strategies on the Doppler and envelope spectra are studied in this work by comparing the spectra of the equivalent signal with that of a single branch. Both of these

spectra are determined by numerically Fourier transforming the computed autocorrelation functions. Since we assume perfect co-phasing of the branches, for the MRC and EGC cases, the RF input spectra are assumed to be that of a double-sideband signal in which the carrier (which is at 0Hz in our baseband case) is Amplitude Modulated (AM) by the Rayleigh fading envelope sequence. Since the envelope sequence is non-deterministic such a spectrum is unknown and therefore the RF input spectra will only be determined for the SEL and SAS cases. The envelope spectra will be determined for each of the diversity strategies.

3.8 THE CDF OF RANDOM FM FOR SELECTION DIVERSITY.

Diversity can also be used to improve the receiver performance against random FM. For MRC and EGC the extent to which the random FM can be reduced depends upon the method of combining used[13]. If one branch is simply co-phased with the other then the random FM will be the same as that for a single branch. If a pilot tone is transmitted together with the information and all branches are co-phased to this tone, then the random FM can be completely eliminated, provided that the frequency separation between the pilot tone and carrier is much less than the coherence bandwidth[14]. Feedback techniques such as those used in the Granlund combiner[15] remove the random FM component by the use of a double mixing process. Both the pilot tone method and Granlund receiver can be used to eliminate the random FM for a single branch. In the following we shall consider the improvement, in random FM statistics, for the SEL case only.

Davis[13] considered the effects of random FM for selection diversity with uncorrelated branches. For M uncorrelated branches the PDF of the random FM is given by[13]

$$p(\dot{\phi}) = \frac{M}{2\Omega} \sum_{k=0}^{M-1} \binom{M-1}{k} (-1)^k \left\{ k + 1 + \frac{\dot{\phi}^2}{\Omega^2} \right\}^{-3/2} \tag{3.42}$$

which reduces to the familiar expression for a single branch when M=1 (see equation 2.60). For two branches the PDF is given by

$$p(\dot{\phi}) = \frac{1}{\Omega} \left[\left(1 + \frac{\dot{\phi}^2}{\Omega^2} \right)^{-3/2} - \left(2 + \frac{\dot{\phi}^2}{\Omega^2} \right)^{-3/2)} \right] \tag{3.43}$$

$$\Omega = \frac{\omega_D}{\sqrt{2}} \tag{3.44}$$

Adachi and Parsons[16] extended Davis' results for SEL diversity to include correlated fading. Davis[13] did not consider the CDF of the random FM noise. Adachi and Parsons gave an expression for the CDF without derivation. The CDF of the random FM, $P(\dot{\phi})$, for uncorrelated branches can be found by integrating the PDF of $\dot{\phi}$

$$P(\dot{\phi}) = \int_{-\infty}^{\dot{\phi}} p(\dot{\phi})\, d\dot{\phi} \tag{3.45}$$

However, $P(\dot{\phi})$ cannot be found using the above limits of integration because of the term at infinity. To solve this integral we can consider two situations. Firstly, we shall consider $P(\dot{\phi})$ when $\dot{\phi} < 0$, in this case

$$P(\dot{\phi}) = \int_{-\infty}^{\dot{\phi}} p(\dot{\phi})\, d\dot{\phi} = \int_{-\infty}^{0} p(\dot{\phi})\, d\dot{\phi} - \int_{\dot{\phi}}^{0} p(\dot{\phi})\, d\dot{\phi} \tag{3.46}$$

Now since $p(\dot{\phi})$ is symmetrical about zero the first integral on the right hand side is simply 1/2 i.e.

$$P(\dot{\phi}) = \frac{1}{2} - \int_{\dot{\phi}}^{0} p(\dot{\phi})\, d\dot{\phi} = \frac{1}{2} - \left[\frac{\frac{\dot{\phi}}{\Omega}}{2\sqrt{2 + \frac{\dot{\phi}^2}{\Omega^2}}} - \frac{\frac{\dot{\phi}}{\Omega}}{\sqrt{1 + \frac{\dot{\phi}^2}{\Omega^2}}} \right] \tag{3.47}$$

The same result is obtained when $\dot{\phi} > 0$. This result differs from that derived elsewhere [16]. Figure 3.9 shows the CDF of the random FM for a single branch and for two uncorrelated branches. It can be seen that two branch SEL diversity provides considerable improvement in reducing the random FM noise at high values of differential phase.

3.9 THE RANDOM FM SPECTRA FOR SELECTION DIVERSITY.

The autocorrelation of $\dot{\phi}$ for selection diversity, with uncorrelated fading, is given by[13]

$$< \dot{\phi}(t).\dot{\phi}(t+\tau) > = 2\left(\frac{\dot{a}^2(t) - a(\tau)\ddot{a}(\tau)}{2a^2(\tau)} \right) \ln\left[\frac{2}{1 + \sqrt{1 - a^2(\tau)}} \right] \tag{3.48}$$

the random FM spectrum is thus given by

$$S_{FM}(f) = F\{ < \dot{\phi}(t).\dot{\phi}(t+\tau) > \} \tag{3.49}$$

again F{.} is the Fourier Transform. The asymptotic spectrum, for diversity, is given by[13]

$$\underset{f \to \infty}{S_{FM}(f)} \simeq \frac{\Omega^3}{2\pi^2 f^2} \tag{3.50}$$

$$\underset{f \to \infty}{S_{FM}(f)} \simeq \frac{\omega_D^3}{4\sqrt{2}\,\pi^2 f^2} \tag{3.51}$$

Figure 3.10 shows the asymptotic random FM spectrum for both a single branch (see equation 2.67) and two uncorrelated branches using SEL diversity for a vehicle speed of 10m/s. The diversity strategy clearly

shows considerable improvement in reducing the random FM components at high frequencies.

3.10 CONCLUSION.

Expressions have been presented for the equivalent output signal envelope of several predetection diversity systems. Closed form expressions have been presented to show the improvement in signal statistics for the various diversity schemes. These expressions have taken into account the degree of correlation which exists between two antenna branches.

The following chapter discusses the design, construction and calibration of a two-branch amplitude and phase measuring receiver. This receiver is used to measure the complex correlation between the signal received on two spaced antennas, at both the mobile and base stations. The complex signal envelopes, which are recorded, are used to characterise the narrowband channel and assess the effectiveness of the various diversity schemes that have been discussed in this chapter.

3.11 REFERENCES.

[1] Parsons, J.D., Henze, M., Ratliff, P.A. and Withers, M.J., "Diversity Techniques for Mobile Radio Reception", The Radio and Electronic Engineer, Vol.45, No.7, pp.357-367, 1975.

[2] Cox, D.C., "Antenna Diversity Performance in Mitigating the Effects of Portable Radiotelephone Orientation and Multipath Propagation", IEEE Trans on Commun., Vol. COM-31, No.5, pp.620-628, 1983.

[3] Bergmann, S.A. and Arnold, H.W., "Polarisation Diversity in Portable Communications Environment", Electron. Lett., Vol.22 No.11, pp.609-610, 1986.

[4] Adachi, F., Feeney, M.T. and Parsons, J.D., "Level Crossing Rate and Average Fade Duration for Time Diversity Reception in Rayleigh Fading Conditions", IEE Proc., Vol.135 Pt. F, No.6, pp.501-506, 1988.

[5] Jakes, W.C. (Ed), "Microwave Mobile Communications", John Wiley and Sons, New York, 1974.

[6] Adachi, F., Feeney, M.T. and Parsons, J.D., "An Evaluation of Specific Diversity Combiners Using Signals Received by Vertically-Spaced Base-Station Antennas", J. IERE Vol.57 No.6(supplement), pp.S218-S224, 1987.

[7] Kahn, L.R., "Ratio Squarer", Proc. IRE, 42, No.11, p1704, 1954.

[8] Rustako, A.J. and Yeh, Y.S., "Performance of Feedback and Switch Space Diversity 900MHz FM Mobile Radio Systems with Rayleigh Fading", IEEE Trans, Commun. Vol. COM-21, No.11, pp.1257-1268, 1973.

[9] Papoulis, A., "Probability Random Variables and Stochastic Processes", McGraw-Hill, 11th print, 1981.

[10] Brennan, D.G., "Linear Diversity Combining Techniques", Proc. IRE, 47, No.6, pp.1075-1102, June 1959.

[11] Henze, E., "Theoretische Unterschungen über einige Diversityverfahren", Arch. Elekt. Übertagung, 11, No.5, pp.183-194, 1957.

[12] Adachi, F., Feeney, M.T. and Parsons, J.D., "Effects of Correlated Fading on Level Crossing Rates and Average Fade Durations with Predetection Diversity Combiners", IEE Proc. Vol.135, Pt.F, No.1, pp.11-17, 1988.

[13] Davis, B.R., "FM Noise with Fading Channels and Diversity", IEEE Trans. Commun. Technol., Vol., COM-19, No.6, pp.1189-1200, 1971.
---,"Random FM in Mobile Radio with Diversity", IEEE Trans. Commun. Technol., Vol., COM-19, No.6, pp.1259-1267, 1971.

[14] Gilbert, E.N., "Mobile Radio Reception", Bell Sys. Tech. J., Vol.48, pp.2473-2492, 1069.

[15] Granlund, J., "Topics in the Design of Antennas for Scatter", Technical Report 135, Lincoln Laboratory, MIT, Nov. 1968.

[16] Adachi, F. and Parsons, J.D., "Random FM Noise with Selection Diversity", IEEE Trans. Commun., Vol.36, No.6, pp.752-755, 1988.

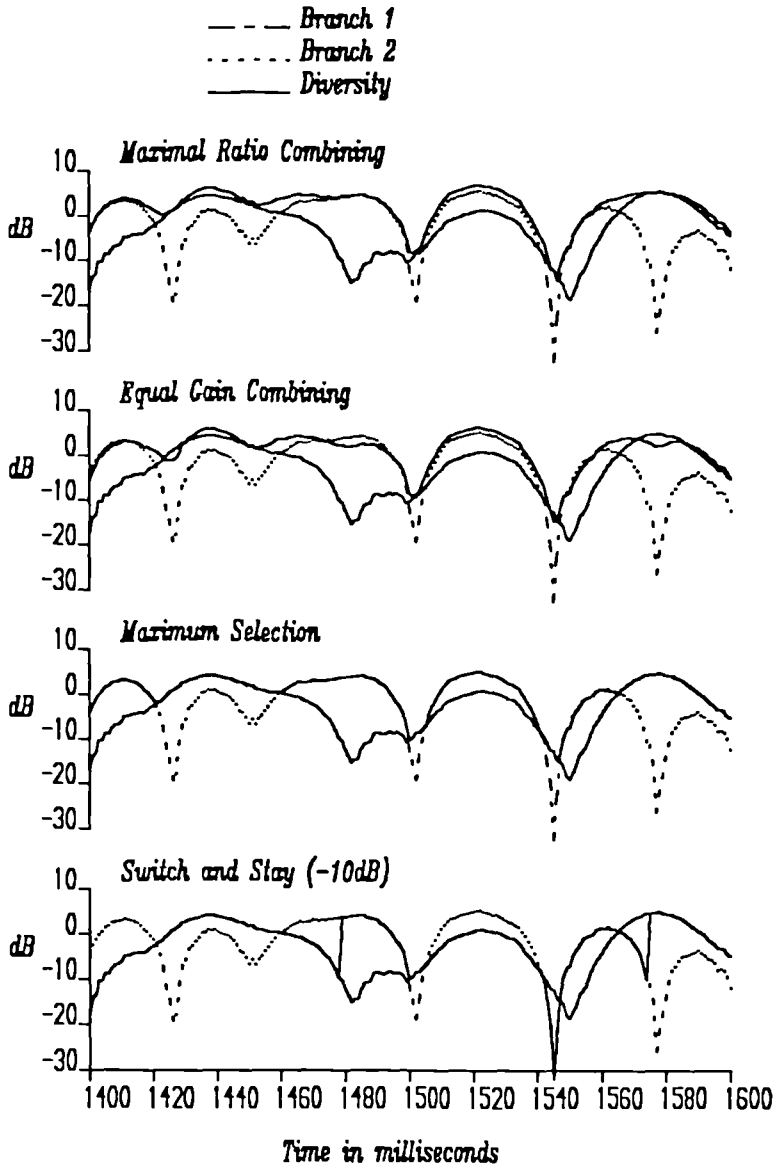

Figure 3.1 Example of individual branch envelopes together with the equivalent envelope for each of the various diversity strategies. A -10dB switching threshold has been used for SAS. The example shown was detected and recorded using the dual branch vector modulator receiver.

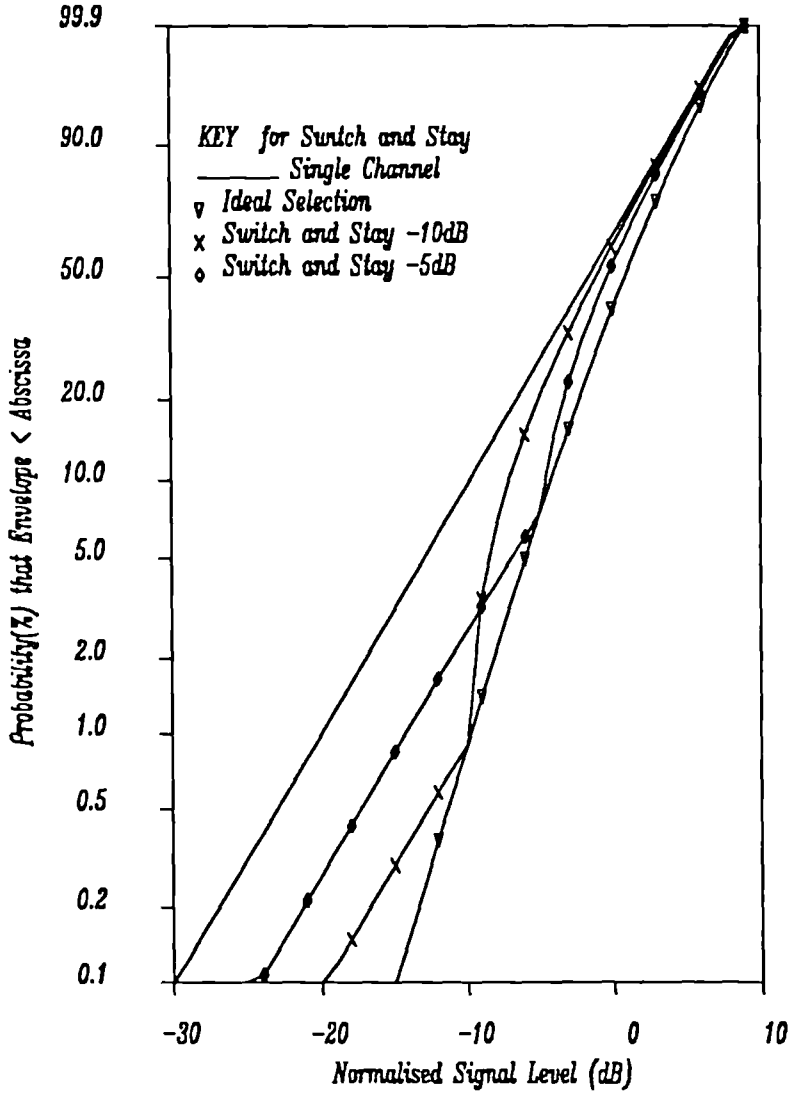

Figure 3.2 The CDF of the envelope for the SAS diversity receiver, using uncorrelated branches, for switching thresholds of -5dB and -10dB. The term 'normalised signal level' means that the envelope has been normalised by the average signal power (σ^2) i.e. $r/\sqrt{2}\,\sigma$.

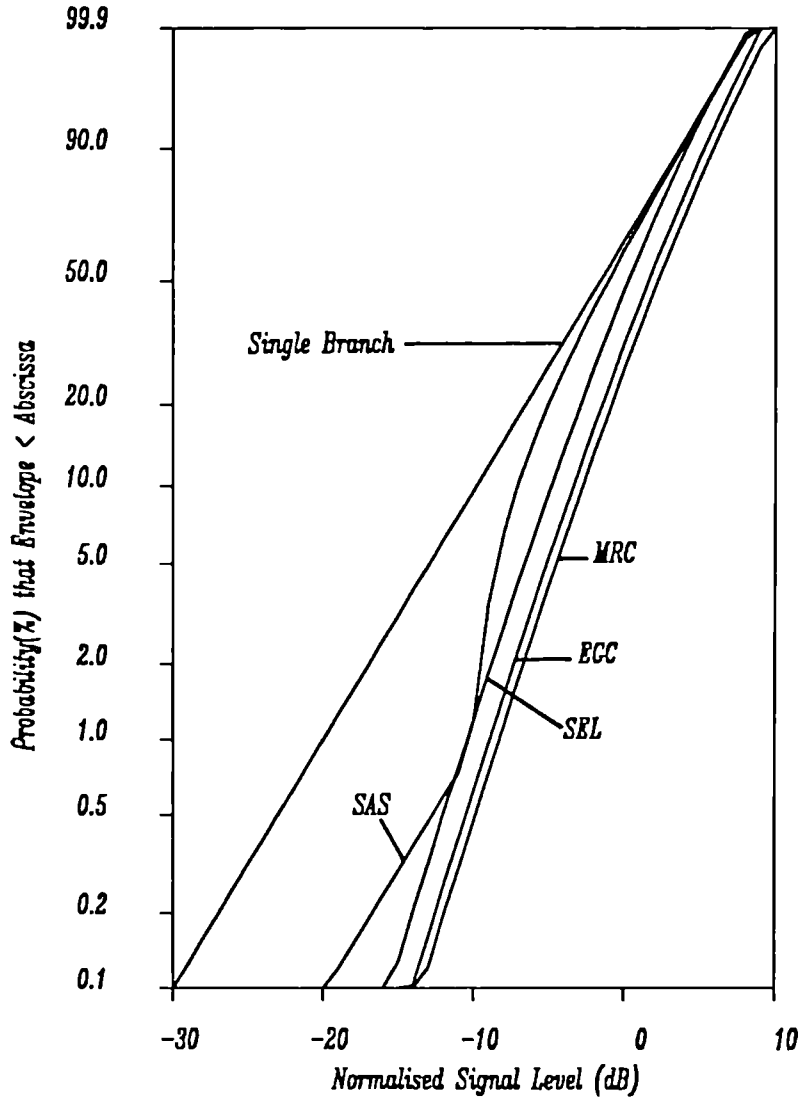

Figure 3.3 The CDF of the envelope for each of the diversity strategies using uncorrelated branches. The term 'normalised signal level' means that the envelope has been normalised by the average signal power (σ^2) i.e. $r/\sqrt{2}\,\sigma$.

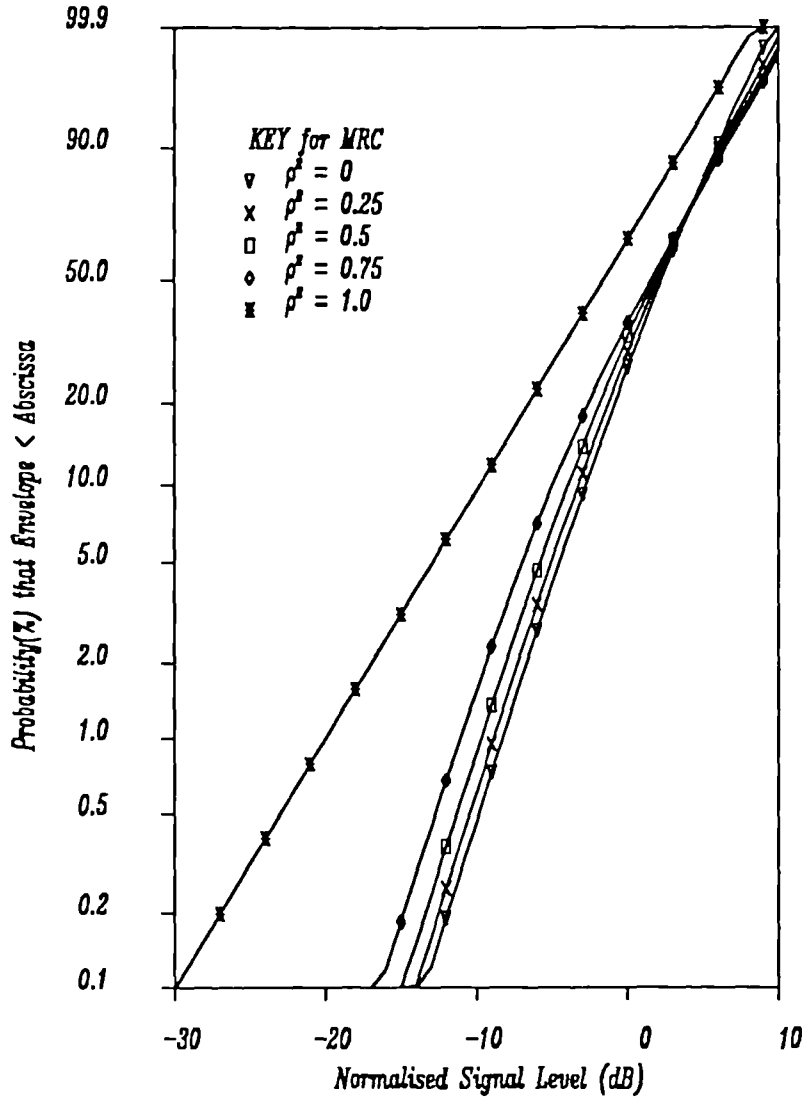

Figure 3.4 The CDF of the envelope as a function of branch crosscorrelation for the MRC strategy. The term 'normalised signal level' means that the envelope has been normalised by the average signal power (σ^2) i.e. $r/\sqrt{2}\,\sigma$.

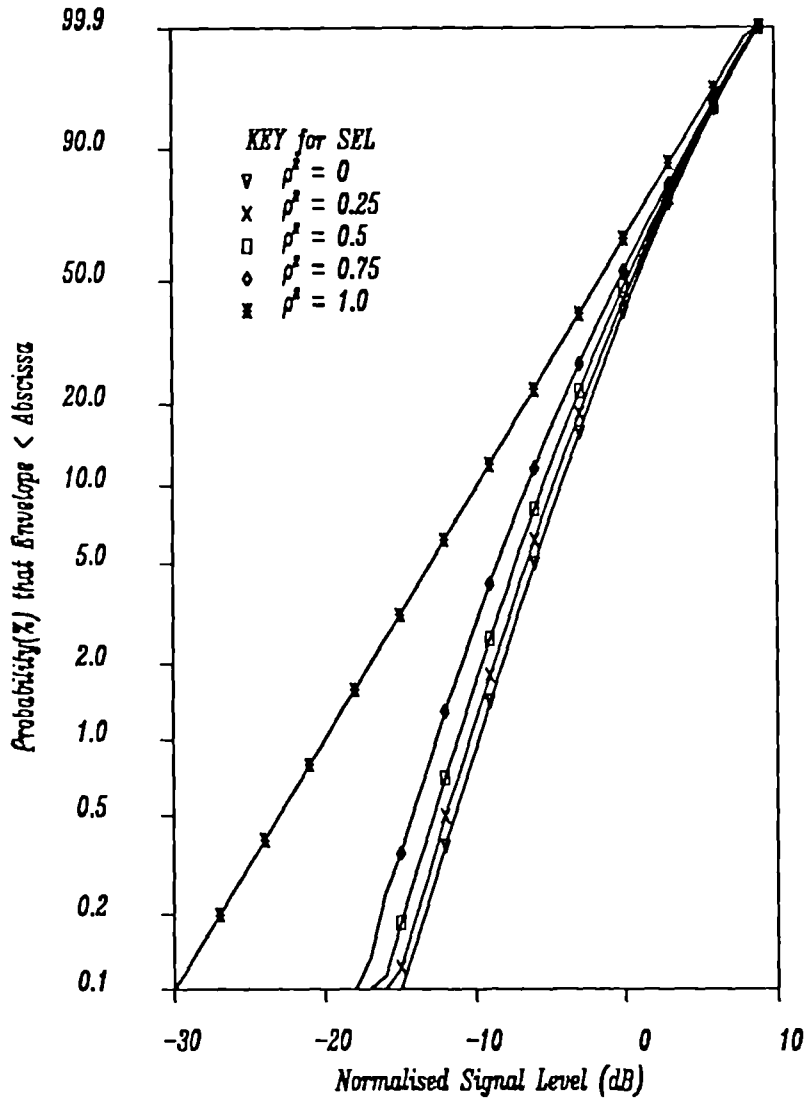

Figure 3.5 The CDF of the envelope as a function of branch crosscorrelation for the SEL strategy. The term 'normalised signal level' means that the envelope has been normalised by the average signal power (σ^2) i.e. $r/\sqrt{2}\,\sigma$.

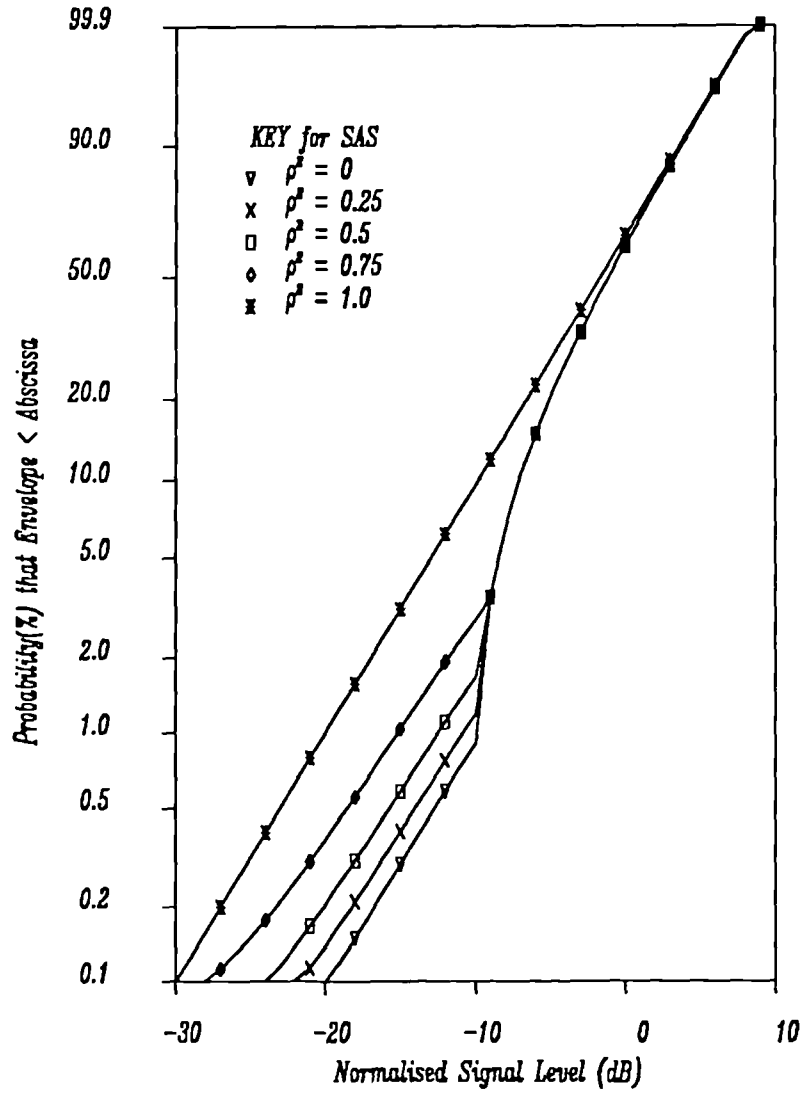

Figure 3.6 The CDF of the envelope as a function of branch correlation for the SAS strategy using a switching threshold of -10dB. The term 'normalised signal level' means that the envelope has been normalised by the average signal power (σ^2) i.e. $r/\sqrt{2}\,\sigma$.

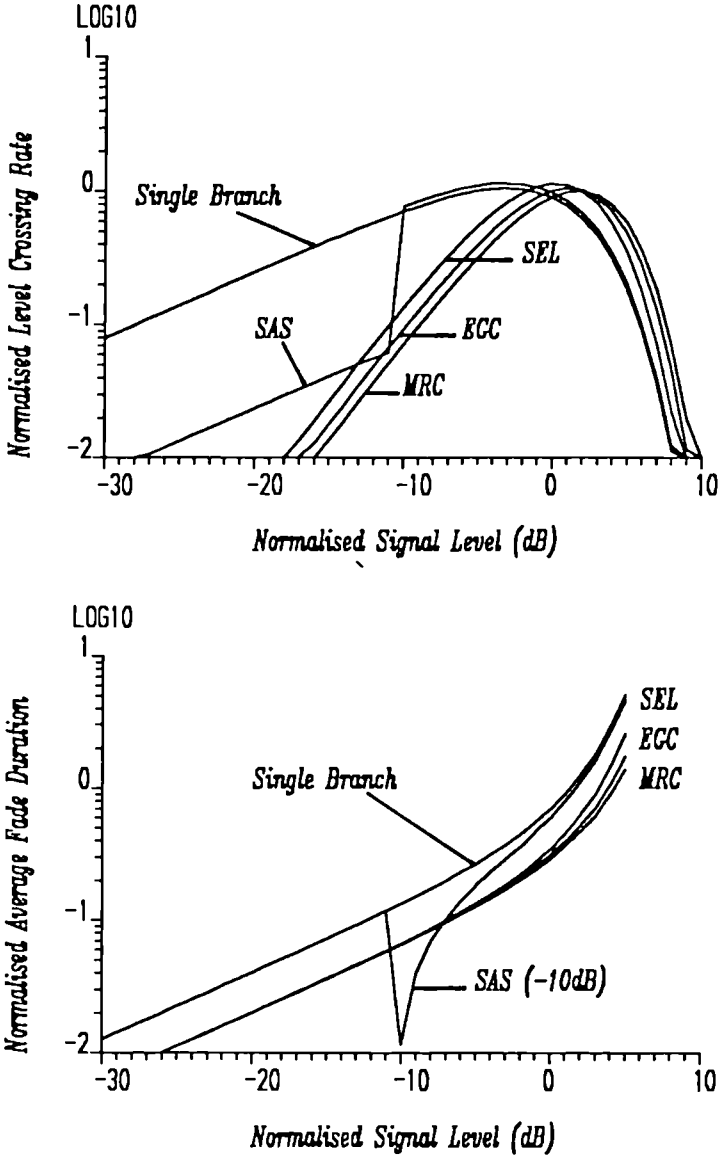

Figure 3.7 The normalised LCR (N_R/f_D) and normalised AFD ($\tau_R f_D$) for the various diversity strategies using uncorrelated branches.

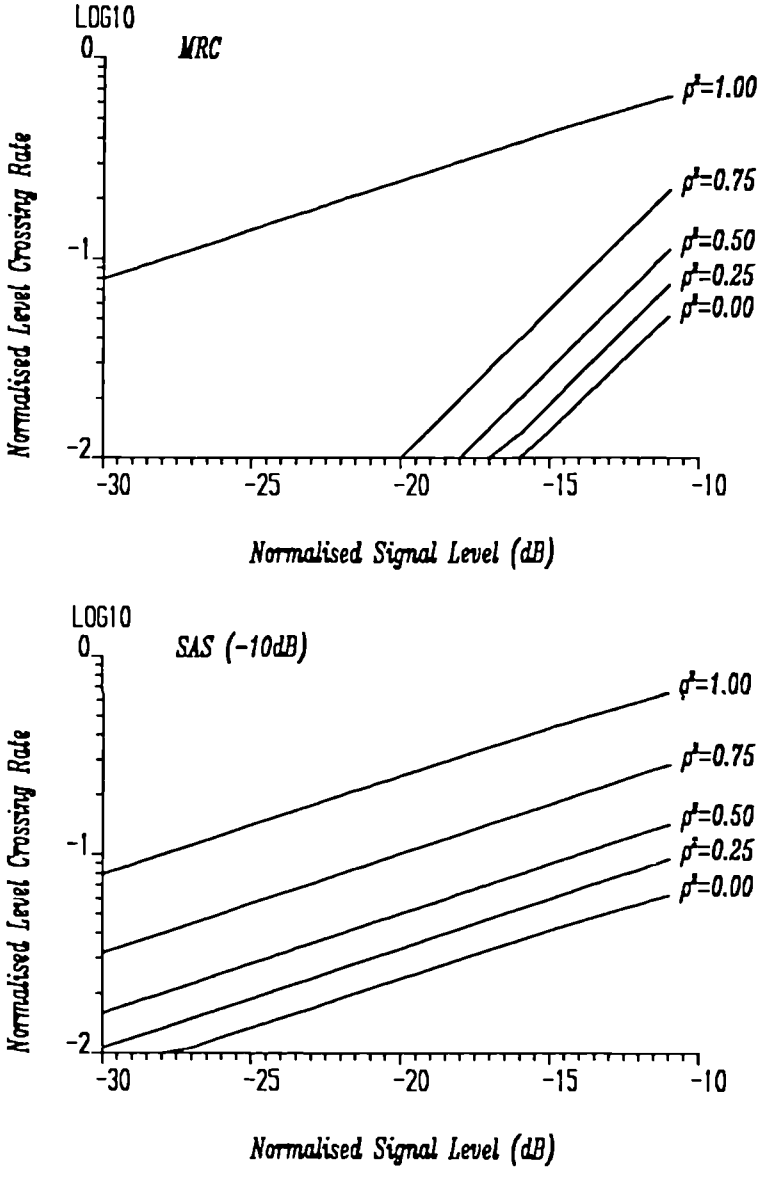

Figure 3.8 The normalised LCR (N_R/f_D) as a function of branch correlation for the MRC and SAS (-10dB switching threshold) strategies.

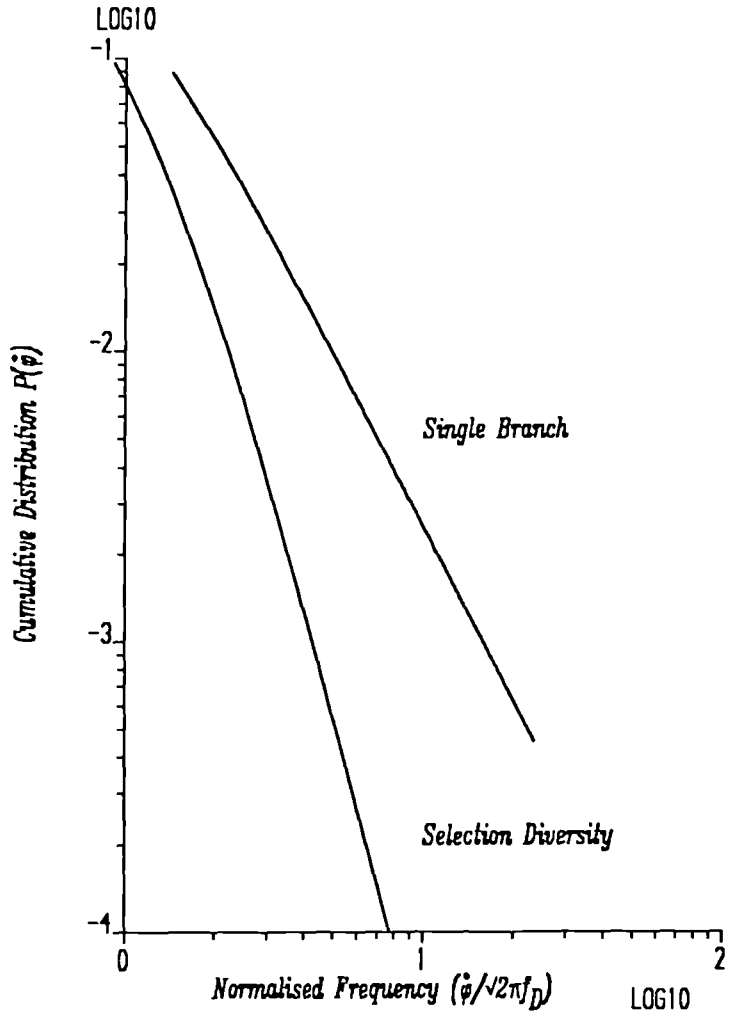

Figure 3.9 The CDF of the instantaneous frequency (random FM) as a function of normalised frequency (i.e. normalised by the maximum Doppler frequency) for a single branch and two uncorrelated branches using SEL diversity.

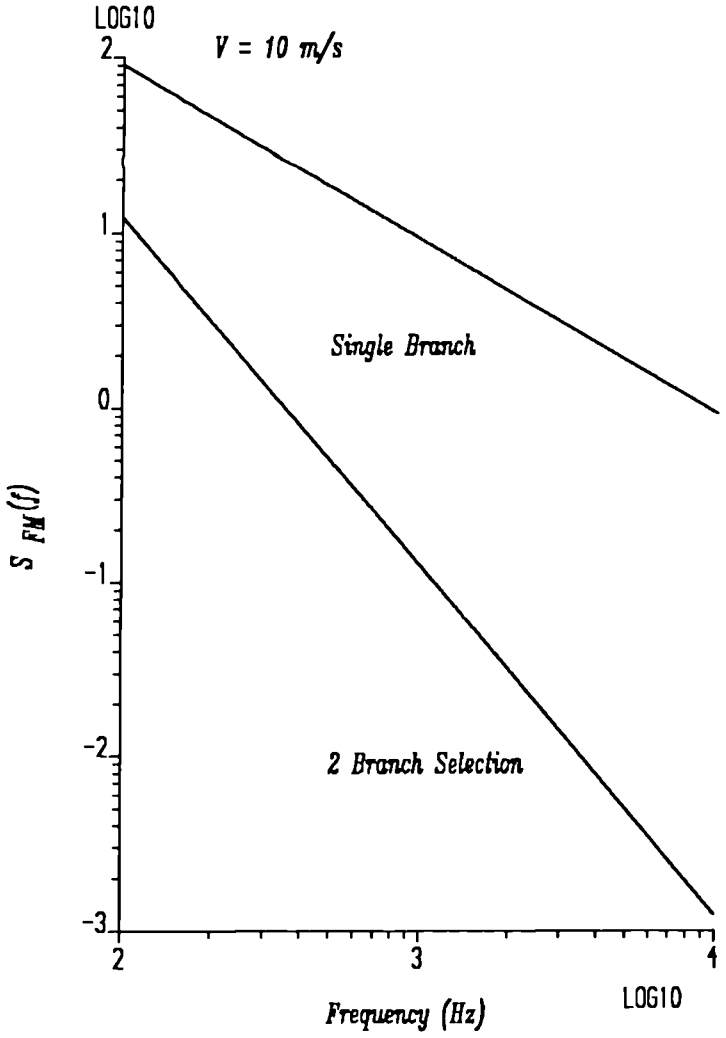

Figure 3.10 Asymptotic spectra of random FM for a single branch and two uncorrelated branches using SEL diversity with a vehicle speed of 10m/s.

CHAPTER 4. THE RECEIVER.

4.1 INTRODUCTION.

To characterise the narrowband mobile radio channel and fully assess the improvement afforded by diversity, requires the use of a different type of receiver than that used in previous studies[1]. Generally, signal strength measuring receivers are used to monitor the fading envelope and not the signal phase. The received carrier phase, of a mobile radio signal, has been used for co-phasing purposes in a dual branch equal gain predetection diversity combiner using single sideband perturbation techniques[2]. However this technique could not resolve the quadrature components and hence was unable to determine the Doppler RF and random FM spectra. At frequencies near 1GHz the relative bandwidth that the received signal occupies is extremely small. For example a vehicle travelling at 15m/s gives rise to a Doppler frequency spread of 100Hz at 1GHz. This proportionally small bandwidth (10^{-7}) coupled with a small signal strength ($\simeq$ -100dBm) makes monitoring such signals difficult, especially in the presence of noise.

This chapter outlines the principle of operation, design and construction of a quadrature receiver which can accurately measure both the amplitude and phase of a fading signal. The signal is received on two phase locked branches coupled to two spaced antennas, for diversity measurements. To the author's knowledge this is the first time such a receiver has been used, in the mobile radio environment, to assess the joint statistics and the improvement obtainable from diversity, using several combining strategies.

4.2 CHOICE OF RECEIVER INTERMEDIATE FREQUENCY.

To measure the carrier phase without ambiguity requires that the RF signal is detected using quadrature demodulation (i.e. vector demodulation). The complex narrowband channel characteristics are measured using coherent detection with the transmitter and receiver quasi-coherently[10] locked together. In this manner only those phase variations introduced by the channel, and not the transmitter/receiver combination, are measured. Naturally, the phase information cannot be realistically studied at the carrier frequency ($\simeq$ 1GHz). The translation of the quadrature information, and hence the phase, to a suitable frequency can be carried out in a number of ways. Heterodyning can be used to translate the carrier information down to a suitable IF (Intermediate Frequency). The choice of IF gives rise to two basic types of IF receiver.

(i) The IF Amplitude and Phase measuring receiver.
(ii) The zero-IF Amplitude and Phase measuring receiver.

These two types of receiver will be discussed in terms of their respective merits and demerits in measuring the amplitude and phase of the received signal.

4.2.1 The IF Amplitude and Phase Measuring Receiver.

In this type of receiver the carrier information is translated, in one or more stages, down to a suitable IF. Care is required in the choice of IF to avoid images, arising from the mixing process, from falling within

[10] The transmitter and receiver, which are physically separated, cannot be absolutely phase locked together in the mobile radio environment. However, the use of extremely stable frequency sources at both the transmitter and receiver can provide limited coherency over the period of an experiment. Hence we shall refer to the two sources as quasi-coherently locked together.

the passband of the IF. This can be achieved by using a first stage frequency upconversion, to displace the images, or through the use of image rejection mixers. All the mixing stages have to be phase locked together, otherwise the signal phase information is swamped by the time varying phase difference between the receiver stages. In addition, careful choice of IF must be made in terms of the IF filters and detectors,[11] which could have non-linear transfer functions. Two advantages of this receiver are that the input operating frequency is not constrained to a narrow RF input frequency band and, in addition, the receiver can be readily tested using network analyser techniques to isolate sources of phase error etc. in the various RF paths of the receiver.

4.2.2 The Zero-IF Amplitude and Phase Measuring Receiver.

In this case the frequency translation is made directly down to baseband such that the IF occurs at dc, i.e. zero-IF. For our purposes we shall consider the frequency conversion to be carried out in one step, and we shall refer to such a receiver as a Direct Conversion Receiver (DCR). This form of receiver naturally has a number of associated disadvantages. Firstly the operating frequency is limited by the availability of mixers which have a sufficiently high operating frequency at the RF port together with a dc operating IF port. The operating frequency is largely limited to the design frequency, due to the constraint of maintaining quadrature in the various RF paths. Secondly, high RF power levels are usually required to drive the mixers in order that an adequate dynamic range is achieved. These disadvantages are largely overcome in this work because only one test frequency was used and the tests were conducted with sufficient proximity to the base station such that the necessary degree of RF amplification required was easily attainable.

---

[11] Two detectors are required for each branch. One to detect the in-phase component and the other to detect the quadrature component.

The architecture associated with this form of receiver has certain distinct advantages over the previous IF receiver. Firstly, the layout is simple in that it lends itself readily to modular construction. Secondly, only one phase locked stage is required, which is particularly useful in this work where more than one branch is employed. The single mixing process, down to zero-IF, also provides an inherent detection function as a result of the mixing process. Images are no longer a problem since these are sufficiently separated from the wanted information so that they are easily removed. Any imbalance between the in-phase and quadrature baseband channels can be reduced through careful calibration, or through the use of digital correction techniques[3].

Because of the advantages outlined above a dual branch DCR zero-IF vector demodulator was designed, constructed and calibrated to measure the complex narrowband mobile radio channel. Before discussing the receiver in detail a brief outline of the operating principles will be presented.

4.3 PRINCIPLE OF OPERATION.

In presenting a simplified description of the vector demodulator we only consider one branch of the receiver. Figure 4.1 shows the DCR with the RF input given by

$$\mathrm{Re}\left\{e^{j(\omega_c t+\phi(t)+\psi_{nT}(t))}\right\} \tag{4.1}$$

where from the above and Fig.4.1

ω_c = RF input carrier angular frequency.
ω_0 = Receiver local oscillator angular frequency.
$\phi(t)$ = Information.
$\psi_{nT}(t)$ = Phase noise associated with the transmitter.
$\psi_{nR}(t)$ = Phase noise associated with the receiver.

The RF input signal is split by a 3dB hybrid whose outputs are fed to two double balanced mixers. The two mixers are fed by quadrature components of the LO(Local Oscillator) to produce in-phase and quadrature outputs given by I(t) and Q(t) respectively

$$I(t) = \cos A \cos B = \frac{1}{2}\,[\,\cos(A - B) + \cos(A + B)] \tag{4.2}$$

$$Q(t) = \sin A \cos B = \frac{1}{2}\,[\,\sin(A - B) - \sin(A + B)] \tag{4.3}$$

where

$$A = \omega_0 t + \psi_{nR}(t)$$
$$B = \omega_c t + \phi(t) + \psi_{nT}(t)$$

In this work the experiments are performed with $f_c \simeq$ 1GHz, therefore the summed terms ($\simeq$ 2GHz) in (4.2) and (4.3) are very high compared with the difference terms. Neither the mixers, or the antialiasing filters (see later sections), are able to pass the high frequency components which are thus filtered out leaving only the difference frequency. The phase noise terms, from the transmitter and receiver, which are uncorrelated, can be considered in terms of an effective phase noise term $\psi_n(t)$

$$\psi_n(t) = \psi_{nT}(t) + \psi_{nR}(t) \tag{4.4}$$

The in-phase and quadrature terms thus become

$$I(t) = \cos[(\omega_0 - \omega_c)t - \phi(t) - \psi_n(t)] \tag{4.5}$$

$$Q(t) = \sin[(\omega_0 - \omega_c)t - \phi(t) - \psi_n(t)] \tag{4.6}$$

where we have dropped the proportionality term without loss of generality. Now ω_c and ω_0 can be arranged, through the use of frequency standards, to be approximately equal such that

$$\omega_0 - \omega_c = \Delta\omega \ll \frac{2\pi}{T_e} \tag{4.7}$$

where T_e is the typical duration of an experiment.

If we consider the Doppler frequencies to be the information then then

$$\phi(t) = \frac{2\pi}{\lambda} Vt \cos\gamma \tag{4.8}$$

where

V = Vehicle speed.
λ = Carrier wavelength ($\lambda \simeq$33cm at 1GHz).
γ = Angular direction of vehicle motion relative to the base station

If we consider also that the signal to phase noise ratio is high i.e. $|\phi(t)| \gg |\psi_n(t)|$ then

$$I(t) = \cos\left\{ -\frac{2\pi}{\lambda} Vt \cos\gamma \right\} \tag{4.9}$$

$$Q(t) = \sin\left\{ -\frac{2\pi}{\lambda} Vt \cos\gamma \right\} \tag{4.10}$$

If I and Q are now monitored on a CRO, in x-y mode, and we assume, for the purpose of illustration, that there is no fading, then the resultant demodulated vector rotates in a circular manner dictated by the Doppler frequency $(2\pi/\lambda)V\cos\gamma$ (+ve Doppler causes the vector to rotate clockwise whilst -ve Doppler causes an anticlockwise rotation). The same effect would be observed if the vehicle was stationary and the transmitter and receiver LOs were offset from one another.

It is easy now *to visualise what happens* to the vector when the received signal has undergone propagation through the mobile radio channel. The received vector moves in a random manner, in the complex plane, with a time varying envelope and phase, as described statistically in Chapter 2. If the same receiver LO is now used to also drive a second identical branch, which is connected to a separate antenna, then the complex narrowband channel can be assessed in terms relevant to the performance of spaced antenna diversity systems.

4.4 THE EXPERIMENTAL AMPLITUDE AND PHASE MEASURING RECEIVER.

The dual branch DCR zero-IF vector demodulator is shown in Figure 4.2. The receiver LO is fed by a 3dB quadrature hybrid (SAGE DC-751) whose outputs provide in-phase and quadrature LO signals to the two branches of the receiver. Each quadrature signal is further split using a 3dB hybrid (MCL ZFSC-2-5). The four LO outputs (two in-phase and two quadrature) are then fed at +7dBm to the LO port of each double balanced mixer (MCL ZFM-2). The RF ports of the mixers are each fed with a split version of the RF input signal from one of the antennas. The split here is achieved using 3dB hybrids (MCL ZFSC-2-4). The resultant baseband signals are dc coupled to amplifier stages with variable dc offset (for x-y alignment purposes). The signals are then fed to antialiasing digital filters (RETICON RF609A). From here the four baseband quadrature signals are fed to a multitrack FM tape recorder (RACAL STORE-7DS).

In the earlier discussion a perfect quadrature relationship was assumed together with matched baseband stages. In a practical receiver neither of these assumptions are necessarily valid. Departure from quadrature and/or amplitude imbalance between the baseband signals, causes errors in the measured signal envelope and phase. In the following section the sources of error associated with quadrature detection are discussed.

4.5 THE SOURCE AND REDUCTION OF AMPLITUDE AND PHASE ERRORS.

In describing the principle of operation, a perfect quadrature relationship was assumed together with perfect channel matching. This is by no means the case in a practical situation. Errors in amplitude and phase can arise in several parts of the system[4]. In the following we

shall discuss three principal sources of error which give rise to errors in determining the amplitude and phase of the received signal. Various methods of reducing the source of amplitude and phase error will also be discussed.

4.5.1 Amplitude Error.

Even if the quadrature phase relationship is perfect then envelope and phase errors can arise if the channels are mismatched in amplitude. The envelope error arises from the fact that the resultant vector, i.e. envelope, is directly related to the channel amplitude. If we consider a fifteen percent difference between I and Q, for the tone measurements discussed earlier, then the envelope will be in error by a maximum of 1.4dB. If this tone is viewed on a CRO, in x-y mode, then what should have appeared as a circle is now an ellipse. The minor axis of the ellipse coincides with the reduced channel, which is orthogonal to the major axis. In this example we consider that the error only occurs in the quadrature branch i.e. the in-phase branch is assumed perfect. In addition, non-linear phase error arises due to the amplitude mismatch, since $\phi = \tan^{1}(Q/I)$. Figure 4.3 shows the effect of channel amplitude mismatch on the envelope and phase.

These errors are easily reduced by altering the appropriate baseband channel gain until both the in-phase and quadrature outputs have the same amplitude.

4.5.2 DC Offset Error.

Even in an otherwise perfect system, envelope and phase errors can still arise if either, or both, of the quadrature components have a fixed dc offset. The effect of dc offset can be seen in Figure 4.4 where errors of 0.3 and -0.2 have been simulated for I and Q respectively. Naturally, the

receiver can no longer detect I and Q as zero mean Gaussian processes for a received Rayleigh distributed signal. DC offset errors are reduced through the use of dc coupled amplifier stages which are calibrated prior to each experimental run. Alternatively the stages could be ac coupled with an accompanying loss of some low frequency information. Small dc offsets can also be further reduced by normalising the I and Q channels by their respective long term average values. Implicit in such an approach would be that I and Q have identical mean values of zero.

4.5.3 Quadrature Error.

Quadrature error refers to the two LO sources, which feed the mixers, not being truly orthogonal. If we again consider the input tone, this time with perfect channel match, the baseband output appears as a skewed ellipse. The degree of skewness is related to the extent of quadrature loss. Figure 4.5 shows this more complicated source of error. Ideally if I has reached a maximum then there should be no signal in Q. Clearly this will not be the case when quadrature error arises. Again this gives rise to error in the envelope and phase of the vector. Quadrature error is reduced by increasing or decreasing the RF path length of either the in-phase or quadrature local oscillator line to the mixer. This is achieved by means of a variable phase shifter or by careful matching of the path lengths.

The extent of the amplitude mismatch and quadrature error can also change as a function of input carrier frequency. In this application the narrow bandwidth ensured that neither of these parameters were adversely affected. When modulation schemes are employed (which occupy a greater bandwidth than the CW signal used in these tests) the effect of input frequency is of greater importance. These errors can be further reduced by the use of digital matching using Fourier transform techniques[3].

The effect of all three sources of error on the envelope and phase can be seen in Figure 4.6. This figure represents the combined effects

of amplitude, dc offset and quadrature mismatch seen in Figures 4.3, 4.4 and 4.5 respectively. Clearly the resultant skewed offset ellipse is dramatically in error compared with the expected circle. In practice each of the three sources of error were reduced, one at a time, in the manner outlined earlier.

4.6 RECEIVER CALIBRATION.

Because the resultant signals occur at baseband, conventional network analyser equipment[12] cannot be used to measure the degree of amplitude mismatch or quadrature error, except in the RF paths. Instead, the sources of error were measured at baseband frequencies using an input tone, at the test frequency, that is phase locked to the LO. The amplitude mismatch was reduced by varying the baseband amplifier gains until both of the quadrature branches exhibited identical amplitudes and zero means for the input tone signal. The quadrature error was reduced by careful tuning of the RF path lengths until the baseband signals, of the input tone, (i.e. tone angular frequency = $|\omega_c - \omega_0|$) had a phase difference of $\pi/2$ radians. The phase difference between the two branches of the receiver, was measured as 13.3°. No attempt was made to eliminate this phase difference since the absolute phase difference between the two branches could be accommodated in subsequent software analysis.

4.6.1 Receiver Dynamic Range.

The receiver dynamic range was measured by injecting an RF tone, at various signal levels, into both branches of the receiver, and digitising

---

[12] Network analysers operate at IF and RF frequencies and hence are ineffective for measurements at baseband frequencies.

the quadrature outputs. Figures 4.7 and 4.8 show the calibrations for branches 1 and 2 respectively. The regression data were used to provide conversion of the I/Q values into envelope (i.e. vector magnitude) signal strength. Note that both branches are extremely well matched and have a large dynamic range for a linear detector system. Input signals of greater than -10dBm cannot be used due to non-linear distortion arising from the mixer diodes becoming saturated. Each of the quadrature mixers acts as an AM linear detector. To assess the non-linear effects of the mixers the harmonics of the fundamental were measured, for each of the mixers, at the point of maximum distortion. These harmonics were found to be greater than 25dB below the fundamental and hence, have little effect on the resultant vector.

4.6.2 Receiver Quadrature Error.

The same data used to measure the dynamic range was used to measure the degree of quadrature error as a function of RF input level. This was achieved by software mixing the baseband quadrature outputs, which contain the tone information, and measuring the departure from quadrature. Figure 4.9 shows the quadrature angular error as a function of RF input level. Again it is noticed that both receivers are well matched and that the absolute quadrature error is small. The quadrature error was not found to vary across the bandwidth of the receiver.

4.7 COHERENT SOURCES.

Measurement of the RF carrier phase, which has undergone propagation through a scattering field, requires that the LOs at both the transmitter and receiver are stable and phase locked together. A number of signal generators were used, as LOs, for the experiments (Marconi-2019,

Marconi-2022C and HP-8656B). Each of the signal generators derives its output frequency from an internal frequency reference. These frequency references are neither stable nor coherent with respect to each other. Each of the generators was therefore driven externally from an extremely stable frequency source. Rubidium frequency standards were used for this purpose (RACAL-DANA 9475). Coherency between the two sources, and hence between the transmitted carrier and receiver LO, was monitored by periodically mixing the two sources and adjusting one of the standards to produce zero-drift.[13] The two signal generators could then be considered to be quasi-coherently locked.

4.7.1 Phase Noise.

If the coherent received signal is viewed on a CRO, in x-y mode, the resultant *point vector*[14] *has a small amount of angular jitter.* This phase jitter, termed 'phase noise', arises from the fact that the frequency standards are not pure sources and the signal generators themselves derive their output frequencies through independent phase locked loops. The degree of phase noise present, using the frequency standards, was considerably smaller than that introduced by the channel. The phase noise introduced by the transmitter and receiver local oscillators was measured for a transmitted tone. The resultant phase was measured and found to have an associated uncertainty, introduced by the phase noise, of 1.1°. Thus the phase of the received RF signal and hence the random FM introduced by the channel could be measured.

---

[13] In fact a very small amount of drift was allowed, between the two sources, provided that the period of the resultant offset frequency was considerably greater than the time required to conduct an experiment.

[14] We have assumed that there does not exist any drift between the two standards.

4.8 THE RECEIVER FRONT-END.

To provide an adequate RF input level to the receiver (-10dBm to -60dBm) and to provide some selectivity, a front-end, comprising of RF amplifiers and a filter, was assembled for each branch of the receiver. This arrangement consisted of a crystal filter (MURATA-DFC3R914P001BTD) centred on the test frequency, preceded and followed by low noise RF amplifiers (HP-8447D and MCL-ZHL-1042J respectively). Sufficient gain and selectivity was achieved, with this combination, to enable maximum use of the receiver's dynamic range for the field trials. The overall gain of this front-end, for both branches, was some 50dB (52dB gain from the amplifiers and 2dB loss through the crystal filter). The receiver was then able to detect and quantify accurately the envelope and phase of an RF signal between -60dBm and -110dBm.

4.8.1 The Receiver Antennas.

Two antennas were used to receive the fading signals for the spaced antenna diversity field trials. These antennas were vertically mounted $\lambda/2$ dipoles designed for the test frequency of 914.5125MHz. Each of the $\lambda/2$ dipoles was mounted on a non-conducting boom to reduce the effects of coupling between the elements and the mast. The separation between the elements, of the dipoles, was adjusted for minimum VSWR. A clamp arrangement was used, on the antenna booms, to facilitate easy adjustment of the vertical antenna spacing between the two antennas.

4.8.2 Data Recording.

The outputs from the four quadrature baseband channels were recorded onto analogue magnetic tape using a multitrack FM tape recorder (RACAL STORE-7DS). In addition, another channel of the recorder was

used to monitor vehicle speed. This was achieved by recording pulses derived from an opto-isolator mounted on the vehicle's drive shaft. When the receiver was located at the base station the pulses were used to modulate the carrier of a FSK transmitter. The tacho pulses were subsequently received, at the base station, by means of an FM receiver and recorded onto tape. A 1 Hz tone was also recorded onto the analogue tape to provide for later digitisation of the recorded information.

4.8.3 The Transmitter.

The transmitter, which was located either at the base station or at the mobile, is shown in Figure 4.10. The Rubidium frequency standard provided an accurate frequency reference for the transmitter, which was coupled with a frequency synthesised signal generator arranged for CW output. A 40dB gain linear amplifier (ENI 603L) was used to provide a 3W signal at the transmitter antenna. The transmitter antenna was a vertical monopole mounted on the roof of the vehicle for reception at the base station, or a mast at the base station for reception at the mobile. Care was necessary at both the base station and mobile to ensure that the antennas did not sway excessively, because such movement manifests itself as phase perturbations on the received signal.

4.9 CONCLUSION.

The principle of vector demodulation has been explained in this chapter together with the design of a dual branch direct conversion vector demodulator receiver. The envelope and phase errors associated with such a receiver have been discussed in terms of their origin and reduction. The calibration of the receiver has shown that both branches are extremely well matched with a usable dynamic range of +45dB. The

use of coherent sources, for both the transmitter and receiver, has been discussed in terms of the coherency between the two sources and their combined phase noise. Finally a selective front-end, for the dual branch receiver, has been described which allows the receiver to measure the envelope and phase of RF input signals down to -110dBm.

4.10 REFERENCES.

[1] Adachi, F., Feeney, M.T., Williamson, A.G. and Parsons, J.D., "Cross-correlation Between the Envelopes of 900MHz Signals Received at a Mobile Radio Base Station Site", IEE Proc. Pt.F, Vol.133, No.6. pp.506-512, 1986.

[2] Henze, M., "A Diversity System for UHF Mobile Radio", Ph.D. Thesis, University of Birmingham, 1975.

[3] Dickinson, M., "Digital Matching of the I and Q Signal Paths of a Direct Conversion Radio", IERE., Vol.56, No.2, pp.75-78, 1986.

[4] Neuf, D. and Piro, P., "Designing with Phase Detectors", Microwave System News, pp.76-82, 1987.

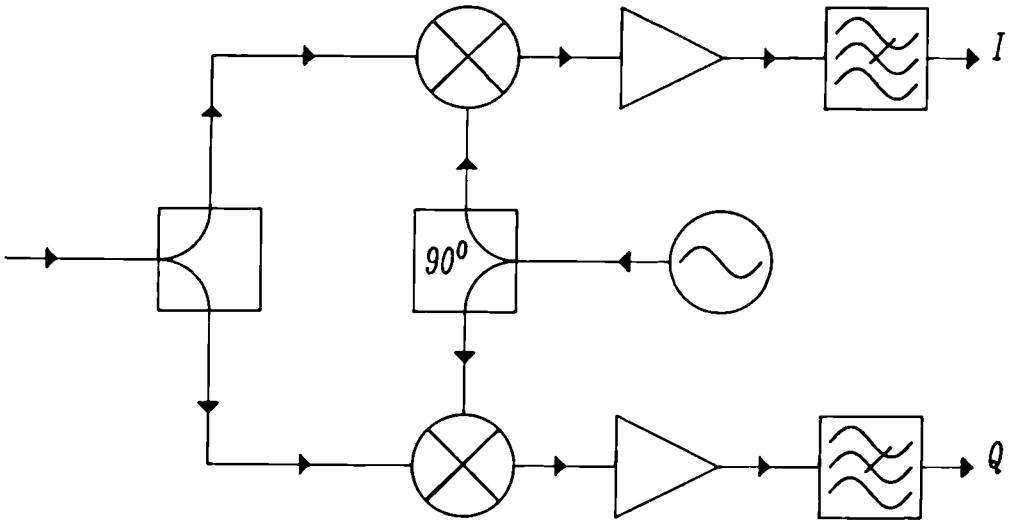

Figure 4.1 The direct conversion vector demodulator receiver.

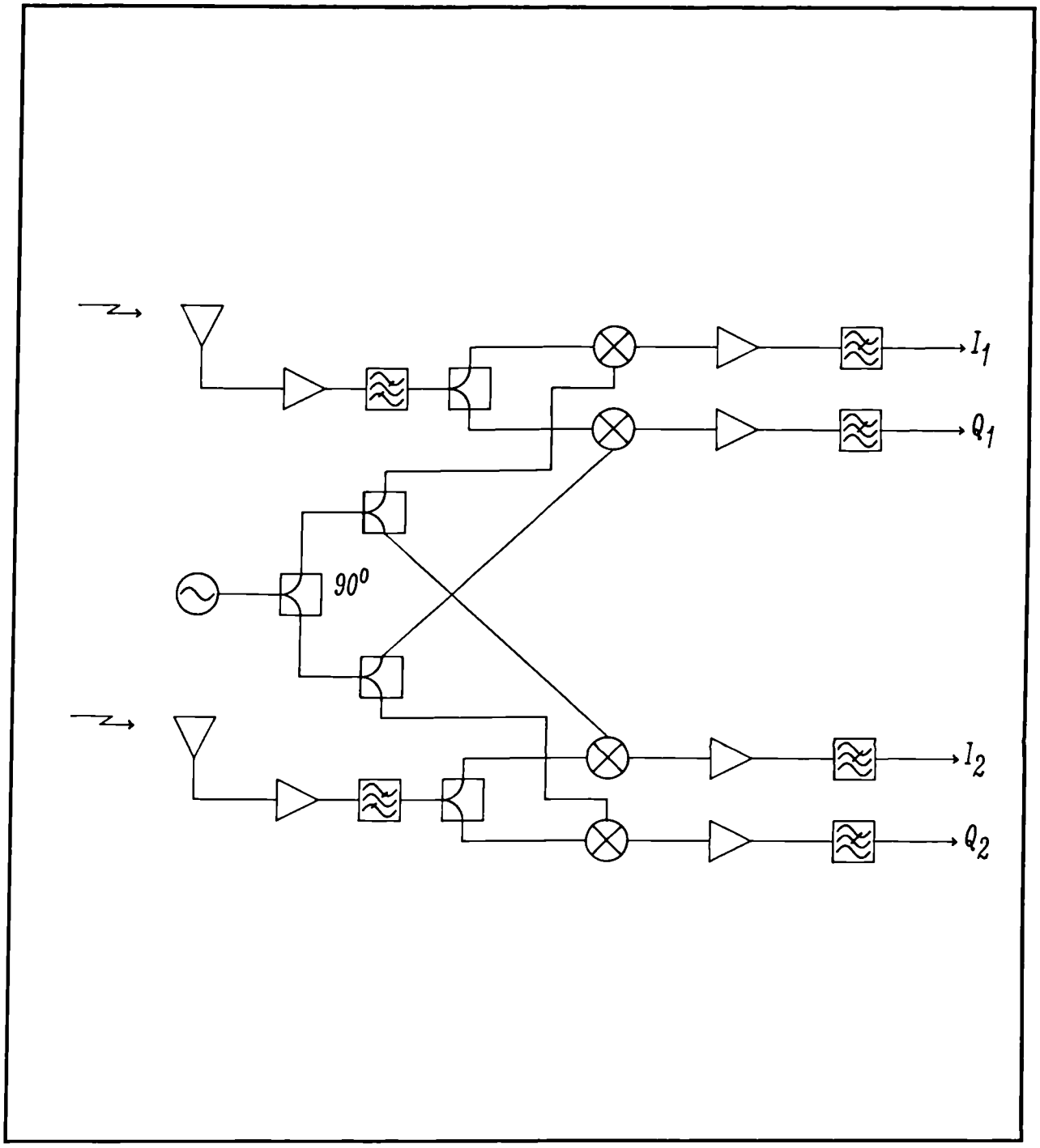

Figure 4.2 The dual branch phase-locked direct conversion vector demodulator receiver.

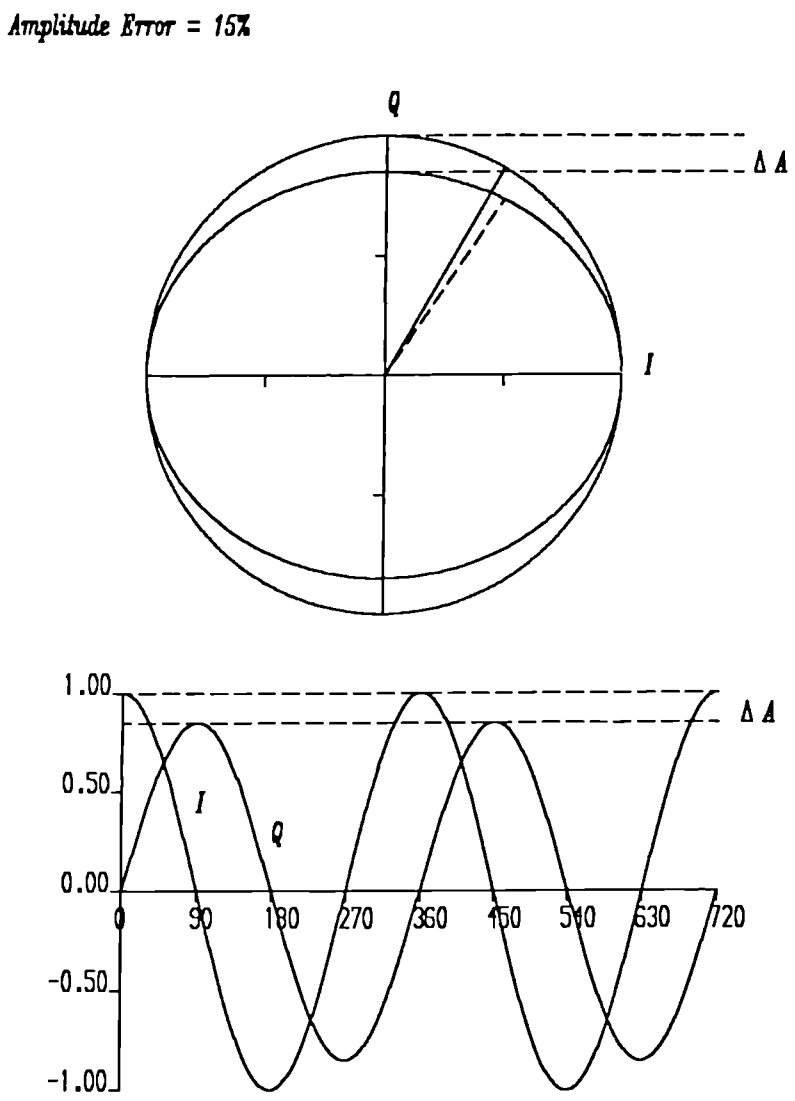

Figure 4.3 Example of amplitude mismatch, between the in-phase and quadrature channels, which produces envelope and signal phase error. The circle represents perfect detection and the ellipse represents the signal detected as a result of the amplitude mismatch. In the upper diagram the solid radius represents the envelope for perfect detection and the dashed radius represents the envelope detected as a result of the amplitude mismatch.

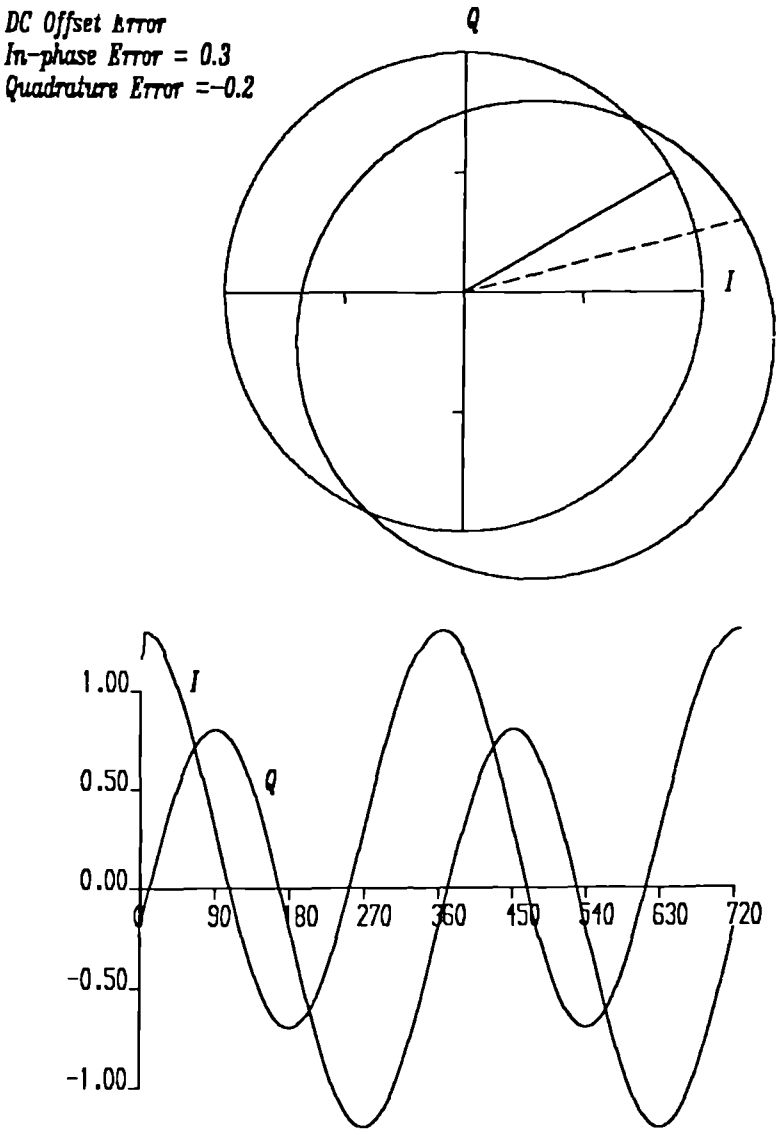

Figure 4.4 Example of dc mismatch, for both in-phase and quadrature channels, which produces envelope and signal phase error. The centred circle represents perfect detection. The offset circle represents the signal detected as a result of quadrature dc offset error. In the upper diagram the solid radius represents the envelope for perfect detection and the dashed radius represents the envelope detected as a result of the dc offset mismatch.

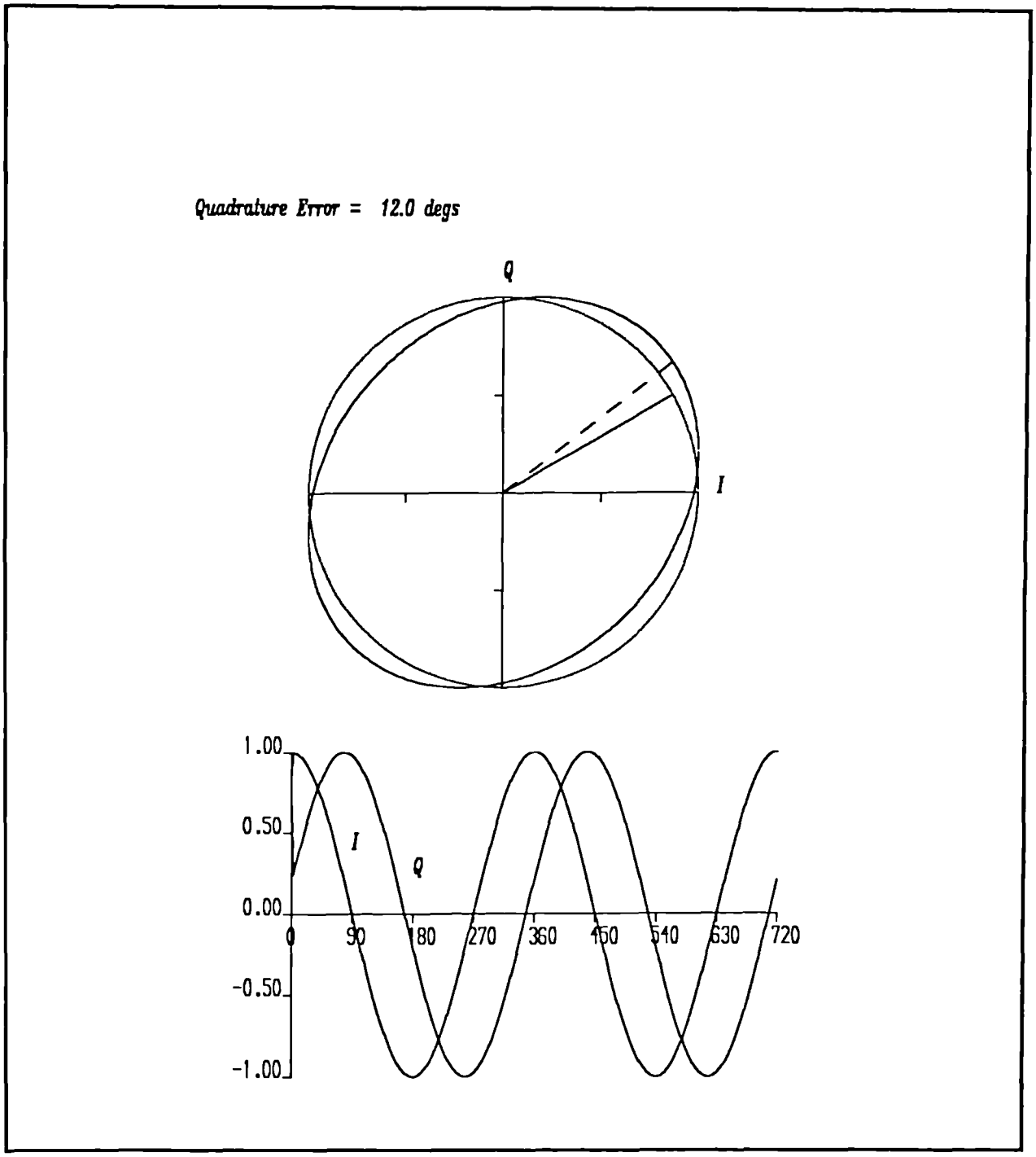

Figure 4.5 Example of quadrature error, between the in-phase and quadrature channels, which produces envelope and signal phase error. The circle represents prefect detection and the skewed ellipse represents the signal detected as a result of quadrature error. In the upper diagram the solid radius represents the envelope for perfect detection and the dashed radius represents the envelope detected as a result of the quadrature error.

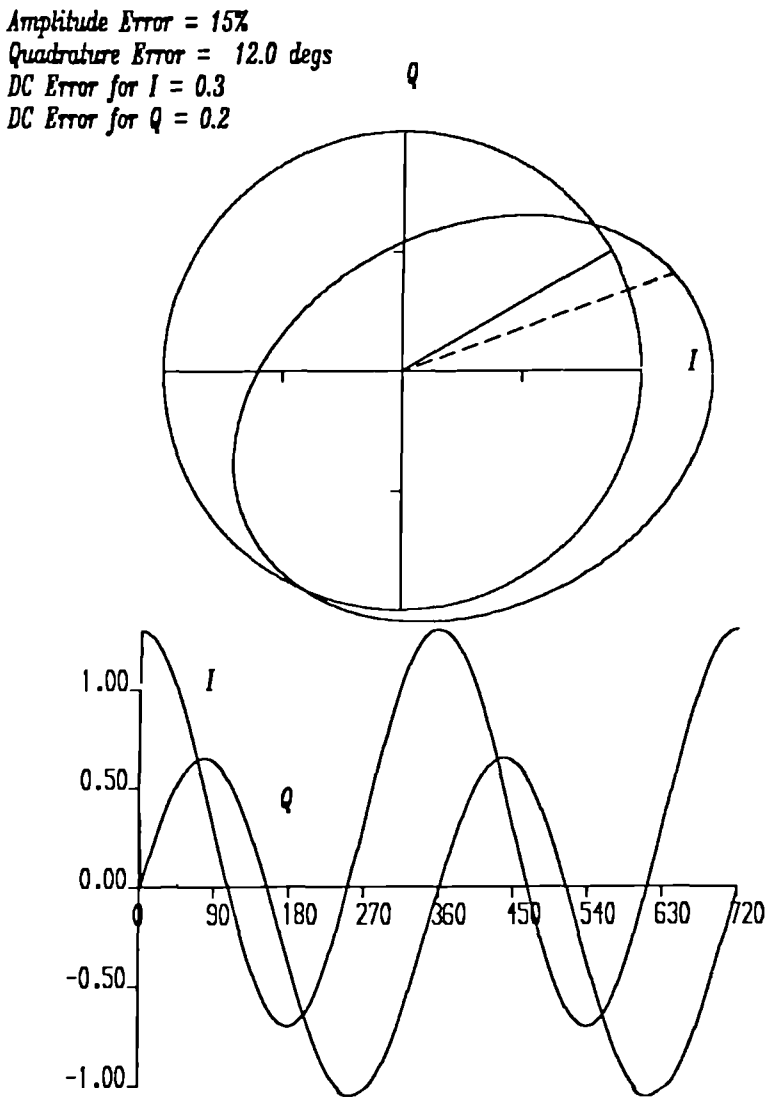

Figure 4.6 Example of amplitude, dc and quadrature mismatch which results in envelope and signal phase error. The circle represents perfect detection. The offset skewed ellipse represents the signal detected with all three forms of error shown in Figures 4.3, 4.4 and 4.5. In the upper diagram the solid radius represents the envelope for perfect detection and the dashed radius represents the envelope detected as a result of the various errors.

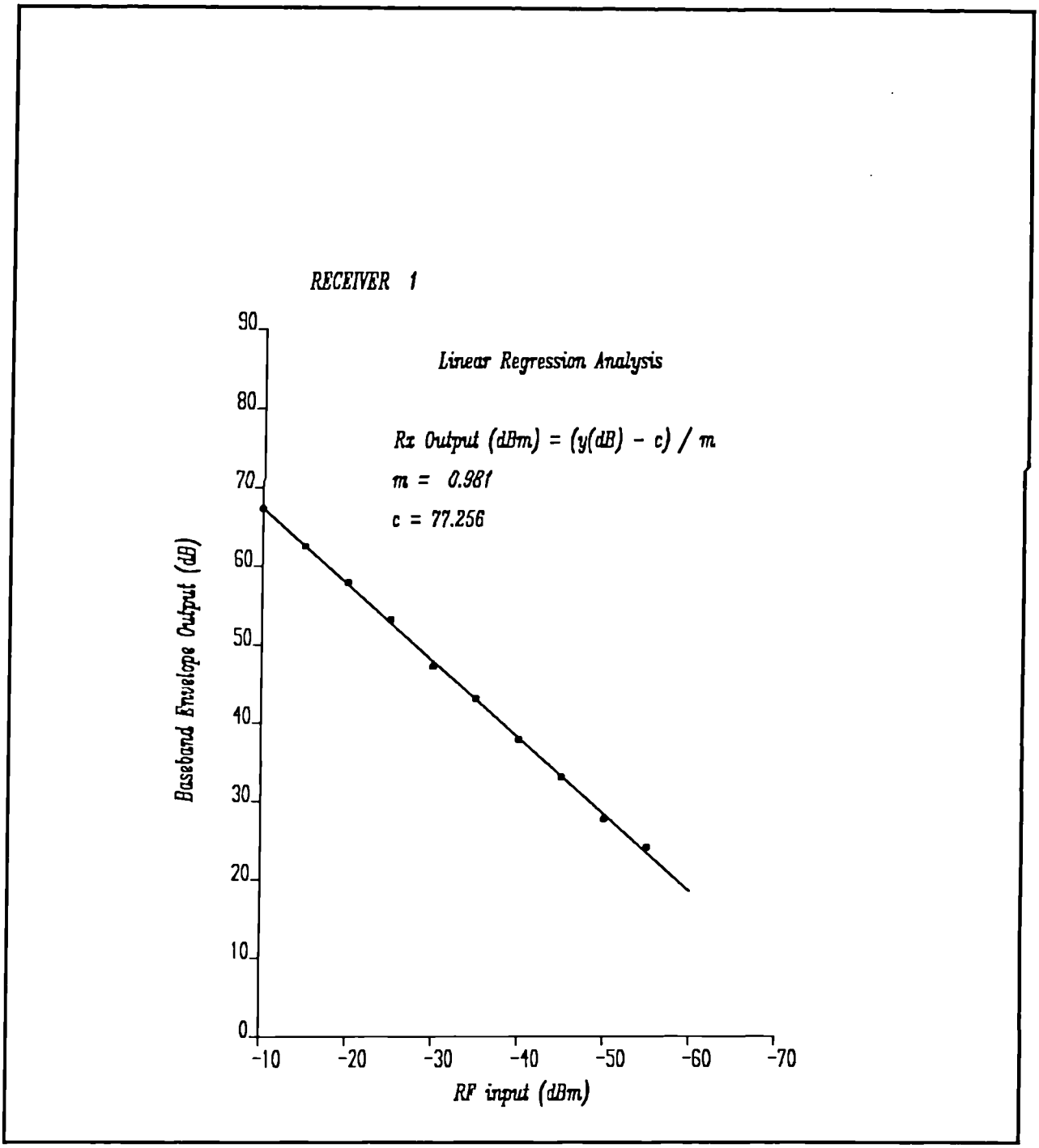

Figure 4.7 Calibration plot and regression analysis data for receiver branch number 1.

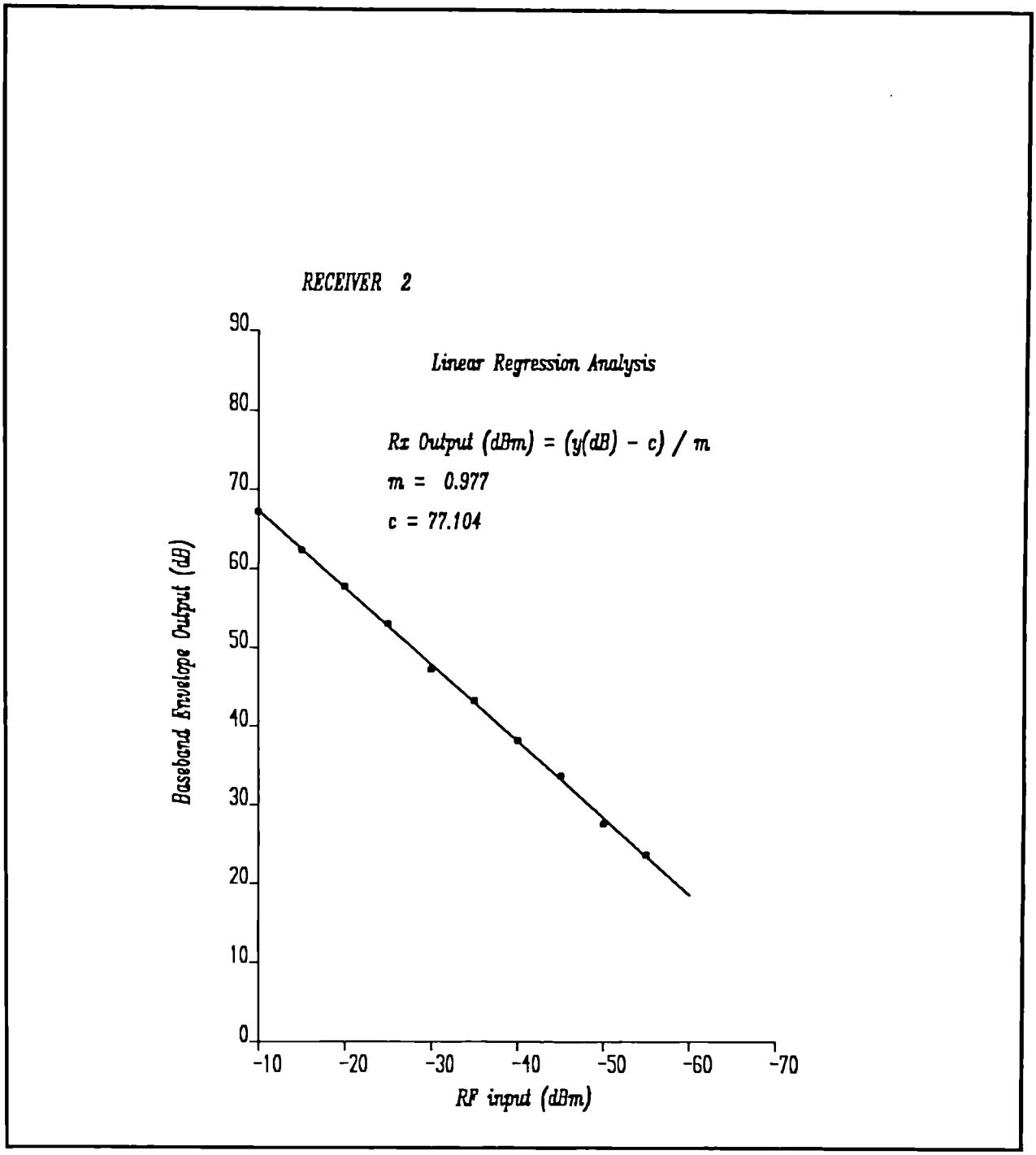

Figure 4.8 Calibration plot and regression analysis data for receiver branch number 2.

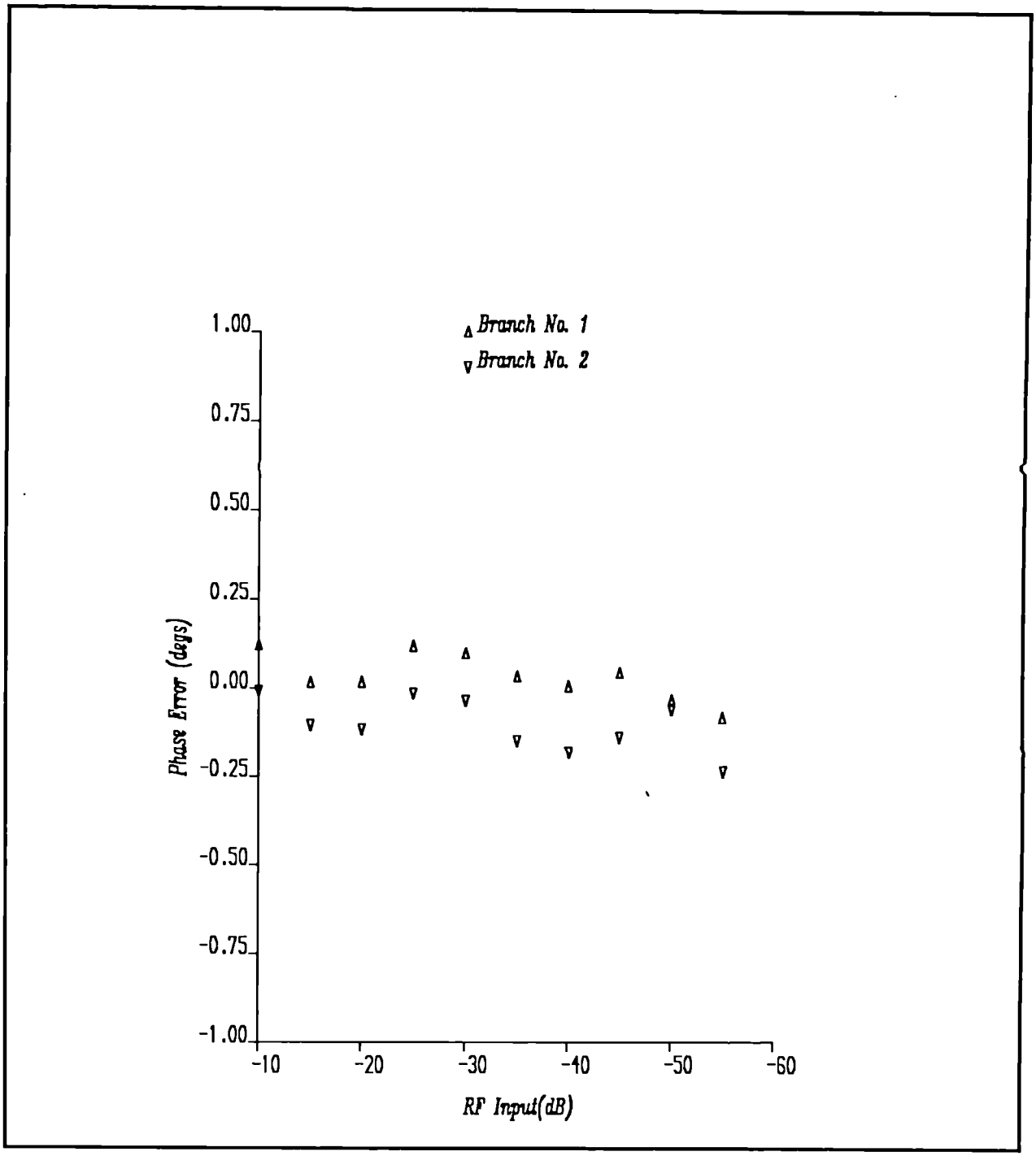

Figure 4.9 Quadrature error as a function of RF input signal level.

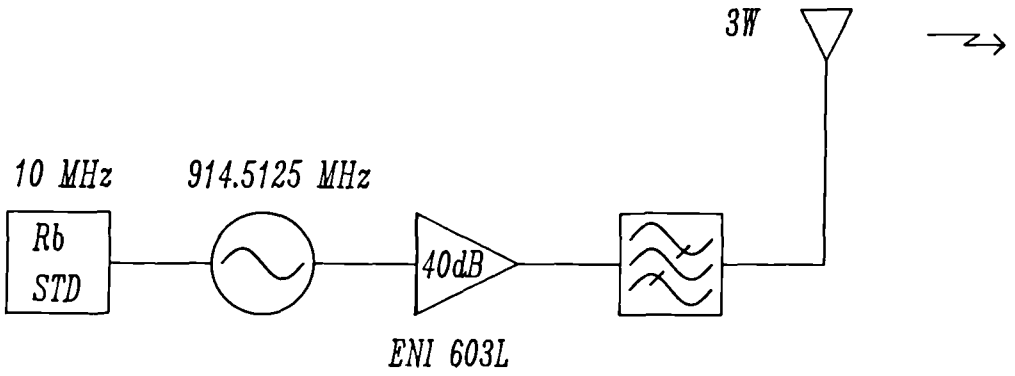

Figure 4.10 The transmitter system.

CHAPTER 5. EXPERIMENTAL PROCEDURE AND DATA REDUCTION.

5.1 INTRODUCTION.

In this chapter an outline of the experiments conducted using the dual branch receiver will be given. In addition, the procedure for digitising the data, which was recorded onto magnetic tape using a multitrack FM recorder, will be discussed. Finally, the initial data reduction, which was carried out on a mainframe computer, will be described.

5.2 EXPERIMENTAL PROCEDURE.

Two series of field trials were conducted during this work. In the first set, the transmitter was located at the mobile and the dual branch receiver at the base station. In the second set, the transmitter and receiver locations were reversed. The vehicle was driven around the test route, at a near-constant speed of 10m/s, for both sets of field trials. The test route, situated some 1.3km from the base station, was the same as that used in an earlier investigation[1]. The principal variable during these trials was the antenna separation between the vertically mounted $\lambda/2$ dipoles used in conjunction with the dual branch amplitude and phase measuring receiver. Three routes were used which had directions, relative to the base station, that were approximately radial(1) or circumferential(2). Each route was traversed in both directions, thus producing six sets of results for each value of antenna separation. The constant vehicle speed and choice of route enabled the data to be analysed in terms of the direction of vehicle motion and maximum Doppler frequency.

5.2.1 Receiver at the Base Station.

In this series of field trials a 3W CW signal was transmitted at 914.5125MHz from the mobile using a monopole antenna mounted on the roof of the vehicle. The scattered signal was received, at the base station, on two vertically mounted and vertically separated $\lambda/2$ dipole antennas. The base station was located on the roof of the Electrical Engineering Building some 35m above ground level. Data were recorded for each of the six routes for nineteen values of antenna separation. The separation between the antennas was adjusted, in steps of 1λ, from 2λ to 20λ.

This series of field trials was a reconstruction of an earlier investigation[1] in which only the signal envelope was recorded. In this more recent survey however quadrature detection was used which enabled both the envelope and phase of the received signal, to be measured. Figure 5.1 shows the test routes in relation to the receiver at the base station.

5.2.2 Receiver at the Mobile Station.

A 3W CW signal was transmitted at 914.5125MHz, from the base station, using a vertical monopole antenna. The receiver, now located at the mobile station, was connected to two vertically mounted and vertically separated $\lambda/2$ dipole antennas. A mast was mounted on the the roof of the vehicle which enabled the antennas to be displaced in $\lambda/2$ steps from[15] $\lambda/2$ to 4λ. The lower antenna was fixed at 1λ above the vehicle roof, which coincided with the optimum position for VSWR and the maximum number of antenna separations which could be easily accom-

---

[15] An antenna separation of exactly $\lambda/2$ could not be used otherwise the elements, of the two antennas, would come into contact with one another. The end elements, of the two antennas, were separated by a few cms where it was noted that little power was lost through cross-coupling.

modated. Again the vehicle covered all six routes for each of the antenna separations.

5.3 DATA DIGITISATION.

The in-phase and quadrature baseband signals from the two antennas, were recorded onto a multitrack analogue FM tape recorder. The analogue tapes were later replayed and the respective quadrature signals simultaneously digitised at a 1kHz rate. The Analogue to Digital Convertor(ADC) used was a 12-bit device with bipolar input ($\pm 2.5V$) which was operated by an IBM Personal Computer(PC). The IBMPC(model AT) also transferred the digitised data onto digital magnetic tape using two bytes per sample. The magnetic tape transport employed (EMI 8800) used an 8-bit byte format. The first recorded byte (lo-byte) stored the first eight bits of the sample and the second byte (hi-byte) contained the higher four bits of information, the upper 4-bits being masked.[16] The data bytes were recorded as coded ASCII characters. The data were recorded in the sequence I_1, Q_1, I_2 and Q_2 (where I_1 is the in-phase component of branch 1 etc.). The data were recorded in blocks of 4080 bytes i.e. 510 samples of each quadrature signal per block. The first record, or block, contained header information pertaining to the experimental configuration e.g. location of receiver, the antenna separation and vehicle route. The digital tapes were later read, decoded and subsequently analysed on the University's mainframe computer (IBM-3081).

---

[16] This lo-byte/hi-byte data storage method could be used for 16-bit information. However, since the ADC was a 12-bit device the upper 4 bits, of the hi byte, were unused and hence masked.

5.3.1 Data File Representation.

The first block of each data file contains information about the experimental arrangement. When the receiver was located at the base station the first five characters of the information block were used. The first two of these characters, 'VB', referred to Vertically spaced antennas at the Base station. The third and fourth characters provided the antenna separation in wavelengths (e.g. '20'). The fifth and final character indicated the test route e.g. 'A' (A to F for the six routes). A typical information character string would then be

VB20A

When the receiver was located at the mobile the first two characters again gave information regarding the test location and antenna arrangement. In this particular case a 'C' is used to represent tests with the receiver at the Car e.g 'VC'. The following three characters provide the antenna separation in 1/2dB steps with a 'P' being used to represent a decimal point e.g. 3P5 = 3.5 wavelengths separation. Again the final character is used to represent the test route for the file. A typical character string would thus be

VC3P5F

These character strings will appear on some of the graphs for the results (see Chapter 6) to provide information of the data source.

5.4 PRELIMINARY DATA REDUCTION.

In order to facilitate a study of the effects of antenna correlation and diversity improvement etc., the data were preprocessed prior to analysis. This data preprocessing was undertaken in two stages. Firstly, the data were decoded from the magnetic tape and secondly the data were converted into signal envelope values using the calibration information shown earlier in Figures 4.7 and 4.8.

5.4.1 Data Decoding.

The data on the digital magnetic tape was stored in ASCII format. The mainframe computer(IBM-3081) uses EBCDIC format, which is not directly compatible with that of the data tapes. The ASCII characters of the first block, which contain header information, are decoded by means of a 'look-up' table arrangement of corresponding characters. The raw baseband data are transformed by using the standard FORTRAN-77 character-to-integer function (ICHAR(arg)), together with the appropriate lo-byte and hi-byte transformation. The baseband signals were then converted from integer to bipolar voltages corresponding to the voltage outputs of the FM tape recorder.

5.4.2 Envelope Calibration.

The quadrature data, for each antenna, was used to store corresponding signal strength values of each associated envelope. The regression data shown in Figures 4.7 and 4.8 were used to convert the voltage quadrature information into relative signal strength values(dBm). In addition, the phase associated with each envelope is determined from the appropriate linear-valued component of the signal on each antenna.

5.5 ESTIMATION OF THE LOCAL MEAN.

The received signal envelope is composed of superimposed fast and slow fading components. To calculate the cross-correlation between the signals received on the two antennas and to assess the diversity improvement requires that the slow fading component, often called the local mean, is removed. To estimate the local mean a moving average method can be used. The received signal strength $R(t)$ can be represented as

$$R(t) = r(t) \bullet m(t) \tag{5.1}$$

where $m^2(t)$ is the local mean power, which is the total power of the incoming multipath waves arriving at the receiver, and $r(t)$ is a normalised received signal strength which varies quickly (i.e. fast fading). In an urban area, the number of multipath waves can be assumed to be very large, and thus $r(t)$ becomes a Rayleigh process having unity power.

An estimate of the local mean power, $m^2(t)$, at a time t_n, for a vehicle moving at a constant speed can be found from a series of N samples using the following moving average method

$$\hat{m}^2(t_n) = \frac{1}{N} \sum_{m=\frac{-(N-1)}{2}}^{m=\frac{(N-1)}{2}} \frac{R^2(t_{n+m})}{2} \tag{5.2}$$

where $\hat{m}^2(t_n)$ is the estimate of the local mean power. Using $\hat{m}^2(t_n)$ the estimated fast fading component $\hat{r}(t)$ is given by

$$\hat{r}(t_n) = \frac{R(t_n)}{\sqrt{\hat{m}^2(t_n)}} \tag{5.3}$$

This estimated fast fading (i.e. normalised signal) is used in the analysis of the cross-correlation between the envelopes and in the assessment of the statistics associated with the various diversity schemes.

The length of time over which m^2 is estimated is $T = N/f_s$, where f_s is the sampling period. If T is chosen too short then the local mean is poorly estimated, since the fast fading components are still present. If T is chosen too long the slow fading is largely lost. A satisfactory value for T, was determined in an earlier investigation[1] where it was found that the local mean could be estimated with an accuracy of between $\pm 1dB$ and $\pm 2dB$ for a normalised sample period of $f_D T = 16$. The vehicle speed of 10m/s corresponded with a maximum Doppler frequency of 33Hz. Thus the observation period was 0.5s, which

coupled with the 1 Hz sampling rate corresponded with a local mean averaging window of 501 points. Appendix E describes the effect of sample size and sampling rate (as a function of f_D) on the variance of of the estimated local mean signal strength (expressed in dB terms).

5.6 CONCLUSION.

The experimental procedure has been given for vertically spaced antenna measurements at the base and mobile stations. The digitisation, of the recorded data, has been described together with preliminary data reduction, which included decoding the magnetic data tapes and calibrating absolute signal strength values. The estimation of the local mean, which is used to normalise the data to the fast fading component only, has been described.

In the following chapter the normalised data are analysed in terms of statistics associated with a single branch, which were outlined in Chapter 2. In addition, the cross-correlation between signals received on two vertically separated antennas is analysed as a function of the antenna separation and their location. The improvement provided by several predetection diversity schemes is then assessed in terms simulated diversity using the data of the signals received on the two correlated antennas, as outlined in Chapter 3.

5.7 REFERENCES.

[1] Adachi, F., Feeney, M.T., Williamson, A.G. and Parsons, J.D., "Cross-correlation Between the Envelopes of 900MHz Signals Received at a Mobile Radio Base Station Site", IEE Proc. Pt.F, Vol.133, No.6. pp.506-512, 1986.

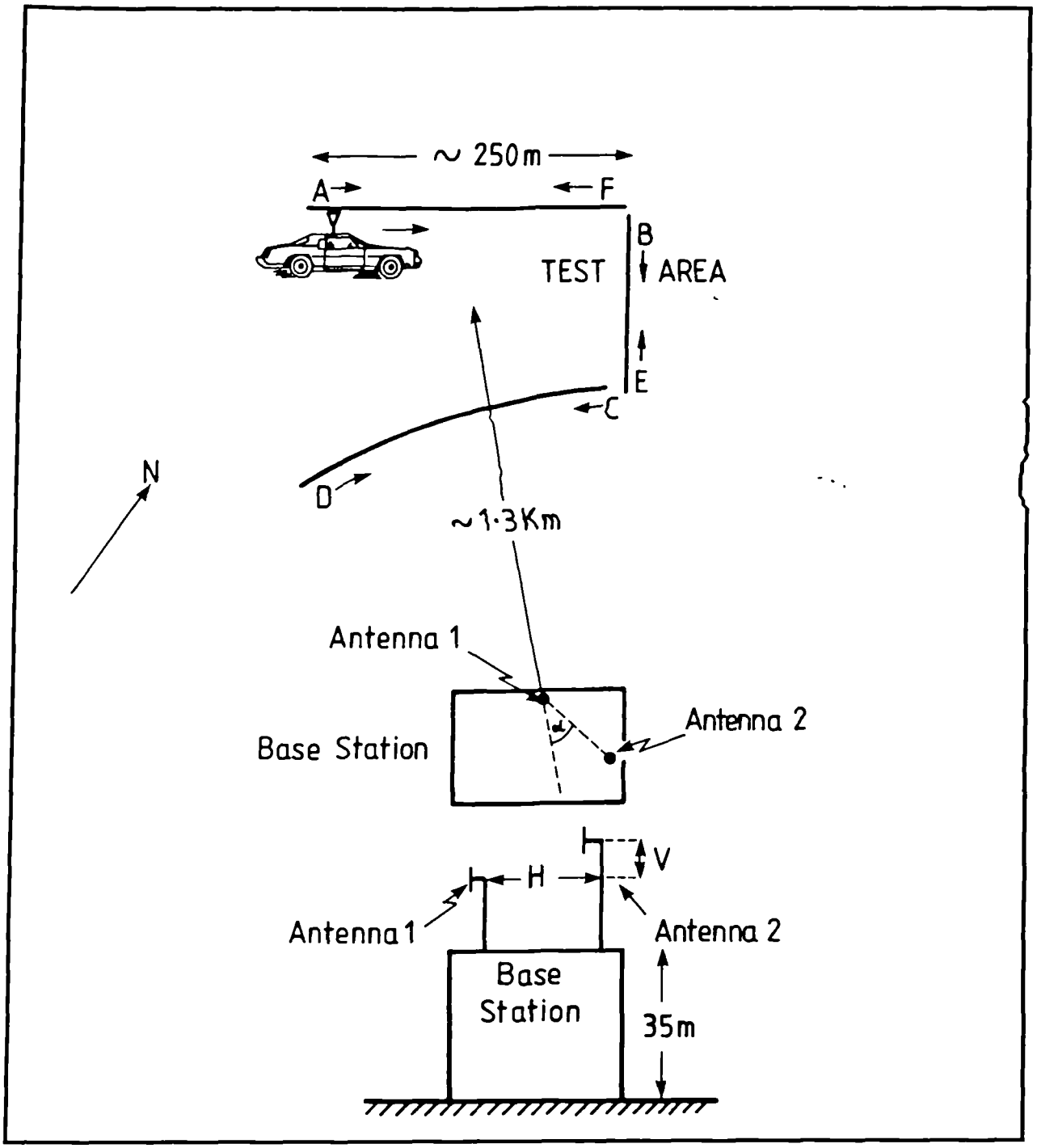

Figure 5.1 The test area in relation to the base station. Sections labelled A to F refer to the data routes. The vertical antenna separation is d_v.

CHAPTER 6. RESULTS.

6.1 INTRODUCTION.

Results of an investigation using the dual branch vector demodulator receiver with vertically spaced receiver antennas at both the mobile and base stations are presented in this chapter. The presentation is in three sections. Firstly, some single branch statistics are presented which show results that are in some cases compatible with a simple Rayleigh fading model whilst in others a dramatic departure is noted. Secondly, the measured cross-correlation between signals received on two vertically spaced antennas is determined for both mobile and base stations, and interpreted in terms of a scattering model which describes the cross-correlation in terms of a scattering geometry. Finally, results illustrating the performance of several simulated predetection diversity strategies using correlated signals are presented, in a similar statistical framework to that described in Chapters 2 and 3.

6.2 SINGLE BRANCH STATISTICS.

Before discussing the results of the various diversity strategies a brief presentation of some single branch statistics will be given. These results are discussed in terms of the theoretical expressions presented in Chapter 2.

6.2.1 The Quadrature Components.

The PDF and CDF of a typical pair of quadrature components (I and Q) detected by the receiver are shown in Figure 6.1. These signals were measured at the mobile and the results agree well with the theoretical PDF and CDF given in Chapter 2 (see equations 2.6 and 2.7 respectively). For the CDF, the ordinate has been scaled such that a normally-distributed variable appears as a straight line with a gradient inversely related to the standard deviation of the distribution.

6.2.2 The CDF of the Envelope.

The CDF of the received signal envelope is shown in Figure 6.2. The ordinate has been scaled such that the CDF of a Rayleigh-distributed envelope appears as a straight line. In this figure two situations have been plotted for comparison. Both the cases depicted were commonly observed when studying propagation in small cells in urban areas. Firstly, a Rayleigh-distributed envelope received at the mobile is shown as a straight line with a CDF accurately given by equation 2.11. In the second case (the curve) deep fades have been recorded at the base station which have a higher probability of occurrence than that observed for a pure Rayleigh fading envelope. The CDF of this latter case arises when a standing wave pattern occurs as a result of the superposition of direct and indirect propagation paths[1,2]. In the case recorded, 30dB fades have occurred approximately ten times more frequently than for a Rayleigh distributed signal. Naturally, this situation would present a serious impairment to information transmitted over such a channel. Indeed such propagation conditions might easily arise in microcellular systems where only a few propagation paths probably exist. In this situation diversity could provide a much improved signal, particularly if the signals received on the antenna branches are uncorrelated (see later sections).

6.2.3 The Received Signal Phase.

Figure 6.3 shows the received signal phase, differential phase (i.e. $\phi(t+1) - \phi(t)$) and envelope, for a typical section of data gathered at the mobile using the receiver. The seemingly abrupt phase changes which occur between 0° and 360° are not real but merely the way transitions between full cycles are plotted. The true large phase changes that occur can be seen to coincide with the deep fades as expected. The small scale ragged appearance of the phase is caused by phase noise resulting from small instantaneous differences in phase between the transmitter and receiver frequency sources (see Chapter 4).

Figure 6.4 shows the measured PDF of the phase, $p(\phi)$, and differential phase, $p(\dot{\phi})$, for a typical section of data. The PDF was measured in phase bins of 1° between 0° and 360°. The reference point, 0°, relates to the in-phase component of the received signal and increases in a counter-clockwise manner, i.e. $0° = I$, $90° = Q$, $180° = -I$, and $270° = -Q$. The measured PDF of the phase agrees well with that predicted by equation 2.30. In this case, since ϕ is in degrees the theoretical value for $p(\phi)$ is given by 1/360 i.e. 0.003, which can be seen as the horizontal line in the figure. The lower plot depicts the measured PDF of the differential phase, $p(\dot{\phi})$. Again, the measured values agree well with that predicted by theory (see Figure 2.11).

6.2.4 PDF of the Differential Phase as a Function of Envelope.

Figure 6.5 shows the conditional probability of the differential phase as a function of the fade depth i.e. $p(\dot{\phi}\,|\,R)$. This plot differs slightly from that given for the theoretical result (see equation 2.63 and Figure 2.12) in that the PDF has not been measured for a specific envelope value but over a range of fade depths. This method of data presentation has been used in order to show the trend of $p(\dot{\phi}\,|\,R)$ when a statistically small number of samples exist for specific envelope values. The form of the result, however, agrees well with theory in that the peak of the PDF

occurs at small $\dot{\phi}$, for the shallow fades whereas, large values of $\dot{\phi}$ are clearly associated with the deep fades, especially when $-10 \leq R \leq -6dB$ and $1 \leq |\phi/\omega_D| \leq 3$.

6.2.5 PDF of the Phase Gradient.

The probability density function of phase gradient as a function of time, or spatial, difference is shown in Figure 6.6. The result shown agrees well with that predicted by equation 2.38. The differences between the experimental and predicted values can be accounted for in the uncertainty of the vehicle speed, which is directly related to l/λ (see equation 2.38 and Figure 2.6). Clearly the PDF maximises at large phase differences (*e.g* π) as $l/\lambda \rightarrow 0.5$. When $l/\lambda \simeq 0.38$ the PDF is approximately constant across the range of $\Delta\phi$. This situation coincides with the samples, at l/λ apart, being independent of one another. In terms of equation 2.38 the normalised autocovariance function is zero and hence $p(\Delta\phi)$ or $p(\phi_1, \phi_2) = p(\phi_1) \bullet p(\phi_2) = 1/4\pi^2$.

6.2.6 The RF Input Spectrum.

In order to determine the spectrum of the RF input signal, the quadrature complex autocorrelation coefficients were first determined for 512 delays using 5000 points of data (i.e. 5 seconds). The complex correlation coefficient for a given delay was then determined using equation (6.5)[17] with z_2 forming the delayed, but replicated, data samples of z_1. The spectral components of the Doppler RF input spectrum were computed using a complex FFT (Fast Fourier Transform) routine[3]. Prior to the Fourier transform however, the data samples were shaped using a Hammin window[4] which combined good frequency resolution with minimum spectral leakage. The FFT routine was carried out over

---

[17] See section 6.3 and therein.

1024 points (i.e. a power of two for fast computation) which, together with a sampling frequency of 1 Hz provided a spectral resolution of 0.97Hz from -500Hz to +500Hz (i.e. the negative and positive Nyquist frequencies). A complex FFT routine[3, 5 and 6] was used in order that both positive and negative Doppler components could be resolved. Several overlapping spectra were determined for each section of data. These spectra were then averaged to provide a representative spectrum for the route. The extent of the overlapping used was half the length of the FFT, i.e. 512 (approximately half a second).

Figures 6.7 and 6.8 show two contrasting cases of Doppler spectra. The upper plot in each figure shows the real part of the complex autocorrelation function, whilst the lower plot depicts the computed spectrum of the carrier, translated to baseband. In the first example the autocorrelation and spectrum closely resemble that predicted in Chapter 2 with sharp frequency cut-offs occurring at $\pm f_D$. In the second example, which was not untypical, the spectrum departs dramatically from that predicted by theory. The dominant components in the spectrum suggest that for some periods along the route a propagation mode existed in which the received signal vector did not move in a random manner, in the I/Q plane. Such a situation might arise in several ways, for example if a dominant direct path existed, the arrival angle of the multipath waves was non-uniform, the multipath waves do not posses a uniformly distributed phase or the combined multipath waves resulted from propagation in elevation as well as azimuth (see Chapter 2). For propagation in very small cells these points probably become increasingly more important. As a result therefore, it could be expected that the Doppler spectrum, for small cells, would differ from that expected under pure Rayleigh fading conditions.

6.2.7 The Envelope Spectrum.

The spectrum of the fading envelope was determined by carrying out a real FFT on the measured autocorrelation coefficients of the envelope.

Again, the autocorrelation coefficients were first transformed using a Hammin window prior to Fourier transformation into spectral values. The same parameters were used for the autocorrelation size and number of lags etc. as those discussed earlier in the previous section.

Figures 6.9 and 6.10 show two contrasting cases of envelope spectrum for the same sections of data used in the previous discussion. In the first case the envelope autocorrelation function (upper plot) and envelope spectrum (lower plot) clearly resemble that predicted in Chapter 2 with a sharp frequency cut-off occurring at $2f_D$. The second example (Figure 6.10) shows a case where the measured values differ markedly from that predicted by theory. This is most noticeable in the spectrum where there is no abrupt frequency cut-off. Indeed the spectrum shows a general decrease in spectral power with increasing frequency, instead of the usual flat response up to the sharp cut-off at $2f_D$. The same explanation is offered for the differences between the two cases as that used in the previous section. The apparent lack of spectral content below 2Hz, in both cases, is solely due to this region of the spectrum being removed by the normalisation of the envelope (see Chapter 5).

6.2.8 The Random FM Spectrum.

Figure 6.11 shows the measured random FM spectrum for a single branch at the base station together with that predicted by theory (see equations 2.64 to 2.66 and Figure 2.13). The spectrum was determined by Fourier transforming the measured autocorrelation function of $\dot{\phi}$. The autocorrelation function was determined using a window of 1500 points and 128 lags. A real FFT routine[3] was used with 512 points which, with points sampled at 1kHz, gave a frequency resolution of 1.95Hz. The spectral values plotted represent data averaged over spectral segments of 39Hz. The measured random FM spectrum agrees well with theory, the greatest energy being concentrated at the lower frequency and the energy of the higher frequency falling asymptotically.

The predicted spectrum was determined by Fourier transforming equation (2.65).

6.3 CROSS-CORRELATION BETWEEN VERTICALLY SPACED ANTENNAS.

Having presented examples of the statistics derived from measurements using a single branch, we now turn attention to the matter of diversity reception. Firstly we present some measured results for the cross-correlation between signals received on vertically separated antennas at both the base and mobile stations. In a previous study[7] the cross-correlation between the envelopes of signals received on two base station antennas was measured for both vertical and horizontal antenna separations. The normalised envelope cross-correlation, ρ_{env} , was calculated using[7]

$$\rho_{env} = \frac{\overline{\hat{r}_1\hat{r}_2} - \overline{\hat{r}_1}\,\overline{\hat{r}_2}}{\sqrt{\overline{\hat{r}_1^2} - \overline{\hat{r}_1}^2}\sqrt{\overline{\hat{r}_x^2} - \overline{\hat{r}_x}^2}} \tag{6.1}$$

$\overline{\hat{r}_n} = \overline{\hat{r}_n}(t)$ is the arithmetic average of the estimated fast fading component (see Chapter 5) of antenna n. Subsequent analyses[8,9] made use of the fact that $\rho_{env} \simeq |\rho_{12}|^2$ [10,11] where $|\rho_{12}|$ is the modulus of the complex correlation between antennas 1 and 2. In the present work, the vector demodulator receiver provides the necessary quadrature information to measure ρ_{12} directly. If we represent the complex signal received on antenna 1 as z_1 and that on antenna 2 as z_2 then the complex cross-correlation between the signals received on the two antennas is defined as [12]

$$\rho_{12} \equiv \frac{\mathrm{COV}(z_1, z_2)}{\sigma(z_1)\sigma(z_2)} \tag{6.2}$$

Since z_1 and z_2 are complex, the signals can be expressed in terms of the quadrature components, I and Q as

$$\begin{aligned} z_1 &= I_1 + jQ_1 \\ z_2 &= I_2 + jQ_2 \end{aligned} \tag{6.3}$$

In equation (6.2) the terms of the complex correlation are

$$\begin{aligned} \mathrm{COV}(z_1, z_2) &= \text{Covariance between } z_1 \text{ and } z_2 \\ \sigma(z_1) &= \text{Standard deviation of } z_1 \end{aligned}$$

Also

$$\begin{aligned} \mathrm{COV}(z_1, z_2) &\equiv E\{(z_1 - E\{z_1\})^*(z_2 - E\{z_2\})\} \\ \sigma(z_1) &\equiv \sqrt{E\{|z_1 - E\{z_1\}|^2\}} \end{aligned} \tag{6.4}$$

Where E{.} is the expectation of the variate (see Chapter 2). Combining equations 6.2 and 6.4, the complex correlation between the signals received on antennas 1 and 2 is given by[18]

$$\rho_{12} = \frac{< (z_1 - < z_1 >)^*(z_2 - < z_2 >) >}{\sqrt{< |z_1 - < z_1 > |^2 >}\sqrt{< |z_2 - < z_2 > |^2 >}} \tag{6.5}$$

The complex cross-correlation, ρ_{12}, was determined for each setting of antenna separation at both the mobile and base stations using two sec-

---

[18] Again, as in Chapter 2 $< . > = E\{.\}$ has been used for clarity of expression.

ond segments of data[7] each of which was approximately Rayleigh distributed.

6.3.1 Cross-correlation at the Base Station.

From experimental data, the complex cross-correlation, ρ_{12}, was determined, using equation (6.5), for each of the antenna separations and for each of the routes travelled. Values of ρ_{12} were found for antenna displacements of 2λ to 20λ in steps of 1λ. Figure 6.12 shows $|\rho_{12}|^2$ plotted against antenna separation, for radial and circumferential routes. The values of $|\rho_{12}|^2$ shown in Figure 6.12 agree well with values of ρ_{env} found in an earlier study[7] from measurements taken over the same routes. It is generally accepted[11] that for $|\rho_{12}|^2 \leq 0.7$ an improvement in performance can be achieved using a two branch diversity system. In the case of vertical antenna separation at the base station values of $|\rho_{12}|^2 \leq 0.7$ can be achieved for antenna separations of 8λ to 13λ for the various routes surveyed. This result agrees well with that found in the earlier investigation[7] where $\rho_{env} \leq 0.7$ was achieved for antenna separations of 11λ to 13λ.

6.3.2 Cross-correlation at the Mobile Station.

In this case, the complex cross-correlation, ρ_{12}, was calculated, using equation (6.5), for measurements using two vertically spaced antennas at the mobile, for the same routes. Values of ρ_{12} were found for antenna displacements of 0.5λ to 4.0λ in steps of 0.5λ. Figure 6.13 shows $|\rho_{12}|^2$ plotted against antenna separation for each of the routes. Regardless of the route travelled, a value of $|\rho_{12}|^2 \leq 0.7$ can be achieved for antenna separations $\lesssim 1.0\lambda$,[19] which, at 1GHz, is physically small ($\simeq$ 33cm). This

[19] Values of $|\rho_{12}|^2 \leq 0.7$ can be achieved at antenna separations $\simeq 0.5\lambda$. However, this value

suggests that, using vertical separation, a small, unobtrusive space diversity antenna could be constructed for use on mobiles. Horizontally-spaced antennas are not an attractive proposition for vehicular use.

6.3.3 Comparison of Envelope and Complex Cross-correlation.

The cross-correlation between the envelopes (ρ_{env}) of the signals received on two spaced antennas was calculated for a radial route, together with the corresponding complex cross-correlation ρ_{12}. The two cross-correlation parameters are shown in Figure 6.14 for one of the routes. This figure shows that ρ_{env} is generally a good approximation to $|\rho_{12}|^2$ [11,13] i.e. $\rho_{env} \simeq |\rho_{12}|^2$ and suggests that it is reasonable to employ conventional signal strength envelope-detection receivers to measure the magnitude of the cross-correlation between signals received on spatially separated antennas.

In the following section a scattering model is used to explain the cross-correlation between the signals received on the two branches, in terms of scatterers in the vicinity of the mobile. This model is based upon the statistical relationship between two complex phase-related signals received on two vertically-spaced antennas. The phase relationship, between the two complex signals, is modelled in terms of the angle of the received multipath waves waves relative to the scatterers surrounding the mobile.

6.3.4 Theoretical Analysis of Cross-correlation using a Scattering Model.

Consider the transmission from a moving vehicle received by two vertically spaced antennas at the base station. It is assumed that no line

is not quoted since at this antenna separation some coupling will occur between the two antennas and thus reduce the received signal power.

of sight propagation path exists, and that all the waves received at the base station come from scatterers surrounding the mobile unit. It is further assumed that there are no local scatterers at the base station, and that the distance between the mobile and base stations is much greater than the antenna separation. The coordinate system (for vertical separation of the antennas) at the base station is shown in Figure 6.15. If we represent the complex signal received on antenna 1 as z_1 and that on antenna 2 as z_2 then

$$z_1(t) = \sum_{n=1}^{N} E_n \exp\{j[(\omega_c + \omega_n)t + \theta_n]\} \tag{6.6}$$

$$z_2(t) = \sum_{n=1}^{N} E_n \exp\left\{j[(\omega_c + \omega_n)t - \frac{2\pi}{\lambda} d_v \sin \varepsilon_n + \theta_n]\right\} \tag{6.7}$$

where

E_n = Amplitude of n^{th} wave.
ω_c = Nominal carrier angular frequency.
ω_n = Angular frequency of n^{th} wave.
d_v = Vertical antenna separation.
ε_n = Elevation angle of n^{th} wave.
θ_n = Phase of n^{th} wave.

Since the multipath waves come from different scatterers, the random phases, θ_n are independent. Substituting (6.6) and (6.7) into (6.5) and noting that for a Rayleigh process $< z_1 > = < z_2 > = 0$ the complex cross-correlation, ρ_{12}, is given by

$$\rho_{12} = \frac{\frac{1}{2}\sum_{n=1}^{N} E_n^2 \exp\left\{ -j\left[\frac{2\pi}{\lambda} d_v \sin \varepsilon_n \right] \right\}}{\frac{1}{2}\sum_{n=1}^{N} E_n^2} \tag{6.8}$$

Assuming the multipath waves all have identical amplitude ($E_n = E$) then ρ_{12} becomes

$$\rho_{12} = \frac{1}{N}\sum_{n=1}^{N} \exp\left\{ -j\left[\frac{2\pi}{\lambda} d_v \sin \varepsilon_n \right] \right\} \tag{6.9}$$

If we assume a large number of received waves with a PDF in elevation given by $p(\varepsilon_n)$ then (6.9) can be replaced by an integral over $p(\varepsilon_n)$ such that

$$\rho_{12} = \int_{-\pi}^{\pi} \exp\left\{ -j\left[\frac{2\pi}{\lambda} d_v \sin \varepsilon_n \right] \right\} p(\varepsilon_n)\, d\varepsilon_n \tag{6.10}$$

In addition, we assume $p(\varepsilon_n)$ to be Gaussian distributed and centred at an angle ε_v. This angle (ε_v) is the angle of elevation of the mobile relative to the base station. The PDF of the multipath waves in elevation for a Gaussian distribution is therefore given by

$$p(\varepsilon_n) = \frac{1}{\sqrt{2\pi}\,\sigma} \exp\left\{ -\frac{(\varepsilon_n - \varepsilon_v)^2}{2\sigma^2} \right\} \tag{6.11}$$

6.3.4.1 Vertically Spaced Antennas at the Base Station.

The elevation angle at which the multipath waves are centred is given by the relative height of the base station with respect to the mobile test area (approx 35m in this case) and the distance of the test area from the base station (1.3km), i.e.

$$\varepsilon_v = \tan^{-1}\left(\frac{35}{1300}\right) = 1.5^\circ \tag{6.12}$$

Since ε_v and the spread in ε_n are small, the directivity of the two $\lambda/2$ dipoles in elevation (*i.e.* $G(\varepsilon)$) need not be considered here (*i.e.* $G_1(\varepsilon) = G_2(\varepsilon) \simeq 1$).

The cross-correlation, $|\rho_{12}|^2$, can thus be determined by numerically integrating equation (6.10). Alternatively, an approximate closed form solution to $|\rho_{12}|^2$, is available[7] which relates the cross-correlation with the vertical antenna separation (d_v), the distance of the mobile from the base station (L) and the distance of the scatterers from the mobile (r_v), this being

$$|\rho_{12}|^2 \simeq \exp\left\{ -\left[\frac{2\pi}{\lambda} \frac{d_v r_v \sin\varepsilon_v \cos\varepsilon_v}{L} \right]^2 \right\} \tag{6.13}$$

Figure 6.16 shows theoretical values of $|\rho_{12}|^2$ plotted using equation (6.13) for various values of σ (in 6.11). The results in Figure 6.16 suggest that σ lies between 1° and 1.4°. From Figure 6.15, σ is given by

$$\sigma = \frac{r_v \sin\varepsilon_v}{L} \tag{6.14}$$

which suggests that the distance of the scatterers from the mobile (*i.e.* $r_v \sin\varepsilon_v$) is some 22.7 to 31.8m.

6.3.4.2 Vertically Spaced Antennas at the Mobile.

In this situation care has to be taken in numerically integrating equation (6.10) because, at the mobile, ε_v is not necessarily the same as that used for vertically separated antennas at the base station. The reason for this is the way the mobile views the incoming multipath waves which arrive at various angles from the scatterers. In addition, the directivity of the vertically displaced $\lambda/2$ dipoles must also be considered. For a vertical $\lambda/2$ dipole the antenna directivity is given by[14]

$$G_1(\varepsilon) = G_2(\varepsilon) = G(\varepsilon) = \frac{\cos\left\{ \frac{\pi \sin \varepsilon}{2} \right\}}{\cos \varepsilon} \tag{6.15}$$

In this situation $|\rho_{12}|^2$ is given by[15]

$$|\rho_{12}|^2 = \frac{\left| \int_{-\pi}^{\pi} G_1^*(\varepsilon) G_2(\varepsilon) \exp\left\{ -j\left[\frac{2\pi}{\lambda} d_v \sin \varepsilon \right] \right\} p(\varepsilon) d\varepsilon \right|^2}{\int_{-\pi}^{\pi} G_1^*(\varepsilon) G_1(\varepsilon) p(\varepsilon) d\varepsilon \int_{-\pi}^{\pi} G_2^*(\varepsilon) G_2(\varepsilon) p(\varepsilon) d\varepsilon} \tag{6.16}$$

In other words, the multipath amplitudes (E_n) and the PDF of the arrival angles in elevation in equation (6.8) are now modified by the directivity of the two antennas.

The complex cross-correlation between the signals on the two antennas was calculated using equation (6.16) for various values of σ. Figure 6.17 shows curves of $|\rho_{12}|^2$ at several values of σ. In this situation σ clearly lies between 3° and 6°. The value of σ can be interpreted as the effective angular radius of the scattering volume as viewed by the vertically spaced antennas. If we consider the angular diameter of the

scattering volume (i.e. 2σ)[20] then the mobile views the scatterers as 6° to 12° in cross-section whereas the base station views the volume as some 2° to 2.8° in cross-section. Hence the mobile antennas have a smaller cross-correlation, for a given separation, compared with that experienced by the base station antennas.

To conclude this section on the measured cross-correlation between signals received on two vertically displaced antennas, we can summarise as follows; a branch cross-correlation of ≤ 0.7, when diversity becomes useful, can be achieved at the base station for antenna separations of 8λ to 13λ for cells of a few km in radius. This arrangement at the base station is particularly useful in that, little roof-top space is required and, unlike horizontally spaced antennas, is not dependent on the relative position of the mobile with respect to the base station. When the diversity antennas are located at the mobile, vertical displacements of only 1λ are required to obtain values of $|\rho_{12}|^2 \leq 0.7$. This is of particular importance as system manufacturers believe that horizontally spaced antennas on the mobile are unacceptable to their customers. Two vertically spaced antennas could be designed to appear as a single antenna which might be acceptable to the consumer. The small separation required at the mobile, compared with that necessary at the base station, is a direct consequence of the uniform angle of arrival of the multipath waves at the mobile and the proximity of the scatterers compared with that experienced at the base station. In addition, it has been shown experimentally that the envelope cross-correlation, ρ_{env}, is a good approximation to the square of the modulus of the complex cross-correlation, i.e. $|\rho_{12}|^2$, between the signals received on two antennas.

---

[20] For a Gaussian distribution of ε_n 63% of the multipath waves arrive within $\pm\sigma$ (i.e. 2σ across).

6.4 DIVERSITY RESULTS.

Results illustrating the performance of the various diversity strategies in terms of the CDF, LCR and AFD of the envelope, for data received by two vertically spaced antennas at the base station, have been presented elsewhere[8,9]. In this section results for the CDF, LCR and AFD will be presented only for data received at the mobile station. These statistical parameters are presented in terms of the normalised equivalent envelope, i.e. the slow fading component is removed (see Chapter 5). The procedure allows a comparison of the improvement provided, in respect of the fast fading, by each of the diversity strategies considered. The small antenna separations involved essentially means that both branches record the same local mean variation. The normalisation of each branch signal by its own local mean value also removes any differences between the overall signal power received by each antenna. In this study the antenna separations used at the mobile are sufficiently small that the differences between the signal powers received on the two antennas was $\leq 1dB$ which has little effect on the performance improvement at the antenna separation of interest. The various spectra and random FM statistics will be presented for data gathered at both the mobile and base stations.

6.4.1 CDF of the Received Envelope.

The CDF of the received envelope at the mobile using antennas vertically separated by $2\lambda(|\rho_{12}|^2 = 0.41)$ for the various diversity strategies (-10dB switching threshold for SAS) is shown in Figure 6.18. The results for MRC, EGC and SEL agree reasonably well with those predicted by theory (see Figure 3.3). The differences between the measured and predicted values can be explained in terms of the measured data having an appreciable value of correlation (0.41) compared with the value of zero assumed in the theoretical case. This can clearly be seen in the case of SAS where the measured data departs significantly from that in Figure 3.3. This is to be expected since in Chapter 3 it was observed that

the SAS strategy is more susceptible to a degradation in performance as a function of increasing correlation. In addition the measured CDFs for the individual branches show a slightly increased probability of deep fades occurring than that predicted for a pure Rayleigh fading environment (see equation 2.11 and Figure 2.4). This suggests that for some period during the length of section A there existed a propagation mode of only a few multipaths (see earlier discussion for a more extreme case). Obviously SAS is more susceptible to such propagation conditions because of its inherent dependence upon the fade falling below the threshold level, which will occur more frequently than for the pure Rayleigh fading case. The other strategies are however remarkably resilient to such a deleterious propagation mode.

6.4.1.1 The CDF of the Envelope as a Function of the Branch Correlation.

The CDF of the envelope for various values of correlation between the two branches is plotted in Figure 6.19 for the MRC case. The antenna separations used are $1\lambda, 2\lambda$ and 4λ which, for this route, correspond to values of $|\rho_{12}|^2$ of 0.68, 0.46 and 0.1 respectively. The experimental values agree well with those predicted in Chapter 3 (see equation 3.33 and Figure 3.4). Again the differences between the measured values and theory can be attributed to slight differences between the measured values of $|\rho_{12}|^2$ and those used in the theory and the fact that the single branch statistics show a slightly increased probability of deep fades occurring than that encountered in pure Rayleigh fading conditions.

Figure 6.20 shows the CDF for different values of correlation for the SAS strategy, using a -10dB switching threshold, for the same section of data as that used for the MRC case above. Immediately apparent in this figure is the fact that the performance of the SAS strategy is highly dependent upon the degree of correlation between the branches, in contrast to that for the MRC case. This feature of the SAS strategy was outlined earlier in Chapter 3 (see equation 3.33 and Figure 3.6).

6.4.2 Level Crossing Rate and Average Fade Duration.

The LCR and AFD of the received envelope at the mobile for an antenna separation of $2\lambda(|\rho_{12}|^2 = 0.41)$ for the MRC, EGC and SEL strategies is shown in Figures 6.21 and 6.22 respectively. In the context of Figure 6.21 the term 'normalised LCR' refers to the measured LCR divided by the maximum Doppler frequency, f_D, which for these experiments was approximately 30Hz. The 'normalised AFD', is simply the measured AFD multiplied by f_D. The form of the experimental results agree well with those predicted by theory (see equations 3.37 and 3.38 and Figure 3.7). The differences between the experimental and theoretical results can be attributed to two sources. Firstly, the theoretical values for N_R and τ_R were determined for zero correlation, whereas the experimental values have an appreciable value of $|\rho_{12}|^2 = 0.41$. Secondly, the normalisation of N_R and τ_R have a certain degree of error associated with them as a result of an inaccurate knowledge of the vehicle speed.

Figures 6.23 and 6.24 shows N_R and τ_R for the SAS strategy using a threshold level of -10dB. Again differences between the experimental and theoretical values can be attributed to the same causes as those discussed above.

6.4.2.1 LCR and AFD as a function of Correlation.

The LCR for different values of correlation between the branches is plotted in Figures 6.25 and 6.26 for the MRC and SAS cases respectively. Again antenna separations of $1\lambda, 2\lambda$ and 4λ have been used with corresponding values of correlation of 0.68, 0.46 and 0.1 respectively. The results agree well with those predicted earlier (see equations 3.40 and Figure 3.8). The differences between experimental and theoretical values can be attributed to the same causes outlined earlier. Clearly the

MRC strategy is quite resilient to increasing values of cross-correlation, whereas the SAS strategy shows a rapidly decreasing degree of improvement with increasing branch correlation.

The AFD for different values of correlation is not plotted here as $|\rho_{12}|^2$ had little effect on τ_R, which remained approximately halved. This result agrees well with that found earlier[8,9] for signals received at a base station site.

6.4.3 The RF Input Spectrum for SEL and SAS Diversity Strategies.

The RF input spectrum was determined for each of the two individual branches and the equivalent signal output for SEL and SAS diversity strategies. In the case of SAS the spectrum was determined for switching thresholds of -5dB to -20dB in steps of -5dB. The two antennas, situated at the base station, were separated by 5λ which corresponded to a value of $|\rho_{12}|^2 = 0.87$. Although the diversity improvement will be minimal at such a high value of cross-correlation, this example is chosen to clearly illustrate both the beneficial and detrimental effects of diversity due to the degree of cross-correlation and consequent switching between branches. The spectra were determined using the same methods outlined earlier for the single branch analysis. Figures 6.27 and 6.28 show the autocorrelation and spectra for the SEL and SAS (-10dB threshold) strategies respectively. The effect of each diversity strategy can clearly be seen. Overall, each strategy basically reduces the power of the lower spectral components at the cost of some spectral broadening. This spectral broadening can be explained in terms of the abrupt switching, that occurs in both diversity strategies, between the two branches. The abrupt change between branches causes a discontinuity to occur in the complex sequence which results in a more impulsive autocorrelation function. Such an autocorrelation function, or complex sequence, when Fourier transformed causes a broadening of the spectral content of the information. SAS diversity shows the largest

spectral broadening because of the larger discontinuities that occur in the complex sequence when switching between branches. Naturally, the choice of switching threshold will alter the switching rate and hence the rate of discontinuity occurrence which affects the degree of spectral broadening.

6.4.4 The Envelope Spectrum with Diversity.

The spectrum of the envelope was determined for each of the individual branches and the equivalent envelope for each of the various diversity strategies. The spectra were determined in the manner described earlier. Figure 6.29 and 6.30 show the envelope spectra for MRC and SAS (-10dB threshold) respectively. Although the maximum Doppler frequency, f_D, appears little changed with diversity the overall effect of the various strategies is to reduce the spectral content of the higher frequency components, whilst increasing that of the lower values. This phenomen ո is associated with diversity smoothing out the envelope time series. Again the abrupt changes in the diversity envelope, for SAS, results in a more impulsive-like autocorrelation function which when Fourier transformed causes broadening of the spectrum beyond $2f_D$.

6.4.5 Random FM.

The PDF, and hence CDF, of the random FM component, i.e. $\dot{\phi}$, was determined for data gathered at the base station using simulated SEL and SAS diversity strategies. The CDFs of $\dot{\phi}$, $P(\dot{\phi})$, are plotted in Figure 6.31 for an antenna separation of 15λ on route A ($|\rho_{12}|^2 = 0.53$) for a single branch and SEL diversity together with SAS using switching thresholds of -5dB to -20dB in 5dB steps. The SEL strategy shows the largest improvement with SAS showing a best performance at a switching threshold of -10dB. The SEL results agree well with expected values given by equation (3.47) and shown in Figure 3.9. The measured single

branch values of $P(\dot{\phi})$ are slightly worse than than those expected theoretically because $\dot{\phi}$ exists in the data not only as a result of the channel but also because of phase noise introduced by the transmitter and receiver frequency sources (see Chapter 4). In addition, discrepancies between experimental values and those predicted by equation (3.47) can be explained in terms of the non-zero correlation between the branches. The theoretical values of $P(\dot{\phi})$ assume independent branches. The tendency for the measured data to show too large a reduction in $P(\dot{\phi})$ at high values of normalised frequency is attributed to the lack of statistical values at such extreme excursions in phase difference.

Figure 6.32 shows $P(\dot{\phi})$ for selection diversity as a function of antenna separation from 5λ to 20λ in steps of 5λ, which corresponds to correlation ($|\rho_{12}|^2$) values of 0.92, 0.81, 0.53 and 0.42 respectively. This figure shows that SEL diversity can significantly reduce the random FM component even at high values of correlation.

Figure 6.33 shows $P(\dot{\phi})$ for SAS diversity, using a switching threshold of -10dB, for the same data as discussed above. Although the switching threshold chosen was near optimum, SAS diversity clearly does not provide the same improvement in reducing the random FM noise as SEL diversity. Indeed, SAS diversity shows little improvement in reducing the random FM noise at high values of normalised frequency.

6.5 CONCLUSION.

The signal received from propagation measurements in small cells showed that in general the phase statistics differ little from those predicted for a purely Rayleigh fading environment. In some, not uncommon, cases the measured CDF of the envelope showed a considerably higher preponderance of deep fades than that expected for Rayleigh fading. In addition, the Doppler and envelope spectra sometimes exhibited markedly different forms than those predicted by Rayleigh fading.

The causes of the departure from Rayleigh, which becomes increasingly apparent in well-illuminated small cells, is largely due to dominant propagation paths and/or significant contributions to the summed multipath components from waves propagating out of the horizontal plane (see Chapter 2).

Results have been presented for the measured correlation (complex and envelope) between vertically separated antennas at the base and mobile stations. Two scattering models have been presented to describe the degree of correlation as a function of antenna separation and reception geometry for both stations. Both sets of results show that vertically separated antennas can provide a sufficient degree of decorrelation for practical diversity to be employed at both base and mobile stations with unobtrusive antenna arrangements requiring little space.

Various predetection diversity schemes have been simulated using data received on the dual branch vector demodulator receiver. Results comparing the diversity strategies have been presented in terms of the envelope statistics for the mobile case only. Statistics associated with the phase have been presented for both the mobile and base station cases. These results show that significant diversity improvement can be achieved at both stations using practical antenna separations. MRC showed the biggest improvement in signal statistics, even at high values of branch correlation. SAS provided significant improvement in the signal statistics provided that the cross-correlation between the branches is low. Both of these results confirm the findings presented in Chapter 3.

In the following chapter the concluding results of this investigation will be given in detail. In addition, recommendations for future work will be presented in the framework of the research carried out in this investigation.

6.6 REFERENCES.

[1] Lee, W.C.Y., "Mobile Communications Engineering", McGraw-Hill, New York, 1982.

[2] Davis, B.R. and Bogner, R.E., "Propagation at 500MHz for Mobile Radio", IEE Proc. Pt.F, Vol.132, No.5, pp.307-320, 1985.

[3] Weinstein, C.J. (Ed), "Programs for Digital Signal Processing", Digital Processing Committee, IEEE Acoustics, Speech and Signal Processing Society, IEEE Press, 1979.

[4] Harris, F.J., "On the Use of Windows for Harmonic Analysis with the Discrete Fourier Transform", Proc. IEEE, Vol.66, No.1, pp.51-83, 1978.

[5] Elliot, D. and Rao, K.R., "Fast Fourier Transforms; Algorithms, Analyses, Applications", Academic Press, New York, 1982.

[6] Ramirez, R.W., "The FFT: Fundamentals and Concepts", Tektronix/Prentice-Hall Englewood Cliffs, N.J., 1985.

[7] Adachi, F., Feeney, M.T., Williamson, A.G. and Parsons, J.D., "Cross-correlation Between the Envelopes of 900MHz Signals Received at a Mobile Radio Base Station Site", IEE Proc. Pt.F, Vol.133, No.6, pp.506-512, 1986.

[8] Adachi, F., Feeney, M.T. and Parsons, J.D., "An Evaluation of Specific Diversity Combiners Using Signals Received by Vertically Spaced Antennas", J. IERE Vol.57, No.6 (Supplement), pp.S218-S224, 1987.

[9] Adachi, F., Feeney, M.T. and Parsons, J.D., "Effects of Correlated Fading on Level Crossing Rate and Average fade Duration with Predetection Diversity Combiners", IEE Proc. Pt.F, Vol.135, No.1, pp.11-17, 1988.

[10] Jakes, W.C. (Ed), "Microwave Mobile Communications", John Wiley and Sons, New York, 1974.

[11] Brennan, D.G., "Linear Diversity Combining Techniques", Proc. IRE, 47, No.6, pp.1075-1102, June 1959.

[12] Papoulis, A., "Probability Random Variables and Stochastic Processes", McGraw-Hill, 11th print, 1981.

[13] Schwartz, M., Bennett, W.R. and Stein, S., "Communication Systems and Techniques", McGraw-Hill, New York, 1966.

[14] Lee, K.F., "Principles of Antenna Theory", John Wiley and Sons, New York, 1984.

[15] Yamada, Y., Ebine, Y. and Nakajima, N., "Base Station/Vehicular Antenna Design Techniques Employed in High-Capacity Land Mobile Communications Systems", Rev. Elec. Comms. Labs., Vol.35, No,2, pp.115-121, 1987.

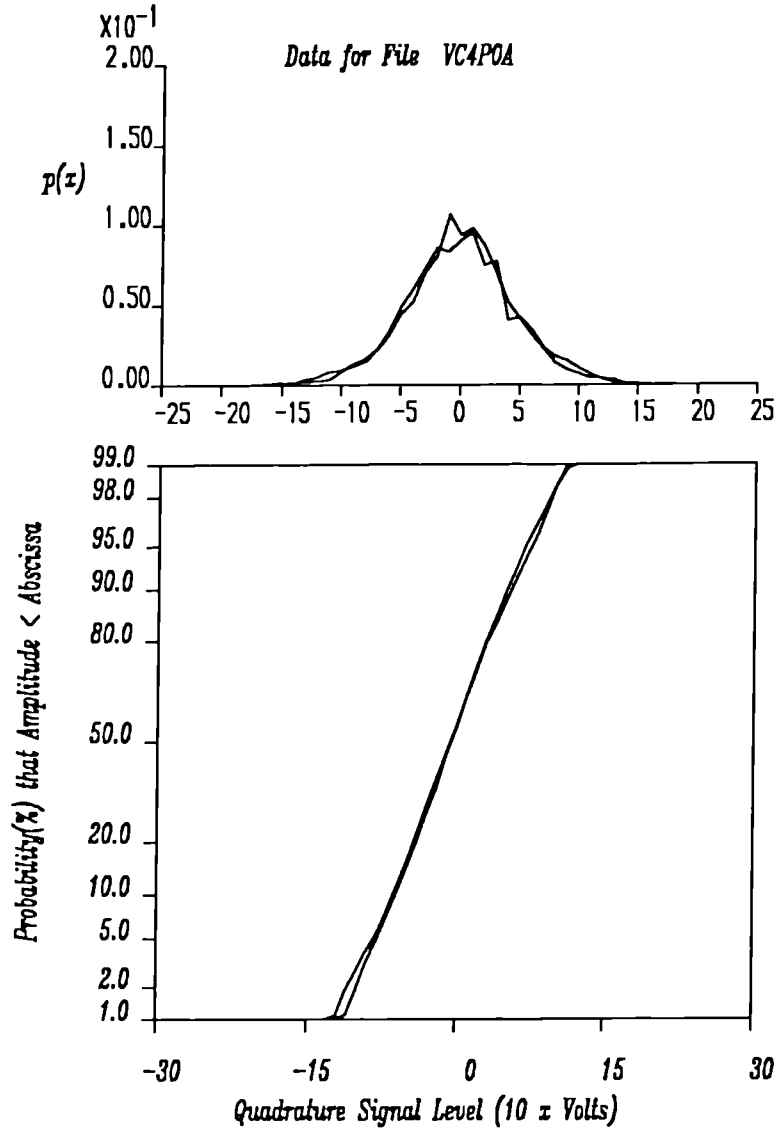

Figure 6.1 Measured PDF (upper) and CDF (lower) of the in-phase and quadrature components. The ordinate, of the CDF plot, is scaled such that a variable with a Gaussian PDF appears as a straight line.

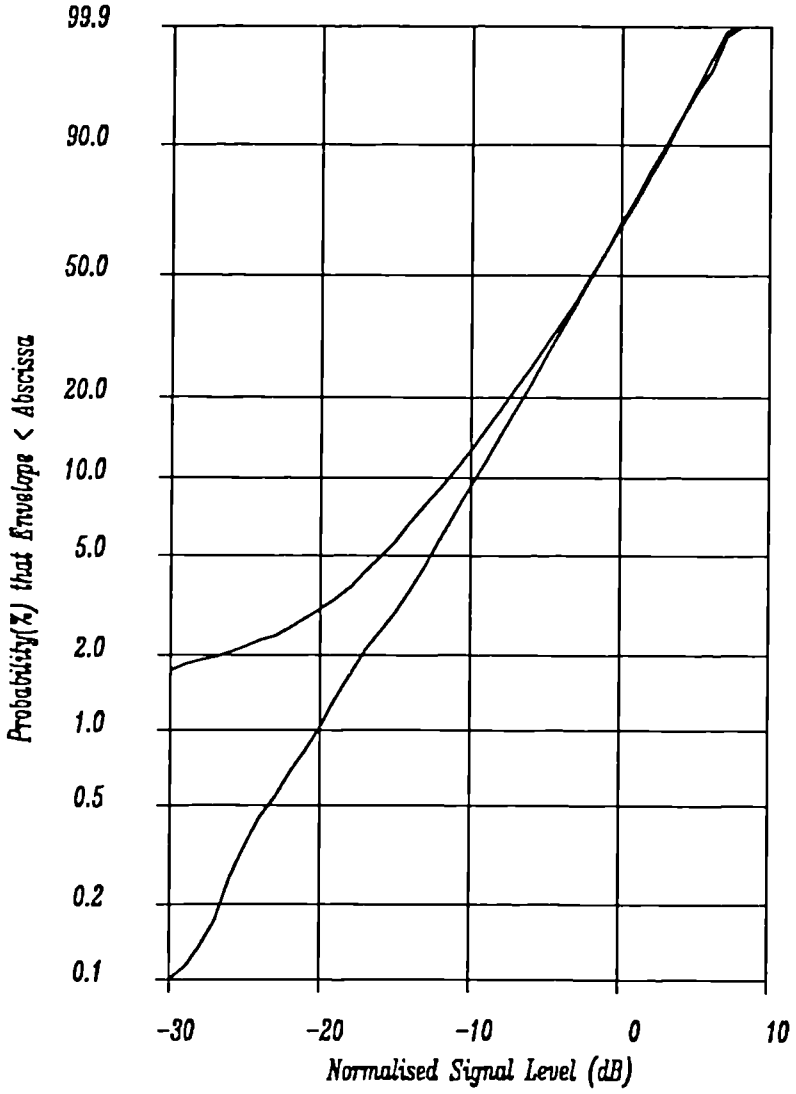

Figure 6.2 CDF of the envelope for a nearly Rayleigh fading (straight line) and severely non-Rayleigh (curved line) fading case. The extreme fading case is caused by destructive interference between a direct and secondary reflected ray which results in a standing wave pattern which has a higher probability of deep fades than occurs in Rayleigh fading. The term 'normalised signal level' means that the envelope sequence has been normalised by the average signal power (σ^2) i.e. $r/\sqrt{2}\,\sigma$.

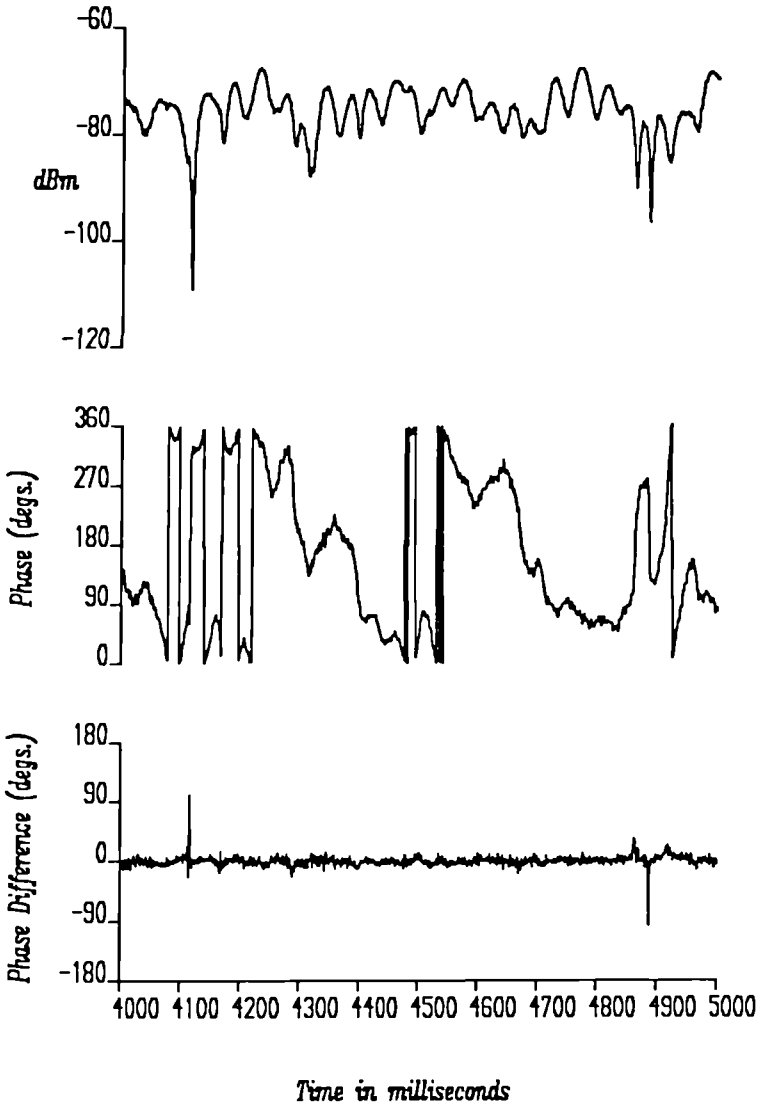

Figure 6.3 Example of envelope, phase and differential phase, for the same time period, for data detected by the vector demodulator receiver. The apparent large phase transitions, in the centre plot, occur merely as a result of the plotting method recording transitions over the 0° and 360° boundary. True large phase transitions can be seen in the lower diagram where they are seen to coincide with the deep fades.

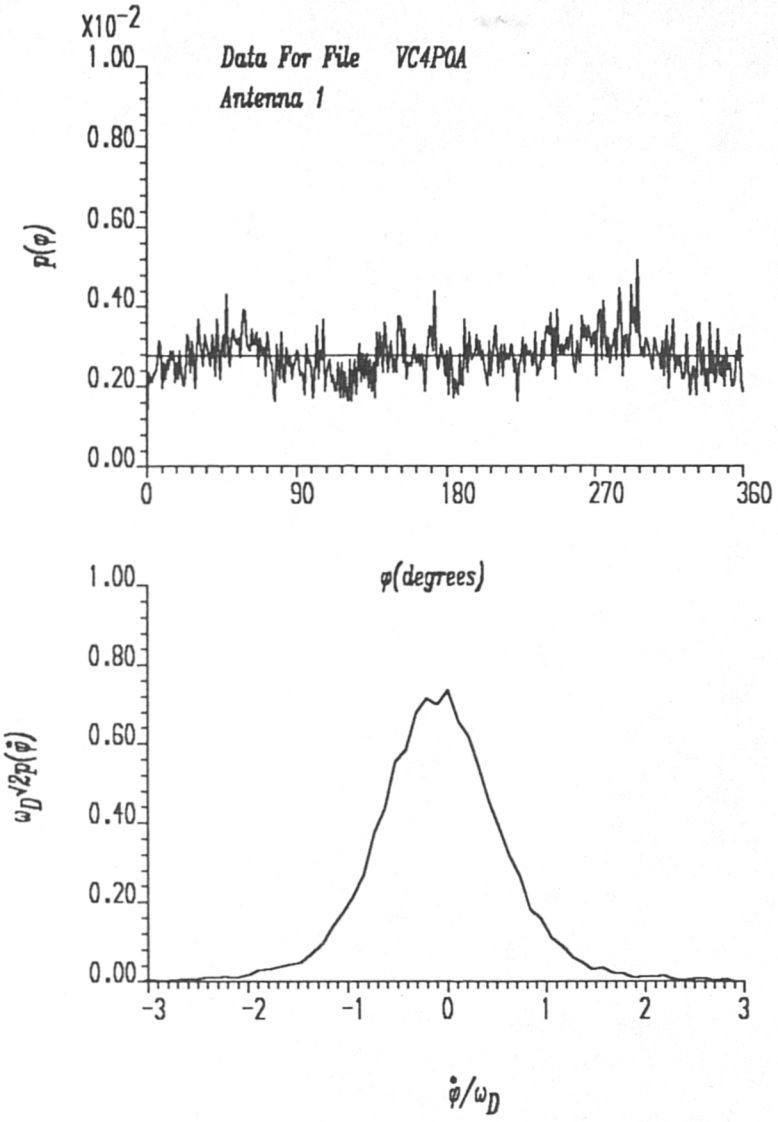

Figure 6.4 Measured PDF of the phase (upper plot) and differential phase (lower plot see Figure 2.11). The horizontal line in the upper diagram represents uniform phase (i.e. $p(\phi) = 1/2\pi$)

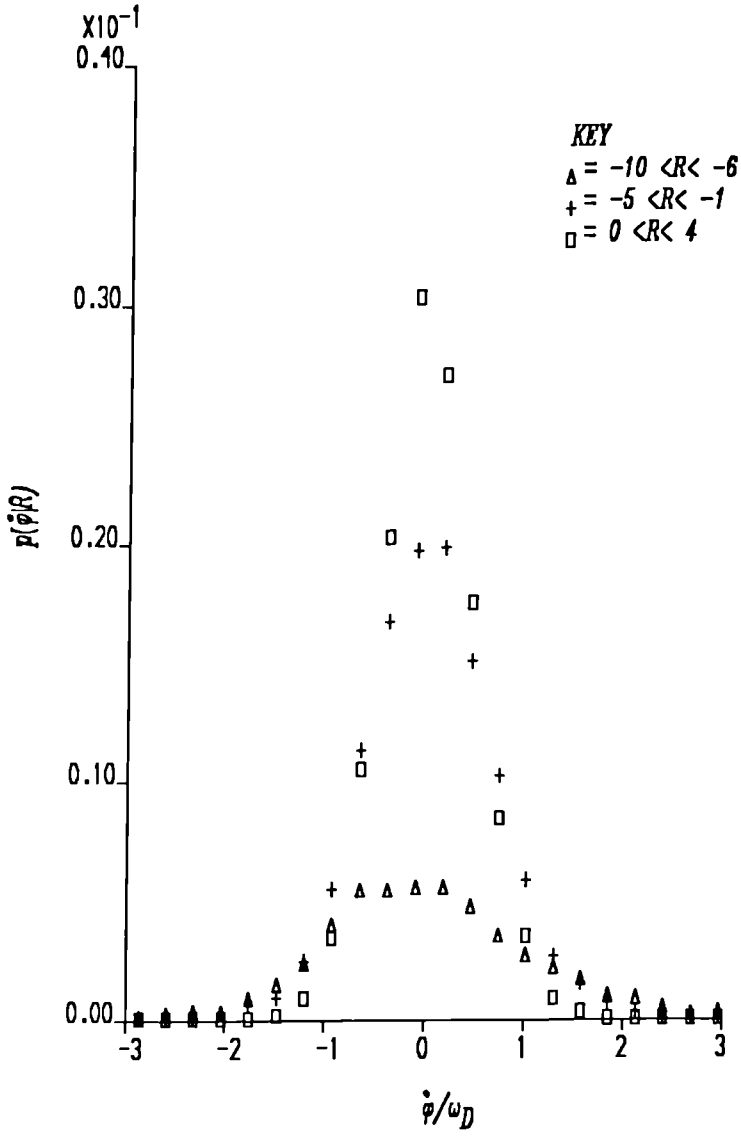

Figure 6.5 Measured conditional PDF of the phase, i.e. $p(\dot{\phi}|R)$, over a range of envelope values. Note that small changes in phase are associated with shallow fades (i.e. small values of R) and that the large phase transitions are associated with the deep fades.

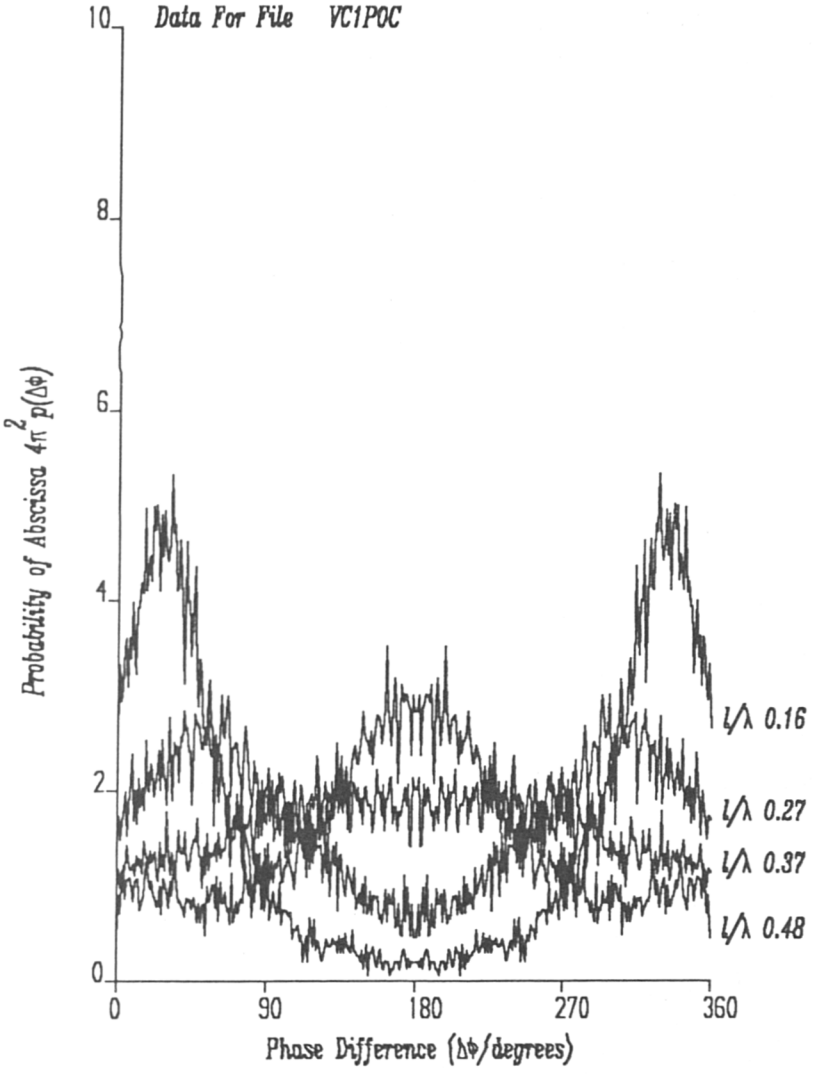

Figure 6.6 Measured PDF of the phase gradient (i.e. $p(\Delta\phi)$) as a function of several values of distance (l/λ). Note that when the distance is $\simeq$0.38 the PDF is uniform i.e. the samples are independent and therefore $p(\Delta\phi) = p(\phi_1).p(\phi_2) = (1/2\pi)^2$.

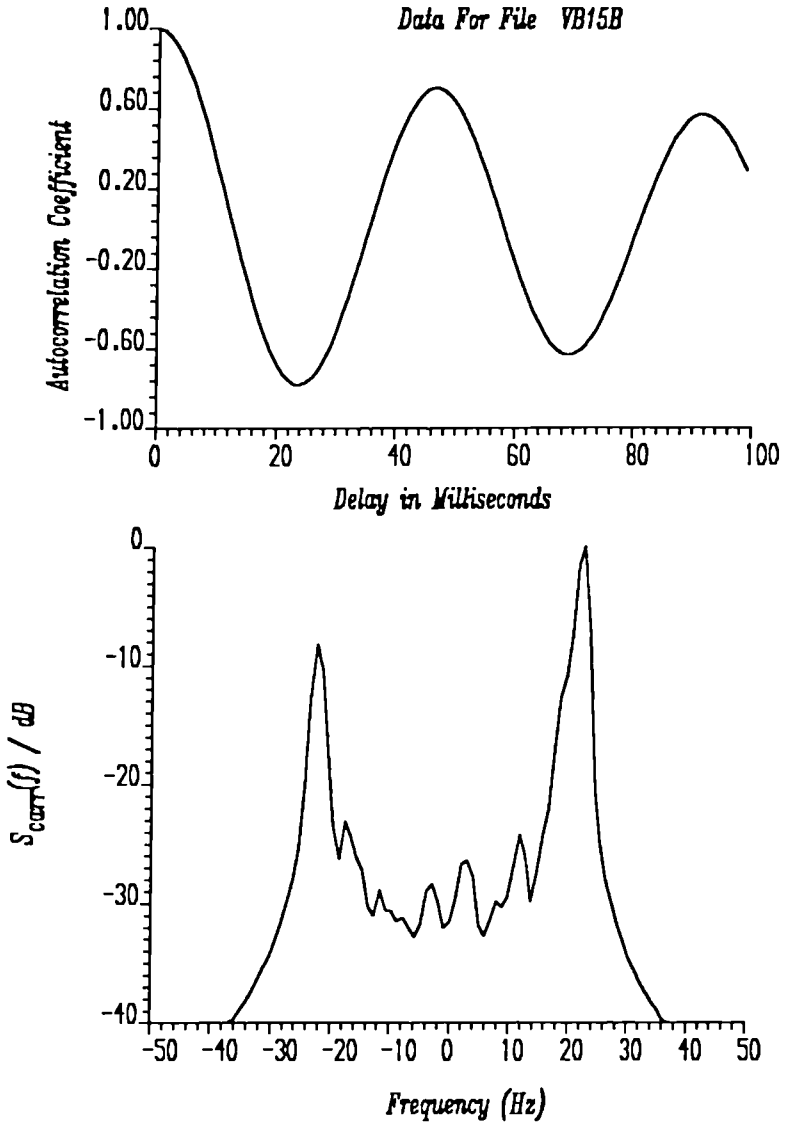

Figure 6.7 Measured quadrature autocorrelation (upper plot) and RF input (i.e. Doppler) spectrum for data gathered from a Rayleigh like fading environment. For comparison with theory see Figure 2.9.

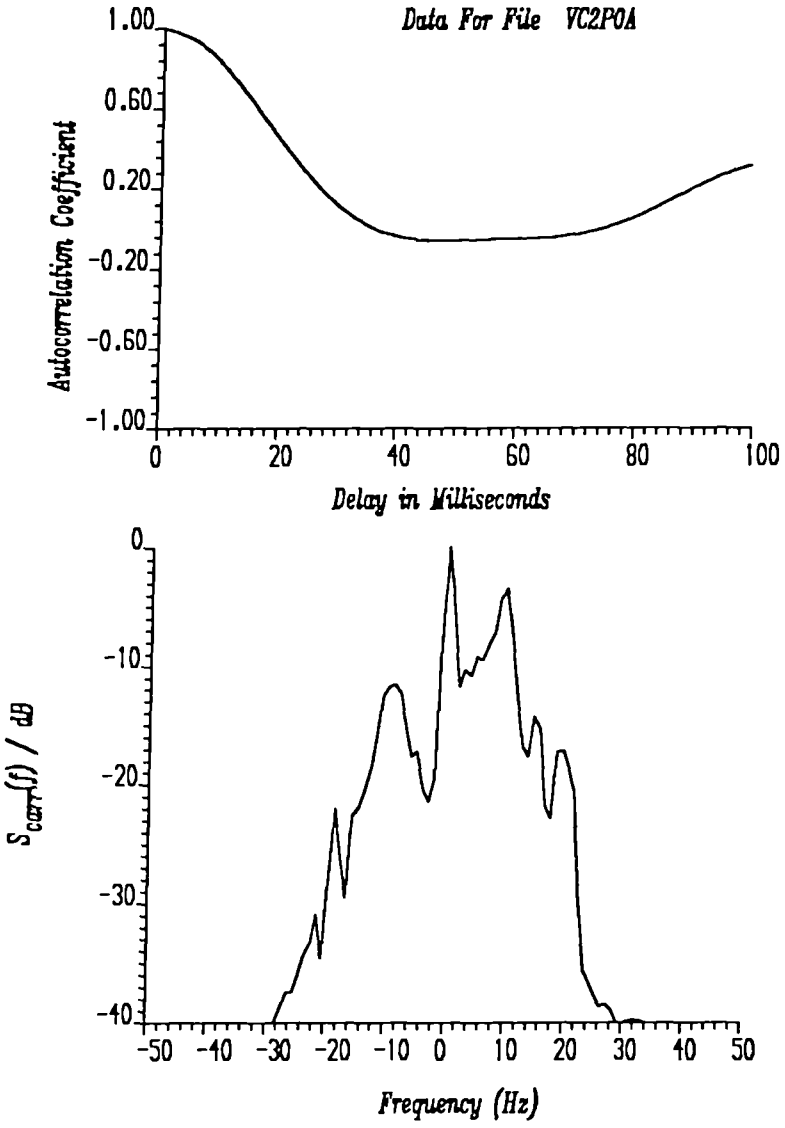

Figure 6.8 Measured quadrature autocorrelation (upper plot) and RF input (i.e. Doppler) spectrum for data gathered from a non-Rayleigh like fading environment. For comparison with theory see Figure 2.9. Note that the characteristic frequency cut-offs at $\pm f_D$ have largely been reduced in sharpness and that the majority of the energy is concentrated at the lower frequencies.

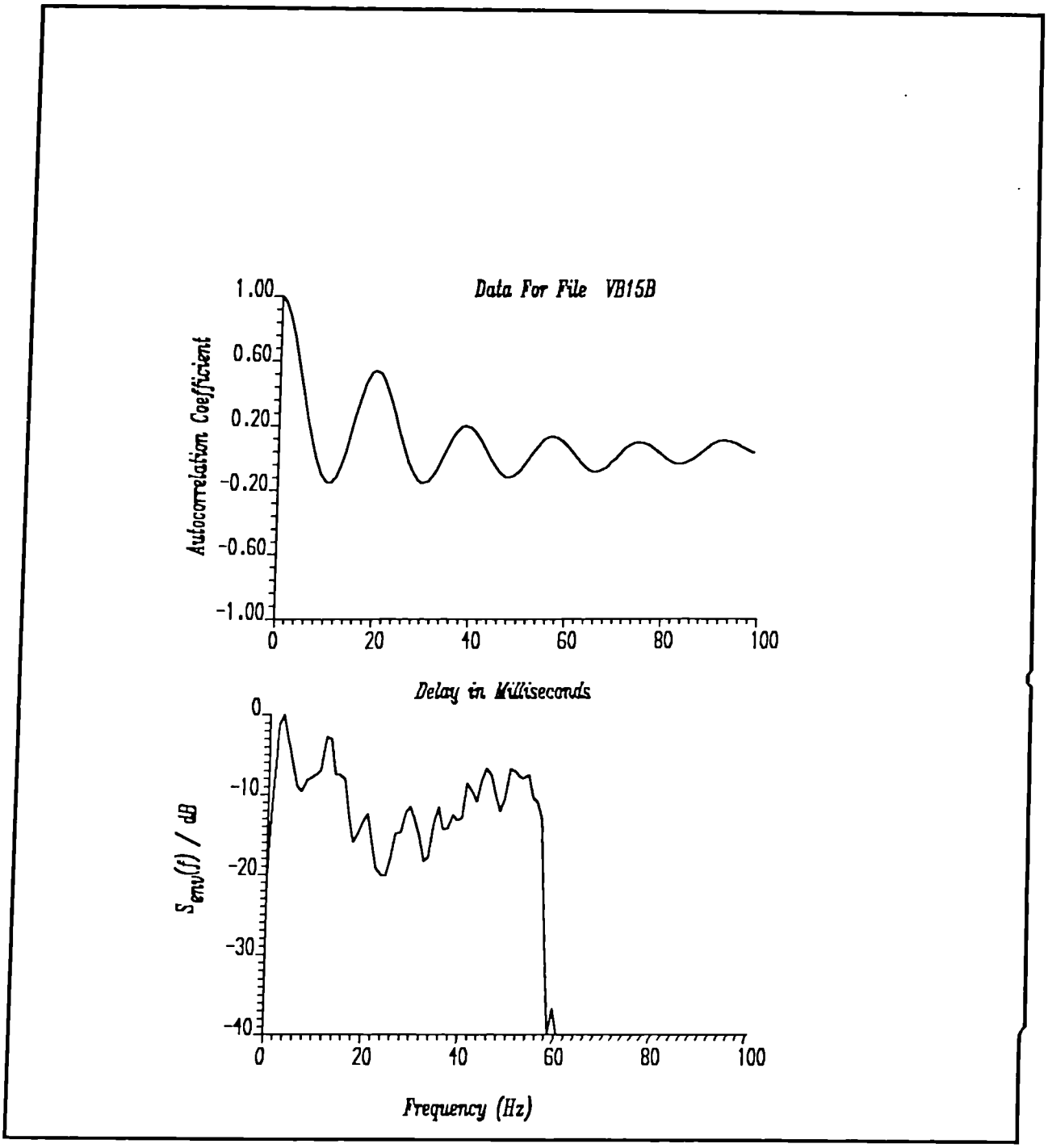

Figure 6.9 Measured envelope autocorrelation (upper plot) and envelope spectrum for data gathered from a Rayleigh like fading environment. For comparison with theory see Figure 2.10.

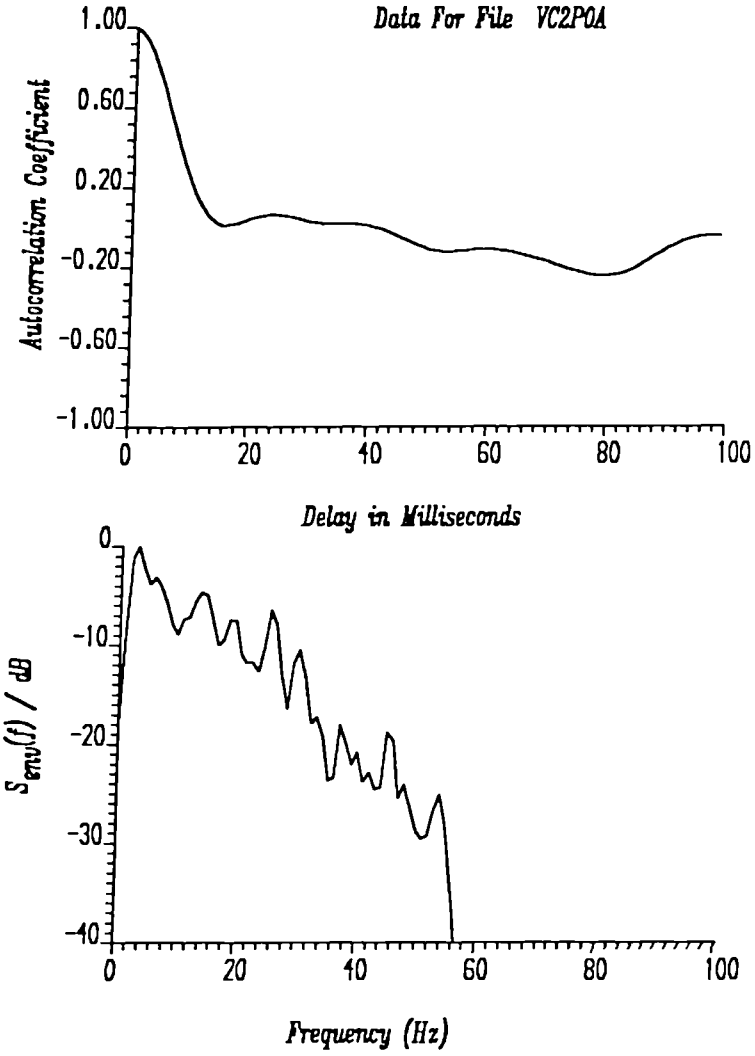

Figure 6.10 Measured envelope autocorrelation (upper plot) and envelope spectrum for data gathered from a non-Rayleigh like fading environment. For comparison with theory see Figure 2.10. Note that the general shape and characteristic frequency cut-off at f_D has been largely replaced by a decaying spectrum.

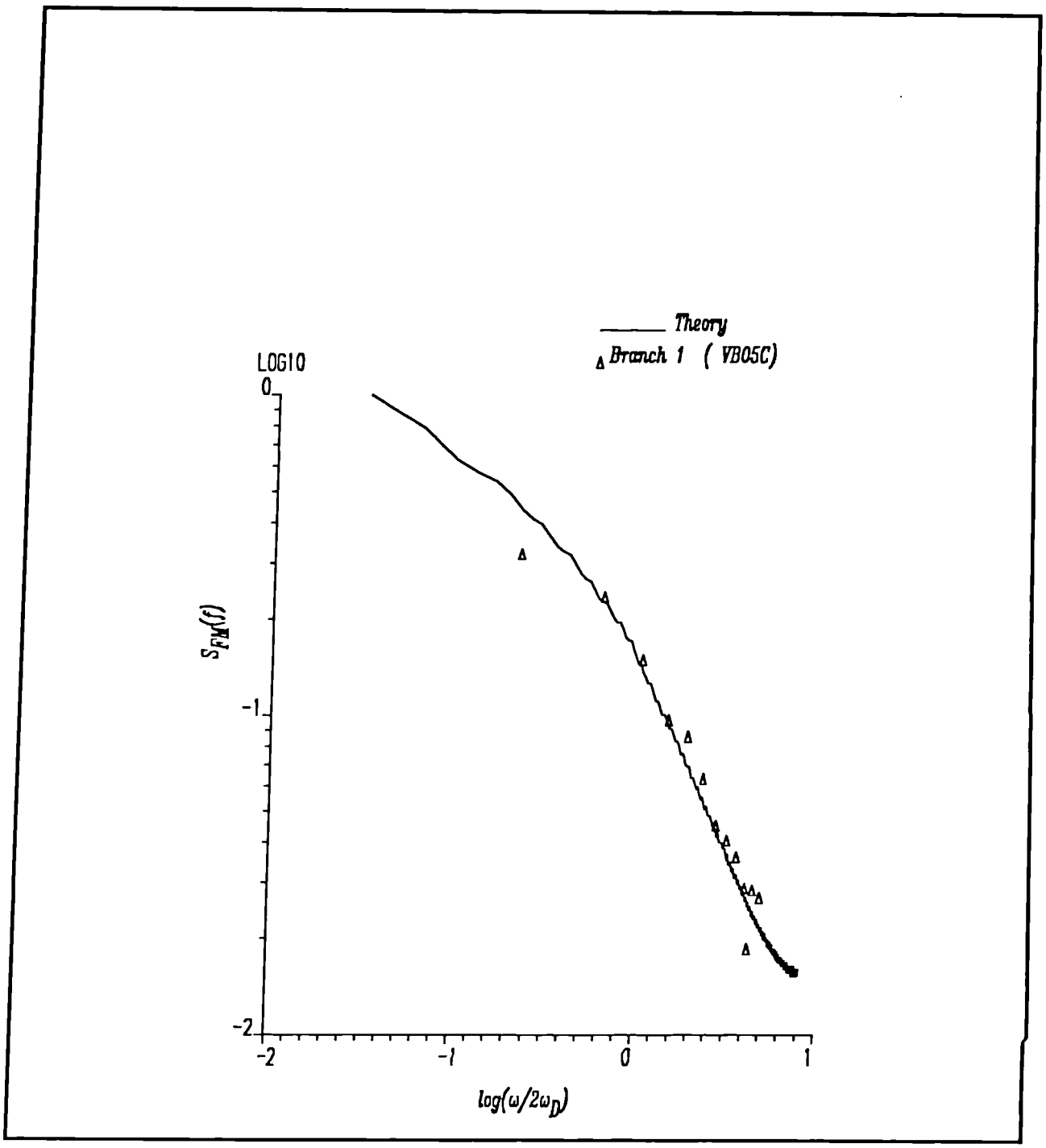

Figure 6.11 The measured random FM spectrum for a single branch and that expected in a Rayleigh fading environment. The measured random FM spectrum was determined by Fourier transforming the measured autocorrelation of the differential phase (i.e. $\dot{\phi}(t)$). The theoretical spectrum was determined by Fourier transforming equation 2.65.

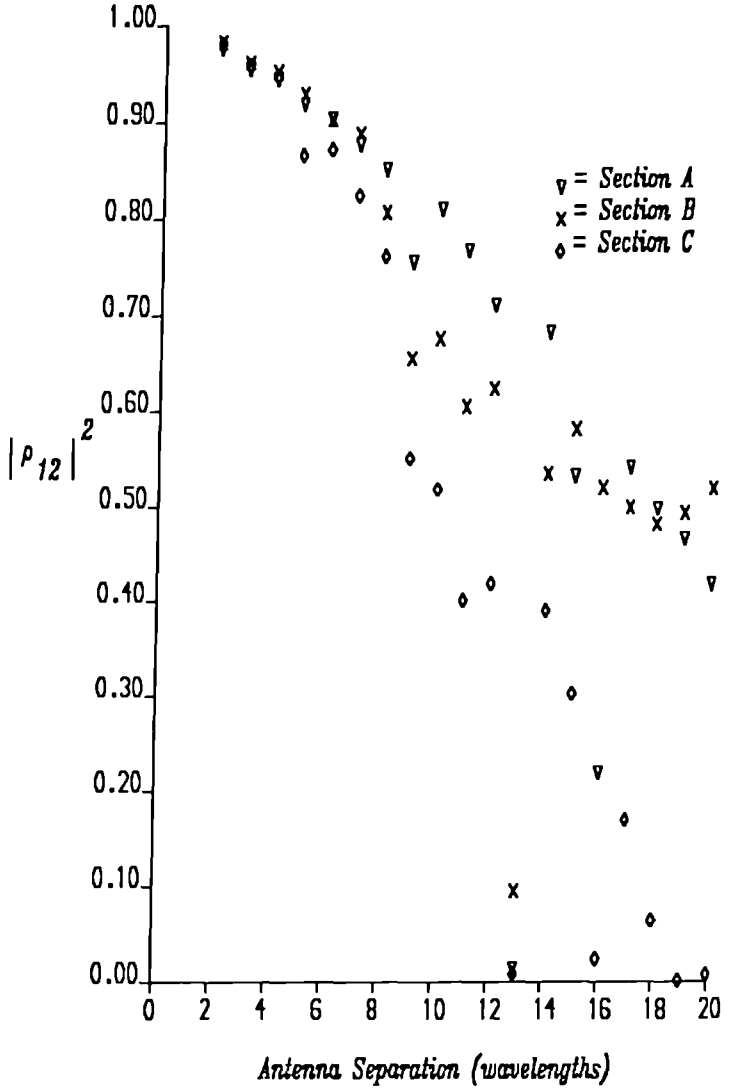

Figure 6.12 Magnitude of the complex crosscorrelation ($|\rho_{12}|^2$) between signals received on two antennas, at various vertical antenna separations, for data received at a base station site from radial(B) and circumferential routes(A,C).

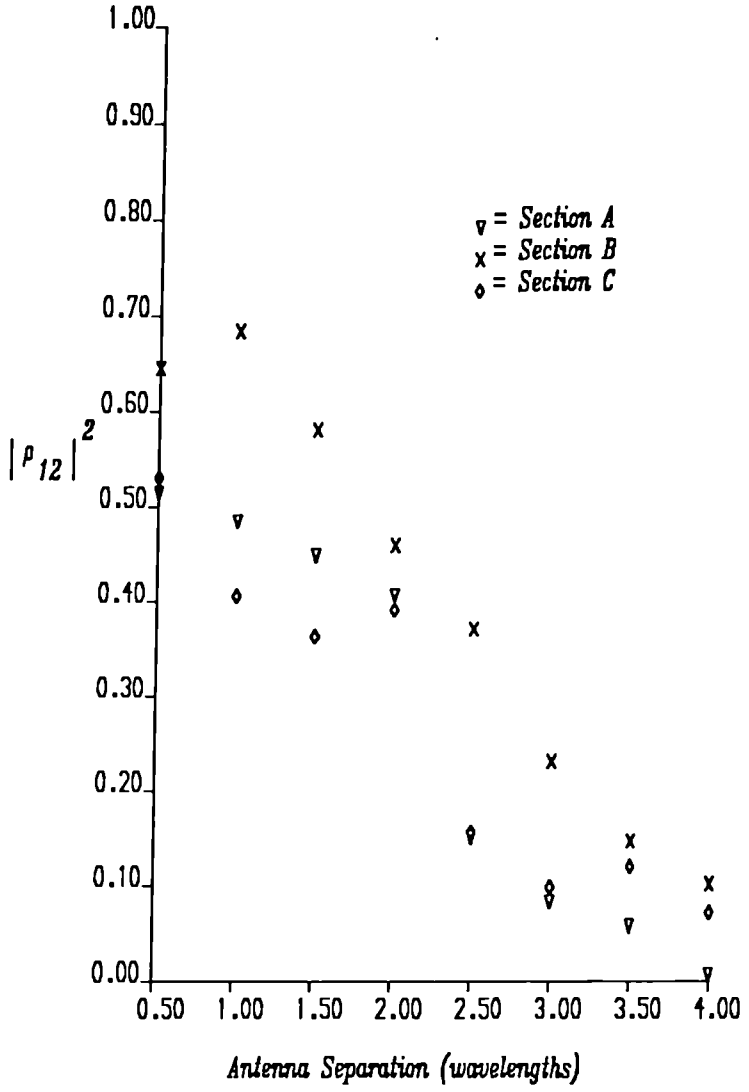

Figure 6.13 Magnitude of the complex crosscorrelation ($|\rho_{12}|^2$) between signals received on two antennas, at various vertical antenna separations, for data received at a mobile travelling radial(B) and circumferential routes(A,C).

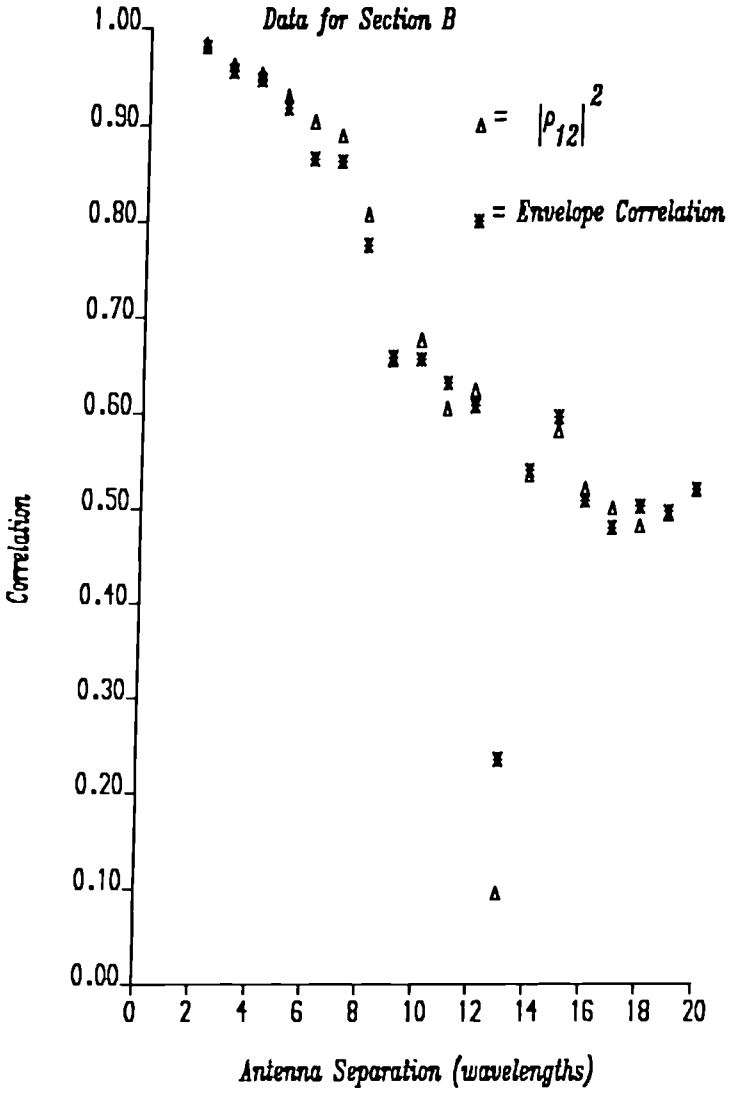

Figure 6.14 Comparison of the magnitude of the complex crosscorrelation ($|\rho_{12}|^2$) and envelope crosscorrelation (ρ_{env}) for data received on two vertically separated antennas at a base station site.

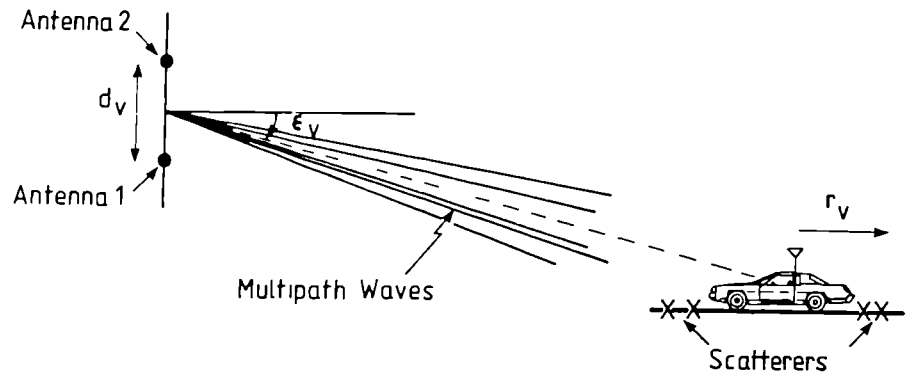

Figure 6.15 Coordinate system for the scattering model in which $|\rho_{12}|^2$ is a function of the vertical elevation angle (ε_v) and the spread in arrival angle (σ) of incoming multipath waves.

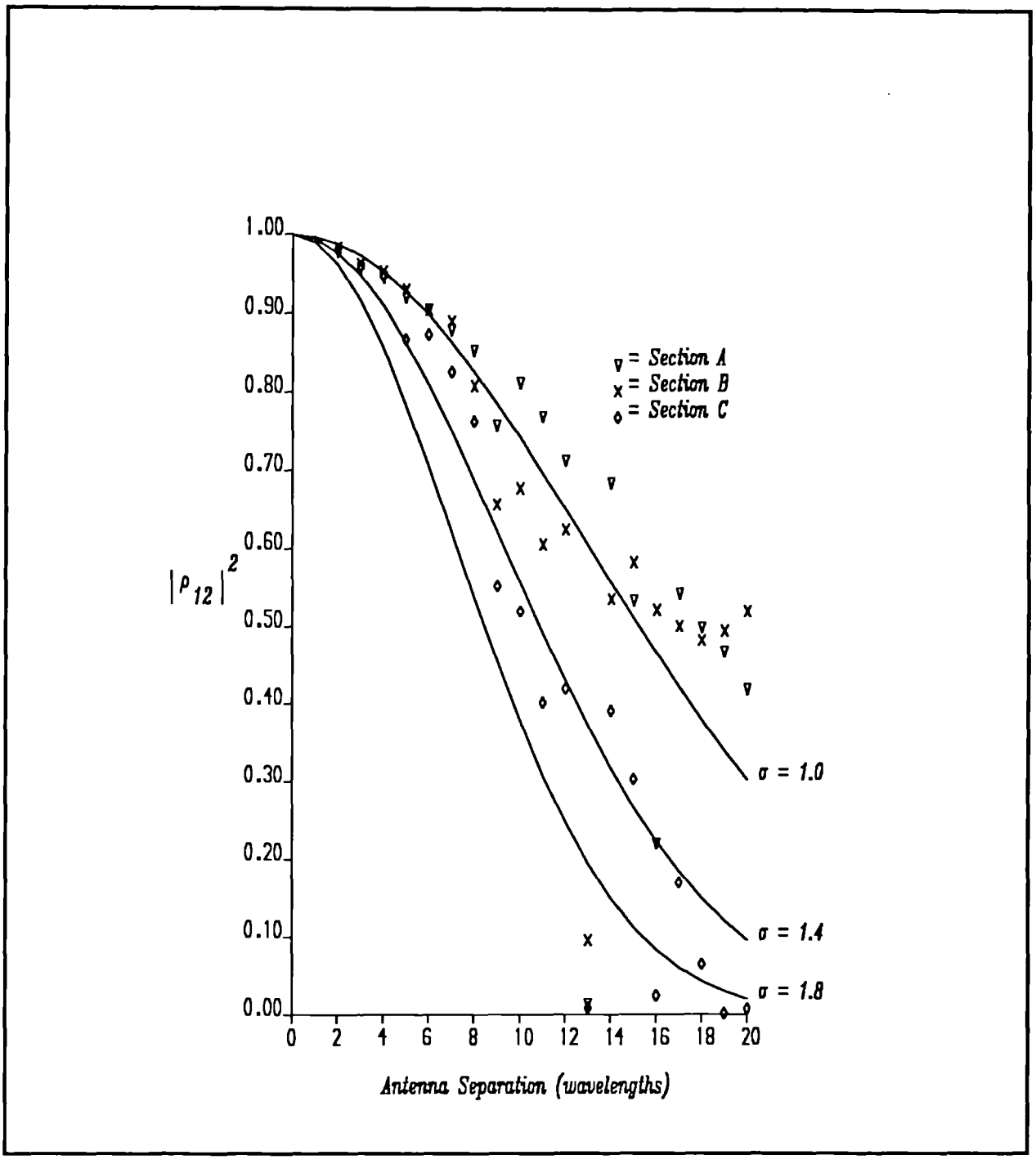

Figure 6.16 Theoretical curves and experimental values of $|\rho_{12}|^2$ as a function of antenna spacing and spread in arrival angle (σ in degrees) of incoming multipath waves for data received at a base station site.

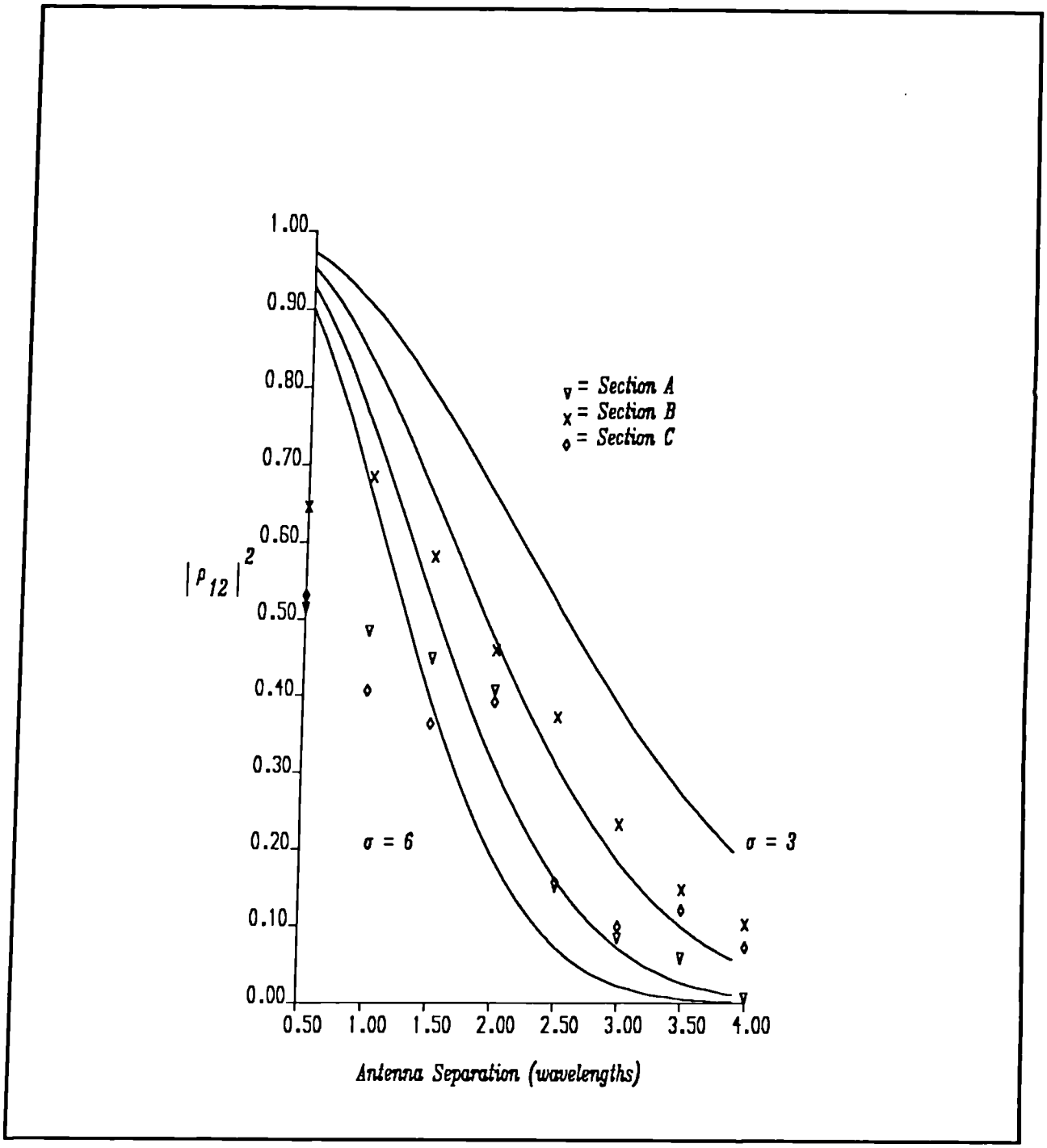

Figure 6.17 Theoretical curves and experimental values of $|\rho_{12}|^2$ as a function of antenna spacing and spread in arrival angle (σ in degrees) of incoming multipath waves for data received at a mobile site.

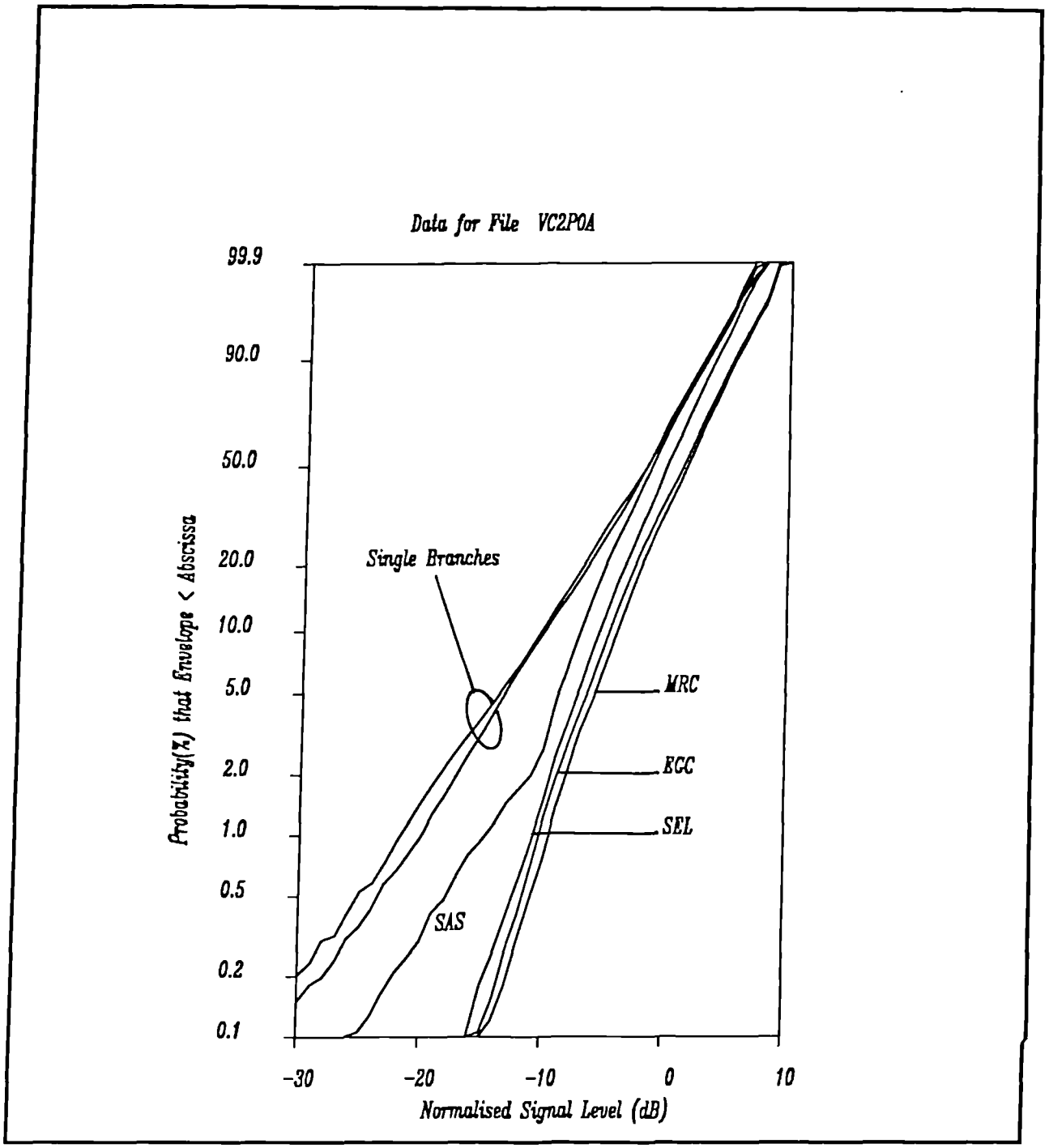

Figure 6.18 The measured CDF of the envelope for individual branches and various diversity strategies at the mobile using a vertical antenna separation of 2λ. The term 'normalised signal level' means that the envelope sequence has been normalised by the average signal power (σ^2) i.e. $r/\sqrt{2}\,\sigma$.

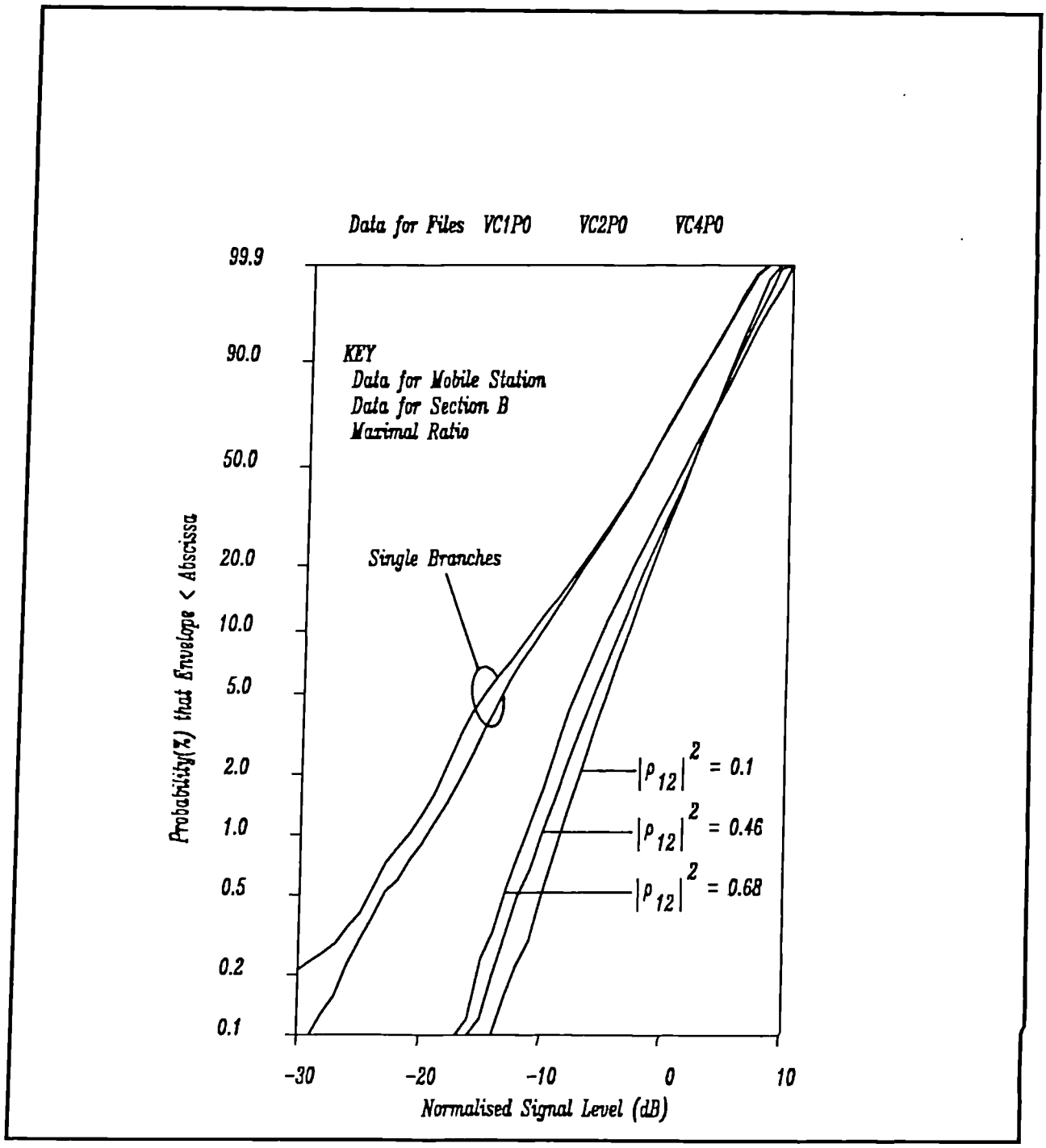

Figure 6.19 The measured CDF of the envelope for individual branches and MRC diversity, as a function of branch crosscorrelation (i.e. antenna separation). The term 'normalised signal level' means that the envelope sequence has been normalised by the average signal power (σ^2) i.e. $r/\sqrt{2}\,\sigma$.

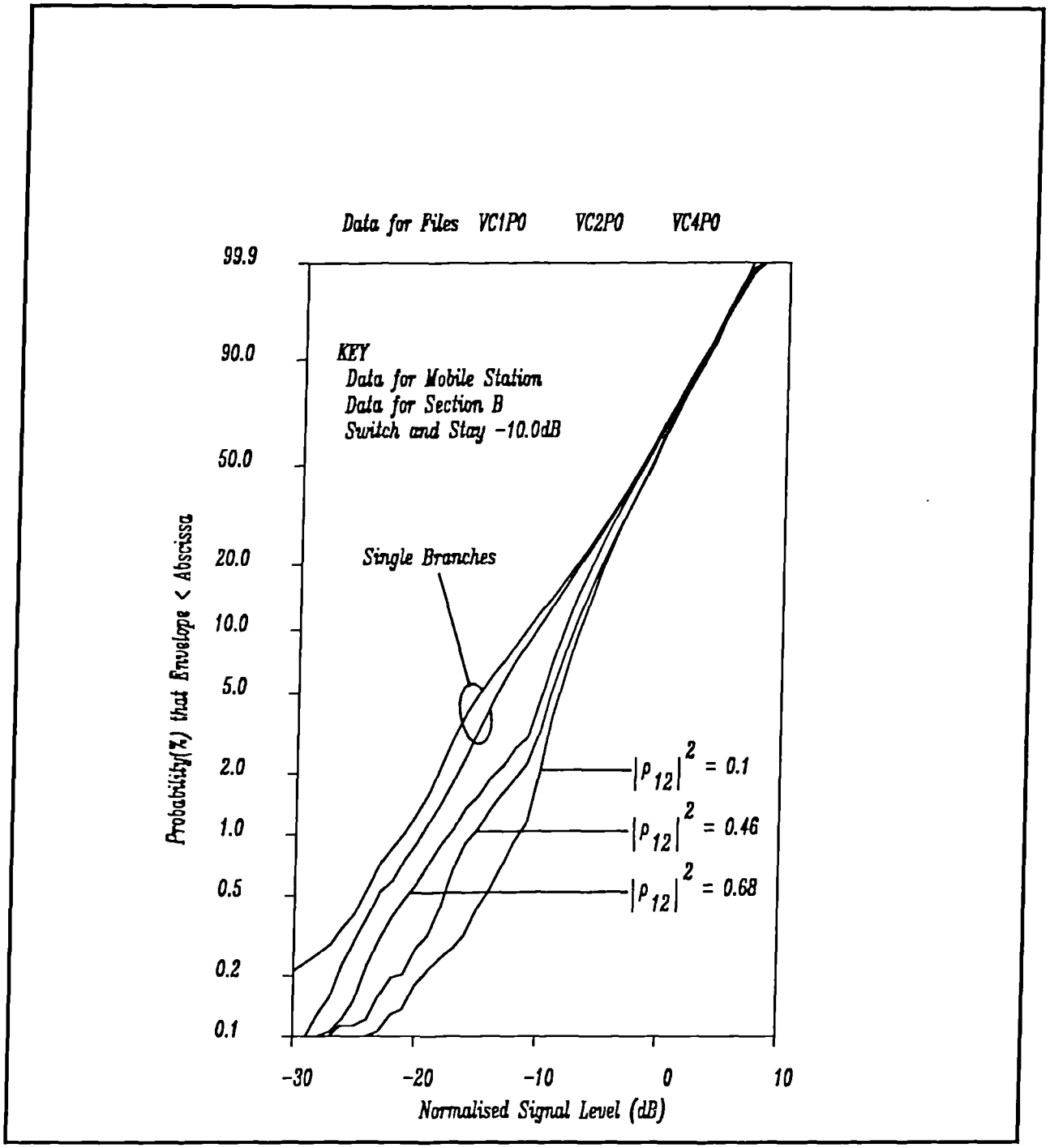

Figure 6.20 The measured CDF of the envelope for individual branches and SAS diversity (-10dB switching threshold), as a function of branch crosscorrelation (i.e. antenna separation). The term 'normalised signal level' means that the envelope sequence has been normalised by the average signal power (σ^2) i.e. $r/\sqrt{2}\,\sigma$.

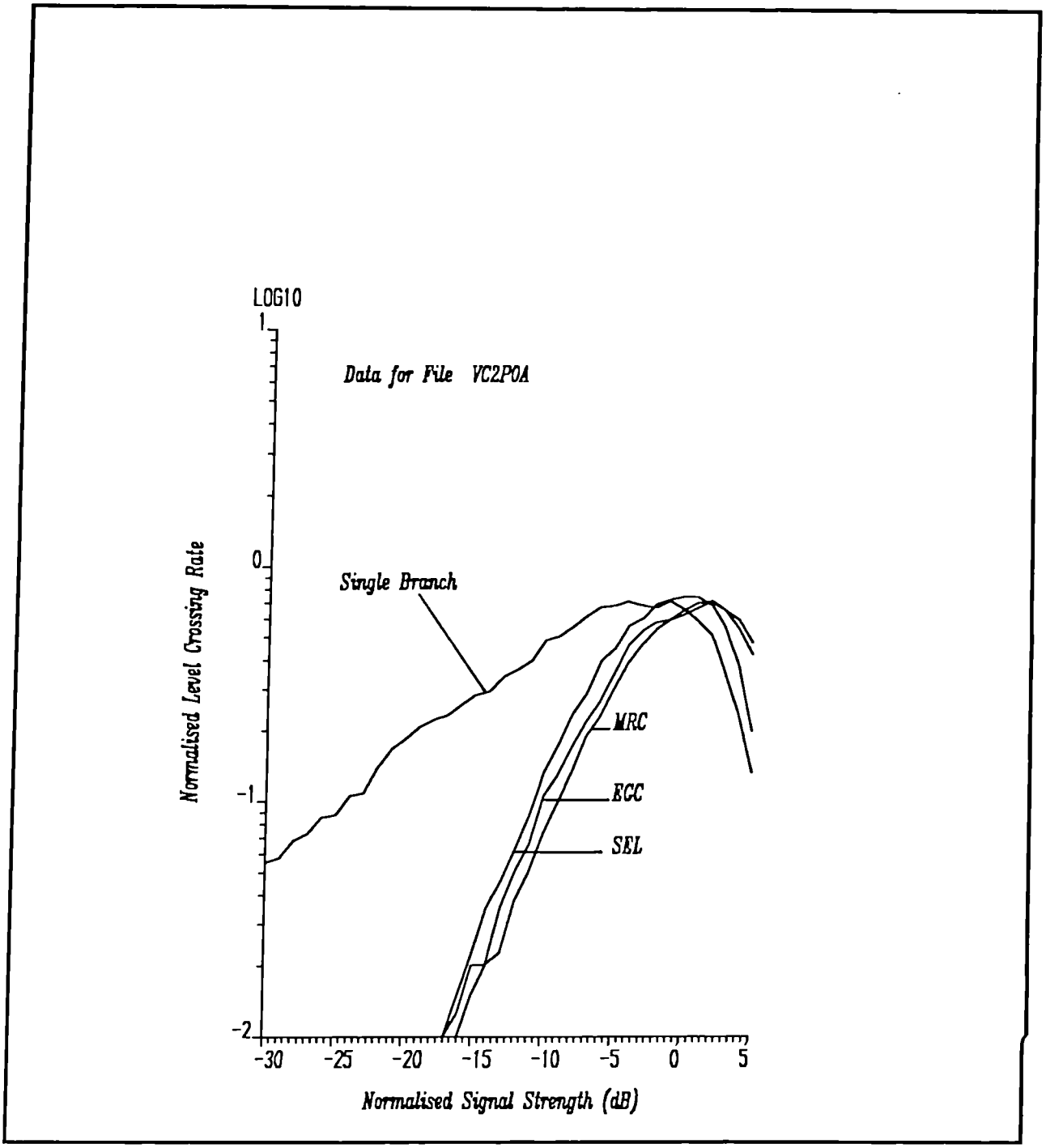

Figure 6.21 The measured LCR, of the envelope, for an individual branch and MRC, EGC and SEL diversity strategies. The term 'normalised signal strength' means that the envelope sequence has been normalised by the average signal power (σ^2) i.e. $r/\sqrt{2}\,\sigma$.

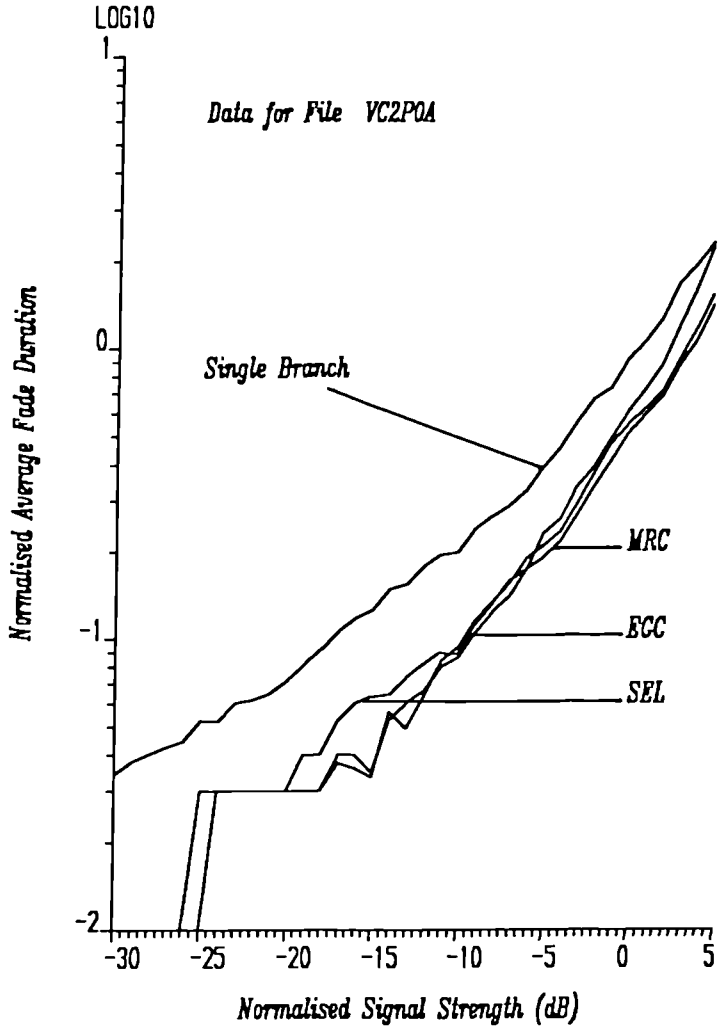

Figure 6.22 The measured AFD, of the envelope, for an individual branch and MRC, EGC and SEL diversity strategies. The term 'normalised signal strength' means that the envelope sequence has been normalised by the average signal power (σ^2) i.e. $r/\sqrt{2}\,\sigma$.

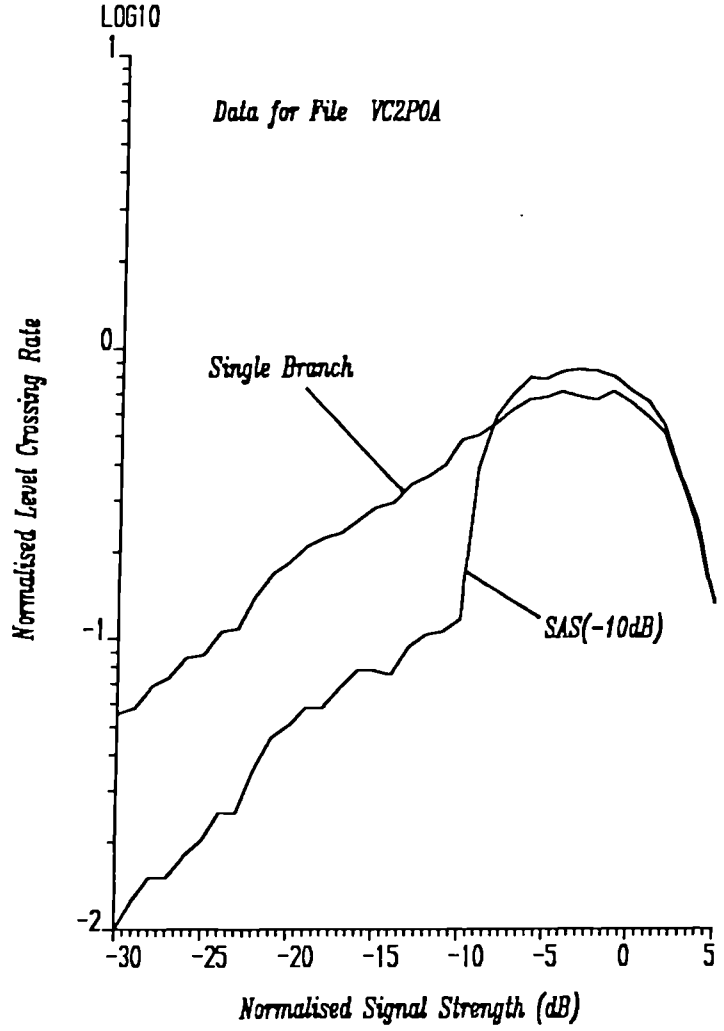

Figure 6.23 The measured LCR, of the envelope, for an individual branch and SAS diversity (-10dB switching threshold). The term 'normalised signal strength' means that the envelope sequence has been normalised by the average signal power (σ^2) i.e. $r/\sqrt{2}\,\sigma$.

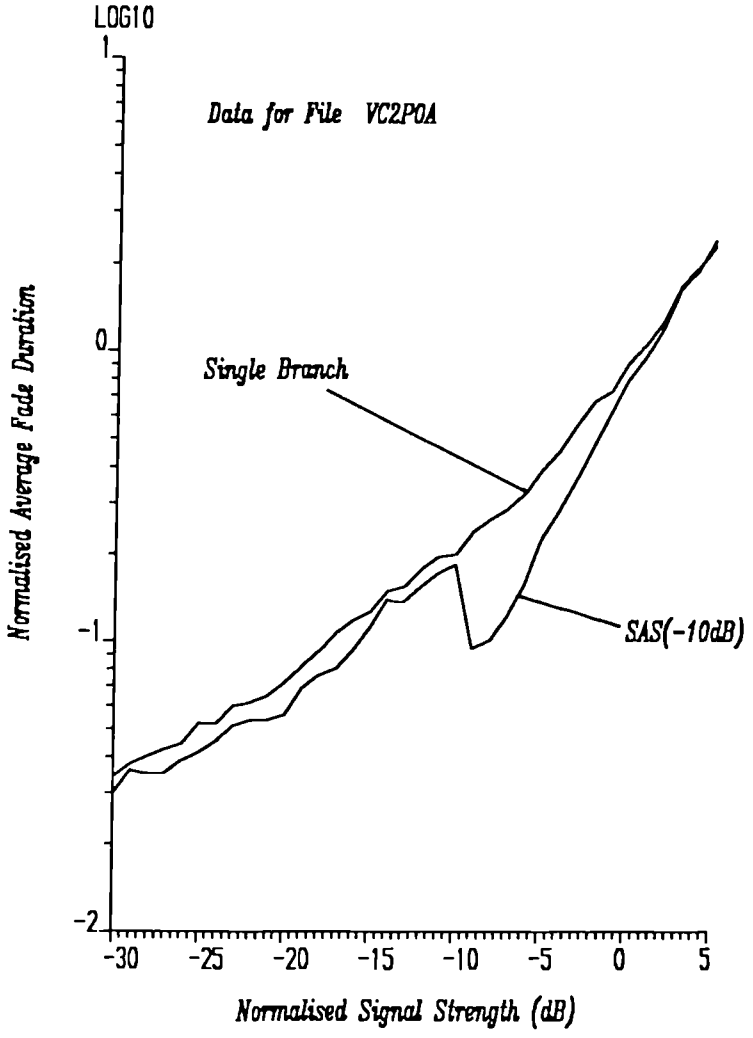

Figure 6.24 The measured AFD, of the envelope, for an individual branch and SAS diversity (-10dB switching threshold). The term 'normalised signal strength' means that the envelope sequence has been normalised by the average signal power (σ^2) i.e. $r/\sqrt{2}\,\sigma$.

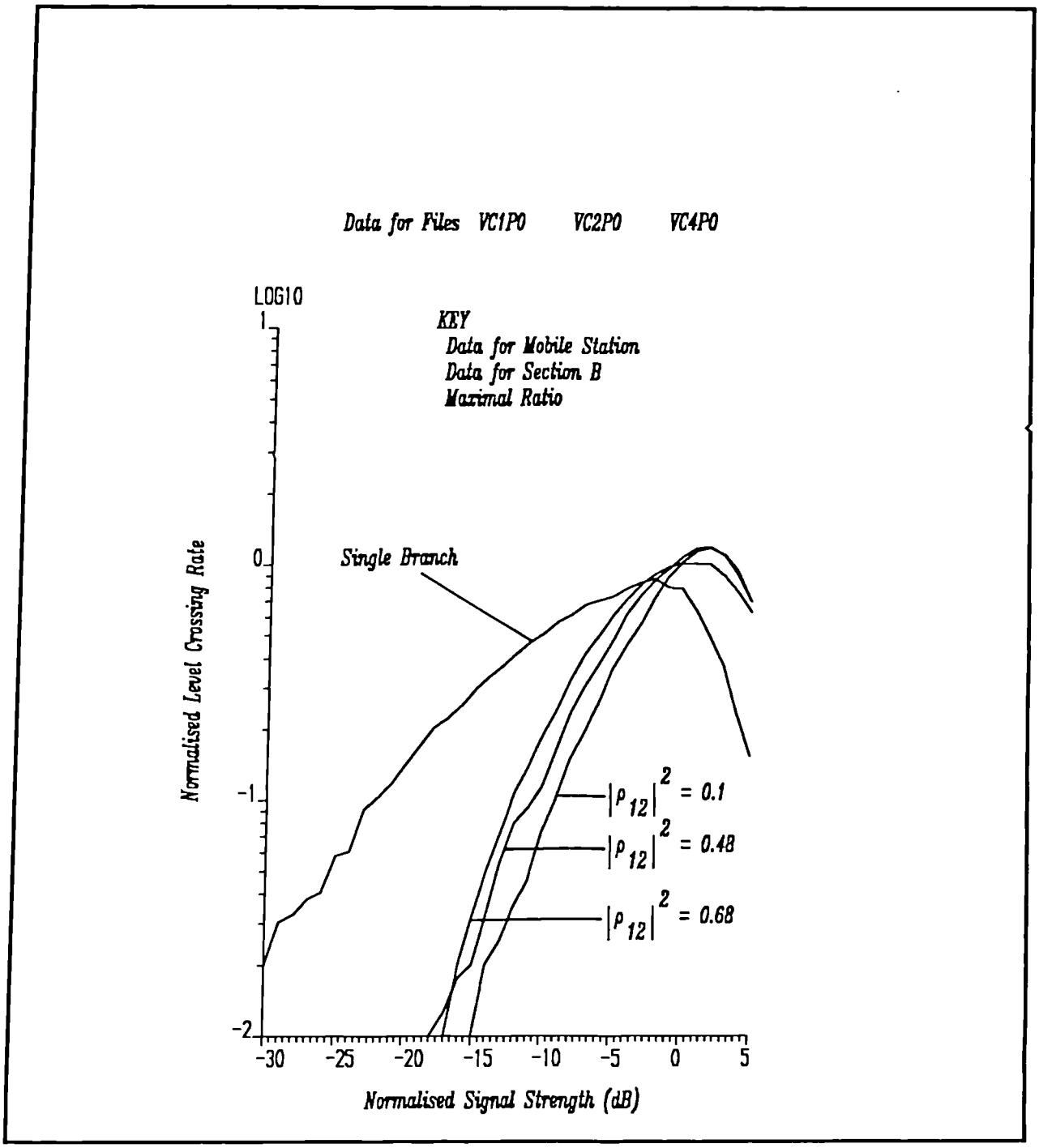

Figure 6.25 The measured LCR, of the envelope, for an individual branch and MRC diversity as a function of branch crosscorrelation (i.e. antenna separation). The term 'normalised signal strength' means that the envelope sequence has been normalised by the average signal power (σ^2) i.e. $r/\sqrt{2}\,\sigma$.

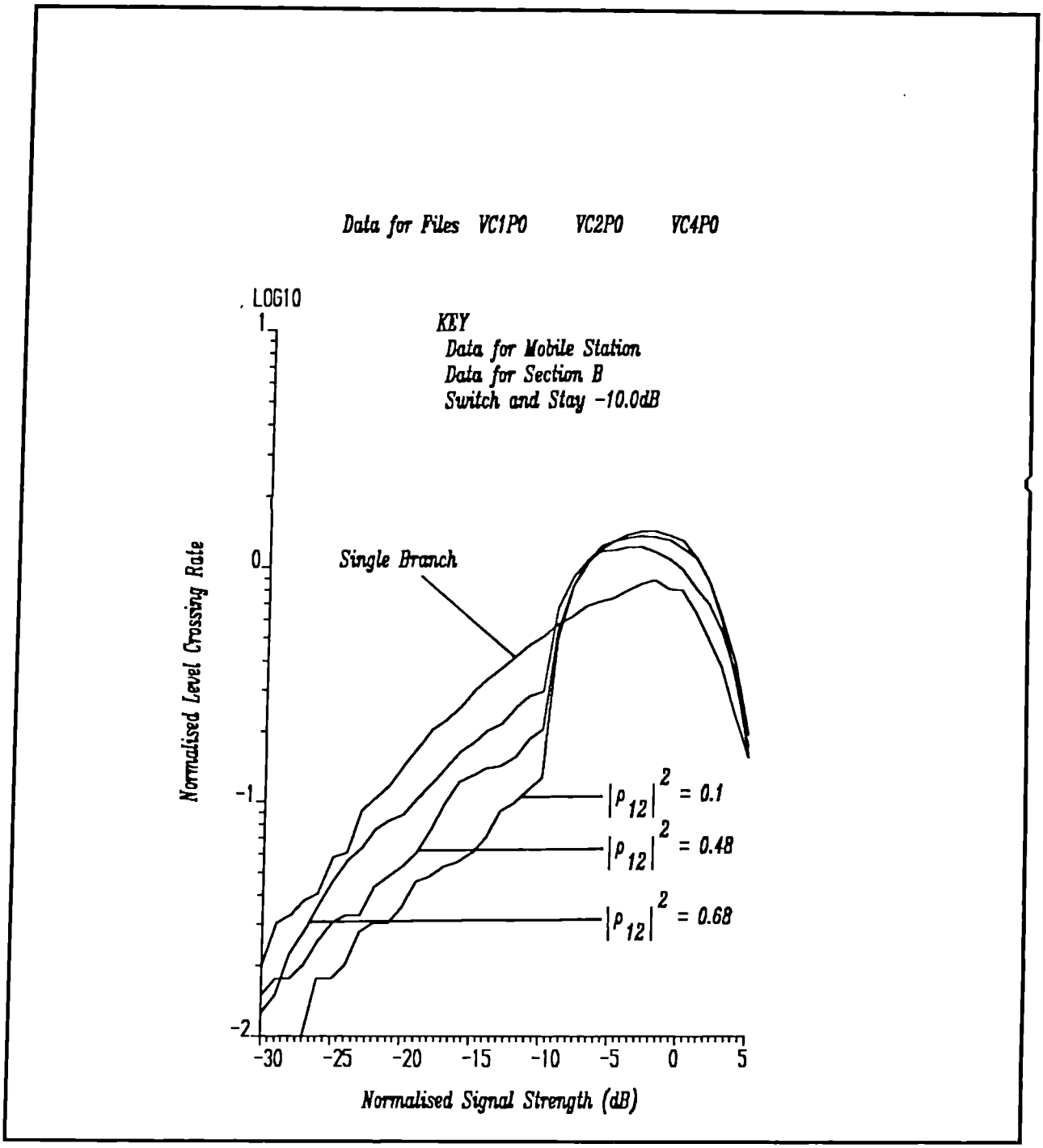

Figure 6.26 The measured LCR, of the envelope, for an individual branch and SAS diversity (-10dB switching threshold) as a function of branch crosscorrelation (i.e. antenna separation). The term 'normalised signal strength' means that the envelope sequence has been normalised by the average signal power (σ^2) i.e. $r/\sqrt{2}\,\sigma$.

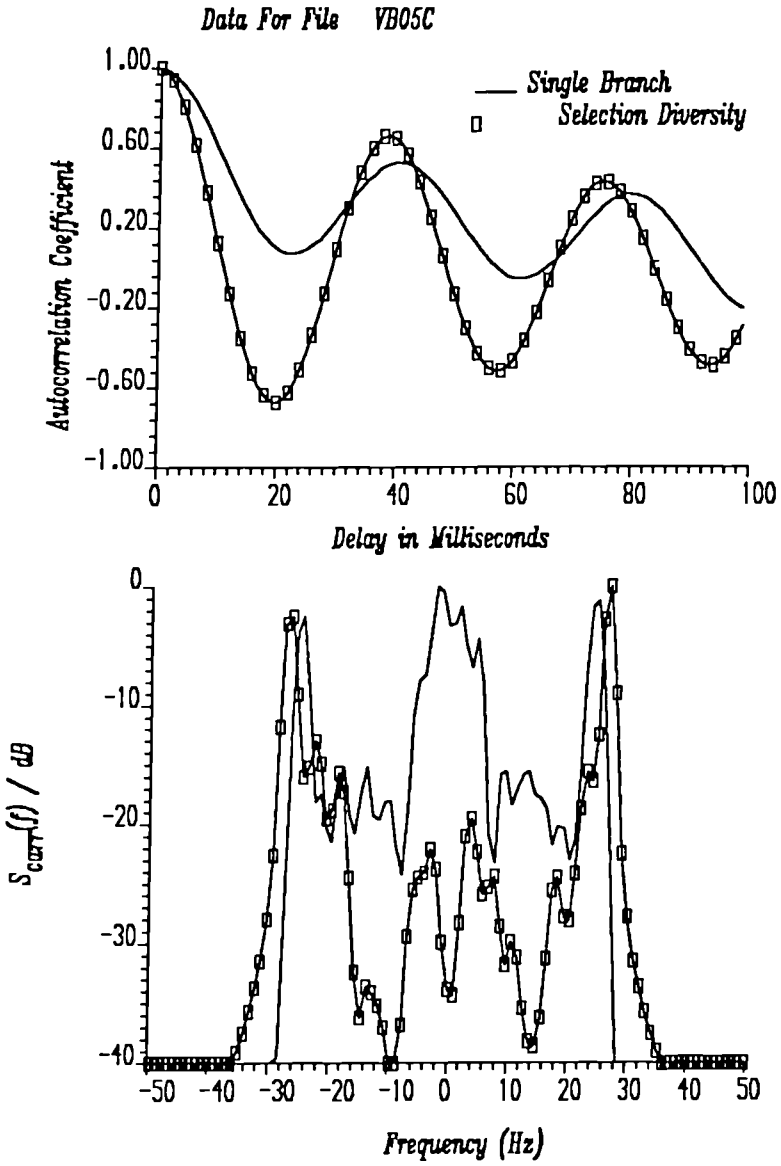

Figure 6.27 The measured autocorrelation and Doppler spectrum for an individual branch and SEL diversity. Note the decreasing of the lower frequency energy and the spectral broadening as a result of SELection diversity.

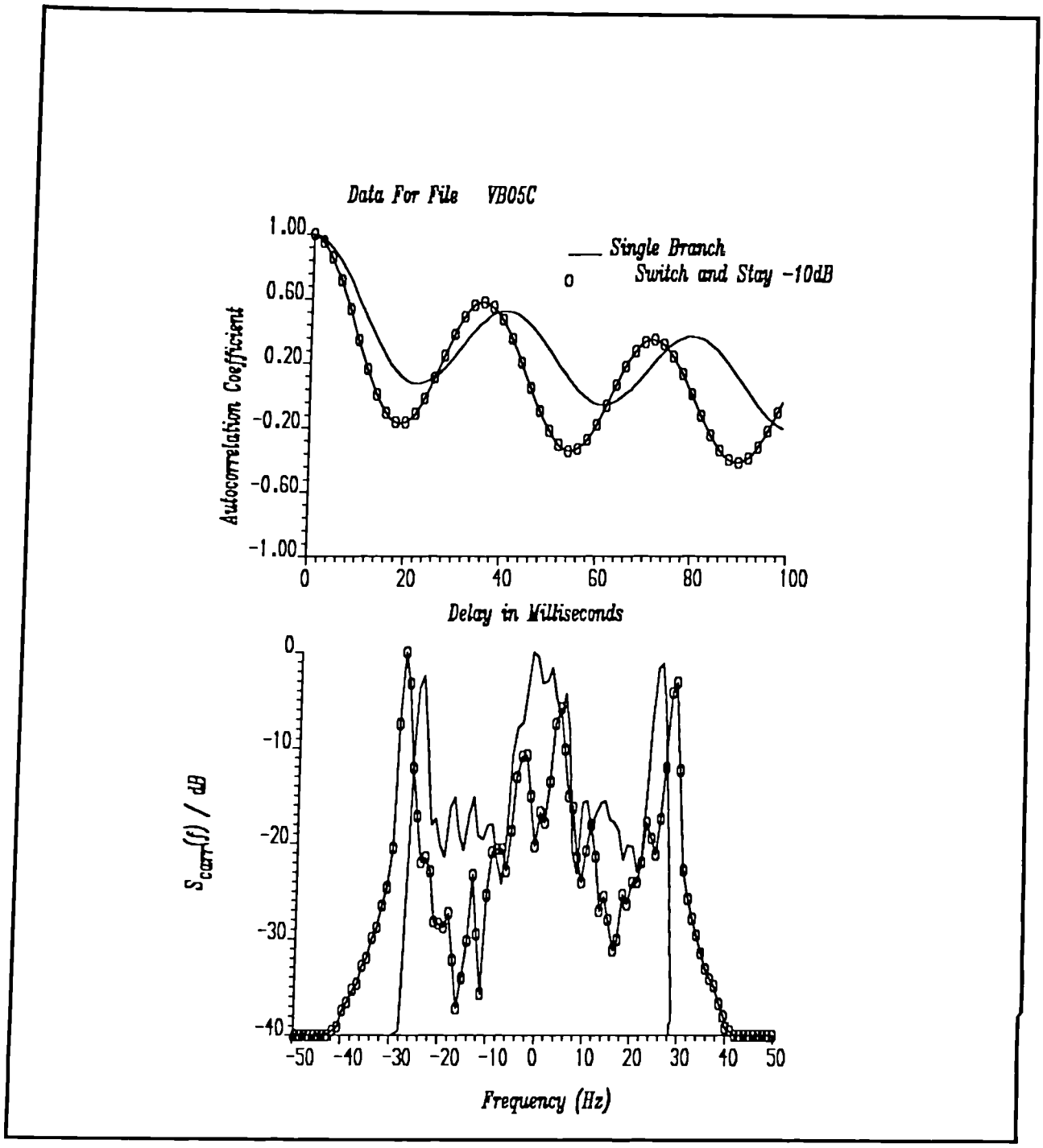

Figure 6.28 The measured autocorrelation and Doppler spectrum for an individual branch and SAS diversity (-10dB switching threshold). Note the decreasing of the lower frequency energy and the spectral broadening, which is greater than that for SEL diversity. The broadening results from frequent large discontinuities that occur when switching between branches.

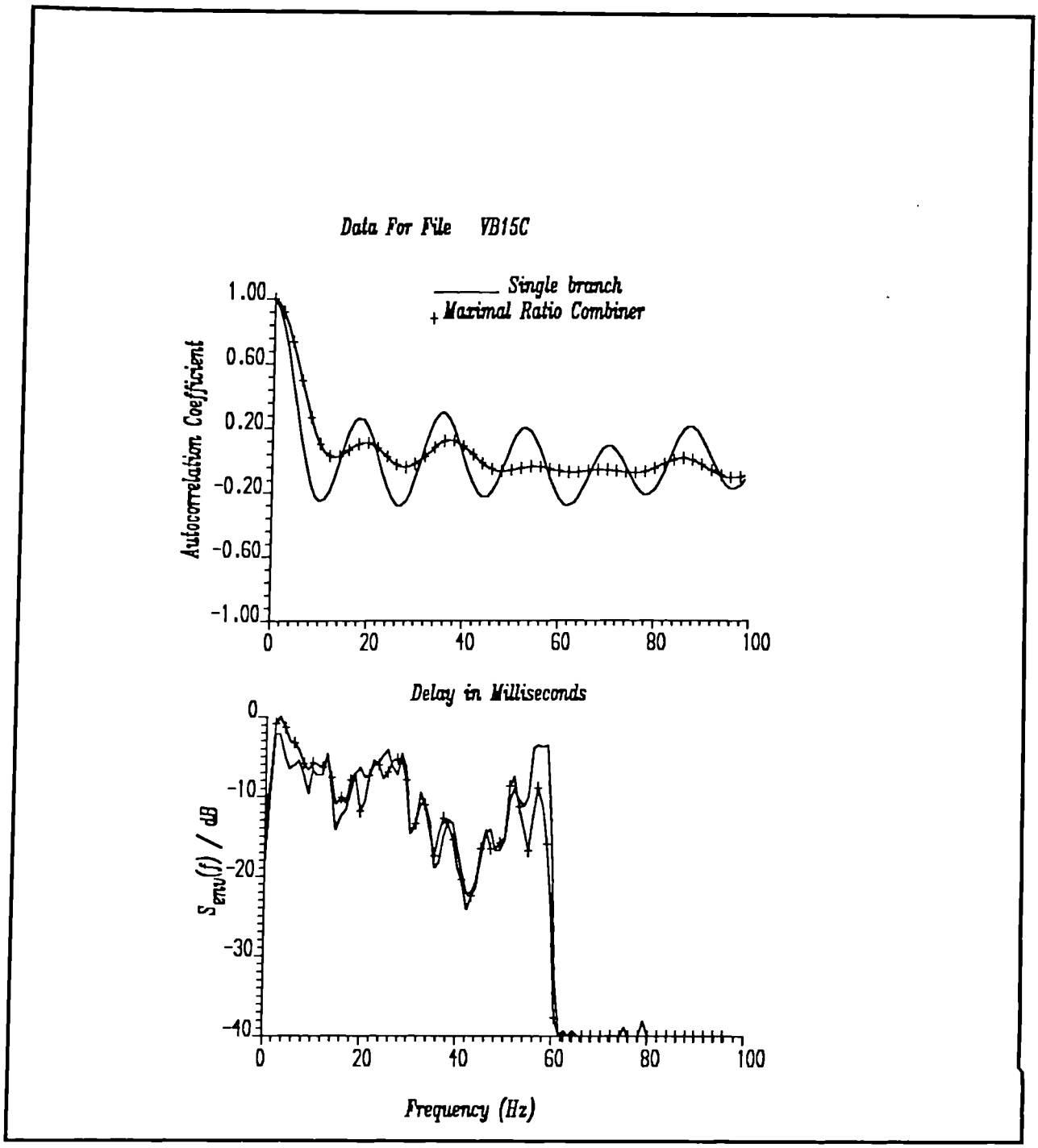

Figure 6.29 The measured autocorrelation and envelope spectrum for an individual branch and MRC diversity. Note the increasing of the lower frequency energy. This phenomena is synonymous with the diversity action smoothing out the envelope time series. The absence of energy below 2Hz is simply due to the normalisation procedure which removes the local mean variation of the envelope.

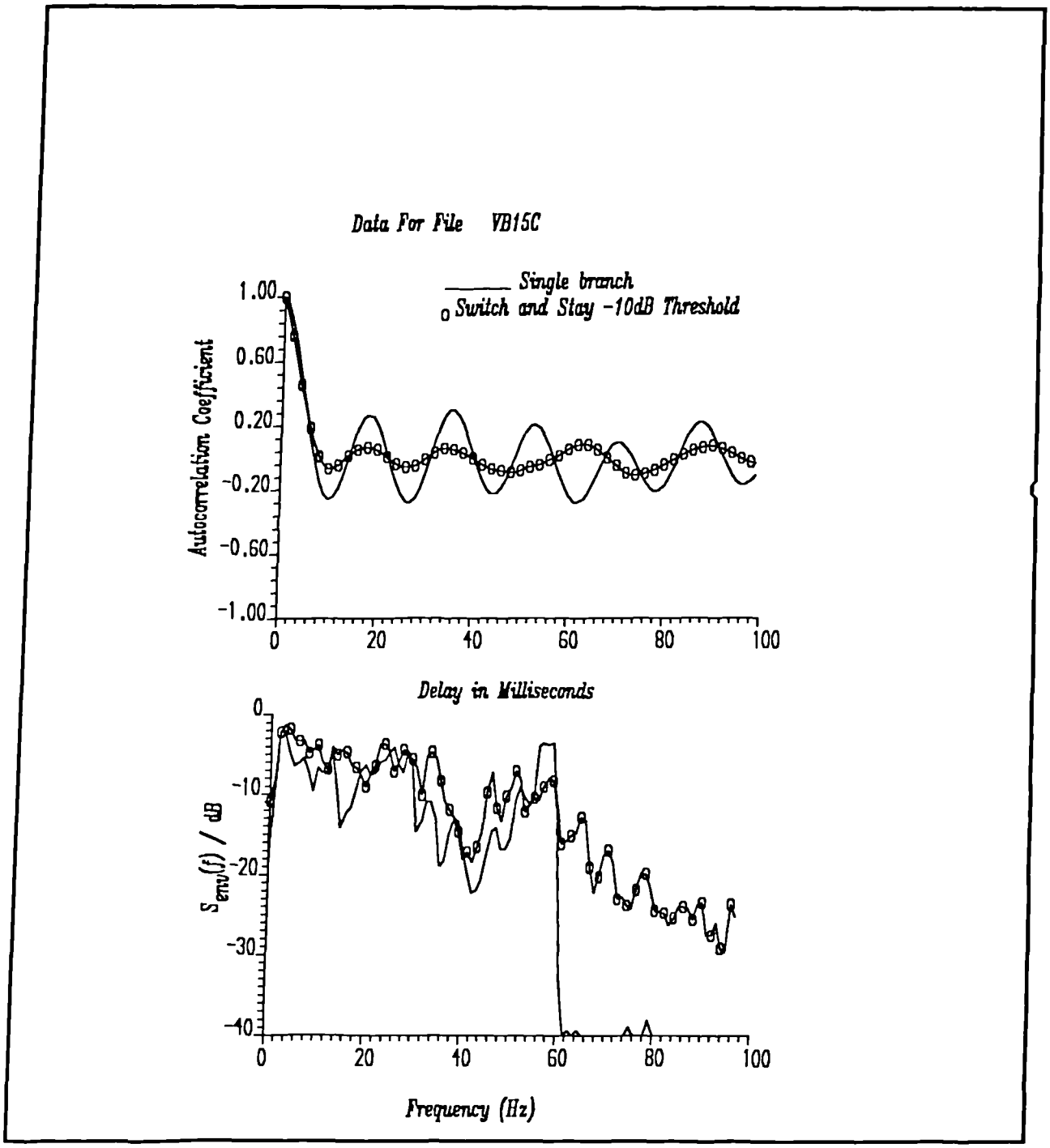

Figure 6.30 The measured autocorrelation and envelope spectrum for an individual branch and SAS diversity (-10dB switching threshold). Note the increasing of the lower frequency energy and the broadening of the spectrum beyond $2f_D$. This phenomena is synonymous with the diversity action smoothing out the envelope time series with the switching transients causing the spectral broadening. The absence of energy below 2Hz is simply due to the normalisation procedure which removes the local mean variation of the envelope.

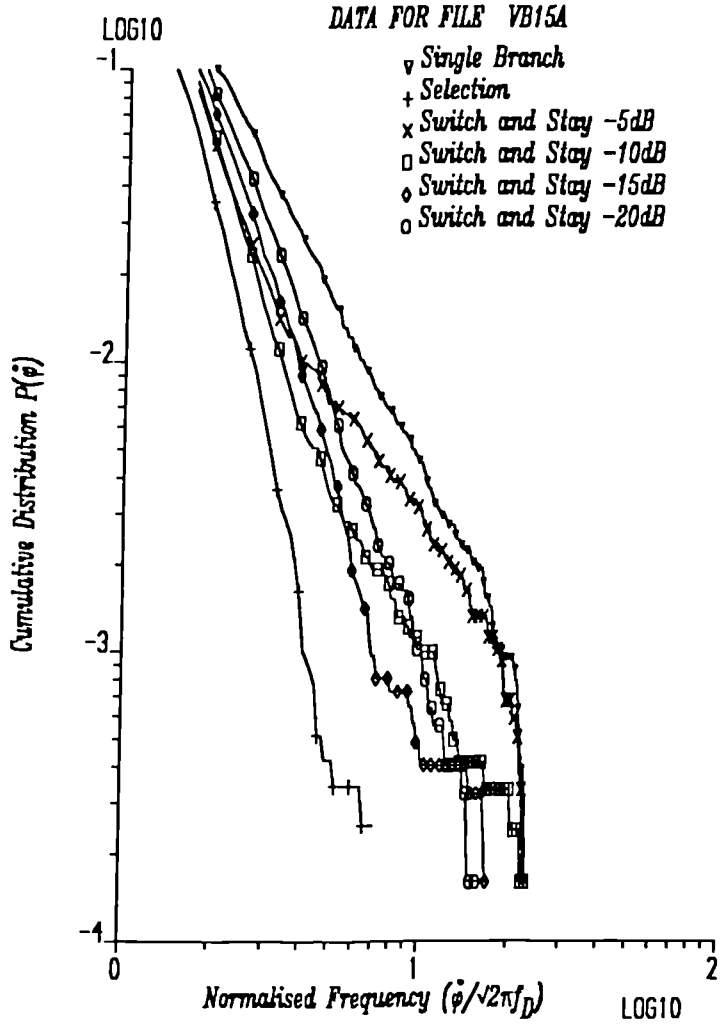

Figure 6.31 The measured CDF of the random FM component for a single branch, SEL and SAS (-5dB to -20dB thresholds) diversity for data gathered from a base station site using a vertical antenna separation of 15λ. Note that SEL provides the best improvement with SAS showing optimum performance with a switching threshold of -10dB to -15dB.

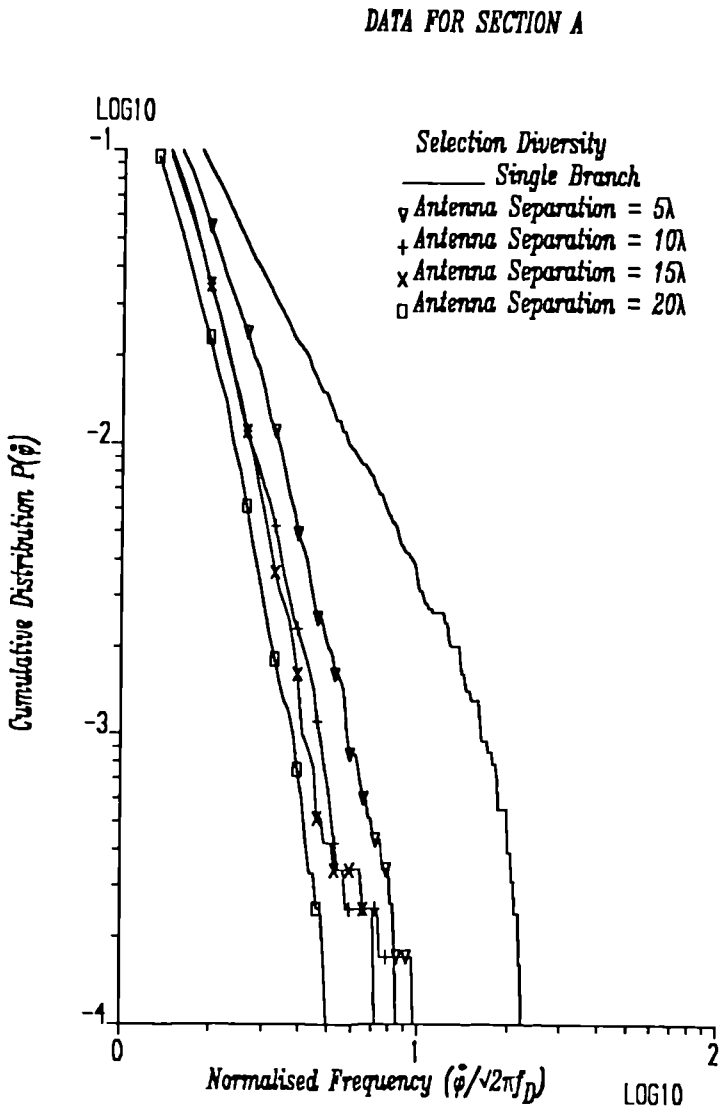

Figure 6.32 The measured CDF of the random FM component for a single branch and SEL diversity as a function of branch crosscorrelation. Note that there is little increase in improvement for antenna separations beyond 10λ.

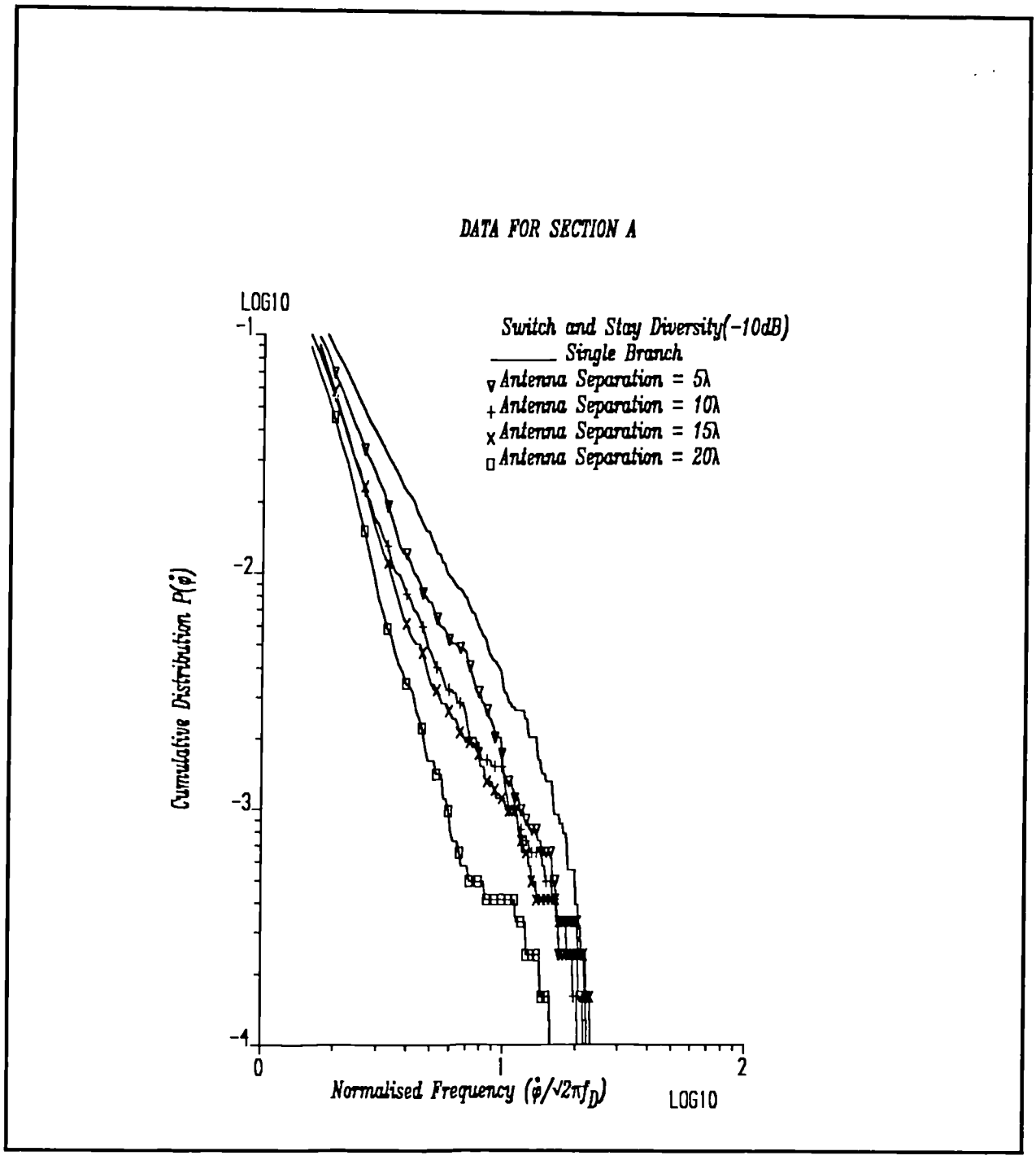

Figure 6.33 The measured CDF of the random FM component for a single branch and SAS diversity (-10dB threshold) as a function of branch crosscorrelation. Note that the improvement is not as good as that provided by SEL diversity and that in this case optimum performance is achieved at maximum antenna separation.

CHAPTER 7. CONCLUSION.

7.1 SUMMARY

This final chapter contains a summary of the work undertaken in this thesis. The summary will be in two parts. Firstly, the results of the investigation will be collated and discussed in terms of the original aims of the work. Secondly, some proposals for future work will be presented as a consequence of the findings of this study.

In the second chapter a review of the received signal statistics was presented in terms of two propagation models. The conventional two dimensional propagation model, where the multipath waves are constrained to propagation in the horizontal plane only, was considered in terms of the classical results associated with Rayleigh fading. The three dimensional model, where the multipath waves are considered to exist in both the azimuthal (i.e. horizontal) and elevation (i.e. vertical) planes was examined and it was found that the major difference between the two models is seen in the spectral statistics and not those statistical parameters pertaining to just the envelope and phase alone. This later model is considered by the author to be of considerable importance to the understanding of the propagation mechanisms associated with small cells where the effects of height probably become increasingly more important and where, in addition, few multipaths may, on occasions, exist.

In the third chapter the envelope statistics of several predetection diversity combiners were presented in a unified form using a number of reference sources. The statistical parameters were found for both the largely unrealistic case of uncorrelated branches and for the more meaningful case of correlated branches. Each of the diversity strategies considered was able to provide a considerable improvement in system performance, as evidenced by the statistical parameters related to the envelope. Maximal Ratio Combining(MRC) provided the biggest im-

provement followed by Equal Gain Combining(EGC) and Selection(SEL) diversity. The improvement in all three cases persisted even for high values of cross-correlation between the branches. Switch And Stay(SAS) diversity showed the least improvement of the diversity strategies. The best improvement provided by SAS was obtained with a switching threshold approximately 10dB below the local mean envelope value. SAS diversity did not show the same resilience to highly correlated signals as the other diversity strategies. The CDF of random FM, for SEL diversity, was derived for uncorrelated branches. The results of this derivation clearly showed that such a diversity scheme could dramatically reduce the effects of the random FM noise.

In the fourth chapter a simple account of vector demodulation was presented in terms of the measurement of carrier signal amplitude and phase. The origins and methods of reducing several sources of error (amplitude imbalance, quadrature dc off-set and quadrature error) were discussed in terms of the appearance of each source of error, on the envelope and phase, in relation to a test signal (a tone) viewed on a CRO. The concept of the vector demodulator receiver was then extended to the design, construction and testing of a dual branch direct conversion vector demodulator receiver with an operating frequency of nearly 1GHz, a dynamic range of +45dB and a sensitivity of -110dBm. To measure the phase characteristics of a mobile radio channel required that the transmitter and receiver were both frequency and phase locked to each other. The practicalities of achieving such coherency, in a mobile radio environment, was then examined in terms of the phase noise performance of the experimental configuration. The overall system, in which the receiver was operated, was then discussed in terms of a dual selective front-end stage, for the receiver, and the recording equipment used to store the dual branch quadrature information. Finally, the transmitter system was discussed for two experimental arrangements, one with the receiver at the base station and the other for the receiver at the mobile.

In the fifth chapter the experimental procedure and initial data reduction were discussed. Two sets of field trials were outlined; one where two vertically spaced receiving antennas were located at the base

station, the other where the two vertically separated antennas were located at the mobile. In each case the vehicle was driven at a constant speed of 10m/s around a preplanned test route using several different values of antenna displacement. The recorded results formed a data set that enabled a realistic comparison to be made between several predetection diversity strategies in terms of both the envelope and phase. Prior to the analyses, the data were reduced to a usable form through decoding and calibration. The envelope statistics were later examined using normalised data whereby the slow fading component (introduced by variations in the gross terrain features and not multipath) was removed using a moving average window technique. This technique was discussed in detail with respect the the vehicle speed and data sampling. Reference to an earlier investigation suggested that an averaging window of half a second together with a vehicle speed of 10m/s and sampling rate of 1 Hz enabled the local mean to be estimated to within $\pm 1dB$ to $\pm 2dB$.

The sixth chapter presented results of the investigation for three distinct areas of interest. The first section of Chapter 6 considered the received signal statistics of a single branch. It was found that for small cells (in this case the cell radius was 1.3km) a not uncommon propagation mode occurred whereby interference between a direct and indirect path resulted in deep fades occurring more frequently than that experienced in the more commonly encountered Rayleigh fading environment. Overall, the statistics associated with the phase were found to conform to those predicted by a Rayleigh fading model (e.g. probability of phase, differential phase and phase gradient). The measured Doppler spectrum however seldom matched the familiar 'U' shape predicted by theory. Instead it was noticed that the low frequency components sometimes dominated the spectrum in a fashion suggested by the three dimensional propagation model (see Chapter 2 and Aulin reference therein). The unusual shaped spectrum could also be explained in terms of a non-uniform angle of arrival for the multipath waves or the summation of only a few multipaths with non-random phases. Both of these later two conditions might easily occur for propagation in small cells.

In the second section the cross-correlation between signals received on two vertically separated antennas was investigated. The cross-correlation was examined in terms of both the envelope and complex signal received on the two branches. It was found that ρ_{env} is a good approximation for $|\rho_{12}|^2$ for the field trials carried out in this work. The cross-correlation between the branches was determined over a range of vertical antenna separations at both the base and mobile stations. The results of the base station experiment confirmed an earlier investigation in that an antenna separation of between 8λ and 13λ is all that is necessary for diversity to provide useful improvements in the received signal statistics (i.e. $\rho_{env} \leq 0.7$). Not only is a small amount of rooftop space required for vertically separated antennas at the base station but also the improvement afforded is not dependent upon the direction of the mobile with respect to a line joining the base station antennas. Both these results are in marked contrast to that experienced using a horizontally separated antenna arrangement. A similar vertical displacement experiment at the mobile suggested that a separation between the antennas of $\leq 1\lambda$ is all that is necessary for diversity to be usefully employed at the vehicle. The cross-correlation results at the mobile suggest that an unobtrusive and physically small antenna arrangement could be used on the vehicle roof. A scattering model was developed for signal reception both at the base and mobile stations in terms of the scatterers surrounding the vehicle. The scattering model fitted the experimental results well, suggesting that the principal scatterers are situated some 20m to 30m from the vehicle. This scattering distance implies that the buildings immediately lining the test routes act as the principal sources of multipath. The degree of cross-correlation between the branches was found to be inversely related to the cross-sectional area of the scatterers viewed by the diversity antennas. The antennas at the mobile therefore viewed a wider scattering area than that experienced by the base station antennas for a given antenna displacement.

The third and final section of Chapter 6 considered the effects of several predetection diversity strategies, using data received on two vertically separated antennas. This analysis allowed a true comparison

to be made, in terms of the envelope and phase, between the various strategies since the same field-recorded data was used in each case. The results were considered in terms of the degree of cross-correlation between the two branches (i.e. antenna separation) and the location of the diversity receiver (i.e. base or mobile). At both receiver locations it was found that a significant improvement in performance, as evidenced by the received signal statistics could be achieved at relatively small values of antenna separation. Maximal ratio combining was found to provide the greatest improvement with little impairment to performance as a result of increasing cross-correlation (i.e. smaller antenna separation). Switch and stay diversity shows a best improvement with a switching threshold of -10dB. This scheme however, suffered a rapidly decreasing improvement with increasing cross-correlation. The effects of MRC and EGC diversity on random FM were not examined in this work. The effects of these two strategies is dependent upon the method of implementation, which can vary from the total elimination of the random FM component to no reduction whatsoever (i.e. the output of the diversity strategy is the same as that of a single branch). The effects of diversity on random FM was examined for the SEL and SAS diversity strategies. SEL diversity provided the best improvement in reducing the deleterious effects of random FM. Again SAS showed an optimum performance using a switching threshold of -10dB. Both the strategies showed a maximum improvement in reducing random FM at the highest values of differential phase. The results found for SEL diversity agreed well with those derived in Chapter 3.

In summary therefore, the designed receiver performed to expectation in measuring the narrowband channel, in terms of both the envelope and phase on two branches, for propagation over small cells in an urban environment. The results have shown that propagation in such an environment cannot be solely described in terms of Rayleigh statistics and that worse propagation conditions, than Rayleigh, sometimes prevail. In addition, predetection diversity can provide a considerable improvement in system performance when used at either base or mobile stations for realistic values of antenna separation.

7.2 RECOMMENDATIONS FOR FUTURE WORK.

As a result of these investigations the author considers that there are four areas in which further studies are worthwhile.

Firstly, it is suggested that the existing data could be used to investigate how various estimator algorithms perform in relation to predicting the amplitude and phase of the measured channel. Such an analysis would be extremely useful since future generation mobile communication systems might utilise estimator/predictor techniques in conjunction with high order digital modulation (e.g. vector modulation) schemes in order that more efficient use is made of the RF spectrum. The existing data is extremely useful for such an analysis because it is real, i.e. it possesses the vagaries of a true channel, and is not subject to the many assumptions used in computer simulation studies. In addition, the data exists in the form of two phase locked branches and hence the various diversity strategies could be assessed using the real data with simulated high order modulation schemes that employ estimator/predictor techniques.

As a consequence of this first recommendation it is further suggested that field trials be conducted in which the dual branch vector demodulator receiver is used in conjunction with the transmission of high order modulation schemes using estimator techniques.

Thirdly, it is recommended that field trials be conducted using the equipment described in this work to investigate the complex signal for propagation in very small cells (i.e. cells with a radius $\ll 1km$) with diversity. The information gathered from such field trials would, the author feels, be of considerable use in further understanding the propagation mechanisms for small cells. In small cells the effects of multipath propagation in the vertical plane would be expected to play an increasingly more important role, especially in terms of the received spectra and degree of cross-correlation between the signals received on two vertically separated antennas. In addition, various diversity strategies could be assessed over the wide range of propagation modes that occur in small cells.

Finally, it is suggested that any future dual branch vector demodulator receiver be constructed to operate at a high IF in order to accommodate a wider range of RF input frequencies. Although such a receiver would be more complicated to build and test than than the unit employed in this work, the higher operating frequency would enable diversity to be assessed at those frequencies where future generation mobile communications systems might be expected to operate.

APPENDIX A. REFERENCE PAPERS.

This appendix contains papers referred to in this work which were either written or co-written by the author. The titles and sources of these papers are;

[1] Williamson, A.G., Adachi, F., Feeney, M.T. and Parsons, J.D., "Base Station Space Diversity for Mobile Radio Systems", Presented at the IREECON (Melbourne Australia) Oct. 1985, pp.228-231.

[2] Adachi, F., Feeney, M.T., Williamson A.G. and Parsons J.D., "Cross-correlation Between the Envelopes of 900MHz Signals Received at a Radio Base Station Site", IEE Proc. Pt.F., Vol.133, No.6, 1986, pp.506-512.

[3] Feeney, M.T. and Adachi, F., "The Performance of Various Diversity Combiners on Signals Received at a Base Station Site", Presented at the IERE Third International Conference on 'Land Mobile Radio', Publication No.65, pp.55-62, 1985.

[4] Adachi, F., Feeney, M.T. and Parsons, J.D., "An Evaluation of Specific Diversity Combiners Using Signals Received by Vertically Spaced Base Station Antennas", J. of IERE Vol. 57, No.6 (Supl.) pp.S218-S224 1987.

[5] Adachi, F., Feeney, M.T. and Parsons, J.D., "Effects of Correlated Fading on Level Crossing Rates and Average Fade Duration with Predetection Diversity Reception", IEE Proc. Pt.F, Vol.135, No.1, pp.11-17, 1988.

[6] Parsons, J.D. and Feeney, M.T., "Comparison of Selection and Switched Diversity Systems for Error-Rate Reduction at Base-Station Sites in Digital Radio Systems", 37th IEEE Vehicular Technology Conference, 1-3rd June 1987, Tampa Florida, pp.393-398.

[7] Adachi, F., Feeney, M.T. and Parsons, J.D., "Level Crossing Rate and Average Fade Duration for Time Diversity in Rayleigh Fading Conditions", IEE Proc. Pt.F, Vol.135, No.6, pp.501-506, 1988.

presented at IREECON '85 (Melbourne 30 Sept - 4 Oct 1985)

Base Station Space Diversity for Mobile Radio Systems

A.G. Williamson
University of Auckland, Auckland New Zealand
F. Adachi
Nippon Telephone and Telegraph Public Corporation, Japan
M. Feeney
J.D. Parsons
University of Liverpool, UK

Aspects of diversity systems for mobile radio are reviewed, and the suitability of space diversity is noted. Details of the receiving antenna system at both the mobile and the base station are discussed, and a recent base station diversity investigation is outlined, and results reported.

INTRODUCTION

The signal received by a mobile operating in an urban environment is subject to deep and rapid fading, a result of the mobile moving through the standing wave set up by the interference of the various scattered waves in the vicinity of the mobile. In most locations no line-of-sight path exists between the base-station and the mobile, and communication is achieved only by the reception of these scattered waves. The received signal can vary by as much as 20-30dB in as short a distance as a quarter of a wavelength (8cm at 900MHz). The signal received at the base station from a moving mobile transmitter suffers the same signal variations.

Clearly, for a given mean signal in, or from, some locality, the reliability of communication will be worse for a transmission suffering fading compared to that for one not so affected. Diversity reception is a technique which can mitigate the effects of fading, and thus provide improved reliability of reception of transmissions subject to fading.

In this paper we briefly review the essential features of a diversity system for mobile radio applications, note the suitability of space diversity systems, and consider the receiving antenna system requirements at both the mobile and base station. A recent experimental study of base station space diversity is reported.

DIVERSITY SYSTEMS

The essence of any diversity system is obtaining and processing two (or more) independent samples of the same transmission.

There are a number of ways of obtaining the samples. While retransmission (time diversity) and frequency diversity are possibilities, they reduce throughput and require greater spectrum, respectively, which make them unattractive solutions for mobile radio applications where demand for service and spectrum is very high. Polarisation diversity is also a possibility, but it requires the transmission of two polarisations. For mobile radio applications we would like to minimise additional equipment requirements and avoid, as far as possible, additional complexity at the mobile. For these reasons space diversity is attractive because it requires the transmission of only one polarisation, and the additional equipment complexity, compared to non-diversity reception, is restricted to the receivers (and receiving antennas).

Having obtained the two (or more) independent samples, there are a variety of processing techniques which can be employed [1]. These techniques each have different degrees of complexity and performance. We shall not be concerned in this paper with discussing the relative merits of the various techniques. It is sufficient for our purposes to note that even the simplest techniques can provide significant improvements in terms of reception reliability. It is also worth noting [2] that while increasing the number of branches (independent signals) provides increasing improvement, the greatest benefit is achieved between non-diversity (one-branch) and two-branch diversity systems. For this reason, in the remainder of this paper we shall think of diversity for mobile radio systems in terms of two-branch systems.

Whatever the technique employed, the basic requirement then is to obtain two samples of the transmission each having approximately the same mean power level, but fading independently. While zero correlation between the signals would produce the greatest benefit, it has been shown [3] that useful advantage can be obtained from signals whose correlation is less than about 0.7. The question which now remains is how do we obtain such signals?

SPACE DIVERSITY FOR MOBILE RADIO SYSTEMS

Space diversity is the means of obtaining the two samples of the transmission from two antennas separated by some distance. The question thus reduces to determining what separation is required in order that the fading of the signals is usefully independent. In the mobile radio situation, the mobile and base station environments are quite different, and this results in quite different required separations. It is thus appropriate to consider the two situations separately.

Mobile

The diffraction and reflection of the signal which permits communication between the base station and the mobile in the absence of a line-of-sight path gives rise to multipath propagation. Moreover, because the clutter in the locality of the mobile more or less completely surrounds the mobile, the multipath signals received by the mobile antennas tend to arrive from all angles in random relationship. The effect of this is that the correlation coefficient between the two signals of two antennas decreases quite rapidily as the separation of the two antennas is increased, even for quite small separations. It has been shown [4] that in practice a separation of only a fraction of a wavelength is all that is necessary at the mobile to obtain signals with a correlation coefficient of less than 0.7.

Consequently obtaining suitable signals at the mobile is not difficult, certainly at VHF and UHF, and we shall consider the matter no further here.

Base station

In contrast to the mobile environment, the base-station is usually much less cluttered, and elevated above the coverage area. As a consequence most of the signals received at the base station arrive within a cone-shaped region centred on the mobile location. Moreover the cone apex angle is quite small, [5] suggests of the order of 0.4° for a range of 3 miles. The consequence of this is that much larger antenna separations are required at the base station than at the mobile in order to obtain signals with low correlation. The antenna separation could, of course, be in the horizontal or vertical planes, or perhaps both.

Horizontal separation base station space diversity has been investigated by a few authors [3,5-7]. It has been found that the required separation between the antennas is dependent on the angle between a line between the mobile and base station and the base station diversity antennas base line. The required separation has been reported to be of the order 15-20λ for the broadside case and 70-80λ for the endfire case [3]. It is also a function of base station height [6]. While such separations may be acceptable at some sites in a system they may be difficult to accomodate at restricted city sites such as may be necessary in cellular systems for example. It is also worth noting in passing that the presence of local scatterers at the base station tends to decrease the correlation between the two received signals [5].

Vertical separation base station space diversity has some attractions for mobile radio systems, since in some situations vertical separation may be more easily accomodated than horizontal separation. Vertical separation systems have however received little attention [7]. The restricted study in [7] found that the signals from two vertically separated antennas were quite highly correlated up to 10λ separation. Moreover it appeared that the relationship between correlation and separation displayed a "standing wave" variation. Separations greater than 10λ were not considered in [7].

CELLULAR MOBILE RADIO

A potential application of diversity reception in mobile radio is in cellular systems. Because of the frequency reuse inherent in cellular mobile radio systems, it is impractical to increase the transmitter power to provide an additional margin against fading in view of the interference implications. This would be particularly so in urban areas where the cells are likely to be small, and the fading quite severe because of the highly obstructed transmission paths. Diversity reception offers the possibility of improving reception reliability without increasing transmitter power. Of course, in areas with small cells, where diversity may be most attractive, there would be many base stations. In view of the restricted size of many base station sites, or the cost of rental etc, we would want, or need, to keep the space requirements to a minimum consistent with the desired performance.

This is the background for a recently conducted study undertaken at the University of Liverpool, U.K.

EXPERIMENTAL STUDY

The aim of the study was to compare the performance of various base station antenna configurations for use in a diversity system. The principal parameter of interest, of course, is the correlation coefficient of the two received signals. The study was undertaken at 900MHz in the Liverpool city area.

The base station which operated in the receiving mode was installed on the roof of the Department of Electrical Engineering and Electronics of the University of Liverpool. The equipment comprised two receivers the input signals to which were from two identical half-wavelength dipoles the relative disposition of which could be altered in both the horizontal and vertical planes. The log video outputs of the two receivers (that is outputs proportional to the input signals in dBm) were recorded on an (8 track) FM tape recorder.

The 900MHz transmitter was operated from the mobile which was driven along a preplanned route. Voice commentary and tacho signals from the vehicle were also transmitted on other frequencies, received at the base station and also recorded on the tape recorder.

The test route of approximately 2km in length contained four separate test sections each of about 200-250m in length. The test area was located approximately 1.3km from the base station, the maximum range possible with the transmitter and equipment available given that it was necessary for the received signal in the deep fades to be above the receiver threshold.

The data collection was accomplished in the following manner. For a particular antenna configuration at the base station the mobile was driven around the test route, in both directions, as the received signal levels were recorded for the four sections (eight records in all). The four test sections comprised: two highly obstructed sections approximately circumferential to the base station, one obstructed section almost radial to the base station and one section neither circumferential nor radial and up an inclined road thus resulting in a progressive reduction of path obstruction.

A number of different base station configurations were investigated so their comparative performance could be assessed. The following situations were considered:

- Horizontal separation only: for separations of multiples of 5λ, from 5λ to 45λ (depending on θ), for θ=0°, 10°, 20°, 30°, 60° and 90° where θ is the angle between a line from the base station to the nominal centre of the test area and the baseline of two antennas.
- Vertical separation only: for separations from 2λ to 24λ in increments of 1λ.
- Joint horizontal and vertical separation: near end-fire case (θ≈0) for horizontal separation in increments of 5λ and vertical separation in increments of 4λ.

The horizontal separation cases were investigated so as to permit comparison with previously published results [3,5,7], and to provide results obtained in the same test environment for comparison with the other results. The range of vertical separation cases studied was more extensive than that in [7].

Joint displacement cases were only considered for cases near end-fire since it is only for such cases that the separation distances required for horizontal separation become large. One purpose of the investigation of joint displacement situations was to assess whether the required horizontal separation for such cases could be reduced by introducing some vertical separation.

In order to calibrate the data gathering system, known signals were fed into each of the receivers prior to commencing the test-runs and the outputs recorded. These records, together with the records for the test sections for the various antenna configurations were subsequently digitized and the results transferred to computer for processing.

RESULTS

The analysis of the data, and calculation of the correlation coefficient follows that in [3]. The initial phase of processing the data has been completed, and results for two situations are shown in Figs 1 and 2.

Fig 1 presents results for the section of the route which was nearly radial, and shows the variation of the correlation coefficient with horizontal separation. Results are shown for θ=0°, 10°, 20°, 30°, 60° and 90°. (It should be noted that θ was measured between the antenna base line and a line to the nominal centre of the test area. The nearly radial route to which Fig 1 relates was approximately 6° from base station/test area centre line.) The key point to note from Fig 1 is that the correlation coefficient tends to decrease with both increasing θ and horizontal separation. This is in agreement with previously published results.

Results for vertical separation cases are given in Fig 2 in terms of the correlation coefficient as a function of vertical separation. (The results are not functions of θ of course because of the omnidirectional character of the receiving antennas arrangement.) Two cases are considered in Fig 2; results are given for the nearly radial test section considered in Fig 1, as well as for a neighbouring almost circumferential test section. The interesting aspect of the results in Fig 2 is that the correlation coefficient decreases with increasing vertical separation. Results for the two other test sections investigated show the same trend. This is in marked contrast to the results of the limited study reported in [7] which tended to indicate that the variation of correlation coefficient with vertical separation displayed a standing wave character. On the basis of the results presented in Fig 2 a vertical separation of the order of 15λ would seem to be satisfactory for vertical separation base station diversity.

Early results for the joint displacement cases have indicated that for a given horizontal separation the correlation coefficient is affected by increasing vertical separation, quite significantly so for small horizontal separations, and that for a given vertical separation the correlation coefficient decreases with increasing horizontal separation. Further analysis and interpretation of the results is continuing.

CONCLUSION

The application of diversity reception in mobile radio has been considered, and the suitability of space diversity noted. Previous work on space diversity for mobile radio was briefly reviewed, and a recent experimental study reported. The results of this study for horizontal separation configurations were broadly in agreement with results published previously, while the investigation of vertical separation configurations was more extensive than that in an earlier study. A significant result of this recent investigation is that vertical separation space diversity systems appear feasible with a minimum separation of 15λ to obtain a correlation coefficient less than 0.7

ACKNOWLEDGEMENTS

This research was undertaken whilst two of the authors were visiting research fellows in the Department of Electrical Engineering and Electronics at the University of Liverpool, U.K.; AGW as Leverhulme Visiting Fellow, FA as a SERC Visiting Research Fellow.

REFERENCES

1. Parsons, J.D., Henze, M., Ratliff, P.A., and Whithers, M.J., "Diversity techniques for mobile radio reception", The Radio and Electronic Engineer, 45, (7), 1975, pp357-367.
2. Jakes, W.C., "A comparison of specific space diversity techniques for reduction of fast fading in UHF mobile radio systems", IEEE Trans Vehicular Tech., VT-20, (4), 1971, pp81-92.
3. Lee, W.C.Y., "Antenna spacing requirement for a mobile radio base-station diversity", Bell Sys Tech Journ, 50, (6), 1971, pp1859-1876.
4. Lee, W.C.Y., Mobile Communication Engineering, McGraw-Hill, New York, 1982, p276.
5. Lee, W.C.Y., "Effects on correlation between two mobile radio base station antennas", IEEE Trans Comm, COM-21, (11), 1973, pp1214-1224.
6. Lee, W.C.Y., "Mobile radio signal correlation versus antenna height and spacing", IEEE Trans Vehicular Tech., VT-25, (4), 1977, pp290-292.
7. Rhee, S.B., and Zysman, G.I., "Results of suburban base station spatial diversity measurements in the UHF band", IEEE Trans Comm., COM-22, (10), 1974, pp1630-1636.

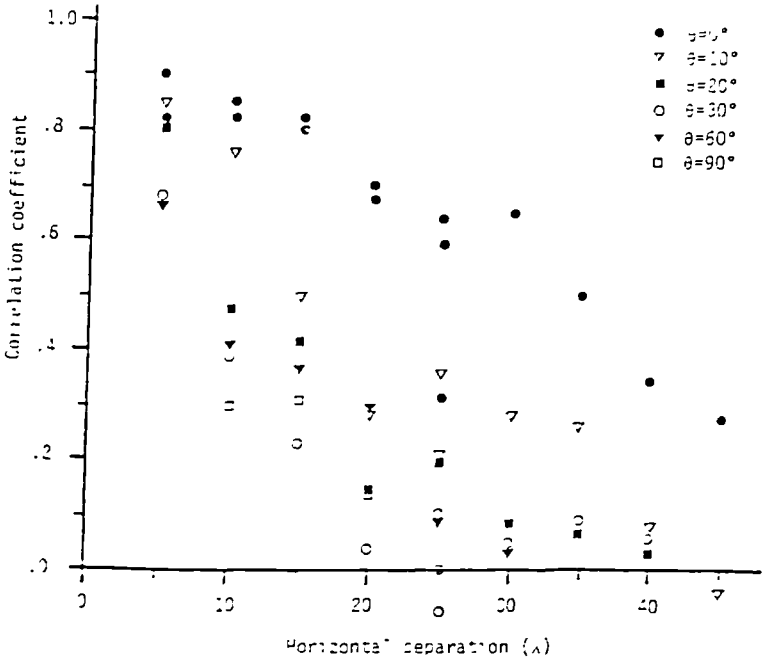

Fig 1. Correlation coefficient for horizontal separation cases for the nearly radial test section.

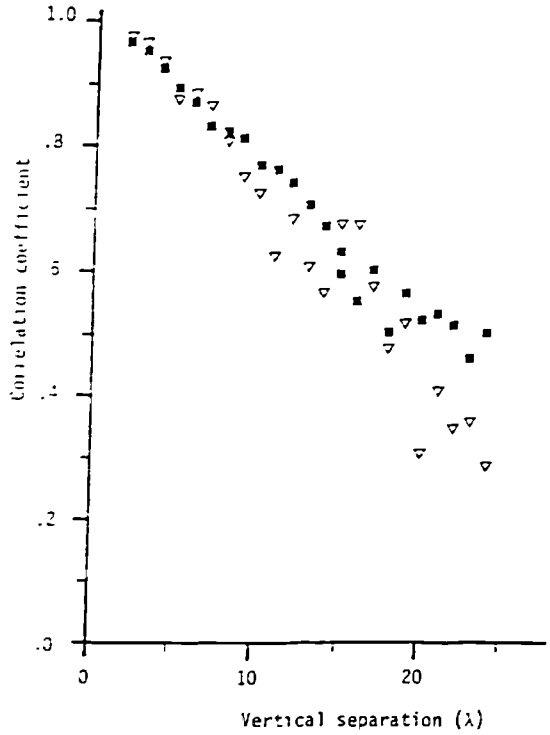

Fig 2. Correlation coefficient for vertical separation cases

▽ nearly radial test section,
■ nearly circumferential test section.

Crosscorrelation between the envelopes of 900 MHz signals received at a mobile radio base station site

F. Adachi, Ph.D., M.T. Feeney, M.Sc., Prof. A.G. Williamson, Ph.D., and Prof. J.D. Parsons, D.Sc.(Eng.), F.I.E.E.

Indexing terms Radiocommunication, Antennas, Radio-wave propagation (Terrain effects)

Abstract: An experimental investigation is reported of the crosscorrelation of 900 MHz signals received by two spatially separated antennas at a base station. The investigation embraced vertical, horizontal and combined horizontal and vertical separation of the antennas, for transmission from test routes 1.3 km from the base station. It was found that a crosscorrelation ≤0.7 (i.e. when diversity improvement becomes significant) can best be achieved using vertical separation of the antennas of between 11 λ and 13 λ, for the 1.3 km cell radius. At 900 MHz such an antenna separation is easily obtained and, in addition, the roof space required is small. Moreover, the crosscorrelation using vertically spaced antennas is independent of the incoming arrival angle (unlike horizontally spaced antennas), and hence low correlation can be achieved while maintaining omnidirectional coverage.

List of principal symbols

l = effective antenna separation
d_H = horizontal separation of base station antennas
d_V = vertical separation of base station antennas
e_i = complex amplitude of ith multipath wave
E = amplitude of ith multipath wave
f_D = maximum Doppler frequency
f = Doppler frequency of ith multipath wave
f_s = sampling frequency
L = distance of mobile from base station
$\hat{m}^2$ = estimate of local mean power
N = number of samples
$p(z)$ = probability distribution function of variable z
r_H = effective distance of scatterers from the mobile for multipath waves received in a horizontal plane
r_V = effective distance of scatterers from the mobile for multipath waves received in a vertical plane
$R(t)$ = time-varying signal strength envelope
$r(t)$ = time-varying Rayleigh-distributed signal strength envelope
T = sampling interval
z^* = complex conjugate of complex variable z
$\bar{z}$ = ensemble average of variable z
α = angle between two base station antennas and a mobile
α_H = arrival angle in horizontal plane of incoming multipath wave
α_i = arrival angle of ith multipath wave
α_V = arrival angle in vertical plane of incoming multipath wave
λ = wavelength
ϕ_i = phase of ith multipath wave
ρ_{env} = crosscorrelation between two signal envelopes
ρ = complex crosscorrelation between two signal envelopes
ω = carrier angular frequency

Paper 4841F (E8), first received 1st April and in revised form 16th July 1986

Dr Adachi is with the NTT Yokosuka Electrical Communication Laboratories, PO Box 8, Yokosuka-shi, Kanagawa-ken 238, Japan; Mr. Feeney and Prof Parsons are with the Department of Electrical Engineering & Electronics, University of Liverpool, Brownlow Hill, PO Box 147, Liverpool L69 3BX, United Kingdom; and Prof Williamson is with the Department of Electrical & Electronic Engineering, University of Auckland, Private Bag, Auckland, New Zealand

1 Introduction

In mobile radio, the received signal envelope is composed of the superposition of fast and slow fading components [1]. The fast fading (Rayleigh fading) is caused by the interference between multipath waves from the surrounding scatterers. The slow fading (sometimes called log-normal fading or shadowing) is caused by gross variations in the terrain between the base and mobile stations.

Diversity reception [2] is one of the most promising techniques available for reducing the effect of the rapid and deep fading. Practical diversity systems for mobile radio are unlikely to employ more than two branches, since as the number of branches increases the incremental improvement decreases and in addition the system becomes more complex. For diversity reception at the mobile the antenna separation need only be around 0.2λ, since the principal scatterers surround the mobile. At the base station, however, the antenna spacings required are considerably larger because the spread in arrival angles is small compared with that experienced at the mobile. Lee [3] studied the crosscorrelation ρ_{env} between the received signal envelopes at two antennas as a function of the horizontal spacing between the antennas (which were at the same height), and the angle α which the two antennas make relative to a line joining the base station with the mobile test area. He concluded that increasing the antenna separation reduced ρ_{env}, and that the smallest values of ρ_{env} occurred for a broadside configuration ($\alpha = 90°$). Recently Kozono and Turuhara [4] carried out an experimental study in the Tokyo area and reported similar results. In another study Rhee and Zysman [5] considered both vertical and horizontal separation. Their results indicated an oscillating tendency for ρ_{env} with increasing vertical separation.

This paper reports the results of a series of field trials in which a mobile transmitted to a base station where the multipath waves were received on two antennas. Various antenna configurations were used: vertical separation over a range from 2 to 24 wavelengths, horizontal separation at various angles α (from endfire to broadside), and a combination of both horizontal and vertical displacements for the endfire case. Results reported here give values for ρ_{env} determined using normalised data which are obtained by dividing the instantaneous signal envelope by an estimate

of the local mean. The values of ρ_{enc} are presented as a function of antenna configuration, and compared with values obtained from a theoretical model which describes the effect that a spread in arrival angles has on ρ_{env}.

2 Crosscorrelation calculation procedure

2.1 Effect of crosscorrelation on diversity improvement

The crosscorrelation ρ_{env} between two Rayleigh fading signal envelopes reduces the effective received signal power, with two-branch diversity, by $(1-\rho_{env})^{1.2}$. However, because deep fades occur only rarely, useful diversity advantage can still be obtained for ρ_{env} as high as 0.7. Since the principal scatterers surround the mobile, it is relatively easy to obtain a low ρ_{enc} at the mobile end of the link, and in such a case the minimum required spacing is around 0.2λ. However, at the base station the required antenna spacing will be larger than at the mobile, since the arrival angles of the multipath waves are concentrated within a small sector. The correlation is a function of the arrival angle of the multipath waves, the distribution of the scatterers surrounding the mobile and the antenna spacing. This means that the orientation of the routes travelled, relative to the base station, and the different types of area (i.e. suburban, urban etc.) affect the crosscorrelation.

2.2 Estimation of local mean

The received signal envelope is composed of superimposed fast and slow fading components. To calculate ρ_{enc} we have to remove the slow fading component, often called the local mean, which varies in a random manner. To estimate the local mean a moving average method can be used. The received signal strength $R(t)$ can be represented as

$$R(t) = r(t)m(t) \tag{1}$$

where $m^2(t)$ is the local mean power, which is the total power of the incoming multipath waves arriving at the receiver, and $r(t)$ is a normalised received signal strength which varies quickly (i.e. fast fading). In an urban area, the number of multipath waves can be assumed to be very large, and thus $r(t)$ becomes a Rayleigh process having unity power.

An estimate of the local mean power, $m^2(t_n)$, at a time t_n, for a vehicle moving at a constant speed can be found from a series of N samples using the following moving average method.

$$\hat{m}^2(t_n) = \frac{1}{N}\sum_{m=-\frac{N-1}{2}}^{\frac{N-1}{2}} \frac{R^2(t_{n-m})}{2} \tag{2}$$

where $\hat{m}^2(t_n)$ is the estimate of the local mean power. Using $\hat{m}^2(t_n)$ the estimated fast fading component $\hat{r}(t)$ is given by

$$\hat{r}(t_n) = \frac{R(t_n)}{\sqrt{[\hat{m}^2(t_n)]}} \tag{3}$$

This estimated fast fading (i.e. the normalised signal) can be used to calculate the crosscorrelation.

The length of time over which m^2 is estimated is $T = N/f_s$. If T is chosen too short then the local mean is poorly estimated, since fast fading components are still present. If T is too long the slow fading is largely lost. To establish a satisfactory value for T, a preliminary study was undertaken using a pure Rayleigh fading signal. It was found that the local mean power could be estimated to within ± 2 dB using a normalised averaging time length $f_D T \simeq 12$, and an estimate within ± 1 dB can be obtained using $f_D T \simeq 64$. For values of $f_D T > 12$, the improvement in the accuracy of the estimate improves very slowly with increasing $f_D T$. In the analysis of our data, $f_D T = 16$ was chosen. The driving speed of the vehicle was kept at a nearly constant 10 m s, which gives a maximum Doppler frequency of around 33 Hz. The observation period is thus 0.5 s, which corresponds to an observation length $L = (f_D T)\lambda = 5.3$ m. The data were sampled at a rate of 1 kHz, which represents 501 data points in the estimation of the local mean.

2.3 Crosscorrelation calculation

The crosscorrelation ρ_{env} between the normalised signals at two antennas is calculated using [6]

$$\rho_{env} = \frac{\overline{\hat{r}_1(t)\hat{r}_2(t)} - \overline{\hat{r}_1(t)}\,\overline{\hat{r}_2(t)}}{\sqrt{[\overline{\hat{r}_1^2(t)} - \overline{\hat{r}_1(t)}^2]}\sqrt{[\overline{\hat{r}_2^2(t)} - \overline{\hat{r}_2(t)}^2]}} \tag{4}$$

where $\hat{r}_1(t)$ and $\hat{r}_2(t)$ are the estimates of the fast fading components of the two received signals, as obtained from eqn. 3. Because the test routes were long (200–250 m), it is reasonable to assume that the principal scatterers surrounding the mobile would change as the vehicle progressed along a test section, and thus so would ρ_{env}. This effect was investigated by determining ρ_{env} for data segments, of 2 s duration, along each of the routes traversed. These segments were found to have normalised signal envelopes which followed a Rayleigh distribution. The values of ρ_{env} varied quite considerably over the segments of a section and for the various antenna configurations. An average value of ρ_{env} was determined for each section.

3 Experimental configuration

A test area, of varying topography, was chosen in the Everton district of Liverpool. Several routes were selected in the test area, these being positioned in approximately radial or transverse directions relative to the base station. The two types of route were chosen since the relative position of the scatterers would create different received signal statistics at the base station. A third type of route was also selected which allowed the mobile to move both radially and transversely (relative to the base station) on a hillside that included some locations giving line of sight propagation. Fig. 1 shows the various sections within the test area in relation to the base station, some 1.3 km distant. The base station was located on the roof of the Electrical Engineering building at the University, some 35 m above ground level.

The mobile transmitted a 5 W CW signal at 896.5 MHz via a vertical monopole antenna mounted on the roof of the vehicle. In addition, the vehicle was equipped with a transceiver for voice communication with the base station. The mobile was driven around the test route at a nearly constant speed of 10 m s. The test route was composed of four sections, each some 200–250 m in length, which were traversed in both directions.

At the base station a pair of half-wavelength dipoles, mounted vertically, were used in a variety of spaced configurations. The following situations were investigated for each section:

(*a*) *Horizontal separation only:* The base station antennas were operated at the same vertical height for horizontal separations from 5 to 50 λ in 5 λ steps for antenna angles α of 0°, 10°, 20°, 30°, 60° and 90°. The antenna angle α is the angle made between the two antennas and a line joining the base station with the centre of the test area.

(*b*) *Vertical separation only:* The antennas were

mounted vertically and separated in 1 λ steps from 2 to 24 λ.

(c) *Joint horizontal and vertical separation:* In this case α was arranged for the endfire configuration ($\alpha = 0$) and the horizontal spacing was increased from 5 to 45 λ in 5 λ increments for vertical separations of 4 to 16 λ in 4 λ steps.

The signal strengths from the two base station antennas were recorded on an eight-track FM recorder using the log-video outputs of two field-strength measuring receivers connected to each of the antennas. Thus the recorded values varied linearly in decibels. Preplanned markers on the test route were used to identify the start of data collection. Subsequently the data on the FM tapes were digitised, at a 1 kHz sampling frequency, and recorded onto

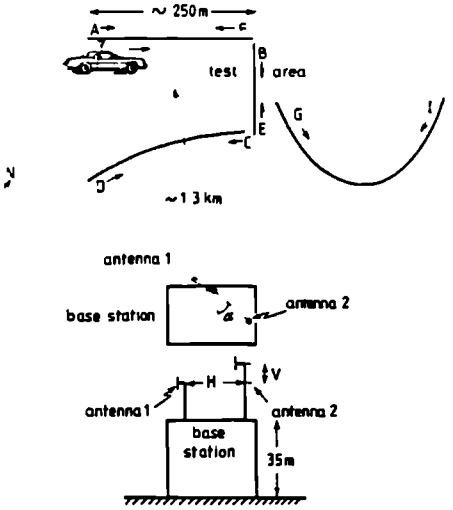

Fig. 1 *Test area in relation to base station and antenna arrangement*
Sections labelled A to I refer to data routes. Parameters H and V refer to horizontal and vertical antenna displacements. α is the antenna angle (see text for definition)

computer magnetic tape. A 'sample-and-hold' circuit was used in conjunction with an analogue digital convertor (ADC) to ensure simultaneity in the data. The ADC was an eight-bit machine with a resolution of 0.3 dB over a dynamic range of 75 dB (−115 dBm to −40 dBm). The 120 Mbyte of data gathered were transferred, in stages, onto one of the University's mainframe computers (an IBM 3083) for analysis.

4 Experimental crosscorrelation

4.1 Vertical separation

Fig. 2 shows the crosscorrelation of the envelopes of the signals received on two antennas at various antenna spacings for radial and circumferential routes. Both routes show a monotonic decline in ρ_{env} with increasing antenna separation. The radial section has, overall, a larger reduction in ρ_{env} for a given antenna spacing than the circumferential route. This is especially pronounced for large antenna spacings. This feature can be explained in terms of the radial route having a larger spread in arrival angles in the vertical plane than the circumferential route (see *Discussion*). It is generally accepted that for $\rho_{env} \leqslant 0.7$ an improvement in the received signal statistics can be achieved using a two-branch diversity system. In the case of vertical separation, $\rho_{env} = 0.7$ can be achieved at an antenna spacing of between 11 λ and 13 λ for radial and circumferential routes, respectively.

4.2 Horizontal separation

The crosscorrelation data at various horizontal antenna spacings and for various antenna angles α over radial and circumferential routes are shown in Figs. 3 and 4, respectively. In both sections it is seen that as the horizontal separation increases ρ_{env} decreases for all antenna angles. In addition, it can be seen that, as the antenna configuration approaches the endfire case ($\alpha = 0$) ρ_{env} increases for nearly all values of horizontal separation, which is in

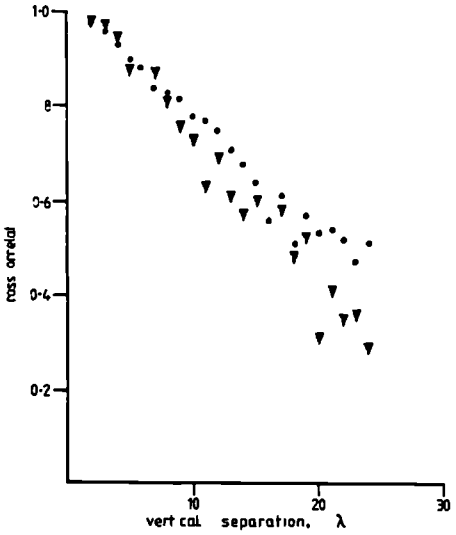

Fig. 2 *Crosscorrelation between signal envelopes (ρ_{env}) received on two antennas spaced at various vertical separations, for data from a radial and a circumferential route*
▼ early radial route B
● nearly circumferential route C

agreement with the trend found by Lee [3]. Overall, the values of ρ_{env} reported in this paper are smaller than those of Lee. It is believed that the differences can be attributed to the larger spread in multipath arrival angles in the Liverpool experiment, these arising because the test area is closer to the base station (1.3 km) than that used by Lee. The overall crosscorrelation is lower for the circumferential route than for the radial one. Again, this is attributed to a difference in the spread of arrival angles in the horizontal plane. In the case of the circumferential route the spread is larger, thus producing a lower value of ρ_{env}.

4.3 Joint separation

The crosscorrelation between the signal envelopes, received at two antennas separated both vertically and horizontally, is shown in Figs. 5 and 6. The endfire case is illustrated, and the Figures show data from radial and circumferential routes, respectively. For both cases it can be seen that an increase in either horizontal or vertical separation produces a reduction in ρ_{env}, with vertical separation having the larger effect. This is consistent with the two individual cases of horizontal and vertical separation dealt with earlier. The overall crosscorrelation is lower for the circumferential route than for the radial route, and again this is consistent with the results for horizontal separation alone at $\alpha = 0°$.

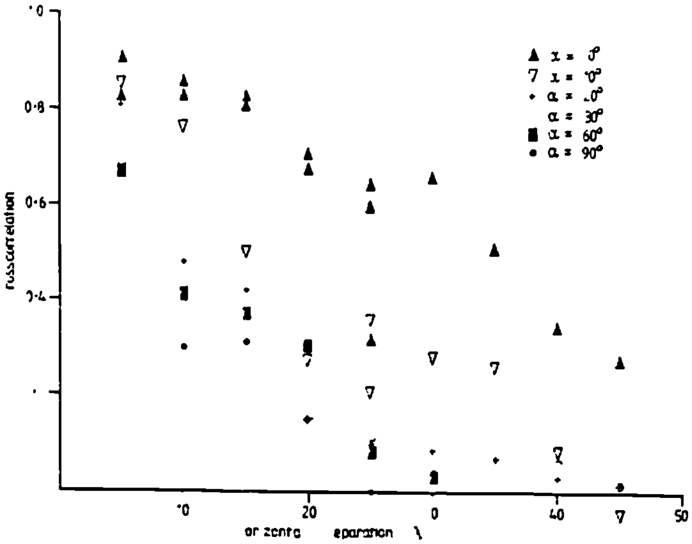

Fig 3 Cr ss rre ation retween ignal nvel pes $\rho_{..}$ received on two antennas eparated horizontally at arious antenna angles (α) or data fr m a radial route

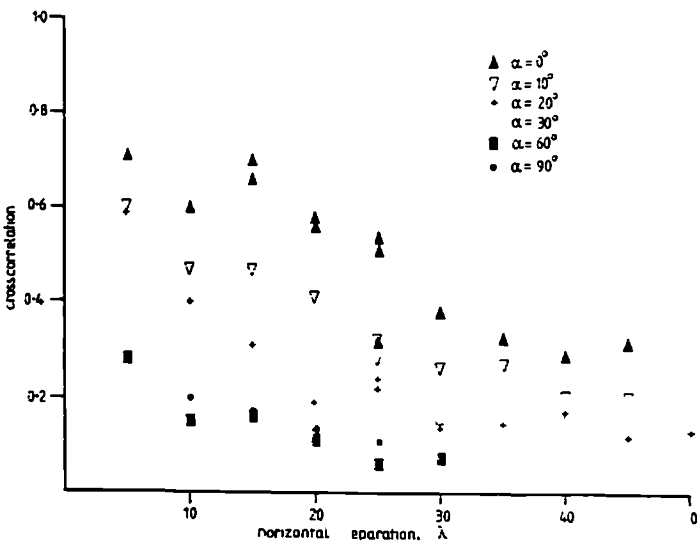

Fig 4 [illegible]

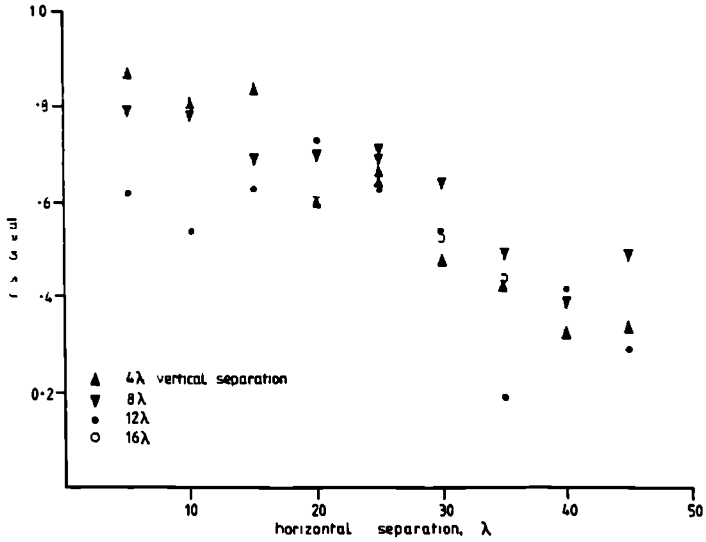

Fig. 5 *Crosscorrelation between signal envelopes (ρ_{env}) received on two antennas separated both horizontally and vertically at α = 0°, for data from a radial route*

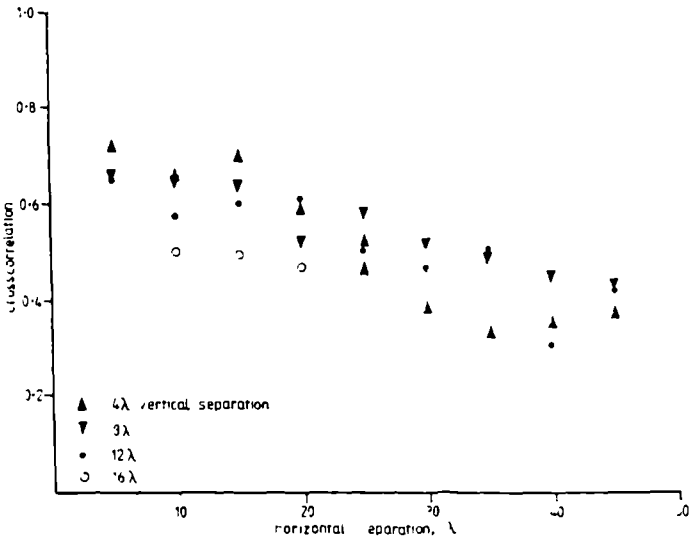

Fig. 6 *Crosscorrelation between signal envelopes (ρ_{env}) received on two antennas separated both horizontally and vertically at $\alpha = 0°$, for data from a circumferential route*

5 Theoretical analysis and discussion

5.1 Horizontal separation case

Consider the transmission from a moving vehicle received by the two antennas at the base station. It is assumed that no line-of-sight propagation path exists, and that all the waves received at the base station come from scatterers surrounding the mobile unit. It is further assumed that there are no local scatterers at the base station, and that the distance between the mobile transmitter and the base station receivers is much greater than the antenna separation. The co-ordinate system for this model is shown in Fig. 7. Under these assumptions, the received signals $e_1(t)$

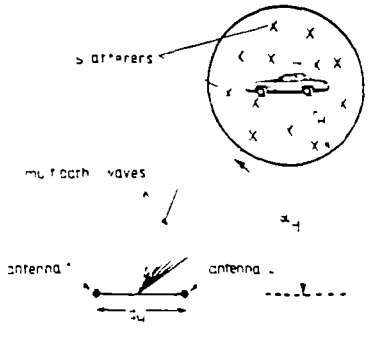

Fig. 7 *Co-ordinate system for calculation of the correlation as a function of the horizontal arrival angle α_H and the received signal envelope correlation with multipath waves*

Parameters r_H and r_i are horizontal antenna separation and distance of the scatterers from the mobile, respectively

and $e_2(t)$ are given by

$$e_1(t) = \sum_{i=1}^{N} E_i \exp\, j[(\omega_c - 2\pi f)t - \phi_i] \tag{5}$$

$$e_2(t) = \sum_{i=1}^{N} E_i \exp\left\{j\left[(\omega_c + 2\pi f_i)t - 2\pi \frac{d_H}{\lambda} \cos \alpha_i + \phi_i\right]\right\} \tag{6}$$

Since the multipath waves come from different scatterers, the random phases ϕ_i are independent.

The normalised crosscorrelation between the two received signals may be obtained from

$$\rho = \frac{\frac{1}{2}\langle [e_1(t) - \bar{e}_1(t)]^* [e_2(t) - \bar{e}_2(t)]\rangle}{\sqrt{\langle [\frac{1}{2}(e_1(t) - \bar{e}_1(t))]^2\rangle \langle [\frac{1}{2}(e_2(t) - \bar{e}_2(t))]^2\rangle}} = \frac{\frac{1}{2}\sum_{i=1}^{N} E_i^2 \exp\left\{-j\left(2\pi \frac{d_H}{\lambda} \cos \alpha_i\right)\right\}}{\frac{1}{2}\sum_{i=1}^{N} E_i^2} \tag{7}$$

Assuming the multipath waves have identical amplitude, i.e. $E_i = E$, then eqn. 7 becomes

$$\rho = \frac{1}{N}\sum_{i} \exp\left\{-j\left(2\pi \frac{d_H}{\lambda} \cos \alpha_i\right)\right\} \tag{8}$$

If we assume a large number of received waves, where $p(\alpha)$ is the probability density function (PDF) of α_i, we have

$$= \int_{-\pi}^{\pi} \exp\left\{-j\left(2\pi \frac{d_H}{\lambda} \cos \alpha_i\right)\right\} p(\alpha_i)\, d\alpha_i \tag{9}$$

Since the arrival angles at the base station are concentrated within a small angular width at an angle α_H, eqn. 9 can be approximated by

$$\begin{aligned}\rho &= \int_{-\pi}^{\pi} \exp\left\{-j2\pi \frac{d_H}{\lambda} \cos \alpha_H \cos(\alpha_i - \alpha_H)\right\} \\ &\quad \times \exp\left\{j2\pi\left(\frac{d_H}{\lambda} \sin \alpha_H\right) \sin(\alpha_i - \alpha_H)\right\} p(\alpha_i)\, d\alpha_i \\ &\simeq \exp\left\{-j2\pi \frac{d_H}{\lambda} \cos \alpha_H\right\} \\ &\quad \times \int_{-\pi}^{\pi} \exp\left\{j2\pi\left(\frac{d_H}{\lambda} \sin \alpha_H\right) \sin(\alpha_i - \alpha_H)\right\} p(\alpha_i)\, d\alpha_i\end{aligned} \tag{10}$$

if the angle α_H is not near 0°.

Thus, the crosscorrelation of the envelopes of two signals can be obtained from [7]

$$\rho_{env} \simeq |\rho|^2 = \left|\int_{-\pi}^{\pi} \exp\left\{j2\pi \frac{d'}{\lambda} \sin(\alpha_i - \alpha_H)\right\} p(\alpha_i)\, d\alpha_i\right|^2 \tag{11}$$

where d is the effective antenna separation, given by

$$d = d_H \sin \alpha_H \tag{12}$$

Eqn. 11 shows that the crosscorrelation is dependent on the arrival angle. To further examine this effect, let us assume that the distribution of arrival angle $p(\alpha_i)$, in the horizontal plane, is a Gaussian distribution with a variance of σ^2:

$$p(\alpha) = \frac{1}{\sqrt{(2\pi)\sigma}} \exp\left[-(\alpha - \alpha_H)^2/2\sigma^2\right] \tag{13}$$

Assuming that the effective scatterers are distributed near the mobile, and that the base-mobile distance is much larger than the distance of the scatterers from the mobile, the spread σ of the arrival angle of the multipath waves is given by

$$\sigma \sim (r_H/L) \tag{14}$$

where r_H is the effective distance of the scatterers from the mobile, measured perpendicular to the mobile to base direction. It can be seen from eqns. 11 and 14 that the crosscorrelation approaches unity as the mobile-base distance becomes larger.

Figs. 8 and 9 show both experimental and predicted values of ρ_{env} against effective antenna separation for

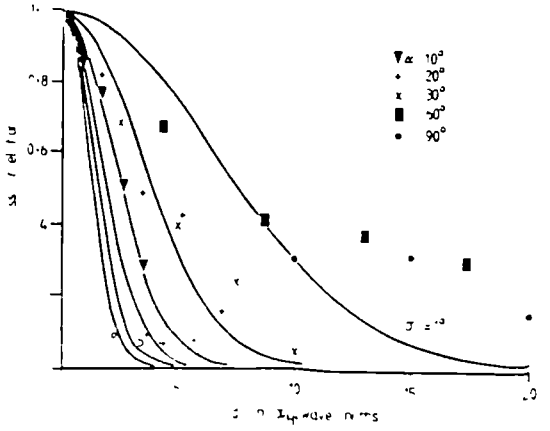

Fig. 8 [illegible]

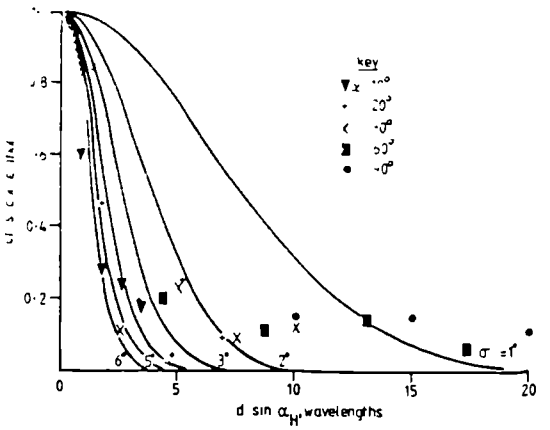

Fig. 9 *Theoretical curves (from eqn. 11) and experimental results of ρ_{env} as a function of effective antenna spacing and spread in arrival angle (σ) of incoming multipath waves for data from a circumferential route*

various arrival angles), for both radial and circumferential test routes. The curves represent values of ρ_{env} obtained from eqn. 11 by numerical integration) for a spread in arrival angles of 1° to 6°. The experimental data and the theoretical model appear to agree quite reasonably for a small spread in arrival angles. The spread in arrival angles for the radial route lies between 1° and 3°, while for the circumferential route it is 2° to 6°. The difference between the two can be explained in terms of the orientation of the routes. The circumferential route, when viewed from the base station, subtends a larger angle than the radial route, leading to lower correlation values for a given base station antenna configuration. Using eqn. 14 we find that the effective distance of the scatterers from the mobile is between 23 and 68 m for the radial route and between 45 and 136 m for the circumferential route. These values suggest that the principal scatterers are along the routes. The effective distances of the scatterers from the mobile are, in general, smaller for the radial route than for the circumferential one in the case of horizontal antenna separation.

5.2 Vertical separation case

The results obtained for horizontal separation of the antennas can be applied to the case of vertical separation with some modification. The co-ordinate system for this model is shown in Fig. 10. The crosscorrelation is given by

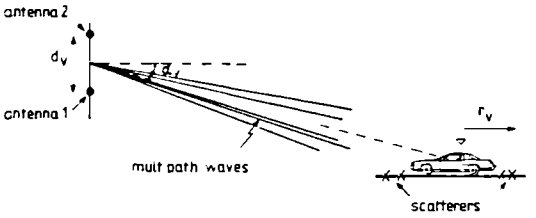

Fig. 10 *Co-ordinate system for a model in which ρ_{env} is a function of the vertical arrival angle (α_V) and spread in arrival angles of incoming multipath waves*

[illegible] transmitter and [illegible] vertical antenna separation and effective horizontal distance [illegible] scatterers from transmitter, respectively

the same expression as eqn. 11, with

$$l = l_1 \cos \alpha_1 \tag{15}$$

$$\sigma \sim \left(\frac{r_1 \sin \alpha_1}{L}\right) \tag{16}$$

where σ is the spread of the multipath arrival angle in the vertical plane. The results for the horizontal separation case suggest that the principal scatterers are located along the route of the mobile in an area 46–136 m wide by 90–272 m long. Hence the effective distance r_1 of the scatterers from the mobile, measured parallel to the mobile to base station direction, is 23–68 m for the circumferential route and 45–136 m for the radial route. Therefore, the radial routes have a larger spread in arrival angle σ in the vertical plane than the circumferential routes, thus producing a lower ρ_{env}. This agrees well with the results shown in Fig. 2.

For a small spread in the arrival angle, a further approximation to eqn. 11 can be made as follows:

$$\rho_{env} \simeq \left| \int_{-\pi}^{\pi} \exp\left\{ j2\pi \frac{d'}{\lambda} (\alpha_i - \alpha) \right\} p(\alpha_i)\, d\alpha_i \right|^2 \tag{17}$$

where $\alpha = \alpha_H$ for the horizontal antenna separation case and α_V for the vertical antenna separation case. The integral on the right-hand side of eqn. 17 is equal to the char-

acteristic function of the variable α_i, which is defined as the Fourier transform $F(\zeta)$ with $\zeta = 2\pi d' \lambda$ on its probability distribution function $p(\alpha_i)$. Assuming that $p(\alpha_i)$ follows a Gaussian distribution function, we then have the following simplified expression:

$$\rho_{env} \simeq \exp\left\{-\left(2\pi \frac{d'}{\lambda}\sigma\right)^2\right\} = \begin{cases} \exp\left\{-\left(\dfrac{2\pi}{\lambda}\dfrac{d_H r_H \sin \alpha_H}{L}\right)^2\right\} \\ \quad \text{for horizontal separation} \\ \exp\left\{-\left(\dfrac{2\pi}{\lambda}\dfrac{d_V r_V \sin \alpha_V \cos \alpha_V}{L}\right)^2\right\} \\ \quad \text{for vertical separation} \end{cases} \tag{18}$$

In general, α_V is very small, even for a small mobile-base distance of 1.3 km, and hence $\cos \alpha_V \simeq 1$. In contrast, however, α_H can vary over $0 \leq \alpha_H < 2\pi$, in which case eqn. 18 suggests that the vertical antenna separation case can achieve a lower ρ_{env} than the horizontal separation case with the horizontal arrival angle α_H of the multipath waves being very small, irrespective of the orientation of the routes travelled. Indeed, a comparison of Figs. 2–4 shows that ρ_{env} for the vertical separation case is lower than that of the horizontal separation case when $\alpha_H = 0$ and higher when $\alpha_H = 10$ 90 .

6 Conclusion

An experimental investigaion of various antenna configurations for use in mobile radio base station space diversity reception has been reported. The results show that a consistent reduction in the crosscorrelation between two signal envelopes, detected at the base station, is best achieved using vertically spaced antennas. This suggests that space diversity systems can be implemented using antennas with vertical separations of between 11 λ and 13 λ when signals received are from a mobile, at a distance of about 1.3 km. At distances greater than 1.3 km it is expected that the trend in reduction of the crosscorrelation will be similar, but that the absolute crosscorrelation will be higher, owing to the smaller spread in multipath arrival angles. A similar argument leads to the conclusion that for vertically spaced antennas the crosscorrelation will be reduced for smaller cells, because of an increase in the angular width of the effective scatterers surrounding the mobile, when viewed from the base station. We also conclude that vertically spaced antennas have a distinct advantage over horizontally spaced antennas in that the crosscorrelation is not a function of the horizontal arrival angle of the multipath waves. In addition, vertically spaced base station antennas require little roof-top space (approximately 4 m at 900 MHz).

7 Acknowledgments

The research for this paper was undertaken while two of the authors were visiting research fellows in the Department of Electrical Engineering & Electronics at the University of Liverpool, UK: A.G. Williamson as a Leverhulme Visiting Fellow, F. Adachi as an SERC Visiting Research Fellow.

8 References

1 DAVIS, B.R., and BOGNER, R.E.: 'Propagation at 900 MHz for mobile radio', *IEE Proc. F, Commun., Radar & Signal Process.*, 1985, **132**, (5), pp. 307–320
2 PARSONS, J.D., HENZE, M., RATLIFF, P.A., and WITHERS, M.J.: 'Diversity techniques for mobile radio reception', *Radio & Electron. Eng.*, 1975, **45**, pp. 357–367
3 LEE, W.C.Y.: 'Effects on correlation between two mobile radio base station antennas', *IEEE Trans.*, 1973, **COM-21**, pp. 1214–1224
4 KOZONO, S., and TURUHARA, T.: 'Correlation between two mobile radio base station antennas', *Trans. IECE Jpn.*, 1983, **J66-B**, pp. 558–559 (in Japanese)
5 RHEE, S., and ZYSMAN, G.I.: 'Results of suburban base station spatial diversity measurements in the UHF band', *IEEE Trans.*, 1974, **COM-22**, pp. 1630–1636
6 SCHWARTZ, M., BENNETT, W.R., and STEIN, S.: 'Communication systems and techniques' (McGraw-Hill, New York, 1966)
7 CLARKE, R.H.: 'A statistical theory of mobile radio reception', *Bell Syst. Tech. J.*, 1968, **47**, pp. 957–1000

THE PERFORMANCE OF VARIOUS DIVERSITY COMBINERS ON SIGNALS RECEIVED AT A BASE-STATION SITE

M. T. Feeney+ and F. Adachi*

SUMMARY

In a multipath environment the received signal, both at the mobile and the base station, is subject to deep and rapid fading. This causes problems for digital and analogue type transmissions. It may be overcome, to some extent, by implementing various diversity techniques. One such technique utilizes diversity combiners e.g. selection, equal-gain, maximal ratio, 'switch and stay' and 'switch and examine') with spaced antenna systems.

Extensive field trials have been carried out in which a mobile transmitted to a base station equipped for spaced antenna diversity reception. Data from these trials have been used to compare various forms of diversity combiner. Results from such comparisons take the form of, the cummulative probability distribution function, the level crossing rate and fade duration. The latter parameters are especially important for digital transmissions since they provide information on the burst error occurrence and length. The results for the diversity combiners are also compared for various fading correlations, which are a consequence of the antenna configurations used.

I. INTRODUCTION

In mobile radio, the received signal is subject to multipath fading. The signal envelope is composed of a fast fading signal superimposed on a slow fading signal. The fast fading results from the interference between scattered radio paths in a region between the base and mobile stations. The slow fading is caused by the varying terrain between the base and mobile stations.

Diversity reception [1] is one of the most promising techniques available which can reduce the fading effect. Since the diversity antennas are close to each other (less than a few tens of wavelengths), the technique has little effect on the slow fading component.

When digital modulation is used, the radio link performance deteriorates rapidly when the received signal fades below some system-determined threshold. The statistical parameters for the rate of occurrence of a signal crossing a particular level, and the duration of fade below a level are important in system design [2].

There does not exist in the literature, to the authors' knowledge, any comparison between calculated and experimental results obtained from several diversity reception scremes. Lee [3] analysed the level crossing rate for just one system assuming a predetection equal-gain combiner and a low cross-correlation among fading signals.

This paper presents the measured data for the statistics of level crossing rate (LCR) and fade duration when predetection selection (SC), equal-gain combining (EGC) and maximal-ratio combining (MRC), schemes are used. In addition, we present results using 'switch and stay' (SS) and 'switch and examine' (SE) strategies. The experimental data are compared with results obtained theoretically for a simple case of no cross-correlation.

II. DIVERSITY OPERATION

The EGC and MRC strategies cophase and combine all the received signals. MRC weights the received signals in proportion to the respective envelopes (assuming the receiver noise power is identical in all of the branches). The SC selects one of the received signals which has the largest signal envelope, and so is the simplest. Practical combiners have been proposed for EGC and MRC for use in mobile radio systems [1]. To realise the action obtained by SC with less complexity, 'switch and stay' and 'switch and examine' strategies have been proposed [4]. SS and SE switch between antennas whenever the received signal falls below a switching threshold. If the new signal is still below the switching threshold, then SE switches back to the previous antenna after a certain examining period. SS and SE are simple to implement and hence are attractive for mobile radio use. However the signal statistics are a function of the switching threshold, and although the SE strategy allows for a quicker return to a higher signal level than the SS strategy, the rapid switching causes accompanying noise bursts.

In order to compare various diversity combiners we introduce the effective signal envelope (R), which is determined from the

+University of Liverpool
*NTT Yokosuka Electrical Communication Laboratories-Japan.

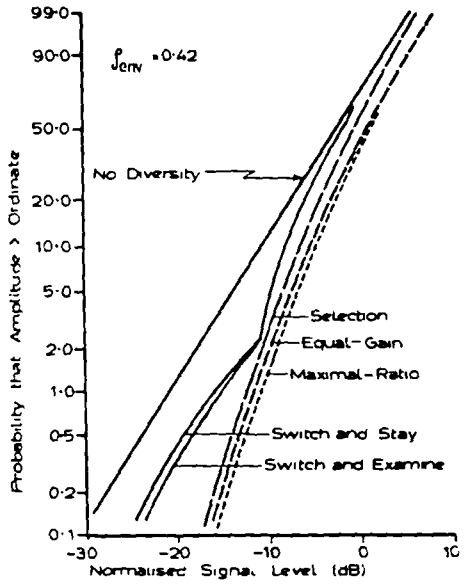

Fig.1. Measured CDF of a normalised fast fading signal envelope for various diversity schemes.

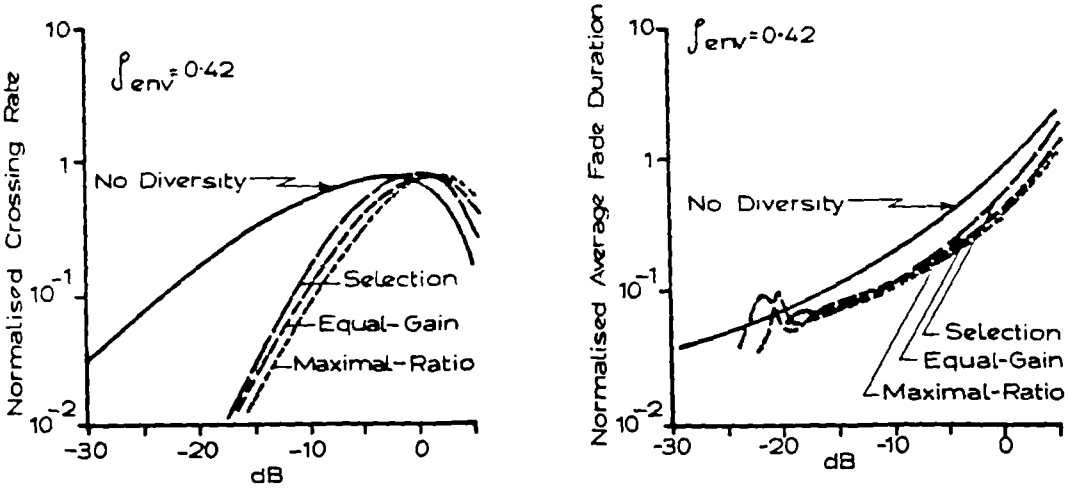

Fig.2. Measured LCR and average fade duration for SC, EGC and MRC strategies.

resultant signal-to-noise ratio (SNR) after combining, since the receiver noises are also added for EGC and MRC. When the received signal envelopes are $R_1, R_2, \ldots R_N$, for a N branch system, the effective signal envelope is given by:

$$R = \begin{cases} R_N & \text{, for SC,SS and SE} \\ \dfrac{R_1+R_2+R_N}{\sqrt{N}} & \text{, for EGC} \\ \sqrt{R^2_1+R^2_2+R^2_N} & \text{, for MRC} \end{cases} \quad (1)$$

If the effective envelopes are the same then the combiner outputs have the same SNR.

As the number of diversity branches increases, the increase in diversity improvement becomes less and the receiver structure becomes more complex. A two-branch diversity N=2) system, which is considered to be the most practical, was adopted for our experiment.

III. EXPERIMENT

The data for this paper originates from field trials carried out in an urban area of Liverpool using a mobile which transmitted to a base station. The data were recorded, at the base station, as signal strength values from the output of field strength receivers that were connected to two antennas. These antennas were positioned for various configurations relative to each other and the mobile test area. The mobile transmitted a 25 watt continuous wave at 896.5 MHz using a vertical monopole antenna mounted on the roof of the vehicle. The vehicle was driven around a predanned route in the test area, some ..5km distance from the base station, at a nearly constant speed of around 10m/sec. The data used in this paper are taken from a route which was some 700m in length that lay nearly circumferential relative to the base station. The base station was located on the roof of the department at a height of 35 meters above the ground level. Two vertically mounted half-wavelength dipoles were used, at the base station, to receive the multipath signals. For this paper we use data obtained when the antennas were configured in a stacked manner for separations of 4, 10 and 20 wavelengths, which corresponds to envelope cross-correlations (ρ_{env}), between the two received signals, of 0.93, 0.75 and 0.42 respectively. These cross-correlations were obtained by averaging cross-correlations for two second segments over the whole section length (approx. 300m). The two received signals were recorded on a multi-track FM tape recorder using the log-video output of the field strength receivers. The FM tapes were later replayed and the two tracks holding the signal strength data were simultaneously digitised by means of a 'sample and hold' circuit and an eight bit analogue to digital converter. The digitised values were then recorded onto computer magnetic tape and later transfered onto one of the Universiy's main-frame computers.

This data base has enabled a true comparison to be made between various diversity reception systems by simulating the diversity action using identical data. The diversity schemes are compared using a number of statistical results such as; the cummulative probability distribution function (CDF), the level crossing rate (LCR) and the average fade duration for the original signal envelope and the effective envelope after diversity has been employed. Prior to determining these parameters the data is filtered to remove the slow fading component. This is achieved by normalising the envelope by the local mean. The received signal envelope R(t), is a combination of a fast r(t) and slow $m_l(t)$ fading components such that:

$$R(t) = r(t)\sqrt{m_l(t)} \quad (2)$$

The local mean power ($m_l(t)$) is estimated using a moving average method by:

$$\hat{m}_l(t_n) = \frac{1}{N}\sum_{m=\frac{-N+1}{2}}^{\frac{N-1}{2}} \frac{R^2(t_{n+m})}{2} \quad (3)$$

where N is the averaging window width. To remove the local mean variation the origional envelope $R(t_n)$ is normalised by the estimated local mean such that;

$$r(t_n) = \frac{R(t_n)}{\sqrt{\hat{m}_l(t_n)}} \quad (4)$$

IVa. EXPERIMENTAL RESULTS

In the following section we present results for the effects that SC, EGC, MRC, SS and SE diversity strategies have on statistical parameters such as the CDF, LCR and average fade duration for data with envelope cross-correlations of 0.93, 0.75 and 0.42. Figure 1 shows the CDF for each of the diversity strategies (using a -10dB switching threshold for SS and SE and a 2 millisecond duration for SE) for data with ρ_{env} = 0.42. All of the schemes show big improvements compared with the case of no diversity, especially when deep fading occurs. Typical improvements at the 1% level are:

5.25 dB using SS
6.93 dB using SE
8.83 dB using SC
9.52 dB using EGC
10.15 dB using MRC

Clearly the choice of switching threshold has a large effect on the improvement which SS and SE strategies can provide. The effect that the various strategies have on the LCR and average fade duration is shown in Figures 2 and 3. In these figures the term 'normalised crossing rate' refers to the number of crossings per second, of a particular level, divided by the maximum Doppler frequency (which for

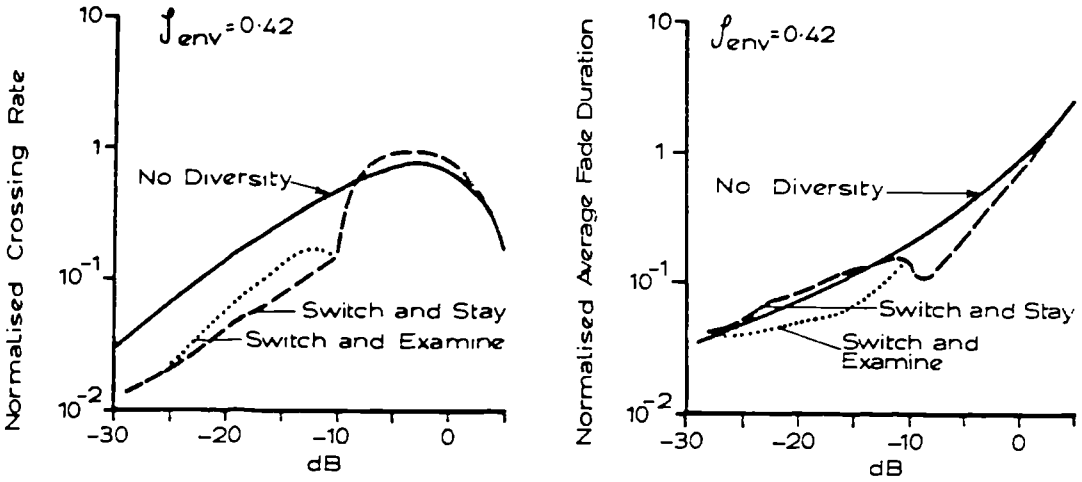

Fig.3. Measured LCR and average fade duration for SS and SE strategies using a switching threshold of -10dB.

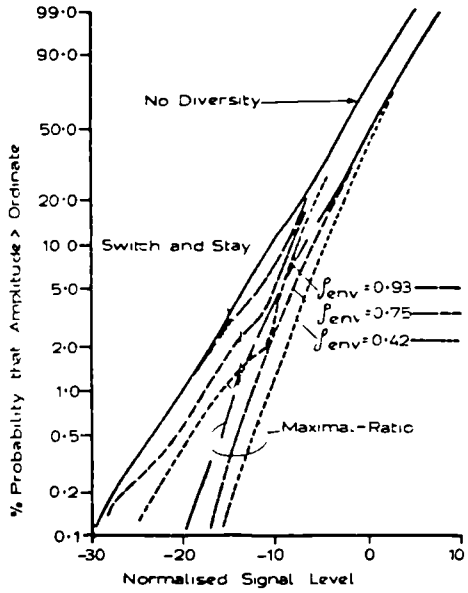

Fig.4. Effect of ρ_{env} on the measured CDF for MRC and SS strategies.

our experiment was 37Hz). The 'normalised average fade duration' is the duration, in seconds, of a fade below a particular level multiplied by the maximum Doppler frequency. In all of the schemes the LCR is considerably reduced for situations when deep fading occurs. The SC, EGC and MRC cases have the largest improvement on LCR with again, the switching threshold affecting the improvement provided by the SS and SE cases. In terms of the average fade duration the SC, EGC and MRC cases show a consistent reduction in the duration of a fade, with the largest improvement being provided by MRC. Below the switching threshold the SS and SE strategies now no reduction in the fade duration.

The effect of envelope cross-correlation is shown in Figure 4 for the MRC and SC cases. In both cases an increase in ρ_{env} reduces the respective improvement. However where as in the limiting case of $\rho_{env} = 1$ the SC, SS and SE strategies show no improvement, the EGC and MRC cases have a minimum 3dB improvement. Figures 5 and 6 now the LCR and average fade duration over a range of ρ_{env} for MRC and SS respectively. For MRC the LCR is maximised for increasing ρ_{env} and even as ρ_{env} approaches a high value there is still a significant reduction in the LCR. The average fade duration, using MRC, changes little with ρ_{env} and remains approximately halved. The SS case, in Figure 6, shows a greater increase in LCR for enlarging ρ_{env} than that for the MRC case, and in addition, the choice of switching threshold considerably affects the performance. The average fade duration tends towards the no diversity case as ρ_{env} increases. Beyond the switching threshold point the average fade duration is not improved for any of the values of ρ_{env}.

It is well known that the advantage of a two-branch diversity system can still be obtained for a cross-correlation up to 0.7. This is seen in all of our results for the CDF, LCR and average fade duration for all strategies except that SS and SE have a reduced improvement with regard to LCR and fade duration. To achieve a ρ_{env} of 0.7 at the mobile an antenna spacing of around half a wavelength is required. To achieve a similar ρ_{env} at the base station, when the mobile is some 1.3km distance, the antennas can be separated vertically apart by around 12 wavelengths.

IV. CALCULATED RESULTS

In Rayleigh fading, the received signal envelope, at each branch, has a probability distribution function (PDF, given by,

$$p(R) = \frac{R}{\Gamma} e^{\frac{-R^2}{2\Gamma}} \qquad (5)$$

where, from now on, R is the envelope, and Γ is the average signal power (viz $m_1(t)$). When predetection diversity is used, the signals are combined in phase or switched. For independent Rayleigh fading, the PDF and CDF are given in Table I for various diversity strategies.

The calculated CDF is shown in Fig.7 for each of the diversity strategies. It can be shown that MRC has the best performance, and that SC and EGC achieve a reduced improvement, relative to MRC, of -1.5dB and -0.88dB respectively. In the case of SS and SE the diversity gain varies according to the switching threshold. The calculated and measured CDF (Figs.7 and 1 respectively) are quite similar.

The LCR is defined as the number of negative or positive-going crossings per second of the equivalent signal envelope R, and is obtained from;

$$N_R = \int_0^\infty \dot{R}\, p(\dot{R}, R)\, d\dot{R} \qquad (6)$$

where $\dot{R}$ is the time derivative of R and $p(\dot{R},R)$ is the joint PDF. If we consider R_1 and R_2 as the equivalent envelopes of each branch then since $\dot{R}_1$ and $\dot{R}_2$ are independent of R_1 and R_2 and they are mutually independent zero-mean Gaussian variables, then their variance is given by;

$$\sigma^2_{\dot{R}} = -\Gamma \ddot{\rho}(o) \qquad (7)$$

where $\rho(t)$ is the normalised autocorrelation function of the received complex signal envelope. Substituting (7) into (6) and using Table I then;

$$N_R = p(R) \sqrt{\frac{-\ddot{\rho}(o)}{2\pi}\Gamma} \qquad (8)$$

If we assume that the scatterers surround the mobile uniformly then;

$$\ddot{\rho}(o) = \frac{\partial^2}{\partial t^2} J_o(2\pi f_D t)\Big|_{t=o} = -\frac{(2\pi f_D)^2}{2} \qquad (9)$$

where f_D is the maximum Doppler frequency (i.e. vehicle speed/wavelength).

The calculated LCR (N_R f_D) for the various diversity schemes are shown in Fig.8, where a -10dB threshold has been used in the SS and SE strategies. The LCR values are underestimated for SE, since the calculations do not take into account the periodic switching, which occurs when both envelopes are below the switching threshold.

The average fade duration is given by;

$$\tau = \frac{P(R)}{N_R} \qquad (10)$$

The results are also shown in Fig.8. The measured and calculated LCR and average fade duration are similar.

It is well known [2] that if two signals are correlated, the effective average power is reduced to $\Gamma_{eff} = \Gamma\sqrt{1-|\rho_{12}|^2}$, where ρ_{12} is the complex fading cross-correlation and is related to $\rho_{env} \approx |\rho_{12}|^2$. When $\rho_{env} = 0.7$ the diversity reduction is about

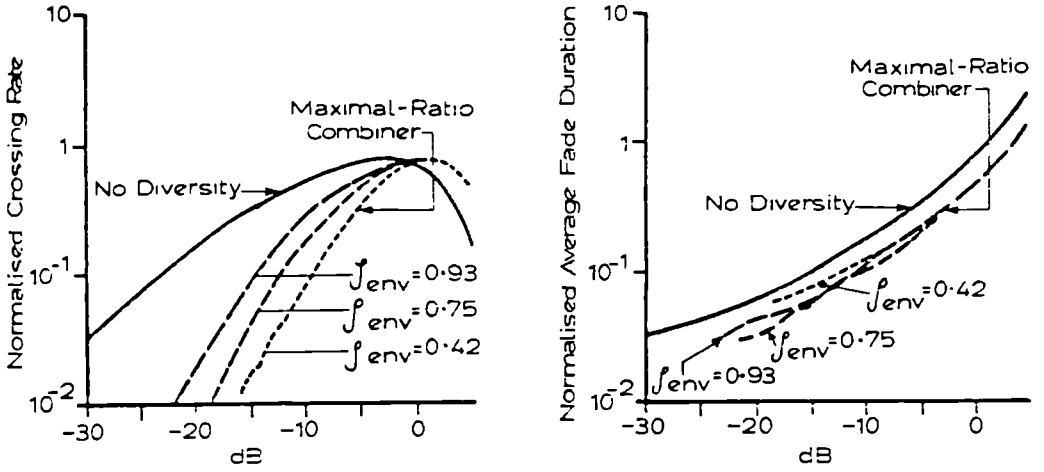

Fig.5. Effect of ρ_{env} on the measured LCR and average fade duration for MRC.

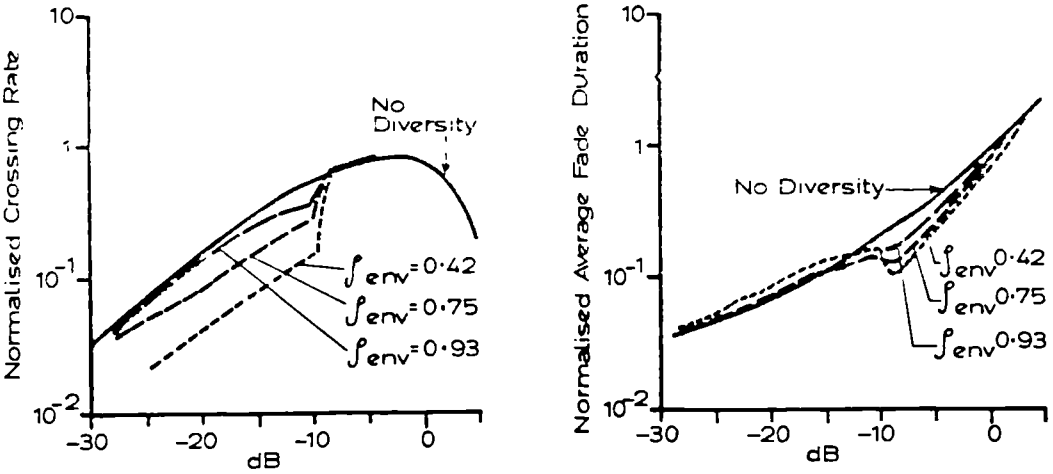

Fig.6. Effect of ρ_{env} on the measured LCR and average fade duration for SS using a switching threshold of -10dB.

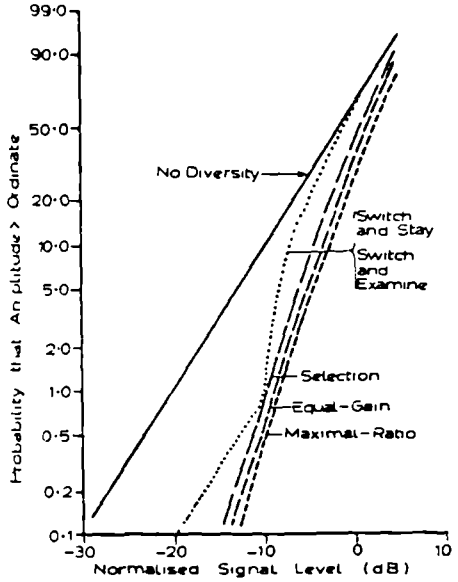

Fig.7. Calculated CDF of a Rayleigh fading envelope for various diversity schemes under a condition of independent fading.

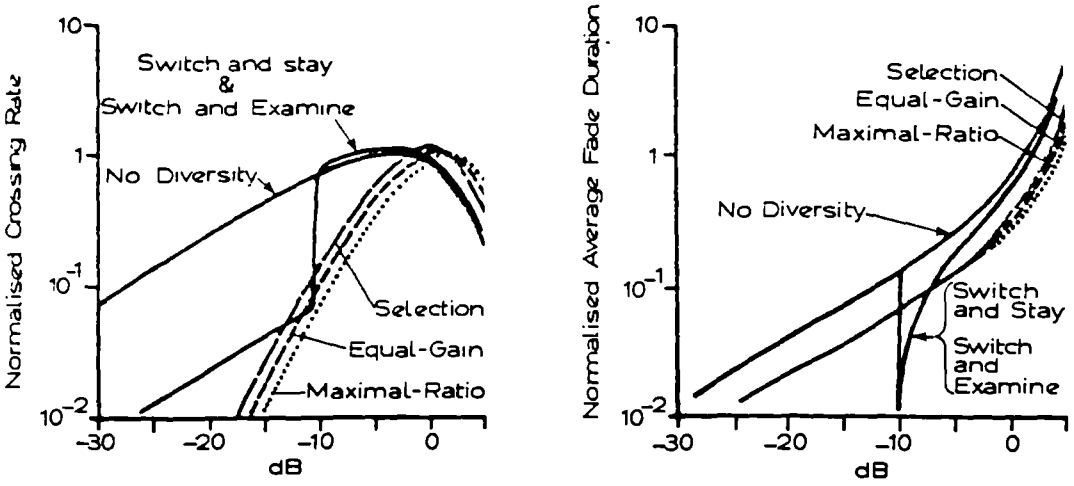

Fig.8. Calculated LCR and average fade duration for various diversity schemes under a condition of independent fading.

2.6 dB. Considering this effect, the measured data agree well with the calculated results. The difference between the two can be attributed to the normalised data not being pure Rayleigh and not having zero cross-correlation.

V. CONCLUSION

The effect of various diversity combiners were compared using the CDF, LCR and average fade duration statistics. Our results show that diversity reception is useful in reducing the effect of fast and deep signal fading, in agreement with theory. The improvement is most noticeable for the CDF and LCR, however the average fade duration is only reduced by about a half. This means that if diversity reception is applied to digital transmissions, then the bit error rate is reduced considerably, and the burst error length is approximately halved. The advantage of a two branch diversity scheme can be obtained for an envelope cross-correlation up to 0.7 for SC, EGC and MRC, except for the SS and SE strategies.

ACKNOWLEDGEMENTS

The authors are indebted to Professor J.D. Parsons of Liverpool University and Associate-Professor A.G. Williamson of the University of Aukland-New Zealand for their assistance and advice throughout this research. One of the authors - F. Adachi, was a SERC Visiting Research Fellow at the University of Liverpool throughout the research.

REFERENCES

[1] Parsons, J.D. et al, "Diversity techniques for mobile radio", Radio & Electron. Eng., vol.45 pp.357-367, July 1975.

[2] Jakes, W.C., Jr., Ed., Microwave Mobile Communications, New York: Wiley, 1974.

[3] Lee, W.C.Y. "Level crossing rates of an equal-gain predetection diversity combiner", I.E.E.E. Trans. Commun. vol., COM-18: pp.417-426.

[4] Rustako, A.J., Yeh, Y.S. and Murray, R.R., "Performance of feedback and switch space diversity 900MHz mobile radio systems with Rayleigh fading", IEEE Trans. Commun., vol. COM-21, pp.1257-1268, 1973.

TABLE I

Diversity Scheme	PDF p(R)	CDF P(R)
MRC	$\frac{R^3}{2\Gamma^2} e^{\frac{-R^2}{2\Gamma}}$	$1 - e^{\frac{-R^2}{2\Gamma}} \sum_{k=1}^{2} \frac{\left(\frac{R^2}{2\Gamma}\right)^{k-1}}{(k-1)!}$
EGC	$\frac{R^3}{2\Gamma_1^2} e^{\frac{-R^2}{2\Gamma_1}}$	$(1 - e^{\frac{-R^2}{2\Gamma_1}})^2 \sum_{k=1}^{2} \frac{\left(\frac{R^2}{2\Gamma}\right)^{k-1}}{(k-1)!}$
SC	$(1 + q \frac{R}{\Gamma} e^{\frac{-R^2}{2\Gamma}}$	$(1 + q)(1 - e^{\frac{-R^2}{2\Gamma}}) - q \quad R \geq R_t$
SE	$\frac{qR}{\Gamma} e^{\frac{-R^2}{2\Gamma}}$	$q(1 - e^{\frac{-R^2}{2\Gamma}}) \quad R < R_t$
SS	$\frac{2R}{\Gamma}(e^{\frac{-R^2}{2\Gamma}} - e^{\frac{-R^2}{\Gamma}})$	$(1 - e^{\frac{-R^2}{2\Gamma}})^2$

where $\Gamma_1 = \Gamma\sqrt{3.2}$

$q = (1 - e^{-R_t^2/2\Gamma})$

R_t = Switching threshold

UDC 621 396 62 621 396 931
Indexing Terms Radio systems, diversity, mobile

An evaluation of specific diversity combiners using signals received by vertically-spaced base-station antennas

F. ADACHI, PhD,*
M. T. FEENEY, MSc†
and
Professor J. D. PARSONS, DSc(Eng), FIEE, FIERE†

SUMMARY

A series of field trials has been conducted in which a 900 MHz CW signal was transmitted from a vehicle moving along a test route some 1·3 km from a base station. The recorded envelopes of the signals received on two vertically-separated antennas at the base station have been used in a computer simulation of two-branch predetection diversity reception Several different systems have been simulated and the computed results show that the theoretical diversity advantages can still be obtained for an envelope cross-correlation (ρ_{env}) of less than 0·7 for all strategies except switching. For a 1 3 km radius cell, a ρ_{env} less than 0·7 can be obtained using antennas with a vertical separation of about 12λ. It has been found that the cumulative distribution and level-crossing rates of the signal are substantially improved and the average fade duration is approximately halved.

* *NTT Electr cal Communications Laboratories P O Box 8, Yokosuka Post Office 238 Japan*
† *Dept of Electrical Engineering and Electronics The University of Liverpool, Brownlow Hill, P O Box 147 Liverpool, L69 3BX*

List of Abbreviations

AFD	average fade duration
CDF	cumulative distribution function
CNR	carrier-to-noise ratio
EGC	equal-gain combining
LCR	level-crossing rate
MRC	maximal-ratio combining
PDF	probability density function
SC	selection combining
SE	switch and examine
SS	switch and stay

1 Introduction

It is well known that in mobile radio the received signal is subject to multipath fading. The signal envelope is composed of a fast-fading component, caused by multiple scattering in the immediate vicinity of the vehicle, superimposed on a slowly varying mean value. The fast-fading component often exhibits Rayleigh statistics whilst the mean value (slow fading component) is log-normally distributed.

When digital modulation is used, the radio link performance deteriorates rapidly whenever the received signal falls below some noise-related threshold. Diversity reception techniques have the potential to reduce error rates substantially,[1] since diversity can improve the signal envelope statistics, reduce the occurrence of deep fades and significantly shorten average fade durations. However, theoretical comparison of the performance of various diversity systems is usually limited to the case of Rayleigh fading with equal mean noise powers on each branch,[2] which may not represent conditions encountered in practice. It is therefore of interest to conduct a practical comparison using real received signals which have statistical properties that may be somewhat different from those theoretically assumed. This paper presents such a comparison using measured signal envelopes obtained at a base station site in an urban area. It had previously been shown that signal envelopes with sufficient decorrelation could be obtained from vertically-separated antennas[3] and signals from two such antennas were used as inputs in a computer simulation of various diversity schemes. A base station site was specifically chosen, firstly because base-station diversity has received much less attention than vehicle diversity and secondly because cellular radio operators in the UK actually use diversity reception at TACS base sites.

In comparing the various diversity techniques it is of interest to examine the cumulative distribution function (CDF) of the output signal, the level-crossing rate (LCR) and the average fade duration (AFD). Although the effect of correlation on the CDF is well-known[2] it is only recently that any attention has been given to the LCR and AFD.[4] Lee[5] has analysed the approximate LCR for just one system assuming a predetection equal-gain combiner and a low crosscorrelation among fading signals. Recently, the LCR and AFD for correlated two branch predetection selection (SC), equal-gain combining (EGC) and maximal-ratio combining (MRC) schemes have been analysed[4] to show that diversity reception is effective in reducing the LCR and AFD. However, the literature does not appear to contain any comparison between calculated and experimental results obtained from several diversity reception schemes.

Extensive field trials were carried out in an urban area of Liverpool to measure the crosscorrelation between the

UDC 621 396 62 621 396 931
Indexing Terms Radio systems, diversity, mobile

An evaluation of specific diversity combiners using signals received by vertically-spaced base-station antennas

F. ADACHI, PhD,*
M. T. FEENEY, MSc†
and
Professor J. D. PARSONS, DSc(Eng), FIEE, FIERE†

SUMMARY

A series of field trials has been conducted in which a 900 MHz CW signal was transmitted from a vehicle moving along a test route some 1·3 km from a base station. The recorded envelopes of the signals received on two vertically-separated antennas at the base station have been used in a computer simulation of two-branch predetection diversity reception. Several different systems have been simulated and the computed results show that the theoretical diversity advantages can still be obtained for an envelope cross-correlation (ρ_{env}) of less than 0·7 for all strategies except switching. For a 1·3 km radius cell, a ρ_{env} less than 0·7 can be obtained using antennas with a vertical separation of about 12λ. It has been found that the cumulative distribution and level-crossing rates of the signal are substantially improved and the average fade duration is approximately halved.

* *NTT Electrical Communications Laboratories, P O Box 8, Yokosuka Post Office 238 Japan*
† *Dept of Electrical Engineering and Electronics, The University of Liverpool, Brownlow Hill, P O Box 147, Liverpool, L69 3BX*

List of Abbreviations

AFD	average fade duration
CDF	cumulative distribution function
CNR	carrier-to-noise ratio
EGC	equal-gain combining
LCR	level-crossing rate
MRC	maximal-ratio combining
PDF	probability density function
SC	selection combining
SE	switch and examine
SS	switch and stay

1 Introduction

It is well known that in mobile radio the received signal is subject to multipath fading. The signal envelope is composed of a fast-fading component, caused by multiple scattering in the immediate vicinity of the vehicle, superimposed on a slowly varying mean value. The fast-fading component often exhibits Rayleigh statistics whilst the mean value (slow fading component) is log-normally distributed.

When digital modulation is used, the radio link performance deteriorates rapidly whenever the received signal falls below some noise-related threshold. Diversity reception techniques have the potential to reduce error rates substantially,[1] since diversity can improve the signal envelope statistics, reduce the occurrence of deep fades and significantly shorten average fade durations. However, theoretical comparison of the performance of various diversity systems is usually limited to the case of Rayleigh fading with equal mean noise powers on each branch,[2] which may not represent conditions encountered in practice. It is therefore of interest to conduct a practical comparison using real received signals which have statistical properties that may be somewhat different from those theoretically assumed. This paper presents such a comparison using measured signal envelopes obtained at a base station site in an urban area. It had previously been shown that signal envelopes with sufficient decorrelation could be obtained from vertically-separated antennas[3] and signals from two such antennas were used as inputs in a computer simulation of various diversity schemes. A base station site was specifically chosen, firstly because base-station diversity has received much less attention than vehicle diversity and secondly because cellular radio operators in the UK actually use diversity reception at TACS base sites.

In comparing the various diversity techniques it is of interest to examine the cumulative distribution function (CDF) of the output signal, the level-crossing rate (LCR) and the average fade duration (AFD). Although the effect of correlation on the CDF is well-known[2] it is only recently that any attention has been given to the LCR and AFD.[4] Lee[5] has analysed the approximate LCR for just one system assuming a predetection equal-gain combiner and a low crosscorrelation among fading signals. Recently, the LCR and AFD for correlated two branch predetection selection (SC), equal-gain combining (EGC) and maximal-ratio combining (MRC) schemes have been analysed[4] to show that diversity reception is effective in reducing the LCR and AFD. However, the literature does not appear to contain any comparison between calculated and experimental results obtained from several diversity reception schemes.

Extensive field trials were carried out in an urban area of Liverpool to measure the crosscorrelation between the

envelopes of signals received at a base station site using two antennas separated vertically, horizontally and a combination of both. Using the envelope data obtained from these field trials, two-branch predetection diversity action was computer simulated and the output CDF, LCR and AFD were determined. We present the measured results when SC, MRC and EGC schemes were used, for various values of envelope crosscorrelation. In addition, results are presented using 'switch and stay' (SS) and 'switch and examine' (SE) strategies.[6] The experimental data are compared with results obtained theoretically.

2 Diversity Operation

The deleterious effects that fading has on signal reception, especially to digital transmissions, can be overcome, to a large extent, by implementing various diversity schemes. Diversity is a convenient method of reducing the depth and occurrence of fades by combining decorrelated versions of the original signal. Of the many diversity schemes, the most useful method for mobile radio is space diversity which utilizes the simultaneous reception of decorrelated signals on two or more spaced antennas. The spacing between the antennas determines the crosscorrelation between the received signal envelopes and thus affects the degree to which the rate and depth of fading can be reduced. The decorrelated signals obtained from the diversity branches can then be processed using various 'combining' schemes. The processing can be performed prior to or after demodulation (pre- or postdetection). In what follows we consider various predetection combining systems for which we assume the noise power to be the same in all branches.

In a predetection MRC the signals from the branches are cophased and added together, each branch being weighted in proportion to its own signal voltage to noise power ratio.[7] Provided the noise in the various branches is uncorrelated, this produces an output signal-to-noise ratio (SNR) equal to the sum of all the input signal-to-noise ratios, which is the best that can be achieved by a linear combiner. Predetection combining can be more simply achieved however by setting all the weighting factors to unity, thereby producing an EGC. Practical realizations of MRC and EGC have been proposed for use in mobile radio systems.[8] SC selects the branch with the largest instantaneous SNR. However to realize an action similar to that of SC with less complexity, SS and SE strategies have been proposed.[6] The essential difference is that in switched systems there is no attempt to find the best input, merely one which is acceptable. A threshold is set and an input is used until it falls below that threshold. Basically there are two switching strategies which can then be used and these cause different behaviour when both signals are in simultaneous fades. Firstly, there is the SE strategy which causes rapid switching between the inputs until one of them rises above the threshold. Secondly, there is the SS strategy in which the receiver is switched to, and stays on, the alternative input as soon as the input in use falls below the threshold, irrespective of whether that input is acceptable or not. Of course, if the alternative input is above the threshold, both systems behave in an identical manner. Although the SE strategy allows a marginally quicker return to an acceptable input when the signals on both branches fade simultaneously, the rapid switching can cause a noise burst and the SS strategy is therefore preferable in most circumstances.

In order to compare various diversity combiners we introduce the concept of an effective signal envelope $R(t)$, which is determined from the resultant SNR after combining, since the receiver noises are also added for EGC and MRC. When the received signal envelopes are $R_1(t), R_2(t), \ldots, R_M(t)$ for an M-branch system, then it is shown in the Appendix that the effective signal envelope is given by

$$R(t) = \begin{cases} R_k(t), & \text{for SS, SE and SC} \\ \dfrac{R_1(t)+R_2(t)+\ldots R_M(t)}{\sqrt{M}}, & \text{for EGC} \\ \sqrt{[R_1^2(t)+R_2^2(t)+\ldots R_M^2(t)]}, & \text{for MRC} \end{cases} \quad (1)$$

where we have assumed that the kth branch is selected for SS, SE and SC. If the effective envelopes are the same, then the combiner outputs have the same SNR. As the number of diversity branches increases, the increase in diversity improvement becomes less and the receiver structure becomes more complex. Two-branch diversity ($M = 2$), which is probably the most practical, is considered in this paper.

3 Experimental Configuration

The data for the simulation originates from field trials carried out in an urban area of Liverpool.[3] A vehicle-borne transmitter radiated a 5 W CW signal at 896·5 MHz using a vertical monopole antenna mounted on the roof of the vehicle which was driven around a route, nearly circumferential relative to the base station, some 1·3 km distant, at a nearly constant speed of 10 m s. The base station was located on the roof of the Electrical Engineering building at the University, some 35 m above ground level. Two vertically-spaced λ 2 dipoles were used at the base station to receive the multipath signals. The signal strengths from the two base-station antennas were recorded on an FM tape recorder using the log-video outputs of field strength receivers connected to each of the antennas. The recorded signal strength data were later simultaneously digitized at a rate of 1 kHz using an eight bit analogue digital converter, and stored on a digital tape, which was subsequently transferred onto one of the

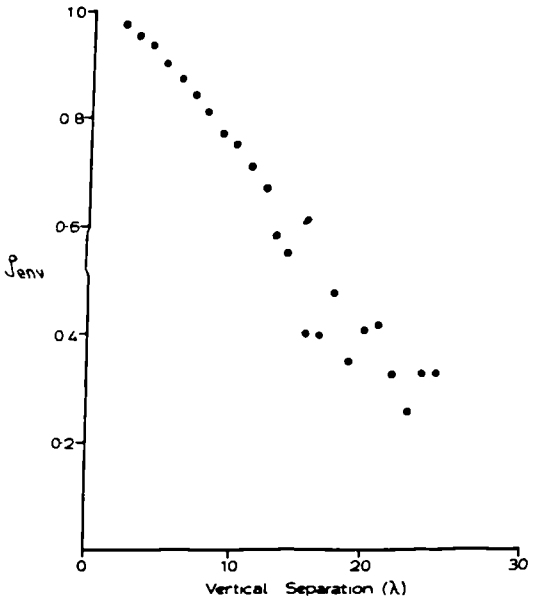

Fig. 1. Crosscorrelation between signal envelopes ρ_{env} received on two antennas spaced at various vertical separations for data from a nearly circumferential route.

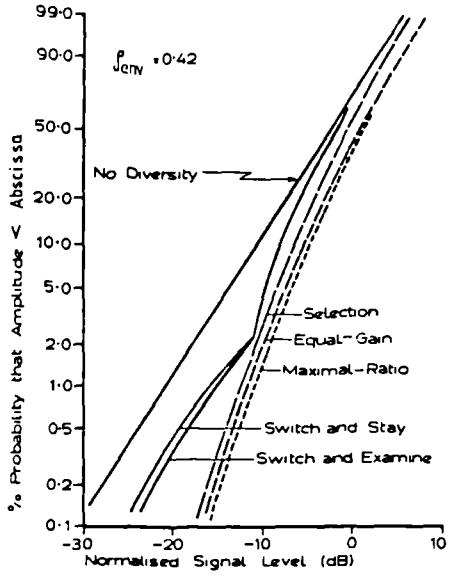

Fig. 2. Measured CDF of a normalized fast fading signal envelope for various diversity schemes

University's mainframe computers (IBM 3083). The data base enabled a true comparison to be made between various diversity combiners by simulating the diversity action using identical data.

Since the diversity antennas are usually close to each other (less than a few tens of wavelengths), there is little effect on the slow fading caused by the varying terrain between the base and mobile stations. The signal envelope data was therefore normalized by the local mean (estimated with a 0·5 s moving-average window) to remove the slow fading component.[3] The various diversity schemes are compared using a number of statistical properties of the fast fading, the cumulative distribution function (CDF), LCR and AFD for the original signal envelope and the effective signal envelope after diversity has been employed.

4 Experimental Results

The measured envelope crosscorrelation, ρ_{env}, between the two received signals is shown in Fig. 1 for vertical antenna separations from 2 to 24λ. These crosscorrelation coefficients were obtained by averaging values obtained for two-second segments over the whole section (approx. 300 m). For the diversity simulation, we used the data obtained when the antenna separations were 4, 10 and 20λ, which correspond to ρ_{env} being 0·93, 0·75 and 0·42 respectively.

4.1 Cumulative Distribution Function (CDF)

Figure 2 shows the CDF for each of the diversity strategies (using a −10 dB switching threshold for SS and SE and a 2 ms duration for SE) using data for which $\rho_{env} = 0{\cdot}42$. Without diversity, the CDF of the individual branch signals follows the Rayleigh distribution as expected. All the schemes show substantial improvements compared with the case of no diversity, especially when deep fading occurs. MRC gives the largest improvement, SE is slightly superior to SS for a signal below the switching threshold, while the CDF is identical above the switching threshold.

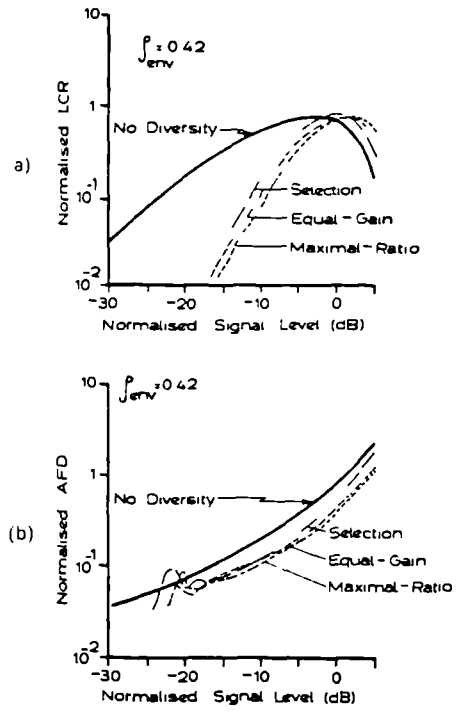

Fig. 3. Measured (a) LCR, and (b) AFD, for SC, EGC and MRC strategies.

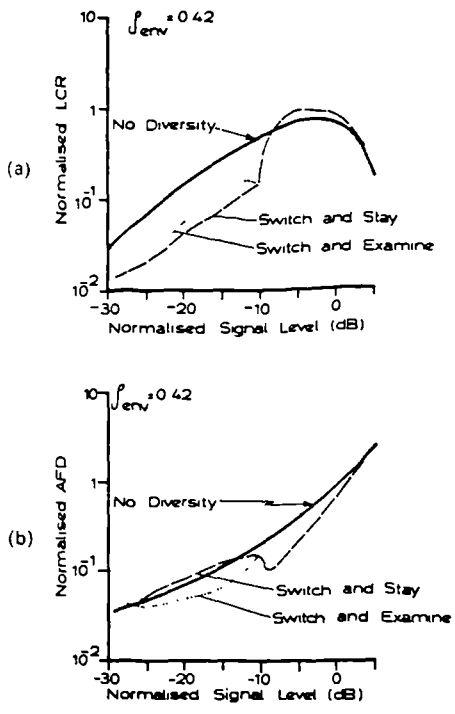

Fig. 4. Measured (a) LCR, and (b) AFD, for SS and SE strategies using a switching threshold of −10dB.

Typical improvements at the 1% level are 5·3 dB for SS, 6·9 dB for SE, 8·8 dB for SC, 9·5 dB for EGC and 10·5 dB for MRC.

4.2 Level Crossing Rate and Average Fade Duration

The effect that the various diversity strategies have on the LCR and AFD is shown in Figs 3 and 4. In these figures, the term 'normalized LCR' refers to the LCR divided by the maximum Doppler frequency, f_D, which for our experiment was 33 Hz. The 'normalized AFD' is the AFD multiplied by f_D. In all the schemes the LCR is considerably reduced for situations where deep fading occurs. The SC, EGC and MRC cases provide the largest improvement in LCR with again the switching threshold affecting the improvement provided by SS and SE. As far as AFD is concerned, the SC, EGC and MRC cases show a consistent reduction, with the largest improvement being provided by MRC. It can be seen in Fig. 3 that the AFD for SC, EGC and MRC is almost halved. Figure 4 shows that the SS and SE strategies yield an identical reduction in the AFD when the signal is above the switching threshold. Below the switching threshold, the SS strategy shows no improvement, whilst SE does, as a result of the periodic switching.

4.3 The Effect of Crosscorrelation

The effect of envelope crosscorrelation on the CDF is shown in Fig. 5 for the MRC and SS strategies. In both cases, an increase in ρ_{env} reduces the improvement. However, whereas in the limiting case of $\rho_{env} = 1$ the SC, SS and SE strategies show no improvement, the EGC and MRC cases have a minimum 3 dB improvement, which is easily understood by reference to equation (1). Figures 6 and 7 show the LCR and AFD over a range of ρ_{env} for MRC and SS respectively. For MRC, even as ρ_{env} approaches a high value, there is still a significant reduction in the LCR. The AFD, using MRC, changes little with ρ_{env} and remains approximately halved. The SS case, in Fig. 7, shows a greater increase in LCR for a larger ρ_{env} than that for the MRC case. The AFD tends towards the no-diversity case as ρ_{env} increases. Below the switching threshold, the AFD is not improved for any value of ρ_{env}.

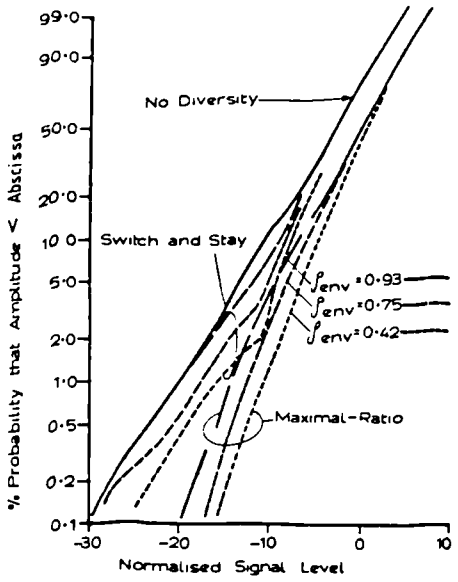

Fig. 5. Effect of ρ_{env} on the measured CDF for MRC and SS strategies.

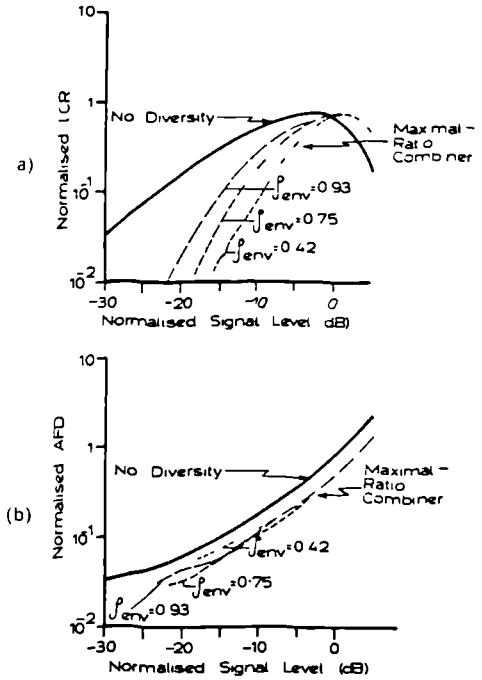

Fig. 6. Effect of ρ_{env} on the measured (a) LCR, and (b) AFD, for MRC.

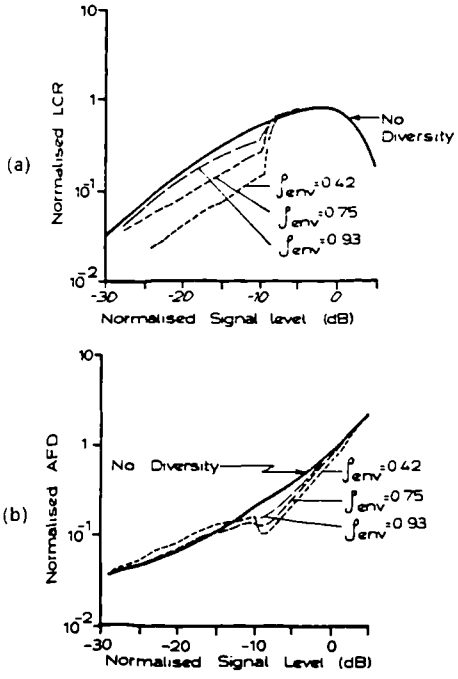

Fig. 7. Effect of ρ_{env} on the measured (a) LCR, and (b) AFD, for SS using a switching threshold of −10dB.

It is well known that in Rayleigh fading conditions the advantages obtainable from diversity are still apparent provided the envelope crosscorrelation does not exceed 0.7.[2] This is confirmed by the results for the CDF, LCR and AFD for all strategies except SS and SE. To achieve a ρ_{env} no greater than 0·7 at the base station, when the mobile is some 1·3 km distant, experiments[3] have shown that when the antennas are approximately 35 m above ground level the vertical separation necessary is only about 12λ.

5 Theoretical Analysis

5.1 Cumulative Distribution Function

In Rayleigh fading, the envelope of the signal received on each branch has a CDF given by

$$P(R) = 1 - \exp\left(-\frac{R^2}{2\sigma^2}\right). \tag{2}$$

where σ^2 is the average signal power (which has been assumed to be unity since the received signal is normalized by the local mean). A closed form expression for the CDF of SE, SC and MRC with correlated fading is given by[9]

$$P(R) = \begin{cases} 1-\exp\left(-\frac{R_t^2}{2\sigma^2}\right) Q\left(\frac{R}{\sigma\sqrt{(1-\rho_{12}^2)}}, \rho_{12}\frac{R_t}{\sigma\sqrt{(1-\rho_{12}^2)}}\right) \\ \qquad -\exp\left(-\frac{R^2}{2\sigma^2}\right)\left\{1-Q\left(\rho_{12}\frac{R}{\sigma\sqrt{(1-\rho_{12}^2)}}, \frac{R_t}{\sigma\sqrt{(1-\rho_{12}^2)}}\right)\right\}, & \text{for SE} \\ 1-\exp\left(-\frac{R^2}{2\sigma^2}\right)\left\{1-Q\left(\rho_{12}\frac{R}{\sigma\sqrt{(1-\rho_{12}^2)}}, \frac{R}{\sigma\sqrt{(1-\rho_{12}^2)}}\right)\right. \\ \qquad \left. +Q\left(\frac{R}{\sigma\sqrt{(1-\rho_{12}^2)}}, \rho_{12}\frac{R}{\sigma\sqrt{(1-\rho_{12}^2)}}\right)\right\}, & \text{for SC} \\ 1-\frac{1}{2\rho_{12}}\left\{(1+\rho_{12})\exp\left(-\frac{R^2}{2\sigma^2(1+\rho_{12})}\right)-(1-\rho_{12})\exp\left(-\frac{R^2}{2\sigma^2(1-\rho_{12})}\right)\right\}, & \text{for MRC} \end{cases} \tag{3}$$

where ρ_{12} is the value of the crosscorrelation function $\rho_{12}(\tau)$ at $\tau = 0$ between the complex envelopes of the two fading signals, $Q(a, b)$ is Marcum's Q-function defined as

$$Q(a, b) = \int_b^\infty x \exp\left(-\frac{a^2+x^2}{2}\right) I_0(ax)\,dx \tag{4}$$

where $I_0(\cdot)$ is the modified zero-order Bessel function, and R_t is a switching threshold. A good approximation for EGC can be obtained by multiplying the average signal power in the expression for the CDF of MRC by $\sqrt{(3/2)}$.[1] An expression for the CDF of SS has not yet been found for correlated fading, but it is identical with that of SE for independent fading.[9] Hence, we use the CDF of SE as an approximation to SS.

The calculated CDFs for independent fading ($\rho_{12} = 0$) are shown in Fig. 8 for each of the diversity strategies. It has been shown[2] that MRC gives the best performance, with SC and EGC achieving a reduced improvement relative to MRC of −1·5 dB and −0·88 dB respectively. The measured and calculated CDFs (Figs 2 and 8 respectively) are quite similar. For small signal envelopes, equation (3) can be approximated as

$$P(R) \approx \begin{cases} \left[\frac{RR_t}{2\sigma^2\sqrt{(1-|\rho_{12}|^2)}}\right]^2, \text{for SS and SE} \quad (R \ll R_t) \\ K\left[\frac{R^2}{2\sigma^2\sqrt{(1-|\rho_{12}|^2)}}\right]^2, \text{for SC, EGC and MRC} \end{cases} \tag{5}$$

where $K = 1$ for SC, 2/3 for EGC and 1/2 for MRC. Since $\rho_{env} \approx \rho_c^2$ in Rayleigh fading,[1] equation (5) shows that the envelope crosscorrelation reduces the effective average power by a factor of $\sqrt{(1-\rho_{env})}$ for all the diversity combiners. When $\rho_{env} = 0{\cdot}42$, 0·75 and 0·93, the diversity gain reductions are 1·2, 3·0 and 5·8 dB respectively. The measured data shown in Fig. 5 agree well with the calculated results.

5.2 Level Crossing Rate and Average Fade Duration

The LCR is defined as the number of negative or positive going crossings per second of the effective signal envelope $R(t)$ at a particular signal level R, and is obtained from

$$N_R = \int_0^\infty \dot{R} p(R, \dot{R})\,d\dot{R}, \tag{6}$$

where $p(R, \dot{R})$ is the joint probability distribution function (PDF) of the signal envelope $R(t)$ and its time derivative $\dot{R}(t)$. The AFD is given by

$$\tau_R = \frac{P(R)}{N_R}. \tag{7}$$

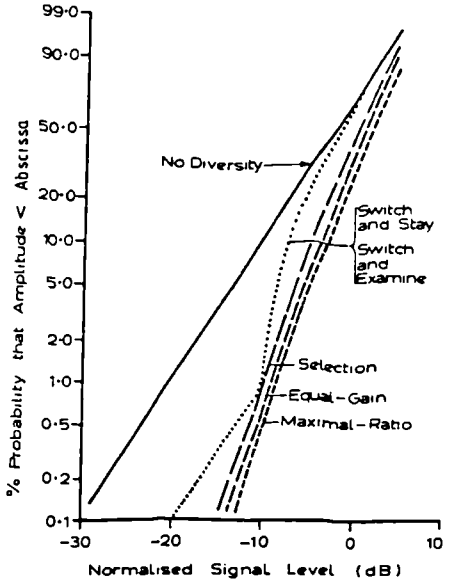

Fig. 8. Calculated CDF of a Rayleigh fading envelope for various diversity schemes under a condition of independent fading.

Recently, the authors have analysed the LCR for predetection diversity combiners.[4] When R is small a simple approximate expression has been obtained, namely

$$N_R \approx \sqrt{-\ddot{\rho}_{11} + \dot{\rho}_{12}^2 \frac{(1-\rho_{12}|^2)}{2\pi}}\, p(R), \qquad (8)$$

where $p(R) = (\mathrm{d}\ \mathrm{d}R)P(R)$ is the PDF of the effective envelope, $\ddot{\rho}_{11} = (\mathrm{d}^2\ \mathrm{d}\tau^2)\rho_{11}(\tau)$ at $\tau = 0$ with $\rho_{11}(\tau)$ being the autocorrelation function of the complex envelope of each received signal and $\dot{\rho}_{12} = (\mathrm{d}\ \mathrm{d}\tau)\rho_{12}(\tau)$ at $\tau = 0$.

Assuming that all the multipath waves received at the base station result from scatterers surrounding a mobile uniformly, $\rho_{11}(\tau) = J_0(2\pi f_D \tau)$ (Ref. 1) and thus $\ddot{\rho}_{11} = -2(\pi f_D)^2$ where f_D is the maximum Doppler frequency (vehicle speed carrier wavelength). No analytical expression is available for $\dot{\rho}_{12}$ with vertically-spaced antennas but we know that for horizontally spaced antennas its effect can be assumed small if the separation of the two antennas is not too small.[4] We therefore assume $\rho_{12} \approx 0$ and hence

$$N_R \approx \sqrt{-\frac{\ddot{\rho}_{11}}{2\pi}}\, p(R) \qquad (9)$$

If the fading signals are independent (ρ_{12} and $\dot{\rho}_{12} = 0$) equation (9) gives the exact expression. The calculated LCR (N_R/f_D) and AFD ($f_D\tau_R$) for various diversity combiners are shown in Fig. 9 for independent fading signals, where a -10 dB threshold has been used in the SS and SE strategies. The measured data are shown in Fig. 3 for SC, EGC and MRC and in Fig. 4 for SS and SE. The measured and calculated LCR and AFD are similar except for SE. The LCR values are underestimated for SE, since the calculations do not take into account the periodic switching, which occurs when both envelopes are below the switching threshold. The difference between the calculated and measured data for SS, SC, EGC and MRC can be attributed to the envelope crosscorrelation not being zero.

When the two fading signals are correlated we have[4]

$$N_R \approx \begin{cases} \dfrac{\sqrt{(2\pi)}f_D\left(\dfrac{R}{\sqrt{2\sigma}}\right)\left(\dfrac{R_t}{\sqrt{2\sigma}}\right)^2}{(1-\rho_{12}|^2)} & \text{for SS and SE } (R \ll R_t) \\ \dfrac{2\sqrt{(2\pi)}f_D K\left(\dfrac{R}{\sqrt{2\sigma}}\right)^3}{(1-\rho_{12}|^2)} & \text{for SC, EGC and MRC} \end{cases} \qquad (10)$$

and

$$\tau_R \approx \begin{cases} \dfrac{1}{\sqrt{(2\pi)}f_D}\left(\dfrac{R}{\sqrt{2\sigma}}\right), & \text{for SS and SE } (R \ll R_t) \\ \dfrac{1}{2\sqrt{(2\pi)}f_D}\left(\dfrac{R}{\sqrt{2\sigma}}\right), & \text{for SC, EGC and MRC.} \end{cases} \qquad (11)$$

Without diversity, the LCR and AFD are given by[1]

$$N_R = \sqrt{(2\pi)}f_D\left(\frac{R}{\sqrt{2\sigma}}\right)\exp\left(-\frac{R^2}{2\sigma^2}\right) \approx \sqrt{(2\pi)}f_D\left(\frac{R}{\sqrt{2\sigma}}\right)$$

$$\tau_R = \frac{\exp\left(\dfrac{R^2}{2\sigma^2}\right)-1}{\sqrt{(2\pi)}f_D\left(\dfrac{R}{\sqrt{2\sigma}}\right)} \approx \frac{1}{\sqrt{(2\pi)}f_D}\left(\frac{R}{\sqrt{2\sigma}}\right) \qquad (12)$$

Equations (10) and (11) show that the LCR increases as the envelope crosscorrelation ρ_{env} ($\approx \rho|^2$) increases (whilst the AFD is unaffected) and becomes 1·7 times, 4 times and 14 times as large as that for the independent fading case for $\rho_{env} = 0{\cdot}42$, $0{\cdot}^{-}5$ and 0·93, respectively. The AFDs for SS and SE strategies are equal to that of no diversity, while SC, EGC and MRC can halve the AFD. Considering the effect of the envelope crosscorrelations, the measured data shown in Figs 6 and $^{-}$ agree well with the calculated results.

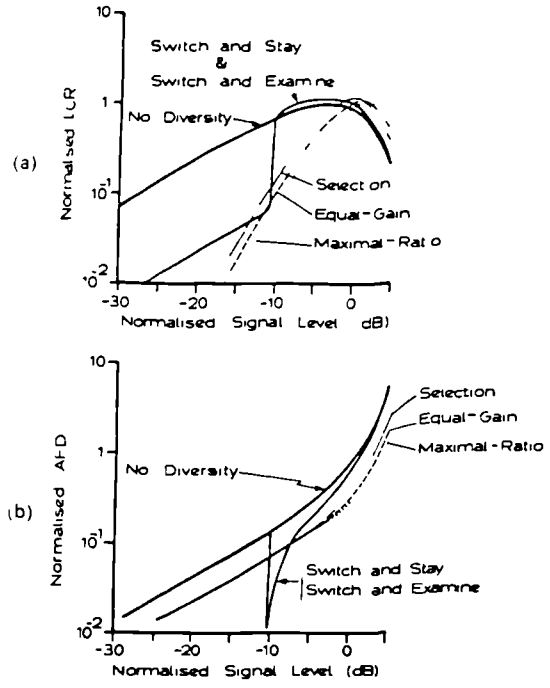

Fig. 9. Calculated (a) LCR and (b) AFD, for various diversity schemes under a condition of independent fading.

6 Conclusion

Recorded signals obtained from vertically-separated antennas at a base station site have been used to compare the effects of various two-branch predetection diversity systems (SS, SE, SC, EGC and MRC) on the measured CDF, LCR and AFD statistics. It has been confirmed that improvements can still be obtained for values of ρ_{env} up to 0·7 for all strategies except switching. A value of ρ_{env} no greater than 0·7 can be obtained at a base station site 35 m above ground level, in a cell of radius 1·3 km, using antennas separated vertically by about 12λ. Diversity produces substantial improvements in the CDF and LCR, but the AFD is only reduced by about half. (Note that there is no improvement in the AFD for SS and SE below the switching threshold.) The results lead to the conclusion that if base station diversity is used with data transmissions then the bit error rate and rate of burst error occurrence can be reduced considerably, whilst the burst error length is approximately halved.

7 Acknowledgments

The authors are indebted to Professor A. G. Williamson of the University of Auckland, New Zealand for his

assistance and advice. One of the authors, F. Adachi, was a UK SERC Visiting Research Fellow at the University of Liverpool throughout the research.

8 References

1 Jakes, W. C. Jr (Ed.), 'Microwave Mobile Communications' (Wiley, New York, 1974).

2 Brennan, D. G., 'Linear diversity combining techniques', *Proc. IRE*, **47**, no. 6, pp. 1075–102, June 1959

3 Adachi, F., Feeney, M. T., Williamson, A. G. and Parsons, J. D., 'Correlation between the envelopes of 900 MHz signals received at a mobile radio base station site', *Proc. IEE pt. F*, **133**, pp. 506–12, 1986

4 Adachi, F., Feeney, M. T. and Parsons, J. D., 'Effects of correlated fading on level crossing rates and average fade durations with predetection diversity reception', *Proc. IEE pt. F* (to be published)

5 Lee, W. C. Y., 'Level crossing rates of an equal gain predetection diversity combiner', *IEEE Trans. on Communications*, **COM-18**, no. 4, pp. 417–26, August 1970

6 Rustako, A. J., Yeh, Y. S. and Murray, R. R., 'Performance of feedback and switch space diversity 900 MHz mobile radio systems with Rayleigh fading', *IEEE Trans. on Communications*, **COM-21**, no. 11, pp. 1257–68, November 1973

7 Kahn, L. R., 'Ratio squarer', *Proc. IRE*, **42**, no. 11, p. 1704, November 1954

8 Parsons, J. D., Henze, M., Ratliff, P. A. and Withers, M. J., 'Diversity techniques for mobile radio reception', *The Radio and Electronic Engineer*, **45**, pp. 357–67, 1975

9 Henze, E., 'Theoretische Untersuchungen uber einige Diversity-verfahren', *Arch. elekt. Übertragung*, **11**, no. 5, pp. 193–94, May 1957

9 Appendix

If a signal with a Rayleigh-fading envelope given by equation (2) is received in the presence of Gaussian noise of mean power N, then it follows directly that the instantaneous carrier-to-noise ratio (CNR) $\gamma = R^2/2N$ and the mean CNR $\gamma_0 = \sigma^2/N$. It is easily shown that the PDF of the CNR is given by

$$p(\gamma) = \frac{1}{\gamma_0} \exp\left(-\gamma/\gamma_0\right)$$

(i) In a maximal ratio combiner (MRC) the output has a CNR given by

$$\gamma_r = \sum_{i=1}^{M} \gamma_i$$

where M is the number of branches. So,

$$\gamma_r = \frac{R_1^2}{2N} + \frac{R_2^2}{2N} + \ldots = \frac{1}{2N} \sum_{i=1}^{M} R_i^2$$

We can define an equivalent output R_r such that

$$\gamma_r = \frac{R_r^2}{2N} = \frac{1}{2N} \sum_{i=1}^{M} R_i^2$$

or

$$R_r = \sqrt{(2N\gamma_r)} = \sqrt{\left(\sum_{i=1}^{M} R_i^2\right)} = \sqrt{(R_1^2 + R_2^2 + \ldots)}$$

(ii) In an equal gain combiner (EGC) the output CNR is

$$\gamma_e = \frac{1}{M}\left(\sum_{i=1}^{M} \sqrt{\gamma_i}\right)^2$$

So

$$\gamma_e = \frac{1}{M}\left(\frac{R_1}{\sqrt{2N}} + \frac{R_2}{\sqrt{2N}} + \ldots\right)^2 = \frac{1}{2MN}\left(\sum_{i=1}^{M} R\right)^2$$

and again we define an equivalent output R_e such that

$$\gamma_e = \frac{R_e^2}{2N} = \frac{1}{2MN}\left(\sum_{i=1}^{M} R_i\right)^2$$

or

$$R_e = \sqrt{(2N\gamma_e)} = \frac{1}{\sqrt{M}}\left(\sum_{i=1}^{M} R_i\right) = \frac{R_1 + R_2 + \ldots}{\sqrt{M}}$$

(iii) For selection diversity

$$\gamma_s = \max\{\gamma_1, \gamma_2 \ldots\}$$

so

$$R_s = \max\{R_1, R_2 \ldots\}$$

Manuscript first received by the Institution on 6th July 1987 and in final form on 4th September 1987
Paper No. 2316 COM/441

Effects of correlated fading on level crossing rates and average fade durations with predetection diversity reception

F. Adachi, PhD
M.T. Feeney, MSc
Prof. J.D. Parsons, DSc(Eng), CEng, FIEE

Indexing terms: Radiocommunication, Receivers

Abstract: General expressions for the level crossing rate (LCR) and average fade duration (AFD) are obtained for several diversity combining schemes employing two-branch predetection reception of correlated Rayleigh fading signals. These expressions are obtained from joint and conditional probability density functions (PDFs) of the received signals, and lead to a unified treatment. This simplified method contrasts with the characteristic function approach used in previous investigations. Numerical results are presented for a space-diversity system using horizontally spaced antennas at a mobile station. It is shown that while the angle between the antenna axis and the direction of vehicle motion does not appear in the cumulative distribution function (CDF) of the combined output signal envelopes, it affects the LCR and AFD when the two fading signals are correlated. When the two antennas parallel with the direction of vehicle motion are used, the LCR can be reduced below the value obtainable from signals which fade independently. When the two antennas are perpendicular to the direction of vehicle motion, the AFD is loosely dependent on the antenna spacing and, provided the antenna spacing is not too small, is approximately half that for the no-diversity case.

List of principal symbols

d = distance between space-diversity antennas
e_i = received amplitude of ith multipath wave
erfc (.) = complementary error function
f_D = maximum Doppler frequency
$J_0(.)$ = zero-order Bessel function
m_R = mean value of $\dot{R}$
N_R = level crossing rate (LCR) at envelope level R
n = conditional level crossing rate
$p(a, b)$ = joint probability density function (PDF) of a and b
$p(a|b)$ = conditional PDF of a with b given
$Re(.)$ = real part of complex value
$R_n(t)$ = time-varying signal strength envelope for Nth branch
$\dot{R}(t)$ = time derivative of time-varying signal strength envelope
z_i = complex amplitude of ith multipath wave
z_i^* = complex conjugate of complex ith multipath wave
$\|z_i\|$ = modulus of complex ith multipath wave
$\langle z_i \rangle$ = ensemble average of complex ith multipath wave
M = mean matrix
M^{-1} = inverse of matrix M
M^T = transpose of matrix M
α = angle between antenna axis and direction of vehicle motion
θ_i = phase of ith multipath wave
θ_{ij} = phase difference between ith and jth multipath waves
λ = wavelength
$\rho_{ij}(\tau)$ = complex crosscorrelation function between ith and jth branches
σ^2 = average received signal power
$\sigma_{\dot{R}}^2$ = variance of $\dot{R}$
τ = time delay
τ_R = average fade duration (AFD) at envelope level R

Paper 5770F (E8), first received 4th September 1986 and in final revised form 26th August 1987

Dr. Adachi is with the NTT Electrical Communications Laboratories, PO Box 8, Yokosuka Post Office, Yokosuka 238, Japan

Mr. Feeney and Prof. Parsons are with the Department of Electrical Engineering & Electronics, University of Liverpool, Brownlow Hill, PO Box 147, Liverpool L69 3BX, United Kingdom

1 Introduction

In UHF land mobile radio, the signal transmission performance deteriorates severely because of multipath fading [1]. If digital signals are transmitted, then burst errors are produced when the signal fades below some noise-related threshold. The rates of occurrence and average length of these burst errors can be estimated from the level crossing rate (LCR) and average fade duration (AFD), respectively [2]. The LCR and AFD in a Rayleigh fading environment have been studied experimentally and theoretically [3].

Predetection diversity reception using selection combining (SC), equal-gain combining (EGC) and maximal-ratio combining (MRC) [4] can be used to reduce the effects of multipath fading on LCR and AFD [5, 6]. Theoretical comparison of the three combining schemes has shown [6] that, for independent Rayleigh fading signals, two-branch diversity reception can substantially reduce the LCR, and can halve the AFD irrespective of

the combining method used. In practical diversity systems, the fading signals received at the different antennas may be partially correlated, but little attention has been given to evaluation of the LCR and AFD of diversity combiners with correlated fading signals. Lee [7] investigated the influence of the fading correlation on the LCR of an EGC. Assuming that the envelope of the combiner output signal and its time derivative are independent random processes, he showed that if space diversity is used at a mobile station, the LCR is affected by the angle between the antenna axis and the direction of vehicle motion. Measured LCRs and AFDs of SC, EGC and MRC in a correlated fading environment are available in Reference 6; however, no analytical results have been presented.

The LCR and AFD for an m-branch equal-gain combiner have been found previously [8] using an approach based on characteristic functions. This approach has restrictions because, to derive one of the fundamental relationships (eqn. 5 of Reference 8), it is necessary to assume that the branch signals and their time derivatives are all Gaussian random variables, that the correlation between the signals is not strong, and that the time derivative $\dot{R}(t)$ of the output signal envelope is a function only of the time derivatives $\dot{R}_1(t)$, $\dot{R}_2(t)$ etc. of the branch signal envelopes. This latter restriction has the further effect of limiting the analysis to the case of equal-gain combiners (see eqn. 4 of this paper).

In this paper we present a unified analysis of the LCR and AFD of two-branch predetection SC, EGC and MRC with correlated Rayleigh fading signals. Our analysis also assumes that the branch signals and their time derivatives are Gaussian random signals, but the method using the joint and conditional probability density functions of the branch signals is conceptually simpler and does not suffer from any restrictions. The general expressions derived in Section 2 can be applied to any type of diversity, such as frequency or space, as can the simpler, approximate expressions which are also given. In Section 3 numerical results are obtained for a space-diversity system using horizontally spaced antennas at the mobile station.

2 Analysis

2.1 Received signal representation

We assume that an unmodulated carrier is transmitted and that the signals received on the two antennas are subject to mutually correlated Rayleigh fading with a symmetrical power spectrum. The fading power spectra of the two received signals are assumed to be identical.

The received signal at the ith antenna ($i = 1, 2$) can be represented in complex form as

$$\begin{aligned} c_i(t) &= \mathrm{Re}\ \{z_i(t)e^{j\omega_c t}\} \\ &= R_i(t)\cos\{\omega_c t + \theta_i(t)\} \end{aligned} \tag{1}$$

where $z_i(t)$ is a zero-mean complex Gaussian process. The envelope $R_i(t)$ ($= |z_i(t)|$) follows a Rayleigh distribution, and $\theta_i(t)$ is a uniformly distributed random phase [1].

2.2 Definition of LCR and AFD with predetection diversity

SC selects the branch having the larger signal envelope; EGC cophases the signals and sums them; MRC cophases, amplifies each signal by a factor proportional to its envelope and sums them. Thus the resultant envelope $R(t)$ can be expressed as

$$R(t) = \begin{cases} \max\{R_1(t), R_2(t)\} & \text{SC} \\ \dfrac{R_1(t) + R_2(t)}{\sqrt{2}} & \text{EGC} \\ \sqrt{(R_1^2(t) + R_2^2(t))} & \text{MRC} \end{cases} \tag{2}$$

In the above we have assumed that the noise power in each branch is identical ($= N_0$), and have taken into account the resultant noise power at the combiner output, such that $R^2(t)/2N_0$ represents the combiner output signal noise power ratio. Hence, we can exactly compare the effects of different types of combiner on the LCR and AFD.

The LCR and AFD of an envelope $R(t)$ at a certain level R can be obtained from eqns. 1.3-32 and 1.3-41, respectively, from Reference 4:

$$\begin{cases} N_R = \displaystyle\int_0^\infty \dot{R}p(R, \dot{R})\,d\dot{R} \\ \tau_R = \dfrac{P(R)}{N_R} \end{cases} \tag{3}$$

where N_R is the number of upward crossings per second, $p(R, \dot{R})$ is the joint probability density function (PDF) of $R = R(t)$ and its time derivative $\dot{R} = \dot{R}(t)$, and $P(R)$ is the cumulative distribution function (CDF). From eqns. 2, $\dot{R}(t)$ is given by

$$\dot{R}(t) = \begin{cases} \dot{R}_1(t), & R_1(t) \geq R_2(t) \\ \dot{R}_2(t), & R_1(t) < R_2(t) \end{cases} \quad \text{SC}$$
$$\dot{R}(t) = \frac{\dot{R}_1(t) + \dot{R}_2(t)}{\sqrt{2}} \quad \text{EGC} \tag{4}$$
$$\dot{R}(t) = \frac{R_1(t)\dot{R}_1(t) + R_2(t)\dot{R}_2(t)}{\sqrt{(R_1^2(t) + R_2^2(t))}} \quad \text{MRC}$$

Using complex notation, $\dot{R}_i$ is represented as

$$\dot{R}_i(t) = \mathrm{Re}\left\{\frac{\dot{z}_i(t)^* z_i(t)}{|z_i(t)|}\right\} \tag{5}$$

The analysis in this paper ignores mutual coupling effects, and the predictions for LCR and AFD may therefore depart from measurements at small antenna spacings, particularly when the signal is very low [9].

2.3 Conditional PDF of $\dot{R}$ (given z_1 and z_2)

From eqns. 4 and 5 it can be seen that with $z_1 = z_1(t)$ and $z_2 = z_2(t)$ being given, $\dot{R}$ becomes a Gaussian variable having the conditional PDF

$$\begin{aligned} p(\dot{R}\,|\,z_1, z_2) &= p(\dot{R}\,|\,R_1, R_2, \theta_{12}) \\ &= \frac{1}{\sigma_{\dot{R}}\sqrt{(2\pi)}} \exp\left[-\frac{(\dot{R} - m_{\dot{R}})^2}{2\sigma_{\dot{R}}^2}\right] \end{aligned} \tag{6}$$

where $\theta_{12} = \arg(z_1^* z_2)$. Values for $m_{\dot{R}}$ and $\sigma_{\dot{R}}^2$ are derived in the Appendix.

2.4 General expressions for LCR

The joint PDF of R_1, R_2 and θ_{12} is given by eqns. 8-31 and 8-102 of Reference 10:

$$\begin{aligned} p(R_1, R_2, \theta_{12}) &= \frac{R_1 R_2}{2\pi\sigma^4(1 - |\rho_{12}|^2)} \\ &\quad \times \exp\left[-\frac{R_1^2 + R_2^2 - 2R_1R_2\ \mathrm{Re}\,(\rho_{12}^* e^{j\theta_{12}})}{2\sigma^2(1 - |\rho_{12}|^2)}\right] \end{aligned} \tag{7}$$

Applying the appropriate variable transformations using eqns. 2, $p(R, \dot{R})$ can be obtained from eqns. 6 and 7, and hence the LCR can be calculated from eqns. 3. To make the LCR calculations simpler, we can change the order of integration with respect to R first. The LCR can be evaluated from

$$N_R = \begin{cases} \int_{\pi}^{\pi}\int_{0}^{R} np(R_1 = R, R_2, \theta_{12})\, dR_2\, d\theta_{12} + \int_{\pi}^{\pi}\int_{0}^{R} np(R_1, R_2 = R, \theta_{12})\, dR_1\, d\theta_{12} & \text{SC} \\ \int_{\pi}^{\pi}\int_{0}^{R\sqrt{2}} n\sqrt{(2)}p(R_1, R_2 = \sqrt{(2)}R - R_1, \theta_{12})\, dR_1\, d\theta_{12} & \text{EGC} \\ \int_{\pi}^{\pi}\int_{0}^{\pi/2} nRp(R_1 = R\cos\psi, R_2 = R\sin\psi, \theta_{12})\, d\psi\, d\theta_{12} & \text{MRC} \end{cases} \quad (8)$$

where n is the conditional LCR and, from eqn. 6, is given by

$$n = \int_0^{\infty} \dot{R}p(\dot{R} \mid R_1, R_2, \theta_{12})\, d\dot{R} = \frac{\sigma_R}{\sqrt{(2\pi)}}\left[\exp\left(-\frac{m_R^2}{2\sigma_R^2}\right) + \sqrt{(\pi)}\left(\frac{m_R}{\sigma_R\sqrt{2}}\right)\mathrm{erfc}\left(-\frac{m_R}{\sigma_R\sqrt{2}}\right)\right] \quad (9)$$

where erfc (.) is the complementary error function.

It is worth noting that the formulation of eqns. 8 is particularly significant. Instead of using a characteristic function approach, it is based on the joint and conditional PDFs $p(R_1, R_2, \theta_{12})$ and $p(\dot{R} \mid R_1, R_2, \theta_{12})$, these being well established relationships. The analysis is unified through eqns. 4, which establish the relationship between R and $\dot{R}$ for each combiner. On this basis, the approach is conceptually more straightforward.

For small values of R, an approximate expression can be obtained. From the Appendix, $m_{\dot{R}}\sqrt{(2)}\sigma_R$ is small and hence $n \sim \sigma_{\dot{R}}\sqrt{(2\pi)}$. Using this and the approximate joint PDF:

$$p(R_1, R_2, \theta_{12}) \simeq \frac{R_1 R_2}{2\pi\sigma^4(1 - |\rho_{12}|^2)} \quad (10)$$

we have the following simplified approximate expression:

$$N_R \simeq \nu\left(-\frac{\ddot{\rho}_{11} + \left(\frac{|\dot{\rho}_{12}|^2}{1 - |\rho_{12}|^2}\right)}{\pi}\right)^{1/2}\frac{\left(\frac{R}{\sigma\sqrt{2}}\right)^3}{1 - |\rho_{12}|^2} \quad \text{for } \frac{R}{\sigma\sqrt{2}} \ll 1 \quad (11)$$

where

$$\nu = \begin{cases} 2 & \text{SC} \\ 4 - \pi/2 & \text{EGC} \\ 1 & \text{MRC} \end{cases} \quad (12)$$

For independent fading signals, ρ_{12}, $\dot{\rho}_{12}$ and $\dot{\rho}_{12} = 0$ for m_R and σ_R^2. Hence from eqn. 9, $n = \sigma\sqrt{(-\ddot{\rho}_{11}\, 2\pi)}$, which is not a function of R_1, R_2 and θ_{12}. Inspection of eqns. 8 shows that the LCR is equal to n times the value of the PDF of R with diversity reception, and is given by

$$\gamma_R = \begin{cases} 2\sqrt{\left(\frac{-\ddot{\rho}_{11}}{\pi}\right)}\frac{R}{\sigma\sqrt{2}}\exp\left(-\frac{R^2}{2\sigma^2}\right)\left\{1 - \exp\left(-\frac{R^2}{2\sigma^2}\right)\right\} & \text{SC} \\ \sqrt{\left(\frac{-\ddot{\rho}_{11}}{\pi}\right)}\exp\left(-\frac{R^2}{2\sigma^2}\right)\left[\frac{R}{\sigma\sqrt{2}}\exp\left(-\frac{R^2}{2\sigma^2}\right) + \left\{\frac{R^2}{\sigma^2} - 1\right\}\frac{\sqrt{\pi}}{2}\mathrm{erf}\left(\frac{R}{\sigma\sqrt{2}}\right)\right] & \text{EGC} \\ \sqrt{\left(\frac{-\ddot{\rho}_{11}}{\pi}\right)}\left(\frac{R}{\sigma\sqrt{2}}\right)^3\exp\left(-\frac{R^2}{2\sigma^2}\right) & \text{MRC} \end{cases} \quad (13)$$

Without diversity, the LCR is given by [4]

$$N_R = \sqrt{\left(\frac{-\ddot{\rho}_{11}}{\pi}\right)}\frac{R}{\sigma\sqrt{2}}\exp\left(-\frac{R^2}{2\sigma^2}\right) \quad (14)$$

2.5 General expression for AFD

We saw in eqns. 3 that the AFD is given by the CDF LCR ratio. The closed-form expressions for the CDF of SC and MRC with correlated fading are given by [4]

$$P(R) = \begin{cases} 1 - \exp\left(-\frac{R^2}{2\sigma^2}\right)\left[1 + Q\left(\frac{R}{\sigma\sqrt{(1 - \rho_{12}^2)}}, \frac{\rho_{12}R}{\sigma\sqrt{(1 - \rho_{12}^2)}}\right) - Q\left(\frac{\rho_{12}R}{\sigma\sqrt{(1 - \rho_{12}^2)}}, \frac{R}{\sigma\sqrt{(1 - \rho_{12}^2)}}\right)\right] & \text{SC} \\ 1 - \frac{1 + \rho_{12}}{2\rho_{12}}\exp\left[-\frac{R^2}{2\sigma^2(1 - \rho_{12})}\right] + \frac{1 - \rho_{12}}{2\rho_{12}}\exp\left[-\frac{R^2}{2\sigma^2(1 - \rho_{12})}\right] & \text{MRC} \end{cases} \quad (15)$$

where $Q(a, b)$ is Marcum's Q-function:

$$Q(a, b) = \int_b^{\infty} x\exp\left(-\frac{x^2 + a^2}{2}\right)I_0(ax)\, dx \quad (16)$$

A good approximation to the CDF of an EGC can be obtained using the CDF of MRC, and is obtained by replacing the average signal power σ^2 of a single branch with $(4 - \pi/2)\sigma^2$ [4]. Hence, the values of AFD can be obtained from eqns. 8 and 15.

A simplified expression for the AFD, particularly for small values of R, can be obtained using eqn. 11:

$$\tau_R \simeq \frac{1}{2}\sqrt{\left(-\frac{\pi}{\ddot{\rho}_{11} + \left(\frac{|\dot{\rho}_{12}|^2}{1 - |\rho_{12}|^2}\right)}\right)}\frac{R}{\sigma\sqrt{2}} \quad \text{for } \frac{R}{\sigma\sqrt{2}} \ll 1 \quad (17)$$

for all diversity combiners.

When two fading signals are independent, an exact expression for the CDF of an EGC can be obtained. The AFD is given by

$$\tau_R = \begin{cases} \frac{1}{2}\sqrt{\left(\frac{\pi}{-\ddot{\rho}_{11}}\right)}\dfrac{\exp\left(\frac{R^2}{2\sigma^2}\right)-1}{\left(\frac{R}{\sigma\sqrt{2}}\right)} & \text{SC} \\ \sqrt{\left(\frac{\pi}{-\ddot{\rho}_{11}}\right)}\dfrac{1-\exp\left(-\frac{R^2}{\sigma^2}\right)-\frac{R}{\sigma_\nu 2}\exp\left(-\frac{R^2}{2\sigma^2}\right)\sqrt{(\pi)}\,\mathrm{erf}\left(\frac{R}{\sigma_\nu 2}\right)}{\exp\left(-\frac{R^2}{2\sigma^2}\right)\left[\frac{R}{\sigma_\nu 2}\exp\left(-\frac{R^2}{2\sigma^2}\right)+\left\{\frac{R^2}{\sigma^2}-1\right\}\frac{\sqrt{(\pi)}}{2}\mathrm{erf}\left(\frac{R}{\sigma_\nu 2}\right)\right]} & \text{EGC} \\ \sqrt{\left(\frac{\pi}{-\ddot{\rho}_{11}}\right)}\dfrac{\exp\left(\frac{R^2}{2\sigma^2}\right)-\left(1+\frac{R^2}{2\sigma^2}\right)}{\left(\frac{R}{\sigma_\nu 2}\right)^3} & \text{MRC} \end{cases} \tag{18}$$

Without diversity reception, the AFD is represented as [4]

$$\tau_R = \sqrt{\left(\frac{\pi}{-\ddot{\rho}_{11}}\right)}\frac{\exp\left(\frac{R^2}{2\sigma^2}\right)-1}{\left(\frac{R}{\sigma_\nu 2}\right)} \simeq \sqrt{\left(\frac{\pi}{-\ddot{\rho}_{11}}\right)}\left(\frac{R}{\sigma_\nu 2}\right) \quad \text{for } \frac{R}{\sigma_\nu 2} \ll 1 \tag{19}$$

Comparison of eqns. 17 and 19 shows that diversity reception can halve the AFD irrespective of the diversity combining scheme used when the two fading signals are independent.

3 Numerical calculations

The expressions derived in Section 2 are general and can be applied to any type of diversity (space, frequency, polarisation or time). In this Section we assume space diversity at the mobile station.

Two antennas with omnidirectional radiation patterns are used as shown in Fig. 1. In this figure d and α denote

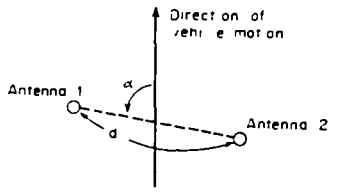

Fig. 1 *Antenna configuration at mobile station*

the antenna spacing and the angle between the antenna axis and the direction of vehicle motion, respectively. Assuming that incoming multipath waves having equal amplitude and independent phases arrive from all directions with equal probability, we have [11]

$$\begin{cases} \rho_{11}(\tau) = J_0(2\pi f_D \tau) \\ \rho_{12}(\tau) = J_0(2\pi\sqrt{[(f_D\tau)^2 + (d/\lambda)^2 - 2(f_D\tau)(d/\lambda)\cos\alpha]}) \end{cases} \tag{20}$$

where $J_0(.)$ is the zero-order Bessel function, λ is the carrier wavelength, f_D is the maximum Doppler frequency (vehicle speed/carrier wavelength), and $\alpha = 0 \sim \pi/2$ rad.

Hence

$$\begin{aligned} \ddot{\rho}_{11} &= -2(\pi f_D)^2 \\ \rho_{12} &= J_0\left(2\pi\frac{d}{\lambda}\right) \\ \dot{\rho}_{12} &= 2\pi f_D \cos\alpha J_1\left(2\pi\frac{d}{\lambda}\right) \\ \ddot{\rho}_{12} &= (2\pi f_D)^2\left\{\frac{J_1\left(2\pi\frac{d}{\lambda}\right)}{\left(2\pi\frac{d}{\lambda}\right)}\cos 2\alpha - \cos^2\alpha J_0\left(2\pi\frac{d}{\lambda}\right)\right\} \end{aligned} \tag{21}$$

where $J_1(.)$ is the first-order Bessel function.

When the antenna spacing is sufficiently large, the two received signal envelopes fade independently. The LCR and AFD for independent Rayleigh fading signals can be

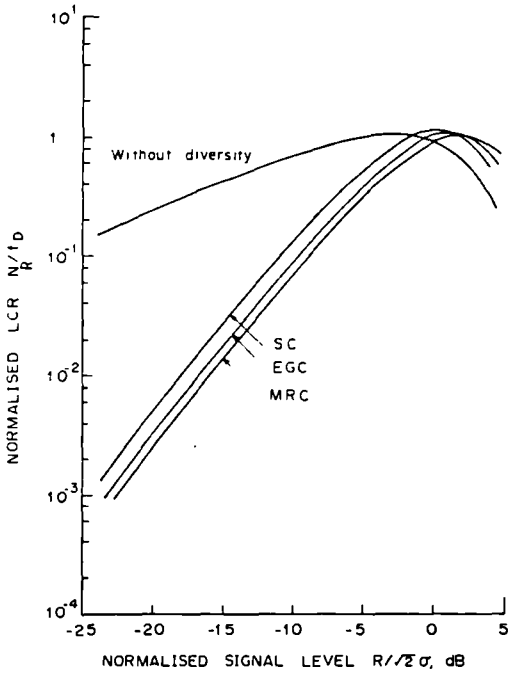

Fig. 2 *LCR curves for independent Rayleigh fading*
$d/\lambda \to \infty$

evaluated from eqns. 13 and 18, respectively. The results are shown in Figs. 2 and 3. For comparison, the results without diversity reception, calculated from eqns. 14 and 19, are also shown. The use of diversity reception reduces the LCR, particularly for the deep fades.

For correlated Rayleigh fading signals, the LCR is calculated using eqns. 8, and is shown in Figs. 4–6. It can be seen in Figs. 5 and 6 that, as the antenna spacing becomes large, the LCR decreases, becoming oscillatory and convergent. For independent fading, the normalised LCR, N_R/f_D, of an MRC at $R_{\searrow}(2)\sigma = -20$ dB is 2.5×10^{-3}. It can be seen in Fig. 5 that when $\alpha \neq \pi/2$, N_R/f_D becomes smaller than 2.5×10^{-3} for small antenna spacings. In particular, when the two antennas are parallel with the direction of vehicle motion ($\alpha = 0$), a minimum LCR can be obtained at $d/\lambda \simeq 0.25$, where it is approximately halved compared with the independent fading case. In Fig. 5 the approximate results calculated from eqn. 11 are shown as broken lines. Except for very small antenna spacings (less than 0.15λ), eqn. 11 is found to be a good approximation.

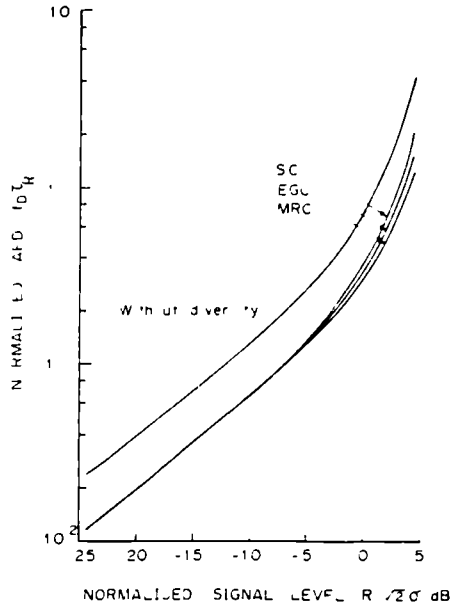

Fig. 3 *AFD curves for independent Rayleigh fading*

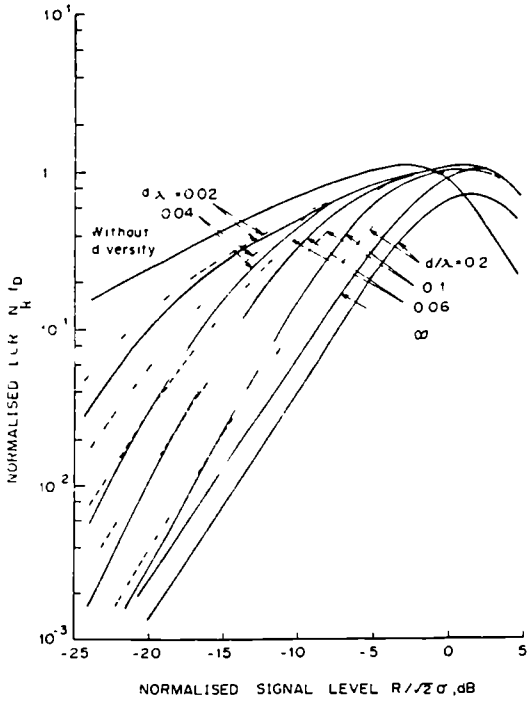

Fig. 4 *LCR curves of MRC for various antenna spacings*
—— $\alpha = 0$ rad - - $\alpha = \pi/2$ rad

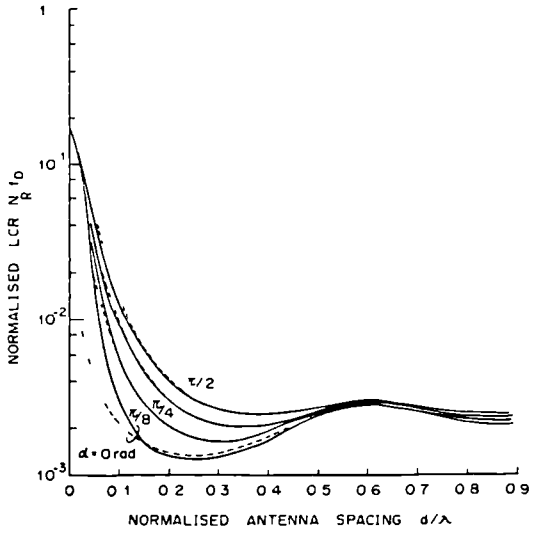

Fig. 5 *Effect of angle α between antenna axis and direction of vehicle motion on LCR curves for MRC*
$R_{\searrow}(2)\sigma = -20$ dB
—— exact - approximate

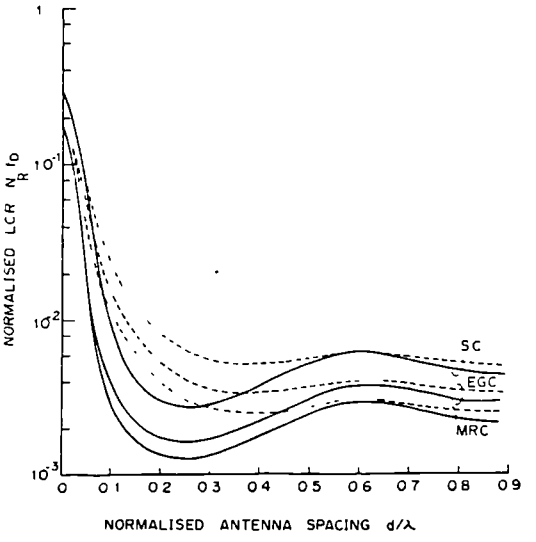

Fig. 6 *Comparison of LCR curves for SC, EGC and MRC*
$R'_{\searrow}(2)\sigma = -20$ dB
—— $\alpha = 0$ rad - - $\alpha = \pi/2$ rad

The AFD evaluated using the above results and the CDF calculated from eqns. 15 are shown in Figs. 7 9.

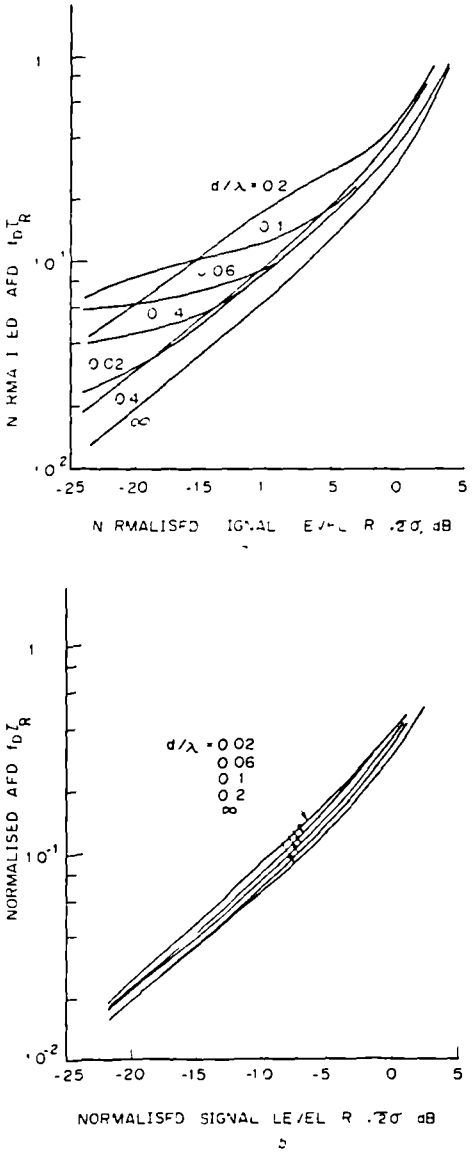

Fig. 7 *AFD curves of MRC for various antenna spacings*
a $\alpha = 0$ rad *b* $\alpha = \pi/2$ rad

The shape of the AFD curves of the MRC for $\alpha = 0$ and $\pi/2$ differ considerably. The AFD curves are loosely dependent on the antenna spacings when the two antennas are perpendicular to the direction of vehicle motion ($\alpha = \pi/2$), and almost identical with those of the independent fading case for antenna spacings $>0.1\ \lambda$. The effect of the antenna angle α is shown in Fig. 8. Broken lines show the approximate results using eqn. 17. Except for small antenna spacings, eqn. 17 is a good approximate expression. The normalised AFD, $f_D\tau_R$, at $R/\sqrt{(2)}\sigma = -20$ dB is 0.04 for no diversity reception; thus the AFD for the MRC is longer than for no-diversity reception for small antenna spacings and $\alpha < \pi/4$. At $\alpha = 0$, the maximum AFD of the MRC is longer by a factor of two. In Fig. 9 the AFDs of SC, EGC and MRC are compared. The AFDs of SC are slightly smaller than those of EGC and MRC.

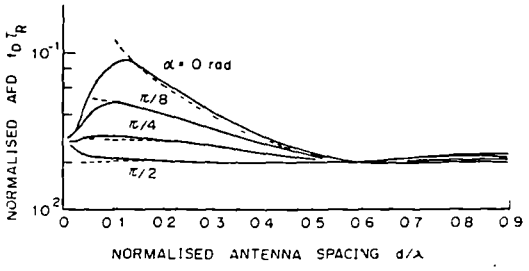

Fig. 8 *Effect of angle* α *between antenna axis and direction of vehicle motion on AFD curves for MRC*
$R/\sqrt{(2)}\sigma$ 20 dB
exact approximate

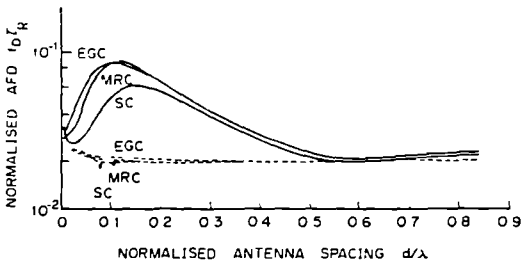

Fig. 9 *Comparison of AFD curves for SC, EGC and MRC*
$R/\sqrt{(2)}\sigma = -20$ dB
—— $\alpha = 0$ rad - - - $\alpha = \pi/2$ rad

4 Conclusions

Expressions have been derived for the LCR and AFD in the case of two-branch predetection SC, EGC and MRC with correlated Rayleigh fading signals. Numerical results were presented for a space-diversity system using horizontally spaced antennas at a mobile station. It has been shown that the angle between the antenna axis and the direction of vehicle motion affects the LCR and AFD curves, while the CDF, which is given by LCR × AFD, is not affected.

A further improvement can be achieved in the LCR over that with independent fading signals by using closely spaced antennas arranged parallel to the direction of vehicle motion. For a signal level of 20 dB below the RMS value and an antenna spacing of 0.25 λ, the LCR of an MRC is about half that of the independent fading case. For the independent fading case, the AFD is halved irrespective of the diversity combining scheme used. When two antennas are perpendicular to the direction of vehicle motion, the AFD is loosely dependent on the antenna spacing, and is almost identical to that for the independent fading case except for very small antenna spacings.

5 Acknowledgment

This study was undertaken while F. Adachi was a UK SERC visiting research fellow in the Department of Electrical Engineering & Electronics at the University of Liverpool, UK.

6 References

1 CLARKE, R.H.: 'A statistical theory of mobile radio reception', *Bell Syst. Tech. J.*, 1968, 47, pp. 957–1000

2 OHTANI, K., DAIKOKU, K., and OMORI, H.: 'Burst error performance encountered in digital land mobile radio channel', *IEEE Trans.*, Nov. 1981, VT-30, pp. 156–160

3 REUDINK, D.O.: 'Properties of mobile radio propagation above 400 MHz', *ibid.*, Nov. 1974, VT-23, pp. [illegible] 159

4 JAKES, W.C. Jr.: 'Microwave mobile communications' (Wiley, New York, 1974)

5 RUSTAKO, A.J. Jr.: 'Evaluation of a mobile radio multiple channel diversity receiver using pre-detection combining', *IEEE Trans.*, Oct. 1967, VT-16, pp. 46–57

6 FEENEY, M.T., and ADACHI, F.: 'The performance of various diversity combiners on signals received at a base station site' *IERE Conf. Proc.* 65, Dec. 1985, pp. 55–62

7 LEE, W.C.Y.: 'Level crossing rates of an equal-gain predetection diversity combiner', *IEEE Trans.*, 1970, COM-18, pp. 417–425

8 LEE, W.C.Y.: 'A study of the antenna array configuration of an *m*-branch diversity combining mobile radio receiver', *ibid.*, Nov. 1971, VT-20, pp. 93–104

9 LEE, W.C.Y.: 'Mobile communications engineering' McGraw-Hill, New York, 1982)

10 DAVENPORT, W.B. Jr., and ROOT, W.L.: 'An introduction to the theory of random signals and noise (McGraw-Hill, New York, 1958)

11 LEE, W.C.Y.: 'An extended correlation function of two random variables applied to mobile radio transmission', *Bell Syst. Tech. J.*, 1969, pp. 3423–3440

12 SCHWARTZ, M., BENNETT, W.R., and STEIN, S.: 'Communication systems and techniques (McGraw-Hill, New York, 1966)

7 Appendix

Let $\dot{z}$ and z be the column matrices of $\dot{z}_i = \dot{z}_i(t)$ and $z_i = z_i(t)$, respectively. Here, $\dot{z}_1$, $\dot{z}_2$, z_1 and z_2 are mutually correlated zero-mean complex Gaussian variables. Applying the matrix theory described on pp. 495–496 of Reference 12, the mean (2 × 1 column) matrix $\mathcal{M}$ and the covariance (2 × 2) matrix Λ of $\dot{z}$, with z given, can be obtained from

$$\begin{cases} \mathcal{M} = \mu z = (cb^{-1})^* z \\ \Lambda = a - cb^{-1}c^{T*} \end{cases} \tag{22}$$

where a, b and c are the partitioned matrices of the correlation matrix

$$\frac{1}{2}\left\langle \begin{pmatrix} \dot{z} \\ z \end{pmatrix}^* \begin{pmatrix} \dot{z} \\ z \end{pmatrix}^T \right\rangle = \begin{pmatrix} a & c \\ c^{T*} & b \end{pmatrix} \tag{23}$$

and $(.)^{-1}$ and $(.)^T$ are the inverse matrix and transposed matrix, respectively. In our case, the components of a, b and c are given by

$$\begin{cases} a_{ij} = -\sigma^2 \dfrac{d^2}{d\tau^2}\rho_{ij}(\tau)\Big|_{\tau=0} = -\sigma^2\ddot{\rho}_{ij}(0) \\ b_{ij} = \sigma^2\rho_{ij}(0) \\ c_{ij} = -\sigma^2 \dfrac{d}{d\tau}\rho_{ij}(\tau)\Big|_{\tau=0} = -\sigma^2\dot{\rho}_{ij}(0) \end{cases} \tag{24}$$

where $\rho_{ij}(\tau) = z_i(t)^* z_j(t+\tau)/2\sigma^2$, and $\sigma^2 = \langle |z_i(t)|^2 \rangle$ is the average received signal power at each antenna.

Since we are assuming a symmetrical fading power spectrum and that the two fading power spectra are identical, $\dot{\rho}_{11}(0) = \dot{\rho}_{22}(0) = 0$ and $\ddot{\rho}_{11}(0) = \ddot{\rho}_{22}(0)$. From eqns. 22 and 23 we then have

$$\mu = \frac{1}{1-|\rho_{12}|^2}\begin{pmatrix} \dfrac{\rho_{12}\dot{\rho}_{12}^*}{\dot{\rho}_{12}} & -\dot{\rho}_{12}^* \\ \dot{\rho}_{12} & -\rho_{12}^*\dot{\rho}_{12} \end{pmatrix}$$

$$\Lambda = -\sigma^2\begin{pmatrix} \ddot{\rho}_{11} + \dfrac{|\dot{\rho}_{12}|^2}{1-|\rho_{12}|^2} & \ddot{\rho}_{12} + \dfrac{\rho_{12}^*(\dot{\rho}_{12})^2}{1-|\rho_{12}|^2} \\ \ddot{\rho}_{12}^* + \dfrac{\rho_{12}(\dot{\rho}_{12}^*)^2}{1-|\rho_{12}|^2} & \ddot{\rho}_{11} + \dfrac{|\dot{\rho}_{12}|^2}{1-|\rho_{12}|^2} \end{pmatrix} \tag{25}$$

where $\rho_{11} = \rho_{11}(0)$, $\rho_{12} = \rho_{12}(0)$, $\dot{\rho}_{12} = \dot{\rho}_{12}(0)$, $\ddot{\rho}_{11} = \ddot{\rho}_{11}(0)$ and $\ddot{\rho}_{12} = \ddot{\rho}_{12}(0)$. Using eqns. 25 with eqns. 4 and 5, m_R and σ_R^2 can be found as

$$m_R = \begin{cases} \dfrac{R_1\,\mathrm{Re}(\dot{\rho}_{12}^*\rho_{12}) - R_2\,\mathrm{Re}(\dot{\rho}_{12}^* e^{j\theta_{12}})}{1-|\rho_{12}|^2} & R_1 \geq R_2 \\ \dfrac{-R_2\,\mathrm{Re}(\dot{\rho}_{12}^*\rho_{12}) + R_1\,\mathrm{Re}(\dot{\rho}_{12}^* e^{j\theta_{12}})}{1-|\rho_{12}|^2} & R_1 < R_2 \\ \dfrac{R_1 - R_2}{\sqrt{2}}\dfrac{\mathrm{Re}(\dot{\rho}_{12}^*\rho_{12}) + \mathrm{Re}(\dot{\rho}_{12}^* e^{j\theta_{12}})}{1-|\rho_{12}|^2} & \text{EGC} \\ \dfrac{R_1^2 - R_2^2}{\sqrt{(R_1^2+R_2^2)}}\dfrac{\mathrm{Re}(\dot{\rho}_{12}^*\rho_{12})}{1-|\rho_{12}|^2} & \text{MRC} \\ -\sigma^2\left\{\rho_{11} + \dfrac{|\dot{\rho}_{12}|^2}{1-|\rho_{12}|^2}\right\} & \text{SC} \end{cases} \tag{26}$$

$$\sigma_R^2 = \begin{cases} -\sigma^2\left\{\ddot{\rho}_{11} + \dfrac{|\dot{\rho}_{12}|^2}{1-|\rho_{12}|^2}\right\} - \sigma^2\,\mathrm{Re}\left\{\left(\ddot{\rho}_{12} + \dfrac{\rho_{12}^*(\dot{\rho}_{12})^2}{1-|\rho_{12}|^2}\right)^* e^{j\theta_{12}}\right\} & \text{EGC} \\ -\sigma^2\left\{\ddot{\rho}_{11} + \dfrac{|\dot{\rho}_{12}|^2}{1-|\rho_{12}|^2}\right\} - \sigma^2\dfrac{2R_1R_2}{R_1^2+R_2^2}\,\mathrm{Re}\left\{\left(\ddot{\rho}_{12} + \dfrac{\rho_{12}^*(\dot{\rho}_{12})^2}{1-|\rho_{12}|^2}\right)^* e^{j\theta_{12}}\right\} & \text{MRC} \end{cases} \tag{27}$$

COMPARISON OF SELECTION AND SWITCHED DIVERSITY SYSTEMS FOR ERROR-RATE REDUCTION AT BASE-STATION SITES IN DIGITAL MOBILE RADIO SYSTEMS

J.D. Parsons and M.T. Feeney

Department of Electrical Engineering and Electronics
The University of Liverpool, P.O. Box 147, Liverpool, L69 3BX, U.K.

ABSTRACT

Recorded envelope data from field trials in which a mobile transmitted a CW signal to a base station equipped with two vertically spaced antennas has been used in a computer simulation of diversity reception. The cumulative distribution function, level-crossing rate and average fade duration have been determined for 2-branch selection and switched diversity systems and the results have been compared with theoretical calculations. Considerable improvements are obtained in general, although switched diversity is not effective in reducing the duration of fades. Provided an optimum switching threshold is used, both types of diversity can reduce BER for uncorrelated envelopes.

INTRODUCTION

The majority of radio communication links are subjected to conditions in which energy can travel from the transmitter to the receiver via more than one path. This "multipath" situation arises in different ways depending upon the application, but in mobile radio systems the major cause is reflection and scattering from obstacles such as trees, hills and buildings along the transmission path. Radio waves therefore arrive at the receiver from different directions, they have different time delays and they combine vectorially at the antenna to give a spatially-varying signal which can be large or small depending upon whether the incoming waves combine in a constructive or destructive manner. The signal fluctuations are known as fading and the rapid fluctuations caused by local multipath are known as fast (or Rayleigh) fading to distinguish them from the much longer-term variation in the mean level which is termed 'slow-fading'.

It is well-known that the location of the receiving antenna does not have to be changed very much to change the signal level by several tens of dB [1]. Moreover, the envelopes of signals received at two points separated by a relatively small distance fade in an uncorrelated manner and this makes space diversity [2] an attractive proposition to mitigate the fading effects. At the mobile end of the link the necessary antenna separation is less than $\lambda/2$; at the base station much larger distances (up to a few tens of λ) are required but the technique can still be used successfully. When digital modulation is used the performance of the radio link deteriorates rapidly when the received signal envelope fades below some system-related threshold. The statistics of the signal envelope, the level-crossing rate and the duration of fades below any given level are important in system design [3].

The literature does not contain any detailed comparison between calculated and measured results for various diversity schemes, although Lee [3] has discussed the case of equal-gain predetection combiners. In this paper we present results for parameters of two-branch predetection selection and switched diversity and compare measurements with theoretical results for the simple case of uncorrelated signals.

DIVERSITY SYSTEMS

The various well-known diversity techniques are extensively described in the literature [4]. In selection diversity and its derivative, switched diversity, only one of the available signals is passed into the receiver at any time. The principle of selection diversity is conceptually very simple, the signal chosen at any instant being the one with the largest signal envelope. In switched diversity the chosen signal continues to be used (whether it is the largest or not) provided it remains above a predetermined threshold level. If it falls below the threshold then it is possible to use the 'switch and stay' strategy in which the new signal is used irrespective of its value, or a 'switch and examine' strategy in which, if the new signal is also below the threshold, the system periodically examines both signals until one rises above the threshold. Although the switch and examine technique allows a marginally quicker return to an acceptable signal when both signals are below the threshold together (a rare event), the rapid switching causes noise bursts which are most undesirable. In selection and switched systems the instantaneous output carrier to noise ratio (CNR) is always equal to the instantaneous CNR of the signal actually in use. The mean output CNR is higher than the mean input CNR although the improvement is marginal and is in itself no justification for using diversity.

EXPERIMENT

The data used for comparison was obtained from a series of field trials in the city of Liverpool [5]. A mobile transmitted a 5 W CW signal at 896 MHz and this was received on two antennas at a base station site approximately 35 m above street level. The vehicle was driven around a pre-planned

route about 1.3 km distant from the base station at a nearly constant speed of 10 m/sec. Two vertically mounted λ/2 dipoles were used for reception and these were mounted one above the other at separations of 4, 10 and 20 wavelengths thereby yielding signals with measured envelope cross-correlation coefficients of approximately 0.93, 0.75 and 0.42 respectively. The two received signals were recorded on a multitrack FM instrumentation tape recorder using the log-video outputs of two field-strength measuring receivers. The recorded signals were later replayed and simultaneously digitised at a 1 kHz rate, the digitised values being transferred to a main-frame computer for analysis.

This data base has allowed a true comparison to be made between various diversity schemes by simulating the action of the diversity schemes on identical data sets extracted from the measured data base. This provides a much more realistic comparison than that obtained by assuming Rayleigh fading. This paper presents results for the cumulative probability distribution function (CDF) the level crossing rate (LCR) and the average fade duration (AFD) for the original signal envelope and the effective envelope after diversity has been employed. The only way in which the original data was modified was by filtering to remove the slow-fading component. This was achieved by normalising to the local/running mean.

RESULTS

The measured envelope cross-correlation ρ_{env}, between the two received signals are shown in Fig. 1 for vertical antenna separations from 2 to 24λ. These cross-correlations were obtained by averaging cross-correlations for 2.0 s segments over the section of the test route used (approx. 300 m). For the following diversity simulation, we use the data obtained when the antenna separations were 4, 10 and 20λ, which correspond to ρ_{env} of 0.93, 0.75 and 0.42 respectively.

Fig. 2 shows the CDF for each of the diversity strategies (using a -10dB switching threshold for SS and SE and a 2 ms duration for SE) for data with ρ_{env}= 0.42. Without diversity, the CDF follows the Rayleigh distribution as expected. All of the schemes show improvements compared with the case of no diversity, especially when deep fading occurs. SE is slightly superior to SS for a signal below the switching threshold, while they have an identical CDF above the switching threshold. Typical improvements at the 1 percent level are 5.3 dB for SS, 6.9 dB for SE and 8.8 dB for SC.

The effect that the various strategies have on the LCR and AFD is shown in Figs. 3 and 4. In these figures, the term 'normalised LCR' refers to the LCR divided by the maximum Doppler frequency f_D, (which for our experiment was 33 Hz). The 'normalised AFD' is the AFD multiplied by f_D. In all of the schemes, the LCR is considerably reduced for situations when deep fading occurs. The largest improvement in LCR is provided by SC with again, the switching threshold affecting the improvement provided by the SS and SE cases. In terms of the AFD, a consistent reduction is obtained from SC with the LCR being

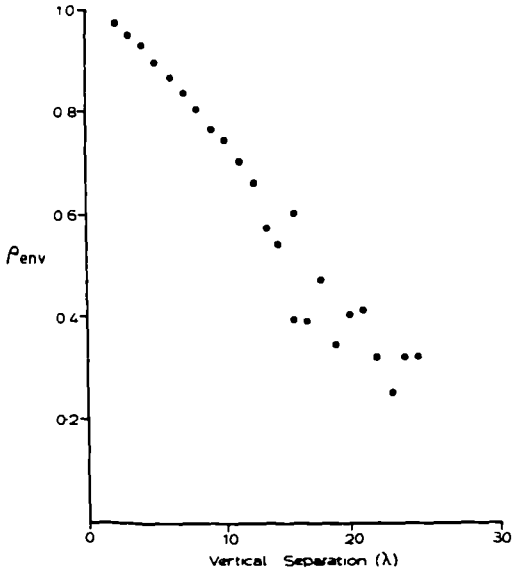

Fig. 1 Cross-correlation between signal envelopes ρ_{env} received on two antennas spaced at various vertical separations for data from a nearly circumferential route.

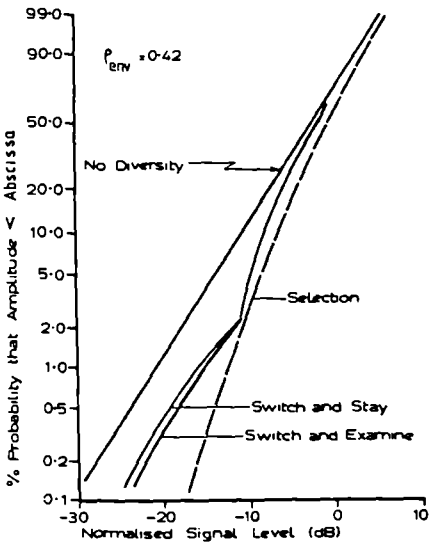

Fig. 2 Measured CDF of a normalised fast fading signal envelope for varous diversity schemes.

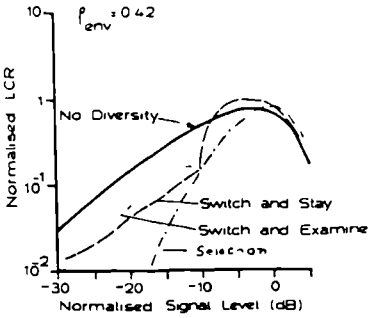

Fig.3 Measured LCR for SS and SE strategies using a switching threshold of -10dB.

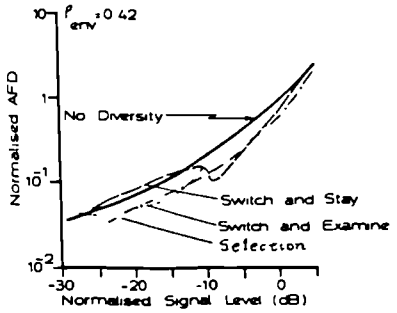

Fig 4 Measured AFD for SS and SE strategies using a switching threshold of - 10dB.

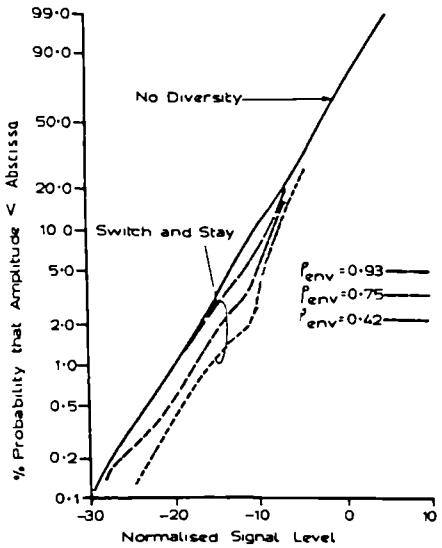

Fig.5 Effect of ρ_{env} on the measured CDF for the SS strategy.

almost halved. Fig. 4 shows that the SS and SE strategies have an identical reduction in the AFD above the switching threshold. Below the switching threshold the SS strategy shows no improvement, whilst SE does, as a result of the periodic switching (2 ms).

The Effect of Correlation

The effect of envelope cross-correlation on the CDF is shown on Fig. 5 for the SS case. An increase in ρ_{env} reduces the improvement until, in the limiting case of $\rho_{env} = 1$, the improvement disappears completely. A similar argument would apply to SC and SE. Figs. 6 and 7 show the LCR and AFD over a range of ρ_{env} for SS. The AFD tends towards the no diversity case as ρ_{env} increases. Below the switching threshold, the AFD is not improved for any value of ρ_{env}.

THEORETICAL ANALYSIS

Cumulative Distribution Function

In Rayleigh fading, the received signal envelope at each branch has a CDF given by

$$P(R) = 1 - \exp\left[-\frac{R^2}{2\sigma^2}\right] \qquad (1)$$

where σ^2 is the average signal power (which has been assumed to be unity since the received signal is normalised by the local mean). The closed form expression of the CDF for SE and SC with correlated fading is given by

$$P(R) = \begin{cases} 1-\exp\left[-\frac{R_t^2}{2\sigma^2}\right] Q\left(\frac{R}{\sigma\sqrt{(1-|\rho_{12}|^2)}}, |\rho_{12}|\frac{R_t}{\sigma\sqrt{(1-|\rho_{12}|^2)}}\right) \\ -\exp\left[-\frac{R^2}{2\sigma^2}\right]\left\{1-Q\left(|\rho_{12}|\frac{R}{\sigma\sqrt{(1-|\rho_{12}|^2)}}, \frac{R_t}{\sigma\sqrt{(1-|\rho_{12}|^2)}}\right)\right\} \quad \text{for SE} \\ 1-\exp\left[-\frac{R^2}{2\sigma^2}\right]\left\{1-Q\left(|\rho_{12}|\frac{R}{\sigma\sqrt{(1-|\rho_{12}|^2)}}, \frac{R}{\sigma\sqrt{(1-|\rho_{12}|^2)}}\right)\right. \\ \left. +Q\left(\frac{R}{\sigma\sqrt{(1-|\rho_{12}|^2)}}, |\rho_{12}|\frac{R}{\sigma\sqrt{(1-|\rho_{12}|^2)}}\right)\right\}, \quad \text{for SC} \end{cases} \qquad (2)$$

where ρ_{12} is the value of the cross-correlation function $\rho_{12}(t)$ at $t = 0$ between the complex envelopes of the two fading signals, Q(a,b) is Marcum's Q-function and R_t is a switching threshold. An expression for the CDF of SS has not yet been found for correlated fading, while it is identical with that of SE for independent fading [6]. Hence,

we use the CDF of SE as an approximation to SS.

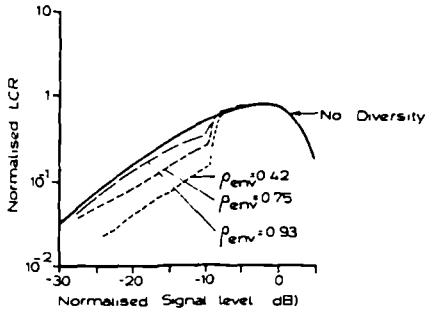

Fig. 6 Effect of ρ_{env} on the measured LCR for SS using a switching threshold of -10dB.

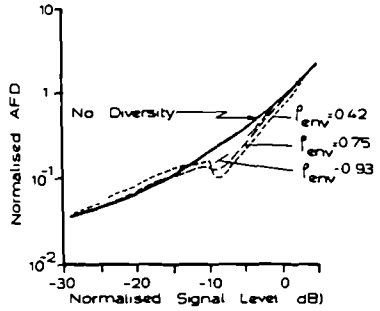

Fig.7 Effect of ρ_{env} on the measured AFD for SS using a switching threshold of -10dB.

The calculated CDFs for independent fading ($\rho_{12} = 0$) are shown in Fig. 8 for each of the diversity strategies. It can be seen that SC has the best performance, with reduced improvements being available from SS and SE. The measured and calculated CDFs (Figs. 2 and 8 respectively) are quite similar. For small signal envelopes, (2) can be approximated as

$$P(R) \approx \begin{cases} \left[\dfrac{RR_t}{2\sigma^2\sqrt{(1-|\rho_{12}|^2)}}\right]^2 , & \text{for SS and SE } (R \ll R_t) \\ \left[\dfrac{R^2}{2\sigma^2\sqrt{(1-|\rho_{12}|^2)}}\right]^2 , & \text{for SC} \end{cases} \qquad (3)$$

Since $\rho_{env} = |\rho|^2$ in Rayleigh fading [1], (3) shows that the envelope cross-correlation reduces the effective average power by a factor of $\sqrt{(1-\rho_{env})}$ for all of the diversity combiners. When $\rho_{env} = 0.42$, 0.75 and 0.93, the diversity gain reductions are 1.2, 3.0 and 5.8 dB respectively. The measured data shown in Fig. 5 agree well with the calculated results.

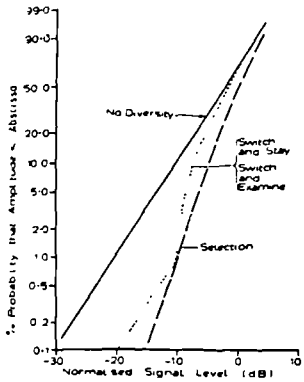

Fig. 8 Calculated CDF of a Rayleigh fading envelope for various diversity schemes under conditions of independent fading.

Level Crossing Rate and Average Fade Duration

The LCR is defined as the number of negative or positive going crossings per second of the effective signal envelope R(t) at a particular signal level R, and is obtained from

$$N_R = \int_0^\infty \dot{R}\, p(R,\dot{R})\, d\dot{R}, \qquad (4)$$

where $p(R,\dot{R})$ is the joint probability distribution function (PDF) of the signal envelope and its time derivative $\dot{R}(t)$. The AFD is given by

$$\tau = \frac{P(R)}{N_R} . \qquad (5)$$

Recently, the authors have analysed the LCR for predetection diversity combiners. When R is small a simple approximate expression has been obtained as

$$N_R \approx \sqrt{\left[-\frac{\ddot{\rho}_{11} + |\dot{\rho}_{12}|^2/(1-|\rho_{12}|^2)}{2\pi}\right]}\, p(R), \qquad (6)$$

where $p(R) = (d/dR)P(R)$ is the PDF of the effective envelope, $\ddot{\rho}_{11}=(d^2/dt^2)\rho_{11}(t)$ at $t=0$ with $\rho_{11}(t)$ being the autocorrelation function of the complex envelope of each received signal and $\dot{\rho}_{12}=(d/dt)\rho_{12}(t)$ at $t=0$.

Assuming that all the multipath waves received at the base station result from scatterers surrounding a mobile uniformly, $\rho_{11}(t)=J_0(2\pi f_D t)$ [1] and thus $\ddot{\rho}_{11}= -2(\pi f_D)^2$. For vertically spaced antennas $\dot{\rho}_{12}$ has not been analytically derived but for horizontally spaced antennas a reasonable distance apart its effect can be assumed small [4]. If we assume $\dot{\rho}_{12} = 0$, then

$$N_R \approx \sqrt{\left[-\frac{\ddot{\rho}_{11}}{2\pi}\right]}\, p(R) \qquad (7)$$

If two fading signals are independent (ρ_{12} and ρ_{12}= 0), (7) gives the exact expression. The calculated LCR (N_R/f_D) and AFD ($f_D\tau$) for various diversity combiners are shown in Fig. 9 for independent fading signals, where a -10 dB threshold has been used in the SS and SE strategies. The measured data are shown in Fig. 3 for SC, and in Fig. 4 for SS and SE. The measured and calculated LCR and AFD are similar except for SE. The LCR values are underestimated for SE, since the calculations do not take into account the periodic switching, which occurs when both envelopes are below the switching threshold. The difference between the calculated and measured data can be attributed to the envelope cross-correlation not being zero.

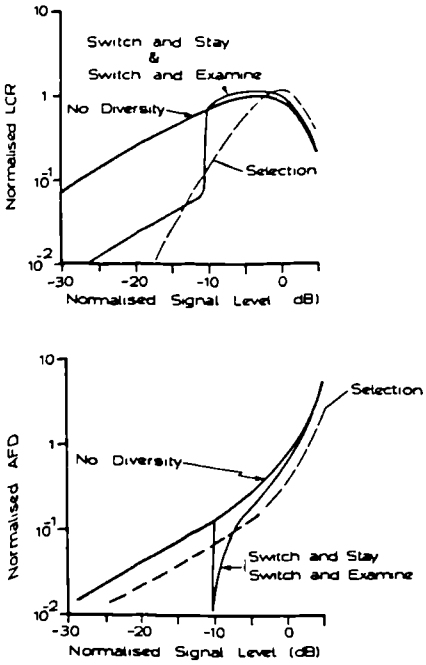

Fig. 9 Calculated LCR and AFD for various diversity schemes under conditions of independent fading.

When the two fading signals are correlated,

$$N_R = \begin{cases} \sqrt{(2\pi)} f_D (\frac{R}{\sqrt{2}\sigma})(\frac{R_t}{\sqrt{2}\sigma})^2/(1-|\rho_{12}|^2), & \text{for SS and SE } (R \ll R_t) \\ 2\sqrt{(2\pi)} f_D (\frac{R}{\sqrt{2}\sigma})^3/(1-|\rho_{12}|^2), & \text{for SC} \end{cases} \quad (8)$$

and

$$\tau = \begin{cases} \frac{1}{\sqrt{(2\pi)} f_D} (\frac{R}{\sqrt{2}\sigma}), & \text{for SS and SE } (R \ll R_t) \\ \frac{1}{2\sqrt{(2\pi)} f_D} (\frac{R}{\sqrt{2}\sigma}), & \text{for SC,} \end{cases} \quad (9)$$

Without diversity, the LCR and AFD are given by [1]

$$N_R = \sqrt{(2\pi)} f_D (\frac{R}{\sqrt{(2}\sigma)}) \exp[-\frac{R^2}{2\sigma^2}] \approx \sqrt{(2\pi)} f_D (\frac{R}{\sqrt{2}\sigma})$$

$$\tau = \frac{\exp[\frac{R^2}{2\sigma^2}] - 1}{\sqrt{(2\pi)} f_D (\frac{R}{\sqrt{2}\sigma})} \approx \frac{1}{\sqrt{(2\pi)} f_D} (\frac{R}{\sqrt{2}\sigma}) \quad (10)$$

Equations (8) and (9) show that the LCR increases as the envelope cross-correlation ρ_{env} ($\approx|\rho|^2$) increases whilst the AFD remains constant and becomes 1.7 times, 4 times and 14 times as large as that for the independent fading case for ρ_{env} = 0.42, 0.75 and 0.93 respectively. The AFDs for SS and SE strategies are equal to those with no diversity, while SC can halve the AFD. Considering the effect of the envelope cross-correlations, the measured data, shown in Fig. 7, agrees well with the calculated results.

COMPARISON OF ERROR RATES

In the case of $|\rho_{12}| = 0$ the expressions for the CDF of SS and SE are identical and can be obtained from (3) as

$$P(R) = \begin{cases} (1+q)[1-\exp(-\frac{R^2}{2\sigma^2})] - q & R \geq R_t \\ q[1-\exp(-\frac{R^2}{2\sigma^2})] & R \leq R_t \end{cases} \quad (11)$$

the CDF of SC is also obtainable from (3) and is given by

$$P(R) = [1-\exp(-\frac{R^2}{2\sigma^2})]^2 \quad (12)$$

where $R^2/2\sigma^2$ can be interpreted as γ/γ_o, the CNR/CNR_{mean} and $q = 1-\exp(-R_t/2\sigma^2)$.

The error rate performance is dependent on the modulation scheme used, but the average error rate can be determined by averaging the conditional probability of error over the ensemble of possible values of R(t) at the diversity combiner output, i.e. by integrating over the PDF of R(t). Taking non-coherent FSK as an example, the probability of

error can be written as $P_e(\gamma) = 1/2\exp(-\gamma/2)$ where γ = CNR and the value of $P_{e,2}$, the value appropriate to 2-branch diversity can be written as

$$P_{e,2} = \int_0^\infty P_e(\gamma)\, p_2(\gamma)\, d\gamma$$

where $p_2(\gamma)$ is the PDF of the CNR at the diversity system output.

For 2-branch selection diversity and Rayleigh fading the value of $P_{e,2}$ is given by

$$P_{e,2} = \frac{4}{(2+\gamma_o)(4+\gamma_o)} \qquad (13)$$

where γ_o is the mean CNR. We know that $P_{e,1}$, the single-branch Rayleigh-fading error rate is given by

$$P_{e,1} = \frac{1}{2+\gamma_o} \qquad (14)$$

So we can further write

$$P_{e,2} = 4\, P_{e,1}^2 \qquad (15)$$

Similarly for SS, it can be shown that

$$P_{e,2} = P_{e,1}\{1-\exp(-\gamma_T/\gamma_o)[1+\exp(-\gamma_T/2)]\} \qquad (16)$$

This expression can be minimised with respect to the threshold value γ_T by differentiation. The optimum threshold is thereby found to be

$$\gamma_T = 2\ln(1+\gamma_o/2)$$

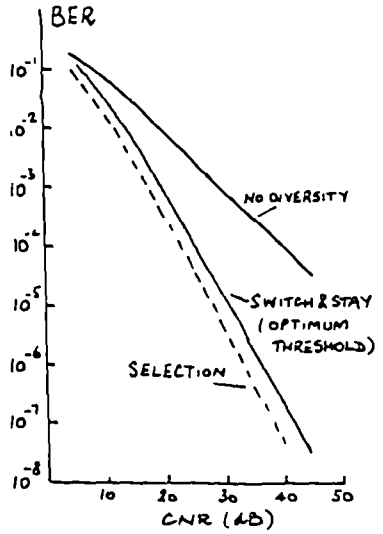

Fig. 10 Error probability for various diversity schemes under conditions of independent fading.

Substituting this back we obtain

$$P_{e,2} = P_{e,1}\left[1 - \left(\frac{\gamma_o}{2+\gamma_o}\right)\left(\frac{2}{2+\gamma_o}\right)^{2/\gamma_o}\right] \qquad (17)$$

Fig. 10 shows the relationship between eqns. (14), (15) and (17) from which it can be seen that provided we set the threshold level to its optimum value, the performance of SS and SE falls only slightly short of that for SC.

CONCLUSION

The effects of various two branch predetection diversity systems (SS, SE and SC) have been compared using the measured CDF, LCR and AFD statistics for vertically spaced antennas at a base station site. A diversity improvement can still be obtained for ρ_{env} up to 0.7 for SC and to obtain this correlation at a base station about 1.3 km from a mobile, the antennas can be separated vertically by around 12λ. The diversity improvement is most noticeable for the CDF and LCR, however, the AFD is only reduced by about half (note that there is no improvement in the AFD for SS and SE below the switching threshold). This means that if diversity reception is applied to digital transmissions, then the bit error rate and rate of burst error occurrence can be reduced considerably, and the burst error length is approximately halved.

ACKNOWLEDGEMENT

The authors wish to acknowledge several useful discussions with Dr. F. Adachi (NTT, Japan) and Dr. A.G. Williamson (University of Auckland, N.Z.) who were both on study leave at the University of Liverpool.

REFERENCES

[1] Jakes, W.C. Jr.(Ed.), "Microwave Mobile Communications", John Wiley and Sons., Inc., New York:1974.

[2] Parsons, J.D., Henze, M., Ratliff, P.A. and Withers, M.J. "Diversity techniques for mobile radio reception", The Radio and Electronic Engineer, Vol.45, No.7, pp.357-367:July 1975.

[3] Lee, W.C.Y. "Level crossing rates of an equal gain predetection diversity combiner", IEEE Trans. Commun. Technol., Vol.COM-18, pp.417-426:Aug.1970.

[4] Brennan, D.G. "Linear diversity combining techniques", Proc.IRE., Vol.47, pp.1075-1102: 1959.

[5] Adachi, F., Feeney, M.T., Williamson, A.G. and Parsons, J.D. "Crosscorrelation between the envelopes of 900MHz signals received at a mobile radio base station site", IEE Proc., Vol.133, Part F, pp.506-512:Oct.1986.

[6] Rustako, A.J., Yeh, Y.S. and Murray, R.R., "Performance of feedback and switch space diversity 900MHz mobile radio systems with Rayleigh fading", IEEE Trans. Commun., Vol. COM-21, pp.1257-1268:Nov.1973.

Level crossing rate and average fade duration for time diversity reception in Rayleigh fading conditions

F. Adachi, PhD
M.T. Feeney, MSc
J.D. Parsons, DSc(Eng), FEng

Indexing terms: Radiocommunication, Receivers

Abstract: Time diversity, in which the same data are transmitted several times, is attractive in digital land mobile radio and is simple to implement because only one antenna is required. Expressions for the level crossing rate (LCR) and average fade duration (AFD) are derived in this paper for a system in which each data symbol is transmitted twice (two-branch diversity). As far as LCR is concerned, the expected diversity advantages can be obtained for a data repetition period, normalised by the maximum Doppler frequency, of about 0.2. For a large data repetition period, the AFD is halved. Measured values of LCR and AFD, obtained from 900 MHz signals received at a base station site, are in good agreement with the predicted values.

List of principal symbols

f_D = maximum Doppler shift = v/λ
R = signal envelope
$\dot{R}$ = time derivative of R
v = vehicle velocity
τ = dummy variable (time delay)
$z_1(t)$ = complex signal envelope
$\phi_1(t)$ = phase modulation
σ = parameter of Rayleigh distribution (σ^2 = mean power)
λ = carrier wavelength
ω_c = carrier angular frequency

1 Introduction

In the UHF mobile radio environment, the received signal is characterised by rapid fading as a result of multipath propagation. Scatterers surrounding the mobile station cause the received signal to be composed of several component waves which combine constructively or destructively, depending upon their relative phase. With digital transmissions, the system performance deteriorates rapidly when the signal falls below some noise-related threshold and this causes bursts of errors to occur. The rates of occurrence and average length of these error bursts can be estimated from the level crossing rate (LCR) and average fade duration (AFD), respectively, of the received signal envelope. Otani and Omori [1] have shown that the measured average length of error bursts in simulated Rayleigh fading conditions are in good agreement with estimated values.

Diversity reception techniques can be used to combat the effects of multipath fading. Of the various possibilities, time diversity has the major advantage over other systems of only requiring a single antenna (space diversity requires two or more antennas) and hence is simple to implement. In a time diversity system, the same data are transmitted several times and in the system considered here, the symbol associated with the largest received signal strength is selected at the receiver.

Closed-form solutions are available for the LCR and AFD without diversity [2 & 3]. However, neither theoretical analysis nor experimental evidence exists for the LCR and AFD using time diversity reception. In this paper we consider a time diversity system in which each data symbol is transmitted twice over a mobile radio channel. It is apparent that, if the data repetition period is small, a finite correlation will exist between the fading signal envelopes associated with the two transmissions of the same data symbol, and one of the aims of the analysis is to establish the relevant relationship. In particular, we are interested in the minimum data repetition period necessary to ensure that the signal envelopes are sufficiently decorrelated to produce improvements in the LCR and AFD. A Rayleigh-fading environment is considered, and the theoretical results derived in Section 3 are compared, in Sections 4 and 5 with experimental measurements taken at a 900 MHz base station site.

2 Time diversity

The basic principle underlying time diversity is that each data symbol is transmitted several times. At the receiver, the various received versions are stored and a decision is taken as to which is correct. The two most obvious techniques are to take a decision either by majority-vote on the various stored versions, or to output the symbol associated with the largest signal strength. For majority voting, the minimum number of repetitions is three (in the UK TACS cellular radio system, which uses this method, words on the forward control channel (FOCC) are repeated five times), whereas if a signal strength indication is used the minimum number of repetitions is two.

Paper 6335F (E8), received 11th November 1987

F. Adachi is with the NTT Electrical Communications Laboratories, PO Box 8, Yokosuka Post Office, 238 Japan and M.T. Feeney and Prof. Parsons are with the Department of Electrical Engineering and Electronics, University of Liverpool, Brownlow Hill, PO Box 147, Liverpool L69 3BX, United Kingdom

If the original data stream is discontinuous, it may be possible to use time diversity, by repeating words, without increasing the data bit rate. However, if the original data stream is continuous, the final data rate has to be doubled or tripled etc. as appropriate. This is the type of system considered by Wong *et al.* [4] and by Miki and Hata [5]; the way in which a transmitted data stream at $2n$ bit/s is generated from an original stream at n bit s, and a version delayed by a time T, are shown in Fig. 1.

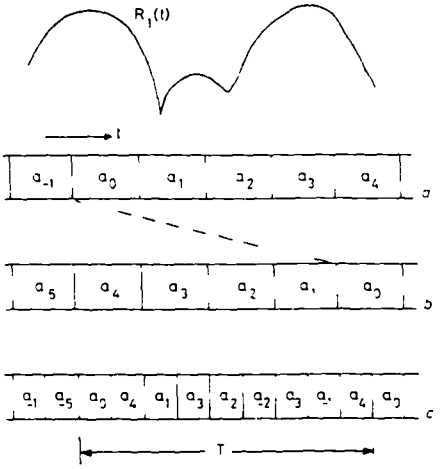

Fig. 1 *Signal envelope and data sequence*
a Original data
b Delayed data
c Transmitted data

This is transmitted over the radio channel which has the fading envelope shown. The precise details of the way in which the final data stream is constructed does not affect the analysis in this paper, which is applicable to any data stream of the kind shown in Fig. 1, i.e. one in which data symbols are repeated after a time T and a decision is taken on the basis of received signal strength. Specifically we consider a system in which the data is transmitted twice and a single antenna is used at the receiver.

The received signal $s(t)$ can be expressed as

$$s(t) = \mathrm{Re}\,\{z_1(t)\exp[j(\omega t + \phi_s(t))]\} \quad (1)$$

where $\phi_s(t)$ depends on the modulation system used. In Rayleigh fading, $z_1(t)$ is a zero-mean complex Gaussian process. A typical relationship between the received signal envelope $R_1(t) = |z_1(t)|$ and the data sequence is depicted in Fig. 1.

In time diversity the transmitted data stream containing the original and repeated data is demodulated from $s(t)$. It can be seen from Fig. 1 that the original data stream has the envelope $R_1(t)$ and the repeated data stream has the envelope $R_1(t - T)$. The nth element a_n ($n = \cdots -1, 0, 1, 2, \ldots$) is received twice and that associated with the larger envelope is selected. Hence the number of diversity branches is two and we can treat this type of time diversity as being equivalent to two-branch selection diversity with the signal envelopes $R_1(t)$ and $R_2(t) = R_1(t - T)$. The resultant envelope $R(t)$, after selection, is represented as

$$R(t) = \max\{R_1(t), R_2(t)\} \quad (2)$$

where $R_2(t) = R_1(t - T)$ and is shown in Fig. 2. The regenerated data symbol a_n is associated with the envelope $R(t_n)$. Since, when digital transmissions are used, error bursts occur when $R(t)$ falls below some noise-related threshold, analysis of the LCR and AFD of $R(t)$ is

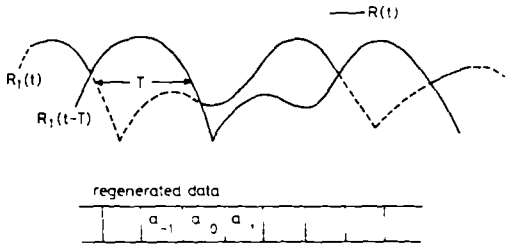

Fig. 2 *Relationship between $R(t)$, $R_1(t)$, $R_1(t - T)$ and regenerated data*

important for estimating the rate of occurrence and average length of these error bursts. In particular, the AFD analysis is important in connection with the application of forward error correcting codes [1].

3 Theory

We assume that the received signal is subject to Rayleigh-fading with a symmetrical power spectrum, i.e. the power spectrum of $z_1(t)$ is symmetrical. The LCR of $R(t)$ at a signal level R is given by Reference 2, p. 32:

$$N(R) = \int_0^\infty \dot{R}p(R, \dot{R})\,d\dot{R} \quad (3)$$

The AFD at the same level is given by

$$\bar{\tau}(R) = \frac{P(R)}{N(R)} \quad (4)$$

where P is the cumulative distribution function (CDF) of $R(t)$. In Reference 6, the present authors have developed an analysis leading to general expressions for the LCR and AFD of two-branch diversity systems, which are applicable in this case.

3.1 Level crossing rate (LCR)

Eqn. 8 of Reference 6 gives general expressions for the LCR using various combining methods. The appropriate relationship here is that applicable to selection diversity; i.e.

$$N = \int_{-\pi}^{+\pi}\int_0^R n_1 p(R_1 = R, R_2, \theta_{12})\,dR_2\,d\theta_{12} + \int_{-\pi}^{+\pi}\int_0^R n_2 p(R_1, R_2 = R, \theta_{12})\,dR_1\,d\theta_{12} \quad (5)$$

where $p(R_1, R_2, \theta_{12})$ is the joint PDF of R_1, R_2 and θ_{12}, given by eqn. 7 of Reference 6, and n_1 and n_2 are the conditional LCRs which can be evaluated from

$$n_1 = \int_0^\infty \dot{R}_1 p(\dot{R}_1 | R_1 = R, R_2, \theta_{12})\,d\dot{R}_1$$
$$n_2 = \int_0^\infty \dot{R}_2 p(\dot{R}_2 | R_1, R_2 = R, \theta_{12})\,d\dot{R}_2 \quad (6)$$

Evaluation of eqn. 6 requires knowledge of $\rho_{12}(0)$ and $\dot{\rho}_{12}(0)$ where $\rho_{12}(x)$ is the normalised crosscorrelation function of the two complex envelopes $z_1(t)$ and $z_2(t)$. In time diversity $z_2(t) = z_1(t - T)$, hence $\rho_{12}(0) = \rho_{11}^*(T)$ and $\dot{\rho}_{12}(0) = -\dot{\rho}_{11}^*(T)$ where $\rho_{11}(x)$ is the normalised

autocorrelation function of $z_1(t)$ and is a real function, since a symmetrical power spectrum has been assumed. The appendix of Reference 6 gives

$$n_1 = \frac{\sigma}{\sqrt{2\pi}}\sqrt{\left(-\ddot{\rho}_{11}(0) - \frac{\dot{\rho}_{11}^2}{1-\rho_{11}^2}\right)} \times \{\exp(-x_1^2) - \sqrt{\pi}\,x_1\,\mathrm{erfc}(x_1)\}$$
$$n_2 = \frac{\sigma}{\sqrt{2\pi}}\sqrt{\left(-\ddot{\rho}_{11}(0) - \frac{\dot{\rho}_{11}^2}{1-\rho_{11}^2}\right)} \times \{\exp(-x_2^2) + \sqrt{\pi}\,x_2\,\mathrm{erfc}(-x_2)\} \quad (7)$$

where we have introduced the simplifying notation $\rho_{11} = \rho_{11}(T)$ and $\dot{\rho}_{11} = \dot{\rho}_{11}(T)$. The variables x_1 and x_2 are

$$x_1 = \frac{\left(\frac{R}{\sigma\sqrt{2}}\right)\dot{\rho}_{11}\rho_{11} - \left(\frac{R_2}{\sigma\sqrt{2}}\right)\dot{\rho}_{11}\cos\theta_{12}}{(1-\rho_{11}^2)\sqrt{\left(-\ddot{\rho}_{11}(0) - \frac{\dot{\rho}_{11}^2}{1-\rho_{11}^2}\right)}}$$
$$x_2 = \frac{\left(\frac{R}{\sigma\sqrt{2}}\right)\dot{\rho}_{11}\rho_{11} - \left(\frac{R_1}{\sigma\sqrt{2}}\right)\dot{\rho}_{11}\cos\theta_{12}}{(1-\rho_{11}^2)\sqrt{\left(-\ddot{\rho}_{11}(0) - \frac{\dot{\rho}_{11}^2}{1-\rho_{11}^2}\right)}} \quad (8)$$

Since $p(R_1, R_2, \theta_{12})$ remains unchanged when R_1 and R_2 are interchanged, we have

$$N = \frac{2\sigma}{\sqrt{2\pi}}\sqrt{\left(-\ddot{\rho}_{11}(0) - \frac{\dot{\rho}_{11}^2}{1-\rho_{11}^2}\right)}\int_{\pi}^{+\pi}\int_0^R \times \{\exp(-x_1^2) + \sqrt{\pi}\,x_1\,\mathrm{erf}(x_1)\} \times p(R_1 = R, R_2, \theta_{12})\,dR_2\,d\theta_{12} \quad (9)$$

This is a general expression, but it is of interest to note that as $T \to \infty$, the independent fading case, then ρ_{11} and $\dot{\rho}_{11} \to 0$, and it becomes

$$N = 2\sqrt{\left(\frac{-\dot{\rho}_{11}(0)}{\pi}\right)}\frac{R}{\sigma\sqrt{2}}\exp\left(-\frac{R^2}{2\sigma^2}\right) \times \left[1 - \exp\left(-\frac{R^2}{2\sigma^2}\right)\right] \quad (10)$$

Conversely, if T is very small then $\rho_{11} \to 1$ and $\dot{\rho}_{11} \to 0$ (symmetrical power spectrum case). Expanding ρ_{11} and $\dot{\rho}_{11}$ in a power series of T gives

$$\rho_{11} = 1 + \dot{\rho}_{11}(0)T + \ddot{\rho}_{11}(0)T^2/2 + \cdots \simeq 1 + \ddot{\rho}_{11}T^2/2$$
$$\dot{\rho}_{11} = \dot{\rho}_{11}(0) + \ddot{\rho}_{11}(0)T + \cdots \simeq \dot{\rho}_{11}(0)T \quad (11)$$

and using the approximate formula for $p(R_1, R_2, \theta_{12})$ with strong correlation (see Appendix 9) it can be shown that

$$N = \sqrt{\left(-\frac{\ddot{\rho}_{11}(0)}{\pi}\right)}\frac{R}{\sigma\sqrt{2}}\exp\left(-\frac{R^2}{2\sigma^2}\right) \quad (12)$$

which is identical to the result for no diversity (Reference 2, p. 36).

3.2 Average fade duration (AFD)

The cumulative distribution function (CDF) with a time diversity system of the type being considered is the same as that of a two-branch selection diversity system with correlated fading [2] viz.

$$P(R) = 1 - \exp\left(-\frac{R^2}{2\sigma^2}\right) \times \left[1 + Q\left(\frac{R}{\sigma\sqrt{1-\rho_{11}^2}}, \frac{|\rho_{11}|R}{\sigma\sqrt{1-\rho_{11}^2}}\right) - Q\left(\frac{|\rho_{11}|R}{\sigma\sqrt{1-\rho_{11}^2}}, \frac{R}{\sigma\sqrt{1-\rho_{11}^2}}\right)\right] \quad (13)$$

where $Q(a, b)$ is Marcum's Q-function

$$Q(a, b) = \int_b^{\infty} x\exp\left[-\frac{x^2+a^2}{2}\right]I_0(ax)\,dx \quad (14)$$

Substitution of eqns. 9 and 13 into eqn. 4 allows us to evaluate the AFD by numerical methods. However, for large T (independent fading) and for small T (no diversity) fairly simple results are obtainable. For large T, $\rho_{11} \to 0$ and hence

$$P(R) = \left[1 - \exp\left(-\frac{R^2}{2\sigma^2}\right)\right]^2 \quad (15)$$

Substituting eqns. 10 and 15 into eqn. 4 gives

$$\bar{\tau} = \frac{1}{2}\sqrt{\frac{\pi}{-\ddot{\rho}_{11}(0)}}\frac{\exp\left(\frac{R^2}{2\sigma^2}\right) - 1}{R\,\sigma\sqrt{2}} \quad (16)$$

For small T, $P(R)$ approaches that without diversity, and

$$\bar{\tau} = \sqrt{\frac{\pi}{-\ddot{\rho}_{11}(0)}}\frac{\exp\left(\frac{R^2}{2\sigma^2}\right) - 1}{R\,\sigma\sqrt{2}} \quad (17)$$

Comparison of eqns. 16 and 17 shows that this kind of time diversity can halve the AFD when T is large (independent fading).

4 Calculated results

If we have knowledge of the normalised autocorrelation function $\rho_{11}(x)$, the LCR and AFD can be calculated. We consider the case when the scatterers surround the mobile uniformly and the antenna has an omnidirectional radiation pattern. Radiowave propagation from base to mobile is reciprocal, and so the autocorrelation function $\rho_{11}(x)$ of the received signal complex envelope $z_1(t)$ at both mobile and base station is given by [2]

$$\rho_{11}(x) = J_0(2\pi f_D x) \quad (18)$$

so that

$$\ddot{\rho}_{11}(0) = -\frac{(2\pi f_D)^2}{2} \quad (19)$$

Using eqns. 9, 13 and 4, we can numerically evaluate the LCR and AFD as a function of the normalised repetition period $f_D T$. In particular we can again write fairly simple expressions in the limiting cases. For $T \to \infty$, we have

$$\frac{N}{f_D} = 2\sqrt{2\pi}\frac{R}{\sigma\sqrt{2}}\exp\left(-\frac{R^2}{2\sigma^2}\right)\left[1 - \exp\left(-\frac{R^2}{2\sigma^2}\right)\right] \quad (20)$$

and

$$\bar{\tau}f_D = \frac{1}{2\sqrt{2\pi}}\frac{\exp\left(\frac{R^2}{2\sigma^2}\right) - 1}{R\,\sigma\sqrt{2}}$$

For small T,

$$\frac{N}{f_D} = \sqrt{2\pi}\,\frac{R}{\sigma\sqrt{2}}\exp\left(-\frac{R^2}{2\sigma^2}\right)$$

$$\bar{t}f_D = \frac{1}{\sqrt{2\pi}}\,\frac{\exp\left(\frac{R^2}{2\sigma^2}\right)-1}{R/\sigma\sqrt{2}} \qquad (21)$$

The calculated CDF, plotted from eqn. 13 is shown in Fig. 3. It can be seen that significant diversity advantages can be obtained at a normalised repetition period $f_DT = 0.2$, which corresponds to $T = 5$ ms if the carrier frequency is 900 MHz and the vehicle speed is 50 km h.

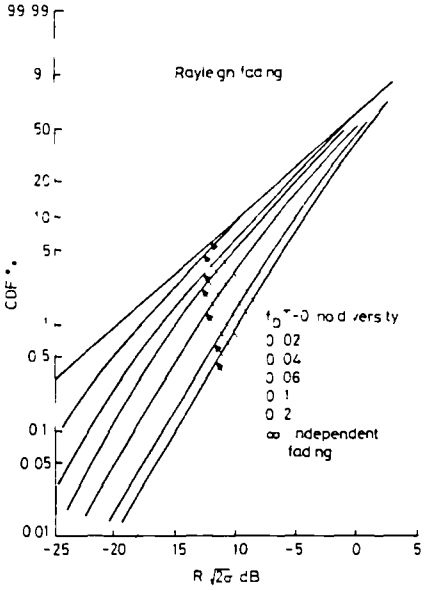

Fig. 3 *Calculated CDF*

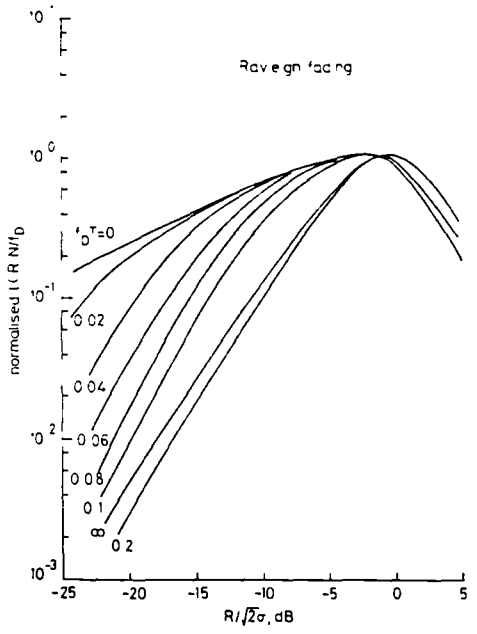

Fig. 4A *Calculated LCR against* $R/\sqrt{2}\sigma$

Some advantages remain, at low signal levels, even if $f_DT = 0.02$. As far as LCR is concerned, Fig. 4A shows that there is always an improvement over the no-diversity case ($f_DT = 0$) and for some values of f_DT near 0.2, the values are less than those for the case of independent fading ($f_DT \to \infty$). This is also apparent from Fig. 4B which shows the oscillatory nature of the curves as a function of f_DT. It is clear that time diversity will be effective in reducing the rate at which error bursts occur in digital land mobile radio.

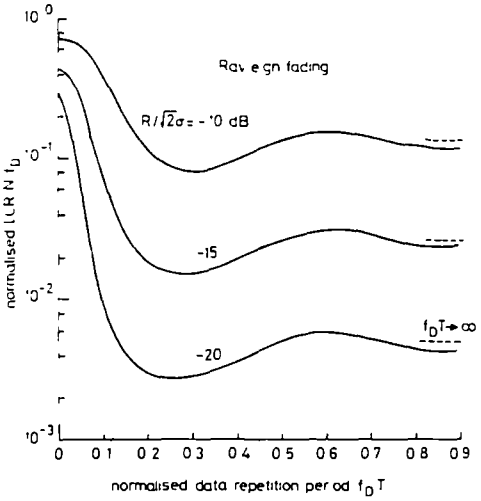

Fig. 4B *Calculated LCR against* f_DT

Calculated results for the AFD are shown in Fig. 5. These curves also have an oscillatory nature (as they must, because at any given level, CDF = LCR × AFD). The AFD is halved, compared with the no-diversity case, for large repetition periods but because of the relationship that exists between CDF, LCR and AFD, values corresponding to f_DT in the range 0.1–0.3 are slightly longer than in the no-diversity case. This is not a serious problem since in all cases there is an overall improvement, i.e. any slight increase in AFD is more than compensated for by the reduction in LCR. For $f_DT > 0.5$ there is always an improvement over the no-diversity case.

5 Experiment

To verify the calculations in the preceding Section, an experiment was set up in which a mobile transmitted a CW signal at 896.5 MHz, this being received on a vertically-mounted $\lambda/2$ dipole antenna at a base station site. The vehicle was driven at a nearly constant speed of 10 m s around a test area, approximately 1.3 km from the base-station which was located on the roof of the Department of Electrical Engineering and Electronics at Liverpool University. The received signal was passed into a signal-strength measuring receiver (Singer NM37-57) and the detected signal envelope was recorded on an analogue FM tape. The envelope was later digitised at a 1 kHz sampling rate for analysis on a mainframe computer.

To remove any effects due to slow fading, the measured signal envelope samples were normalised by using a running mean [7], and variations in the local mean value were removed using a moving-average process with a 0.5 s averaging window. A computer program was

written to simulate the time-diversity action for various repetition periods.

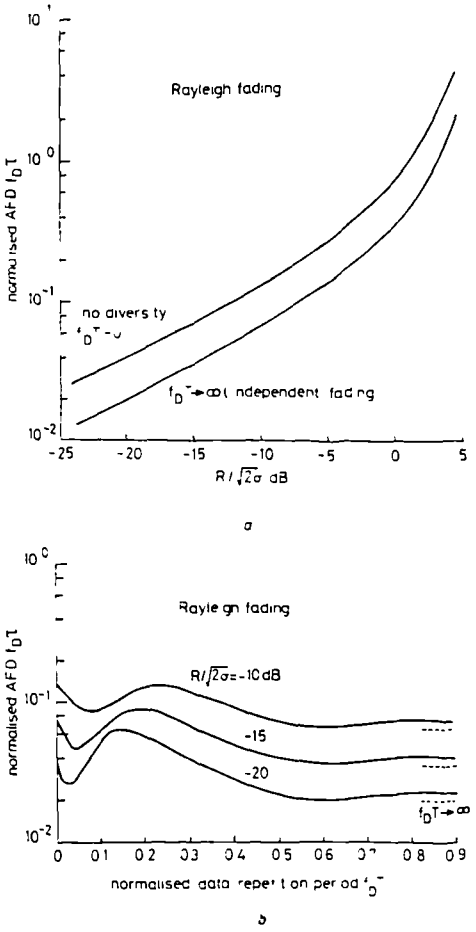

Fig. 5 *Calculated AFD*
a AFD against $R\sqrt{2}\sigma$
b AFD against f_DT

The measured results are shown in Figs. 6–8. It can be seen from Fig. 6 that the signal is below a value of $R\sqrt{2}\sigma = -15$ dB for about 3% of the time without diversity, but this value is reduced to 0.7% when $T = 5$ ms, and 0.3% when $T = 10$ ms. For a vehicle speed of 10 m s a repetition period of 10 ms corresponds to $f_DT = 0.3$ and at this value the measured results are in good agreement with values given by Fig. 3. At the same envelope level, Fig. 7 shows that the LCR is reduced by a factor of 20 for $T = 10$ ms and the measured AFD in the range $R\sqrt{2}\sigma = -10$ to -5 dB is about 0.7 times the value with no diversity. Again these values are in quite good agreement with the calculated values in Figs. 4 and 5.

6 Discussion and conclusions

In this paper we have presented an analysis leading to expressions for the LCR and AFD of a two-branch time diversity system in Rayleigh-fading conditions. It has been shown that the AFD is halved by the use of a large repetition period and that significant diversity advantage, as far as CDF and LCR are concerned, can be obtained using a normalised data repetition period of about 0.2.

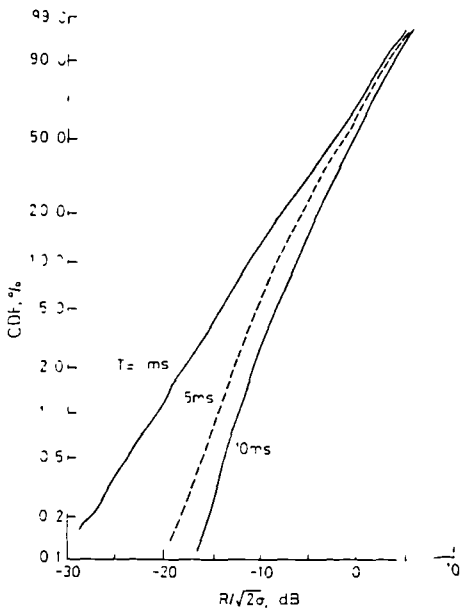

Fig. 8 *Measured CDF*
Carrier frequency = 896.5 MHz
Vehicle speed = 10 m s

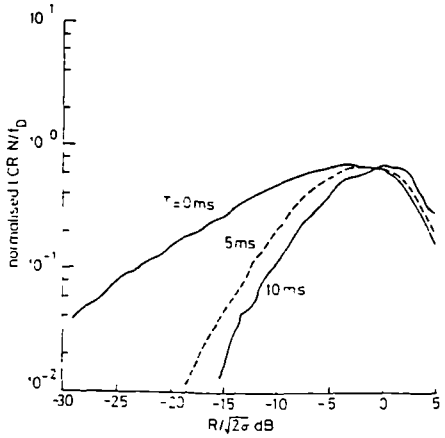

Fig. 7 *Measured LCR*
Carrier frequency = 896.5 MHz
Vehicle speed = 10 m s

Although the analysis has been specifically directed towards systems in which a decision is taken on the basis of received signal strength, the results can also be used as an indicator of how systems based on majority voting will perform. For example, in the UK TACS system, data are transmitted at 8 kbits/s and on the FOCC the word length is 40 bits (28 information plus 12 parity) which occupies a time of 5 ms. In practice, words are interleaved to improve the probability of correct reception so that the interval between repeats of any particular data symbol is 10 ms. The results given in Section 4 show that at this repetition period it should be possible to obtain some very considerable advantages at 25 km/h, since at

this speed a value of $T = 10$ ms corresponds to $f_D T = 0.2$. Figs. 3 and 4 show how the CDF and LCR are modified, and it is apparent that there is a very low probability that a data symbol received erroneously at a certain

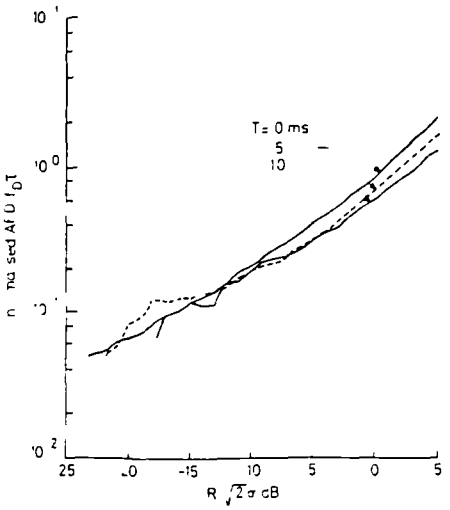

Fig. 8 *Measured AFD*
Carrier frequency 896.5 MHz
Vehicle speed 10 m/s

time will also be in error if repeated after 10 ms. In practice, the improvement only deteriorates very slowly as $f_D T$ is reduced, and so much slower speeds can be accommodated. In the TACS system, the added protection given by coding, and the fact that words are repeated five times, makes the technique viable even for hand portable equipment. However, the precise trade-offs between error probability and number of repeats remains to be investigated, as does a comparison between majority voting systems and those treated in this paper.

Nevertheless, analysis of data gathered from field trials has shown that time diversity yields a substantial improvement in the envelope CDF, and the measured LCR and AFD agree well with calculated results over a range of values of $f_D T$. We conclude that time diversity can provide a significant improvement in system performance and is easily implemented, compared with spaced-antenna systems.

7 Acknowledgment

This work was undertaken while F. Adachi was an SERC visiting research fellow in the Department of Electrical Engineering and Electronics, University of Liverpool.

8 References

1 OTANI, K., and OMORI, H.: 'Distribution of burst error lengths in Rayleigh fading radio channels', *Electron. Lett.*, 1980, **16**, (23), pp. 889–891
2 JAKES, W.C. (Ed.): 'Microwave mobile communications' (John Wiley & Sons, New York, 1974)
3 RICE, S.O.: 'Mathematical analysis of random noise', *Bell Syst. Tech. J.*, 1944, **23**, pp. 282–332 (also 1945, **24**, pp. 46–156)
4 WONG, W.C., STEELE, R., GLANCE, B., and HORN, D.: 'Time diversity with adaptive error detection to combat Rayleigh fading in digital mobile radio', *IEEE Trans.*, 1983, **COM-31**, pp. 378–387
5 MIKI, T., and HATA, M.: 'Time diversity effects in digital land mobile radio', *Trans. Inst. Electron. & Commun. Eng. Jpn. Part B*, 1983, **J66-B**, pp. 543–549
6 ADACHI, F., FEENEY, M.T., and PARSONS, J.D.: 'Effects of correlated fading on level crossing rates and average fade durations with predetection diversity reception', *IEE Proc. F, Commun., Radar & Signal Process.*, **13**, (1), pp. 11–17
7 CLARKE, R.H.: 'A statistical theory of mobile radio reception', *Bell Syst. Tech. J.*, 1968, **47**, pp. 957–1000

9 Appendix

An approximate expression for $p(R_1, R_2, \theta_{12})$ for small T

For time diversity with a symmetrical fading power spectrum, the original expression for $p(R_1, R_2, \theta_{12})$, presented in Reference 2, can be written as

$$p(R_1, R_2, \theta_{12}) = \frac{R_1 R_2}{2\pi\sigma^4(1-\rho_{11}^2)} \times \exp\left[-\frac{R_1^2 + R_2^2 - 2R_1R_2\cos\theta_{12}}{2\sigma^2(1-\rho_{11}^2)}\right]$$
$$= \frac{R_1 R_2}{2\pi\sigma^4(1-\rho_{11}^2)} \exp\left[-\frac{R_1^2+R_2^2}{2\sigma^2(1-\rho_{11}^2)}\right] \times \sum_{n=0}^{\infty} \varepsilon_n I_n\left[\frac{|\rho_{11}| R_1 R_2}{\sigma^2(1-\rho_{11}^2)}\right]\cos n\theta_{12} \quad (22)$$

where $I_n(\cdot)$ = modified Bessel function

$\varepsilon_n = 1 (n = 0)$,

$= 2 (n > 0)$

When T is small, we have from eqn. 11 that

$$1 - \rho_{11}^2 \simeq -\ddot{\rho}_{11}(0)T^2$$

and hence the argument of the modified Bessel function in eqn. 22 becomes very large. Using

$$I_n(y) = \frac{\exp(y)}{\sqrt{(2\pi y)}} \quad \text{for large } y$$

we have

$$p(R_1, R_2, \theta_{12}) \simeq \frac{R_1 R_2}{\sigma^4\{-\ddot{\rho}_{11}(0)T^2\}} \frac{1}{\sqrt{\left(2\pi \frac{R_1 R_2}{\sigma^2\{-\ddot{\rho}_{11}(0)T^2\}}\right)}} \times \exp\left[-\frac{(R_1-R_2)^2 - R_1R_2\ddot{\rho}_{11}(0)T^2}{2\sigma^2\{-\ddot{\rho}_{11}(0)T^2\}}\right] \times \frac{1}{2\pi}\sum_{n=0}^{\infty}\varepsilon_n \cos n\theta_{12} \quad (23)$$

$$= \frac{\sqrt{(R_1R_2)}}{\sigma^3 T\sqrt{(-2\pi\ddot{\rho}_{11}(0))}} \times \exp\left[-\frac{(R_1-R_2)^2 - R_1R_2\ddot{\rho}_{11}(0)T^2}{2\sigma^2\{-\ddot{\rho}_{11}(0)T^2\}}\right]\delta(\theta_{12}) \quad (24)$$

where $\delta(\cdot)$ is the delta function. Since $-\ddot{\rho}_{11}(0)T^2$ is very small, there is a high probability that the value of R_2 is very close to R_1, and so $R_1R_2 \simeq R_1^2$ and we obtain the approximate expression

$$p(R_1, R_2, \theta_{12}) \simeq \frac{R_1}{\sigma^2}\exp\left[-\frac{R_1^2}{2\sigma^2}\right] \times \frac{1}{\sqrt{(2\pi\sigma^2\{-\ddot{\rho}_{11}(0)T^2\})}}\exp\left[-\frac{(R_1-R_2)^2}{2\sigma^2\{-\ddot{\rho}_{11}(0)T^2\}}\right]\delta(\theta_{12})$$

APPENDIX B. RAYLEIGH PDF IN DB TERMS.

For ease of computing, the statistical distributions are determined in terms of dB and not linear units. In order that the PDFs etc. can then be compared we need to consider the equivalent distributions in dB terms. The output from the receiver is usually calibrated in dBs, what then is the equivalent distribution for the dB values? If we consider the Rayleigh distribution for a linear expressed signal then

$$p(r) = \frac{r}{\sigma^2} \exp\left\{ -\frac{r^2}{2\sigma^2} \right\} \qquad (B.1)$$

Let y be the output from the receiver i.e.

$$y = 20 \log r = 2a \ln r \qquad \text{i.e. } a = 10/\ln 10 \qquad (B.2)$$

Then

$$r = e^{y/2a} \qquad (B.3)$$

and

$$\frac{dr}{dy} = \frac{1}{2a} e^{y/2a} \qquad (B.4)$$

Remembering that probability space must be conserved i.e.

$$p(y) = p(r) \frac{dr}{dy} = \frac{e^{y/2a}}{\sigma^2} \exp\left\{ -\frac{e^{y/a}}{2\sigma^2} \right\} \frac{1}{2a} e^{y/2a} \qquad (B.5)$$

Rearranging we have

$$p(y) = \frac{1}{2a\sigma^2} e^{y/a} \exp\left\{ -\frac{e^{y/a}}{2\sigma^2} \right\} \qquad (B.6)$$

Since we normalise by the average signal power $= E\{r^2/2\} = \sigma^2$ then let $\sigma^2 = 1$ then

$$p(y) = \frac{1}{2a} e^{y/a} \exp\left\{ -\frac{e^{y/a}}{2} \right\} \qquad (B.7)$$

which can be rearranged as

$$p(y) = \frac{1}{2a} \exp\left\{ \frac{y}{a} - \frac{\exp(\frac{y}{a})}{2} \right\} \qquad (B.8)$$

APPENDIX C. VARIANCE OF DB EXPRESSED ENVELOPE.

The standard deviation of the dB expressed envelope values, $\sigma_r(dB)$, can be found using classical definitions in the following manner. let y be the dB output from the receiver i.e.

$$y = 20 \log r = 10 \log r^2 = a \ln r^2 \qquad a = 4.34 \tag{C.1}$$

now

$$\sigma_r^2(dB) = < y^2 > - < y >^2 \tag{C.2}$$

Firstly $< y >$

$$< y > = \int_0^\infty y p(y)\, dy = \int_0^\infty a \ln r^2 p(r)\, dr \tag{C.3}$$

remembering that probability space must be conserved i.e.

$$p(y)\, dy = p(r)\, dr \tag{C.4}$$

$$< y > = \int_0^\infty a \ln r^2 \frac{r}{\sigma^2} e^{-r^2/2\sigma^2} dr \tag{C.5}$$

let $x = r^2/2\sigma^2$ then $dx = \frac{r}{\sigma^2} dr$

$$< y > = \int_0^\infty a \ln r^2 \frac{r}{\sigma^2} e^{-x} \frac{\sigma^2}{r}\, dx = \int_0^\infty a \ln(2\sigma^2 x) e^{-x}\, dx \tag{C.6}$$

$$< y > = a \int_0^\infty [\ln 2\sigma^2 + \ln x] e^{-x}\, dx \tag{C.7}$$

now

$$\int_0^\infty \ln x e^{-x}\, dx = -C \qquad (C.8)$$

i.e. Eulers constant, where C = 0.5772157

$$< y > = a[\ \ln(2\sigma^2) - C] \qquad (C.9)$$

Secondly $< y^2 >$

$$< y^2 > = \int_0^\infty (a \ln r^2)^2 \frac{r}{\sigma^2} e^{-r^2/2\sigma^2}\, dr \qquad (C.10)$$

$$= a^2 \int_0^\infty (\ln 2\sigma^2 x)^2 e^{-x}\, dx \qquad (C.11)$$

$$\text{let } z = 2\sigma^2 x \qquad dz = 2\sigma^2 dx$$

$$< y^2 > = \frac{a^2}{2\sigma^2} \int_0^\infty (\ln z)^2 e^{-z^2/2\sigma^2}\, dz \qquad (C.12)$$

now from [1]

$$\int_0^\infty (\ln z)^2 e^{-\mu z}\, dz = \frac{1}{\mu}\left[\frac{\pi^2}{6} + (C + \ln \mu)^2\right] \qquad (C.13)$$

$$< y^2 > = a^2\left[\frac{\pi^2}{6} + \{C - \ln 2\sigma^2\}^2\right] \qquad (C.14)$$

hence

$$\sigma_r^2(dB) = = \frac{a^2\pi^2}{6} \qquad (C.15)$$

$$\sigma_r(dB) = \frac{a\pi}{\sqrt{6}} = 5.57 \text{ dB} \qquad (C.16)$$

REFERENCES.

[1] Gradshteyn, I.S. and Ryzhik, I.W., "Table of Integrals, Series and Products", Academic Press, New York, 1965.

APPENDIX D. RICIAN PDF IN DB TERMS.

For ease of computing, the statistical distributions are determined in terms of dB and not linear units. In order that the PDFs etc. can then be compared we need to consider the equivalent distributions in dB terms. The output from the receiver is usually calibrated in dBs, what then is the equivalent distribution for the dB values? If we consider the Rician distribution for a linear expressed signal then

$$p(r) = \frac{r}{\sigma^2} \exp\{ - \frac{r^2 + d^2}{2\sigma^2} \} I_0\{ \frac{rd}{\sigma^2} \} \qquad (D.1)$$

Let y be the output from the receiver i.e.

$$y = 20 \log r = 2a \ln r \qquad \text{i.e. } a = 10/\ln 10 \qquad (D.2)$$

Rearranging we have

$$r = e^{y/2a} \qquad (D.3)$$

differentiating r with respect to y

$$\frac{dr}{dy} = \frac{1}{2a} e^{y/2a} \qquad (D.4)$$

Remembering that probability space must be conserved then the PDF of the dB values is given by

$$p(y) = p(r) \frac{dr}{dy} = \frac{e^{y/2a}}{2a\sigma^2} \exp\left\{ - \frac{e^{y/a} + d^2}{2\sigma^2} \right\} I_0\left\{ \frac{e^{y/2a} d}{\sigma^2} \right\} \qquad (D.5)$$

Since we normalise by the average signal power $= E\{r^2/2\} = \sigma^2$ then let $\sigma^2 = 1$ then

$$p(y) = \frac{1}{2a} \exp\left\{ \frac{y}{a} - \frac{e^{y/a} + d^2}{2} \right\} I_0\{e^{y/2a} d\} \qquad (D.6)$$

APPENDIX E. SAMPLE SIZE FOR LOCAL MEAN ESTIMATION.

In order to study the fast fading signal and compare recorded data with theory requires that any local mean variation (i.e. slow fading) be removed from the raw data. The local mean variation of the recorded data can be estimated over a particular measurement length. An improvement in the estimation of the local mean, of a fading signal, can be achieved through a knowledge of the effects that the sampling rate and measurement length have on the standard deviation of the estimate. It is insufficient to simply increase the sample size N, since for a high sampling rate and small measurement length the values could lie on an unrepresentative portion of the fading envelope. Similarly, a long measurement length and a sampling rate that is insufficient to resolve the fading envelope could inadequately represent the local mean. It is not only necessary to have a sufficiently large sample size N, but also that the samples should cover a suitable measurement length. In the following the effects that the sampling rate and measurement length have on the standard deviation of the estimated local mean, σ_e, (expressed in dB terms) are considered.

The variance of a random variable x can be found from

$$\sigma^2 = E\{x^2\} - E\{x\}^2 \qquad (E.1)$$

where $E\{x\}$ is the expected value of x. The estimate of the dB expressed envelope $\hat{r}(dB)$[21] is given by

$$\hat{r}(dB) = \frac{1}{N}\sum_{n=1}^{N} a \ln r^2 \qquad (E.2)$$

since

---

[21] The hat symbol, $\hat{w}$, is used to represent an estimate of the variable w.

$$r(dB) = 20 \log r = a \ln r^2 \qquad a = 10/\ln 10 \tag{E.3}$$

Using E1 and E2, the variance can be expressed as[1]

$$\sigma_e{}^2 = \frac{1}{N}\left[\psi(0) + 2\sum_{n=1}^{N-1}\left(1 - \frac{n}{N}\right)\psi(n\Delta T)\right] \tag{E.4}$$

where ΔT is the sampling interval (i.e. $\Delta T = 1/f_s$, f_s = sampling frequency) and $\psi(\tau)$ is the autocovariance of the dB expressed envelope in Rayleigh fading conditions. Now $\psi(\tau)$ was given in Chapter 2 and [2] as

$$\psi(\tau) = a^2 \sum_{n=1}^{\infty} \frac{|\rho|^{2n}}{n^2} \tag{E.5}$$

The autocovariance at zero lag, i.e. $\psi(0)$, was also derived in Chapter 2 and Appendix C as

$$\psi(0) = 5.57^2 \tag{E.6}$$

The sample size N is related to the measurement time T or spatial length $L(= VT)$ by

$$N = f_s T \tag{E.7}$$

$$N = \frac{f_s}{f_D} f_D T = \frac{f_s}{f_D}\frac{L}{\lambda} \tag{E.8}$$

Thus equation E4 can be written as

$$\sigma_e^2 = \frac{f_D/f_s}{f_D T}\left[\psi(0) + 2\sum_{n=1}^{N-1}\left(1 - n\frac{f_D/f_s}{f_D T}\right)\psi(n/f_s)\right]$$
$$= \frac{f_D/f_s}{L/\lambda}\left[\psi(0) + 2\sum_{n=1}^{N-1}\left(1 - n\frac{f_D/f_s}{L/\lambda}\right)\psi(n/f_s)\right] \qquad (E.9)$$

Figure E1 shows σ_e as a function of normalised measurement length ($f_D T$ or L/λ) and normalised sampling rate (i.e. f_s/f_D). Note that for a given measurement length, the standard deviation decreases as the sampling rate f_s increases and asymptotically approaches some low value for high values of sampling rate. To reduce the standard deviation of the estimate, large measurement lengths ($f_D T$ or L/λ) are necessary. However, in real fading conditions, we then run the risk that the average signal power (i.e. σ^2) would no longer remain constant. From Figure E1 $f_D T$ or $L/\lambda > 20$, the standard deviation decreases very slowly. Therefore, it is reasonable to conclude that a practical measurement length lies in the range of $f_D T$ or $L/\lambda = 20 \simeq 40$.

In the case of this work a vehicle speed of 10m/s coupled with the operating frequency (914MHz) relates to a Doppler frequency (i.e. f_D) of $\simeq$30Hz. Which, with a moving average window of 0.5s (i.e. 501 points at a sampling frequency f_s = 1 Hz) produces a normalised measurement length of $f_D T = 15$. From Figure E1 this value of $f_D T$ corresponds with estimating the local mean to within $\pm$ 1dB.

REFERENCES.

[1] Davenport. W.B. and Root, W.L., An Introduction to the Theory of Random Signals and Noise, McGraw-Hill, New York, 1958.

[2] Davis, B.R. and Bogner, R.E., "Propagation at 500MHz for Mobile Radio", IEE Proc., Vol. 132, Pt.F, pp.307-320, 1985.

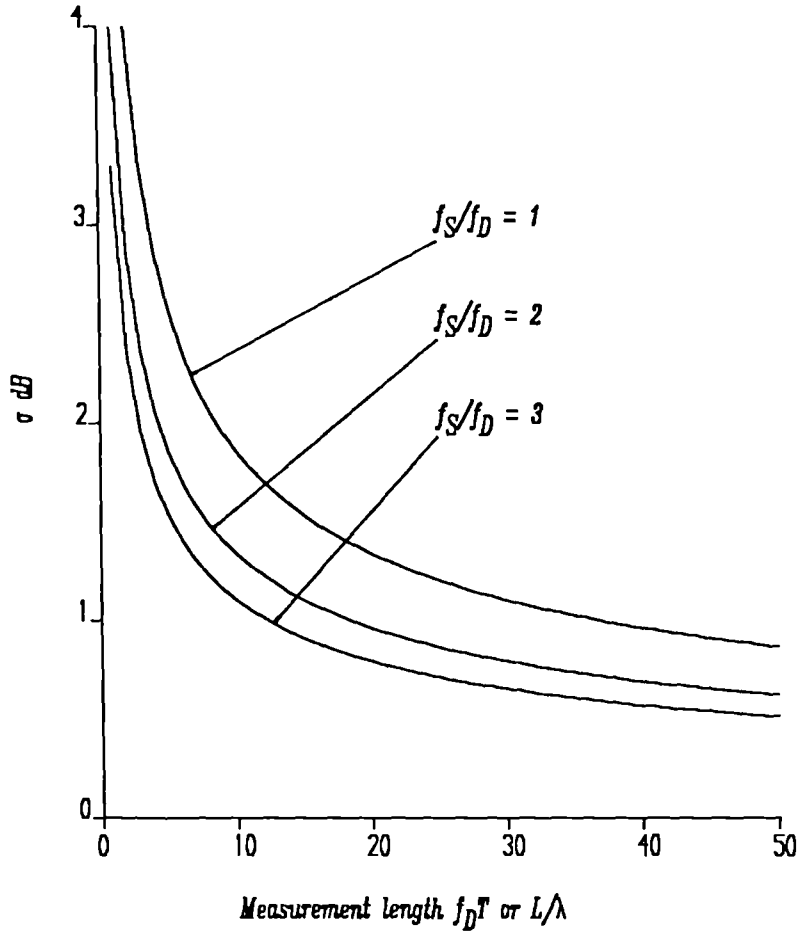

Figure E.1 Standard deviation for the estimate of the mean strength in dB units as a function of normalised sampling rate (f_s/f_D) and measurement length (f_DT or L/λ).